Contributions in Mathematical Oncology: When Theory Meets Reality

Sébastien Benzekry

▶ **To cite this version:**

Sébastien Benzekry. Contributions in Mathematical Oncology: When Theory Meets Reality. Mathematics [math]. Université de Bordeaux, 2017. tel-01658070

HAL Id: tel-01658070
https://theses.hal.science/tel-01658070

Submitted on 7 Dec 2017

HAL is a multi-disciplinary open access archive for the deposit and dissemination of scientific research documents, whether they are published or not. The documents may come from teaching and research institutions in France or abroad, or from public or private research centers.

L'archive ouverte pluridisciplinaire **HAL**, est destinée au dépôt et à la diffusion de documents scientifiques de niveau recherche, publiés ou non, émanant des établissements d'enseignement et de recherche français ou étrangers, des laboratoires publics ou privés.

Université de Bordeaux

Thèse présentée pour obtenir le diplôme

HABILITATION A DIRIGER DES RECHERCHES

Spécialité : Mathématiques appliquées

par

Sébastien Benzekry

Contributions in Mathematical Oncology: When Theory Meets Reality

---

soutenue publiquement le 13 novembre 2017

après avis favorable des rapporteurs:

Mark CHAPLAIN	Professor, St. Andrews University, Scotland
Emmanuel GRENIER	Professeur, Ecole Normale Supérieure de Lyon, France
Larry NORTON	Deputy physician-in-chief for breast cancer programs, Memorial Sloan Kettering Cancer Center, USA

devant le jury composé de:

Dominique BARBOLOSI	PR, Université Aix-Marseille, Marseille
Fabrice BARLÉSI	PU-PH, Assistance publique - Hôpitaux de Marseille, Marseille
Andreas BIKFALVI	PR, Université de Bordeaux, Bordeaux
Jean CLAIRAMBAULT	DR, Inria Paris, Paris
Thierry COLIN	PR, ENSEIRB-MATMECA, Bordeaux
John EBOS	Assist. Prof., Roswell Park Cancer Institute, Buffalo, USA (Invité)
Adeline LECLERQ SAMSON	PR, Université Grenoble-Alpes, Grenoble
Rodolphe THIÉBAUT	PU-PH, Inria Bordeaux & Inserm, Bordeaux

Remerciements

Je tiens tout d'abord à remercier Mark Chaplain, Emmanuel Grenier ainsi que Larry Norton qui m'ont fait l'honneur de rapporter sur mes travaux. Leurs recherches en modélisation du cancer sont pionnières à bien des égards et ont constitué une grande source d'inspiration.

Ensuite, je voudrais exprimer ma gratitude aux membres du jury. C'est un grand plaisir pour moi de voir rassemblés des médecins (merci à messieurs Barlési, Clairambault et Thiébaut), des biologistes (merci à messieurs Bikfalvi et Ebos) et des mathématiciens (merci à madame Leclerq Samson et messieurs Barbolosi et Colin), sans que ces catégories ne soient exclusives. C'est en particulier un grand plaisir de retrouver Dominique Barbolosi qui dirigea ma thèse de doctorat et continue d'être un "mentor" pour moi.

Je mesure aujourd'hui à quel point l'expérience de mon post-doctorat au Center of Cancer and Systems Biology à Boston fut instructive en termes de projets multidisciplinaires mélangeant cliniciens, biologistes, physiciens et mathématiciens au sein d'un même laboratoire et travaillant ensemble au jour le jour. Je souhaite ici remercier la directrice et instigatrice de ce laboratoire Lynn Hlatky dans les nombreux combats pour faire exister cet organe quasi-unique et aujourd'hui le faire renaître de ses cendres. Elle est épaulée par Philip Hahnfeldt avec qui j'ai eu l'honneur de travailler et pu apprécier la profondeur de sa compréhension du cancer et bénéficier de ses idées à la fois simples et puissantes. De plus, je voudrais aussi remercier les autres membres du labo avec qui j'ai échangé et qui m'ont tous appris beaucoup : Giannoula, Abdo, Ryan, Katherine, Clare, Afshin, Janusz, Ed, Jaspreet, Nava,...

Depuis janvier 2013, j'ai la chance de travailler en tant que chargé de recherches au sein de l'équipe-projet Inria MC2 devenue depuis MONC (Modélisation en ONCologie). Son ambiance détendue et ses ambitions de faire de la recherche avec des applications biologiques ou cliniques concrètes m'offre le cadre idéal pour développer mes travaux en toute liberté et je remercie Thierry Colin et Olivier Saut, directeurs d'équipe respectifs, pour leur bienveillance à mon égard et le soutien qu'ils ont apporté ou apportent à mes différents projets. De plus, merci Thierry de donner une sacré dose de bonne humeur malicieuse dans le travail quotidien et merci Olivier pour ton humour moins voyant mais tout aussi fin, ainsi que pour endosser la charge de diriger l'équipe avec grande responsabilité. C'est aussi un plaisir d'interagir avec les autres membres permanents de l'équipe, Clair, Annabelle et Baudoin. Enfin, merci aux membres non-permanents actuels et passés, cités ici dans le désordre le plus total : Sergio, Vivien, Manon, Perrine, Agathe, Thibaut, Cynthia (go the chorus line Bordeaux ! !), Boris, Claudia, Olivier, Thomas, Guillaume L, Guillaume D, Julien. Une mention spéciale pour Benjamin Taton avec qui c'est toujours un grand plaisir d'échanger, sur la science, les stats, la médecine ou autre ! Et bienvenue à ceux qui arrivent cette année : Cristina, Thibauld, Erwan et Costanza.

Dans mes travaux – j'espère que cela sera clair à la lecture de ce manuscrit – j'attache une part fondamentale à la pertinence des problèmes cliniques ou biologiques, ainsi qu'aux données em-

piriques. Ainsi, aucun de ceux-ci n'aurait pu être conduit sans des interactions étroites avec des biologistes ou médecins. Je tiens donc ici à les remercier chaleureusement. Clare Lamont pour avoir effectué les expériences animales d'interactions entre tumeurs avec moi, m'avoir montré tous les détails expérimentaux et être restée jusqu'à des heures tardives pour mesurer toutes les tumeurs, tous les jours de l'étude. John Ebos pour me faire profiter des quantités astronomiques de données générées au sein de son laboratoire (notamment par le travail acharné de Michalis Mastri). Wilfried Souleyreau, Lin Cooley et Andreas Bikfalvi du LAMC et Emeline Ribot du RMSB pour notre collaboration sur le cancer du rein. Enfin, plusieurs des études que j'ai effectuées l'ont été aux côtés de l'inénarrable Joseph Ciccolini et de son harem pharmacocinétique. Merci à vous tous le SMARTc, merci Cindy, Diane, Raouf, Anne, Arnaud.

Le présent mémoire a été écrit en vue d'obtenir l'habilitation à diriger des recherches. J'ai déjà eu la chance d'encadrer plusieurs étudiants, et les travaux qui suivent leur doivent beaucoup. Je tiens ici à les mentionner et à leur dire que ce fut un grand plaisir de travailler avec eux. Merci Aristoteles, Maxime, Simon, Laura et Maria ainsi que Chiara que j'encadre actuellement. De plus, ce fut un immense honneur pour moi d'accompagner les premiers pas en recherche d'Etienne Baratchart, brillant et vif d'esprit mais aussi un grand ami. Etienne, je te souhaite toute la réussite dans ta carrière de chercheur, et tout le bonheur du monde dans ta vie.

La vie, surtout dans la recherche, est ponctuée de hauts et de bas. Parfois, on le sent, tout marche, tout s'enchaîne parfaitement. Mais souvent aussi, on doute, on pense que tout ça ne sert à rien, ne mène à rien. Dans ma vie, il y en a deux qui sont toujours là pour moi, qui croient toujours en moi et qui, je le sais, sont toujours fiers de moi. Merci papa et maman, merci de tout mon coeur.

Merci aussi à mon frangin, au talent débordant. Big up, comme on dirait. Et j'en profite pour déposer deux gros bisous à Romy et Sacco ainsi qu'à Salomé et Tito.

Enfin, merci à toi, mi amor. Tu me supportes dans toutes mes facéties, toutes mes folies. Tu es toujours là pour m'écouter, pour me conseiller, pour m'aider à me repérer dans ce monde. Merci d'être dans ma vie.

Contents

Introduction

Cancer diseases are a major health concern in the modern society. Taken together, they represent the second leading cause of death worldwide (they were responsible for 8.8 million deaths in 2015, which represents nearly 1 in 6 deaths) and the first cause of death in France[1] [Ferlay et al., 2013, InVS and INCa, 2011]. In face of such a public health challenge and considering the "unreasonable effectiveness of mathematics in natural sciences" [Wigner, 1960], one might wonder: can mathematical models be of help in oncology?

Since a wide variety of mathematical tools could be considered, some – such as epidemiological statistical models, stochastic evolutionary models or bioinformatics algorithms – being beyond the scope of my research, I should start by defining what I mean by a "mathematical model". In the context of the work reported here it will be: a function, most often (but not necessarily), deterministic, depending on the time and a set of parameters, intended to describe the **dynamics** of a biological system and thus often defined by a set of ordinary or partial differential equations.

With the development of novel measurement methods (especially from molecular biology and imaging), accumulation of biological and clinical data is currently driving oncology toward a quantitative science, which raises the question of inferring general patterns and structures behind the data as well as extracting the most information from these. Meanwhile, the number of mathematical models developed by theoreticians in the field of so-called "mathematical oncology" [Gatenby and Maini, 2003] has been exponentially growing in the last decades [Barbolosi et al., 2016, Altrock et al., 2015, Byrne, 2010, Anderson and Quaranta, 2008, Bellomo et al., 2008]. However, these formal constructs have often remained confined to qualitative conclusions and rarely been confronted to the observations. The driving force behind my work since my PhD has been to try to **bridge the gap between theories/models and empirical data**. Crucially, my objectives have always been to do so motivated by a specific biological or clinical question, thus not considering the modeling process as an end in itself but rather as a mean. So far, my work has been focused about two possible aims of mathematical modeling in oncology:

1. better **understand the biology**. Indeed, by allowing the simulation (or analysis) of the implications of biological hypotheses, mathematical and computational models provide a way

[1] In France, cancer represents 27.3% of deaths, before cardio-vascular diseases (26% of deaths) [InVS and INCa, 2011]. Cumulative lifetime risk of death by cancer are 14.3% in males and and 9% in females in more developed areas of the world versus respectively 12% and 8.1% in less developed areas (excluding nonmelanoma skin cancer) [Torre et al., 2015]

to test these hypotheses against experimental data. This improves our understanding of the biology by discriminating theories that are able to describe the data and, perhaps even more importantly, reject theories that are not.

2. **predict** the future of a cancer disease or the impact of a therapeutic strategy. In this case, even if the model is only phenomenological (i.e., weakly connected to a mechanistic description of the biological process), if its predictive power of the model is properly validated, it can provide a powerful numerical tool for clinical applications. To this regard, I believe applications can be divided into (at least) two subclasses:
   (a) the rational design of **treatment regimen** in clinical trials
   (b) patient-specific predictive tools of help for **personalized medicine** (personalized prognosis of tumor growth, decrease or relapse and/or metastatic state or relapse in order to plan the individualized intervention).

With this in mind, my research has been focused on **specific problems** concerning processes in cancer that have a **dynamical** component, including tumor growth, metastasis and anti-cancer systemic treatments. Although these biological, clinical and therapeutic problems shall be defined at a later stage in this document, one canonical example is the prediction of the occult burden of metastases at diagnosis in breast cancer, for personalized adaptation of peri-operative treatment. To address these open problems, I consider fundamental to depart from the published knowledge on the biological processes on one hand and from **experimental or clinical data** on the other. Therefore, several of the studies reported here were done in collaboration with biologists or clinicians, including people from the Center of Cancer and Systems Biology (Tufts University, Boston, MA, USA), the Roswell Park Cancer Institute (Buffalo, NY, USA), the Laboratoire de l'Angiogénèse et du Microenvironnement des Cancers (LAMC, Inserm, Bordeaux, France) and the "Simulation & Modelling: Adaptive Response for Therapeutics in Cancer" team (SMARTc, Inserm, Marseille, France). My strategy in these integrative *in vivo/in silico* works has been the following:

1. define, from the current state of the art, a clinically or biologically relevant problem *addressable by mathematical modeling methods* (not all of them are), given the obtainable data
2. design an experiment (this part having been sometimes performed by myself and other times by others) or collect relevant existing data from the literature and/or collaborations with biologists and clinicians
3. define mathematical models to be tested against the data
4. implement the models numerically
5. confront the models to the data using statistical tools (nonlinear mixed-effects), test their relative likelihood and identify the ones that can be *rejected*
6. and most importantly, use this methodology to **derive biologically or clinically meaningful results**.

As a whole, my research contributions have been done with the aim to be part of a ***quantitative* mathematical oncology** approach rather than a purely theoretical and qualitative approach. Specific details of the biological and clinical findings from my research are summarized below and exposed in more details in the document. Although several of the models are applicable to a broad range of solid cancer types, the experimental and clinical data employed in the research reported here come from breast, lung and kidney cancers.

Curriculum vitae

Sébastien Benzekry

French
Born February 22nd, 1985
benzekry@phare.normalesup.org
http://benzekry.perso.math.cnrs.fr/

Inria team MONC
Institut de Mathématiques de Bordeaux
University of Bordeaux
351 cours de la Libération
33405 Talence Cedex, France

Situation

2013 -	Research Scientist (CR1) at Inria Bordeaux, team MONC Grant bonus for doctoral management and research achievements (PEDR)
2017 -	Affiliate Assistant Professor, Biomedical Sciences Department, Iowa State University, USA

Formation

2012	Postdoctoral fellow in mathematical modeling of cancer from January 2012 until November 2012 at the Center of **Cancer and Systems Biology** at Tufts University, School of Medicine, Boston, under the supervision of Philip Hahnfeldt
2008 - 2011	**Doctorate of applied mathematics** LATP and Laboratoire de Pharmacocinétique et Toxicocinétique, Marseille
Title	**Modeling, mathematical and numerical analysis of anti-cancerous therapies for metastatic cancers**
2008	Laureate of the **Agregation of mathematics**, option Scientific calculus.
2007 - 2009	Student at the Ecole Normale Supérieure of Cachan.
2004 - 2007	Mathematics magister at the Ecole Normale Supérieure of Paris
2006 - 2007	Master 2 **Mathematics of modeling** at the University Pierre et Marie Curie, Paris, specialty biology Master 2 internship at the mathematics department of the UPC in **Barcelone** : Exploration of deterministic and stochastic neuron networks
2004 - 2006	Bachelor and Master 1 degrees of Mathematics, ENS Paris.

Foreign research visits

Fall 2016	Short sabbatical at the **Roswell Park Cancer Institute** (J. Ebos' lab), Buffalo, NY, USA Stay at the **Integrated Mathematical Oncology** department of the Moffitt Cancer Center, Tampa, FL, USA
September 2015	**Mathematical Oncology Laboratory (Môlab)**, Ciudad Real, Spain. Collaboration with V. Pérez-Garcia and A. Martinez-González
May 2011	Instituto di Analisi dei Sistemi ed Informatica "Antonio Ruberti", Consiglio Nazionale delle Ricerche, Rome. Collaboration with A. Gandolfi et A. d'Onofrio

Oral communications

International conferences (invited)

December 2017	Mathematical Methods and Modeling of Biophysical Phenomena, Rio de Janeiro, Brazil
June 2017	XXV Congreso de ecuaciones diferenciales y aplicaciones. XV congreso de matemàtica aplicada, Cartagena, Spain. *Optimization of the timing of sequential administration of bevacizumab plus cytotoxics in non-small cell lung cancer by a mathematical model*
May 2016	Metronomics @ Mumbai, Mumbai, India
December 2015	Present challenges of mathematics in oncology and biology of cancer, Marseille, France
November 2015	Dynamique et contrôle des croissances tumorales, Rouen, France
November 2015	Contrôle des EDP et applications, Marseille, France
October 2015	Journées du Groupe de Métabolisme et Pharmacocinétique, Paris, France
June 2015	Micro and Macro Systems in Life Sciences (MMSLS 2015), Bedlewo, Poland
March 2015	Workshop on hybrid and multiscale modelling in cell and cell population biology , Laboratoire Jacques-Louis Lions, Paris, France *Combined in vivo and in silico quantitative modeling of post-surgery metastatic development*
March 2015	Mathematical Methods and Modeling of Biophysical Phenomena, Cabo Frio, RJ, Brazil. *A modeling study of metastatic initiation and tumor-tumor spatial interactions*
January 2015	36th EORTC PAMM Winter meeting , Marseille, France *A translational in vivo/in silico quantitative modeling study of the impact of surgery on metastatic relapse and survival in breast cancer*
October 2014	Autumn School by Japanese and French Mathematicians , Osaka, Japan. *Mathematical modeling of tumor growth and metastatic spread. Data, theories and predictions*

July 2014	10th AIMS Conference on Dynamical Systems, Differential Equations and Applications , Madrid, Spain. *A mathematical model of systemic inhibition of angiogenesis in metastatic development*
November 2013	French-Mexican Meeting on Industrial and Applied Mathematics, Villahermosa, México. *Classical Mathematical Models for Description and Forecast of Preclinical Tumor Growth*
May 2013	Bi-annual congress of the SMAI, Seignosse, France *Mathematical modeling of systemic inhibition of angiogenesis and metastatic dynamics*
March 2013	Workshop on Mathematical Methods and Modeling of Biophysical Phenomena, Cabo Frio, Brazil. *Mathematical modeling of systemic inhibition of angiogenesis and metastatic dynamics*
July 2012	2nd Annual Workshop on Cancer Systems Biology - Tumor Metronomics: Timing and Dose Level Dynamics, Center for Cancer and Systems Biology, Boston, USA. *Mathematical modeling of metastatic development and scheduling optimization of anti-cancerous therapies*
July 2011	7th International Congress of Applied and Industrial Mathematics (ICIAM 2011), Vancouver. *Mathematical modeling of the metastatic process and optimization of anti-cancerous therapies*, in the session Tumor growth modeling and system identification for clinical applications
July 2011	Workshop on Systems Biology of Tumor Dormancy. St. Elizabeth's Medical Center, Boston, USA. *A modeling approach for therapies in metastatic cancers*
May 2011	Journée Emergence de l'Institut Gustave Roussy (IGR), Paris. *Un exemple de modélisation du processus métastatique*
May 2010	2nd Workshop on Metronomic Anti-Angiogenic Chemotherapy in Paediatric Oncology, Marseille. *Mathematical modeling of MTD and metronomic temozolomide*
May 2010	8th conference of the American Institute of Mathematical Sciences (AIMS), Dresde. *Modeling and mathematical analysis of metastatic growth under angiogenic control*, in the session Evolution equations and mathematical biology

Accepted communications

March 2017	38th EORTC-PAMM Winter meeting, Split, Croatia. *Optimization of the timing of sequential administration of bevacizumab plus cytotoxics in NSCLC by a mathematical model.* (Oral communication)
October 2015	Journées du cancéropôle Grand Sud-Ouest , Bordeaux, France *Modeling spontaneous metastasis following surgery: an in vivo-in silico approach* (Poster)
June 2015	Mathematical Methods in Systems Biology, Dublin, Ireland. (Oral communication)

June 2014	European Conference on Mathematical and Theoretical Biology, Göteborg, Sweden. *Metastatic dynamics, systemic inhibition of angiogenesis and implications for surgery* (Oral communication)
June 2014	International Tumor Dormancy Symposium , Lille, France *Metastatic dynamics and systemic inhibition of angiogenesis. Implications for dormancy and surgery* (Poster)
October 2011	Journées du Groupe de Métabolisme et Pharmacocinétique. Paris. *Biomathematical modeling for description of metastatic processes and optimization of combined anti-angiogenic + cytotoxic therapies* (Poster and oral communication)
June 2011	8th European Conference of Mathematical and Theoretical Biology, Krakow. *Optimal schedules for therapies in metastatic cancers*
June 2010	CANUM 2010, Gironde. *A model of metastatic growth under angiogenic control*
May 2010	CMPD 3, Bordeaux. *A model of metastatic growth under angiogenic control*
November 2009	Conference of biomathématics et biomechanics, Tozeur, Tunisie. Poster *Analysis and modeling of metastatic growth including angiogenesis*

Seminars

May 2017	Laboratoire d'Analyse Topologie et Probabilites, Institut de Mathematiques de Marseille. *Mathematical Oncology: Theory Meets Reality.* Marseille, France
November 2016	Integrated Mathematical Oncology Department, Moffitt Cancer Center. *Mathematical Modeling of Metastasis: Theory Meets Reality.* Tampa, Florida, USA
October 2016	Department of Genetics, Roswell Park Cancer Institute (invitation by John ML Ebos). *Mathematical Modeling of Metastasis: Theory Meets Reality.* Buffalo, NY, USA
October 2016	Robert Kerbel's laboratory at Sunnybrook Research Institute. *Mathematical Modeling of Metastasis: Theory Meets Reality.* Toronto, Canada
October 2016	Mathematics Department Colloquium, Ryerson University. *Mathematical Modeling of Metastasis: Predicting the invisible.* Toronto, Canada
May 2016	Seminar at the laboratory of Génétique, Immunothérapie, Chimie et Cancer" of the University of Tours, Tours, France *Data-based mathematical modeling analysis of preclinical studies in oncology*
January 2016	Seminar at the laboratoire d'imagerie biomédicale, Paris, France *Classical Mathematical Models for Description and Prediction of Experimental Tumor Growth*
May 2015	Biomathematics Seminar, University of Gothenburg, Sweden *Modeling spontaneous metastasis following surgery: An In vivo/ in silico approach*

March 2014	Seminar of the inria team Dracula, Lyon, France *Classical Mathematical Models for Description and Prediction of Experimental Tumor Growth*
April 2013	ANEDP team, Orsay, France *Mathematical modeling of systemic inhibition of angiogenesis and metastatic dynamics*
February 2013	LATP, Marseille. *A math walk in a biology lab*
December 2011	Team MC2, Bordeaux. *Modeling, mathematical and numerical analysis of anti-cancerous therapies*
Novembee 2011	EDP Seminar of the Mathematics department, Besançon. *Modeling, mathematical and numerical analysis of anti-cancerous therapies*
Mai 2010	Math-Bio seminar Maths-Bio of the university Lyon 1. *Modeling and mathematical analysis of metastatic growth under angiogenic control*
October 2009	Maths-Cancer working group, School of Pharmacy, Marseille. *Modeling of angiogenesis*
June 2009	Bucolic days of the doctoral seminar, LATP, Marseille

Teaching and supervision

Postdoctoral fellows

2015 - 2017 Diane-Charlotte Imbs (Amidex MARS project), co-supervision with Dominique Barbolosi and Joseph Ciccolini. Current position: Clinical pharmacologist for early drug development oncology, Ipsen innovation

2015 - 2017 Raouf El Cheikh (Amidex MARS project), co-supervision with Dominique Barbolosi. Current position: Modeling and simulation, Sanofi

PhD students

2017 - 2020 Cristina Vaghi: "Improving intra-tumor drug distribution of anti-cancer nanoparticles by data-informed mathematical modeling" (co-supervision with Clair Poignard and Joseph Ciccolini)

2016 - 2019 Chiara Nicolò: "Mathematical modeling of systemic aspects of cancer and cancer therapy" (co-supervision with Olivier Saut)

2013 - 2015 Etienne Baratchart: "Quantitative study of the metastatic process using mathematical modeling" (co-supervision with Thierry Colin and Olivier Saut). Current position: postdoc in the Integrative Mathematical Oncology department of the Moffitt Cancer Center, Tampa, FL, USA

Master 2 internships

2017 M. Bilous (Ecole Polytechnique, M2 of biomechanical engineering): "Mathematical modeling and prediction of clinical brain metastases in non-small cell lung cancer"

2014 Aristoteles Camilo (IMPA, Rio de Janeiro, Brazil and University Pierre et Marie Curie, Paris, France): " An experimentally-based modeling study of the effect of anti-angiogenic therapies on primary tumor kinetics for data analysis of clinically relevant animal models of metastasis"

Other internships

2016 - 2017	Anass Jeffal and Guillaume Lechene (University of Bordeaux, M1): "Optimal control for administration of chemotherapies"
2016	Laura Lumale (INSA engineering school, 2nd year (M1)): "Around a mathematical model of the concomitant tumor resistance phenomenon"
2015	Simon Evain ("Ponts et Chaussées" engineering school, 2nd year (M1)): "Mathematical modeling of tumor and metastatic growth when treated with sunitinib"
2015	Maxime Prodhomme (ENS Cachan, 1st year (L3))

Teaching

2015 - 2017	Teaching assistant for ordinary differential equations in the first year of engineering school Matmeca, Bordeaux, France
2014 - 2017	Supervision of various projects in applied mathematics in Matmeca (L3) or University of Bordeaux (L3 and M1), Bordeaux, France
2009 - 2011	Teaching duties in mathematics (analysis, topology and differential calculus, numerical analysis, preparation to the agregation), 192 hours, University of Aix-Marseille, France

Scientific community activities

Reviewer for grant applications submitted to: the Austrian Science Fund, the Centre d'Excellence Africain en Technologies de l'Information et de la Communication and the TEAM program (European Union and Foundation for Polish Science)

Invited editor of a special issue for the journal Complexity : "Mathematical Oncology: Unveiling Biological Complexity Using Mathematical Methods"

Reviewer for several international journals including **modeling journals** (Journal of Theoretical Biology, Bulletin of Mathematical Biology, PloS One, Mathematical Biosciences, Theoretical Biology and Medical Modeling, Mathematical Biosciences and Engineering, Journal of Biological Informatics, Journal of Biological Systems, ESAIM:Proc, Mathematics and Computers in Simulation) and **biological/medical journals about cancer and pharmacokinetics** (British Journal of Cancer, Clinical Pharmacokinetics, BMC Cancer, Breast Cancer Research and Treatment)

April 2017	Member of the **PhD defense jury** of Karima El Alaoui (University of Lorraine, Heath and Life Sciences department)
January 2017	Interview for the french science popularization journal “Sciences et Avenir”
July 2015	Member of the **scientific committee** of the MB2 conference (Biomathematics modeling days of Besançon)
June 2015	Interview for a local radio (Radio campus)
March 2012	Member of the **organizing committee** of the 2nd Thematic school “Present challenges of mathematics in oncology and biology of cancer: modeling and mathematical analysis"

Research grants

2017	Inria associate team METAMATS: Modeling ExperimenTAl MetAsTaSis (co-PI: John Ebos). 13 k€/year for 3 years. Role: PI
2016	CNRS “First support for an exploratory project” (PEPS). 4.3 k€. Role: PI
2014 - 2017	Amidex MARS (Modeling Anticancer Research & Simulation) project (PI: Pr Fabrice Barlesi. Multidisciplinary and therapeutic innovation Unit, AP-HM, Marseille). Role: Partner

List of publications

Publications are distinguished between journal articles and other publications (such as popularization articles, book chapters, proceedings, articles only submitted or protocols). Emphasized papers in italics are the ones considered as representing the most important contributions. Unless otherwise stated, the order of the authors follows the convention employed in the biomedical field, i.e. the rank goes with the contribution to the study except for the last (senior) author, who in general initiated and supervised the study.

Journal articles

Tumor growth

1. Mollard, S., Fanciullino, R., Giacometti, S., Serdjebi, C., **Benzekry, S.**, and Ciccolini, J. (2016). In Vivo Bioluminescence Tomography for Monitoring Breast Tumor Growth and Metastatic Spreading: Comparative Study and Mathematical Modeling. *Nature Sci Rep*, 6:36173

2. Beheshti, A., **Benzekry, S.**, McDonald, J. T., Ma, L., Peluso, M., Hahnfeldt, P., and Hlatky, L. (2015). Host age is a systemic regulator of gene expression impacting cancer progression. *Cancer Res*, 75(6):1134–1143

3. ***Benzekry, S.**, Lamont, C., Beheshti, A., Tracz, A., Ebos, J. M. L., Hlatky, L., and Hahnfeldt, P. (2014c). Classical mathematical models for description and prediction of experimental tumor growth.* PLoS Comput Biol*, 10(8):e1003800*

Metastasis

4. ***Benzekry, S.***, *Lamont, C., Barbolosi, D., Hlatky, L., and Hahnfeldt, P. (2017). Mathematical Modeling of Tumor-Tumor Distant Interactions Supports a Systemic Control of Tumor Growth.* Cancer Res*, 77(18):5183–5193*

5. ***Benzekry, S.***, *Tracz, A., Mastri, M., Corbelli, R., Barbolosi, D., and Ebos, J. M. L. (2016). Modeling Spontaneous Metastasis following Surgery: An In Vivo-In Silico Approach.* Cancer Res*, 76(3):535–547*

6. *Baratchart, E.,* ***Benzekry *, S.****, Bikfalvi *, A., Colin *, T., Cooley, L. S., Pineau, R., Ribot, E. J., Saut, O., and Souleyreau, W. (2015). Computational Modelling of Metastasis Development in Renal Cell Carcinoma.* PLoS Comput Biol*, 11(11):e1004626 * = joint supervising authors*

7. **Benzekry, S.**, Gandolfi, A., and Hahnfeldt, P. (2014b). Global Dormancy of Metastases Due to Systemic Inhibition of Angiogenesis. *PLoS ONE*, 9(1):e84249–11

8. **Benzekry, S.** (2012b). Passing to the limit 2D–1D in a model for metastatic growth. *J Biol Dynam*, 6(sup1):19–30

9. **Benzekry, S.** (2012a). Mathematical and numerical analysis of a model for anti-angiogenic therapy in metastatic cancers. *ESAIM Math Model Numer Anal*, 46(2):207–237

10. **Benzekry, S.** (2011a). Mathematical analysis of a two-dimensional population model of metastatic growth including angiogenesis. *J Evol Equ*, 11(1):187–213

Treatments

11. *Imbs, D.-C., El Cheikh, R., Boyer, A., Ciccolini, J., Mascaux, C., Lacarelle, B., Barlesi, F., Barbolosi, D., and* ***Benzekry, S.*** *(2017). Revisiting bevacizumab + cytotoxics scheduling using mathematical modeling: proof of concept study in experimental non-small cell lung carcinoma.* CPT Pharmacometrics Syst Pharmacol*, accepted*

12. Mollard, S., Ciccolini, J., Imbs, D.-C., El Cheikh, R., Barbolosi, D., and **Benzekry, S.** (2017). Model driven optimization of antiangiogenics + cytotoxics combination: application to breast cancer mice treated with bevacizumab + paclitaxel doublet leads to reduced tumor growth and fewer metastasis. *Oncotarget*, 8(14):23087–23098

13. Henares-Molina, A., **Benzekry, S.**, Lara, P. C., García-Rojo, M., Pérez-García, V. M., and Martínez-González, A. (2017b). Non-standard radiotherapy fractionations delay the time to malignant transformation of low-grade gliomas. *PLoS ONE*, 12(6):e0178552

14. Serre, R., **Benzekry, S.**, Padovani, L., Meille, C., André, N., Ciccolini, J., Barlesi, F., Muracciole, X., and Barbolosi, D. (2016). Mathematical Modeling of Cancer Immunotherapy and Its Synergy with Radiotherapy. *Cancer Res*, 76(17):4931–4940

15. Pantziarka, P., Hutchinson, L., André, N., **Benzekry, S.**, Bertolini, F., Bhattacharjee, A., Chiplunkar, S., Duda, D. G., Gota, V., Gupta, S., Joshi, A., Kannan, S., Kerbel, R., Kieran, M., Palazzo, A., Parikh, A., Pasquier, E., Patil, V., Prabhash, K., Shaked *, Y., Saulnier Sholler, G., Sterba, J., Waxman, D. J., and Banavali, S. (2016). Next generation metronomic chemotherapy—report from the Fifth Biennial International Metronomic and Anti-angiogenic Therapy Meeting, 6–8 May 2016, Mumbai. *Ecancermedicalscience*, 10

16. **Benzekry, S.**, Pasquier, E., Barbolosi, D., Lacarelle, B., Barlesi, F., André, N., and Ciccolini, J. (2015b). Metronomic reloaded: Theoretical models bringing chemotherapy into the era of precision medicine. *Semin Cancer Biol*, 35:53–61

17. Ciccolini, J., **Benzekry, S.**, Lacarelle, B., Barbolosi, D., and Barlesi, F. (2015). Improving efficacy of the combination between antiangiogenic and chemotherapy: Time for mathematical modeling support. *Proc Natl Acad Sci USA*, 112(27):E3453

18. **Benzekry, S.**, Tuszynski, J. A., Rietman, E. A., and Lakka Klement, G. (2015c). Design principles for cancer therapy guided by changes in complexity of protein-protein interaction networks. *Biol Direct*, 10:32

19. **Benzekry, S.** and Hahnfeldt, P. (2013). Maximum tolerated dose versus metronomic scheduling in the treatment of metastatic cancers. *J Theor Biol*, 335:235–244

20. Lignet, F., **Benzekry, S.**, Wilson, S., Billy, F., Saut, O., Tod, M., You, B., Adda Berkane, A., Kassour, S., Wei, M. X., Grenier, E., and Ribba, B. (2013). Theoretical investigation of the efficacy of antiangiogenic drugs combined to chemotherapy in xenografted mice. *J Theor Biol*, 320:86–99

21. **Benzekry, S.**, André, N., Benabdallah, A., Ciccolini, J., Faivre, C., Hubert, F., and Barbolosi, D. (2012a). Modelling the impact of anticancer agents on metastatic spreading. *Math Model Nat Phenom*, 7(1):306–336

22. **Benzekry, S.**, Chapuisat, G., Ciccolini, J., Erlinger, A., and Hubert, F. (2012b). A new mathematical model for optimizing the combination between antiangiogenic and cytotoxic drugs in oncology. *C R Acad Sci Paris, Ser I*, 350(1-2):23–28

Book chapters

23. **Benzekry, S.** (2017). Les lois de la croissance tumorale. *Bibliothèque Tangente*, Hors Série

24. Barbolosi, D., Benabdallah, A., **Benzekry, S.**, Ciccolini, J., Faivre, C., Hubert, F., Verga, F., and You, B. (2013). A Mathematical Model for Growing Metastases on Oncologists's Service. In *Computational Surgery and Dual Training*, pages 331–338. Springer New York, New York, NY

Proceedings, protocols and submitted articles

Tumor growth

25. **Benzekry, S.**, Beheshti, A., Hahnfeldt, P., and Hlatky, L. (2015a). Capturing the Driving Role of Tumor-Host Crosstalk in a Dynamical Model of Tumor Growth. *bio-protocol*, 5(21)

Metastasis

26. **Benzekry, S.** and Ebos, J. M. (2015). On the growth and dissemination laws in a mathematical model of metastatic growth. *ITM Web of Conferences*, 5:00007

27. **Benzekry, S.**, Gandolfi, A., and Hahnfeldt, P. (2014a). A mathematical model of systemic inhibition of angiogenesis in metastatic development. *ESAIM Proc Surv*, 45:75–87

Treatments

28. Fanciullino, R., **Benzekry, S.**, Lacarelle, B., Ciccolini, J., and Rodallec, A. (2017). Pharmacokinetics of nanoparticles in oncology: clues for anticipating interpatient variability. *submitted*

29. Benguigui, M., Alishekevitz, D., Timaner, M., Shechter, D., Raviv, Z., **Benzekry *, S.**, and Shaked *, Y. (2017). Dose- and time-dependence of the host-mediated response to paclitaxel therapy: a mathematical modeling approach. *submitted* * = joint supervising authors

30. Boyer, A., Imbs, D.-C., Cheikh, R. E., Mascaux, C., Barlesi, F., Barbolosi, D., **Benzekry, S.**, and Ciccolini, J. (2017b). Abstract 4529: Optimization of the sequence for the administration of bevacizumab in combination with pemetrexed and cisplatin in NSCLC : a pharmacology based in vivo study . *Cancer Res*, 77(13 Supplement):4529 –4529

31. Henares-Molina, A., **Benzekry, S.**, Lara, P., García-Rojo, M., Pérez-García, V., and Martínez-González, A. (2017a). OS06.6 Optimized radiotherapy protocols delay the malignant transformation of low-grade gliomas in-silico. *Neuro-Oncology*, 19(suppl 3):iii12–iii12

32. Boyer, A., Ciccolini, J., Mascaux, C., Imbs, D. C., El Cheikh, R., Barlesi, F., and **Benzekry, S.** (2017a). Étude de l'effet séquence bévacizumab/pémétrexed/cisplatine chez la souris porteuse de cancer du poumon non à petites cellules. *Rev Mal Respir*, 34:A52

33. Mollard, S., **Benzekry, S.**, Giacometti, S., Faivre, C., Hubert, F., Ciccolini, J., and Barbolosi, D. (2014). Abstract 3677: Model-based optimization of combined antiangiogenic + cytotoxics modalities: application to the bevacizumab-paclitaxel association in breast cancer models. *Cancer Res*, 74(19 Supplement):3677–3677

Short summary of research contributions since the PhD

As stated above, departing from a PhD where my research had focused on theoretical, numerical and simulation aspects of a few mathematical models in oncology, my subsequent research efforts have concentrated on confronting the models to the observations, in order to answer meaningful clinical or biological problems. Reported below is a short summary of a selection of results that I obtained, which are described in more details in the following chapters.

The driving force has been to establish mathematical models that would *in fine* have clinical use. This often means a situation with metastatic patients, treated with systemic agents. However, as a pre-requisite, I considered essential to further first my understanding of the *biology* of the processes and thus started with experimental data on biological studies, which are often richer than what is obtainable in the clinic. To build and validate the models step by step on solid ground, instead of directly starting with the case of metastases under treatment, the path I followed was the following:

1. first, to assess the descriptive and predictive power of classical models of tumor **growth** [Benzekry et al., 2014c]
2. then, model the natural history of metastasis, in the pre-surgical [Baratchart et al., 2015] or post-surgical [Benzekry et al., 2016] settings (thus adding **dissemination** to growth)
3. study the organism-scale **interactions** between established tumors, mostly qualitatively when considering the full tumor-metastases system [Benzekry et al., 2014b] but also quantitatively in a two-tumors system [Benzekry et al., 2017]
4. and finally, investigate models of the effect of **therapies** (combination of chemotherapy and anti-angiogenics) [Mollard et al., 2017, Imbs et al., 2017].

Of course, I don't pretend to any exhaustivity since the topics mentioned above cover an extremely wide range of processes. Rather, I followed a specific path, driven by the identification of concrete

problems where mathematical modeling was of help. The publications mentioned above don't cover the entirety of my contributions but are the ones that I consider most meaningful. To enlighten the reading, in this summary, no reference to the literature is given. We refer the reader to the body of the document for this matter.

0 Methodological prerequisite: a software for fitting models to data

To accomplish the research program stated above, one first key aspect was to dispose of a numerical tool to fit models to data, i.e. to estimate the parameters, to quantify the uncertainty of this estimation and to statistically compare the goodness-of-fit of the models. Therefore, I programmed a software for nonlinear regression of models in oncology and statistical inference named CARCINOM (for Computer-Assisted Research about Cancer growth and INsights on Oncological Mechanisms).

Given a data set of longitudinal measurements of in a population, it fits user-provided models, computes several goodness-of-fit statistical metrics, identifies the parameters of the models and estimates the uncertainty associated to their determination. It provides several graphical and numerical outputs that I extensively use in my daily work (in the form of LaTeX tables). Three options are available to the user: fitting the average population data, fitting each subject's data individually (and independently) or using a population approach (nonlinear mixed-effects modeling) to estimate a population distribution of the parameters from the pooled data of all subjects. The latter is based on the SAEM[2] algorithm already implemented in Matlab.

The library of models implemented so far include models of tumor growth, metastatic development and effect of specific therapies.

The software is developed in two versions, one written in Matlab and one in python. Currently, the population parameter estimation is only available in the Matlab version.

1 Tumor growth

Despite internal complexity, tumor growth kinetics follow relatively simple laws that can be expressed as mathematical models. To explore this further, I performed a quantitative analysis of the most classical of these: exponential, exponential-linear, power law, Gompertz, logistic, generalized logistic, von Bertalanffy and a model with dynamic carrying capacity. The models were assessed against data from two in vivo experimental systems: an ectopic syngeneic tumor (Lewis lung carcinoma) and an orthotopically xenografted human breast carcinoma. One biological problem that I wanted to address was:

[2]Stochastic Approximation of Expectation-Maximization

Biological problem 1. *What are the general laws of macroscopic tumor growth? What are minimal biological processes able to recover the kinetics of tumor growth curves?*

The goals of the study were then threefold: 1) to determine a statistical model for description of the measurement error of the tumor volumes, 2) to establish the descriptive power of each model, using several goodness-of-fit metrics and a study of parametric identifiability, and 3) to assess the models' ability to forecast future tumor growth.

For point 1) we found that both a constant and a proportional error model had to be rejected. Therefore, we designed and validated a specific error model.

1.1 Theories of tumor growth

The first finding was that the exponential model was not able to fit the tumor growth curves during the entire measured period. Consistently with previous observations, this means that there is a non-constant relative growth rate, with **growth retardation** (i.e. the larger the tumor the slower the growth). For the breast data, the dynamics were best captured by the Gompertz and exponential-linear models. For the lung data, the Gompertz and power law models provided the most parsimonious and parametrically identifiable description.

Interestingly, although often pushed forward in the literature for description of tumor growth and despite its attractive biological explanation of growth retardation as caused by competition for space or nutrients, **the logistic model exhibited substantially lower descriptive power**, suggesting rejection of this theory for explanation of tumor growth retardation. This finding was consistently confirmed in several other data sets that I was given to analyze, including melanoma and kidney experimental tumors.

In line with classical results, the Gompertz model $\left(\frac{dV}{dt} = (\alpha - \beta \ln(V))\, V\right)$ had excellent descriptive power. However, its etiology is still unresolved and its parameters not all physiologically defined. In contrast, I found that another simple and biologically grounded model was equally able to describe the tumor growth curves, the power law model:

$$\frac{dV}{dt} = aV^{\gamma}$$

This model has the interpretation that the **proliferative tissue has a fractal dimension** (equal to 3γ), possibly not equal to 1. The origin of this fractal dimension might stem from the fractal dimension of the tumor vasculature (since the proliferative cells are the one that have access to the nutrients and thus are close to the blood vessels). Following this interpretation, a fully infiltrative (and functional) vasculature would mean a value of $\gamma = 1$ while blood vessels limited to the surface of the tumor would imply $\gamma = 2/3$. Supporting this model further, I found in the case of the lung data a value of the parameter a close to the *in vitro* proliferation rate, which would make sense because a is the growth rate when $V = 1$, corresponding to the initial tumor size at injection ($V = 10^6$ cells $\simeq 1$ mm^3).

1.2 Predictive power of classical models of tumor growth

For the breast data, the exponential-linear model exhibited the highest predictive power, with excellent prediction scores (80%) extending out as far as 12 days in the future and using only 3 data points with two days interval. In contrast, for the lung data, not one of the models was able to achieve a substantial prediction rate (70%) beyond the next day data point even when using 5 data points (one or two days interval) to estimate the parameters.

In this context, a major result that I obtained was that **adjunction of *a priori* information on the parameter distribution led to considerable improvement**. For instance, forecast success rates went from 14.9% to 62.7% when using the power law model to predict the full future tumor growth curves (i.e. up to 14 days in the future), using just three data points with one day interval.

Together, my results not only have important implications for biological theories of tumor growth and the use of mathematical modeling in preclinical anti-cancer drug investigations, but also may assist in defining how mathematical models could serve as potential prognostic tools in the clinic.

This study is the subject of the publication [Benzekry et al., 2014c].

2 Metastasis

2.1 Modeling Spontaneous Metastasis following Surgery: An In Vivo-In Silico Approach

Rapid improvements in the detection and tracking of earlystage tumor progression aim to guide decisions regarding cancer treatments as well as predict metastatic recurrence in patients following surgery. Mathematical models may have the potential to further assist in **estimating metastatic risk**, particularly when paired with in vivo tumor data that faithfully represent all stages of disease progression. One clinical problem associated with this can be stated as

Clinical problem 1. *Estimate the amount of occult distant metastases at diagnosis*

In order to have data about metastatic development necessary to quantitatively investigate the process – typically hard to obtain due to the intravital nature of the process – I collaborated with a biologist (John Ebos, Roswell Park Cancer Institute, Buffalo, USA) who investigates mouse experimental systems of spontaneous metastasis developing after surgical removal of orthotopically implanted primary tumors. The particular biological problem that was investigated was:

Biological problem 2. *What are the qualitative and quantitative differences among experimental models of metastasis for different cancer types? Is the growth of secondary tumors identical to the growth of the primary tumor, in a given experimental system? How does the dissemination process depend on the size of the primary tumor? What is the impact of surgery on metastatic growth and dissemination?*

To do so, the data were confronted to a previously established class of mathematical models for the dissemination and growth of a population of secondary tumors. The models are written as physiologically structured partial differential equations of transport type for the density $\rho(t, v)$ of metastases with size v at time t. Considering that the primary tumor volume $V_p(t)$ follows a model

$$\begin{cases} \frac{dV_p(t)}{dt} = g_p(V_p(t)) \\ V_p(0) = V_0 \end{cases}, \tag{1}$$

the equation on ρ then depends on two fundamental (functional) coefficients g and d both quantifying the two main aspects of metastatic development: dissemination (d) and growth (g). It writes

$$\begin{cases} \partial_t \rho(t, v) + \partial_v(g(t, v)\rho(t, v)) = 0 &]0, T[\times]V_0, +\infty[\\ g(V_0)\rho(t, V_0) = d(V_p(t)) &]0, T[\\ \rho(0, v) = 0 &]V_0, +\infty[\end{cases} \tag{2}$$

where V_0 is the minimal size of a lesion (typically, the size of one cell) and T is the final time.

Two models for the two experimental systems (breast and kidney) were able to fit and predict pre/postsurgical data at the level of the individual as well as the population. These revealed different metastatic dynamics for the two systems:

1. For the breast: **same growth law** (Gompertz-exp) and parameter values for the primary and secondary tumors and metastatic burden dynamics mostly **driven by proliferation**
2. For the kidney: same growth law (exponential) but **different values** of the parameters for the primary and secondary tumors and metastatic burden dynamics mostly **driven by dissemination**

Our approach also enabled retrospective analysis of clinical data describing the probability of metastatic relapse as a function of primary tumor size. In my data-based models, inter-individual variability was quantified by a population distribution of **one key parameter of intrinsic metastatic potential**. My analysis also identified a **highly nonlinear relationship between primary tumor size and postsurgical survival**, suggesting possible threshold limits for the utility of tumor size as a predictor of metastatic recurrence.

These findings validated the descriptive and predictive power of specific quantitative mathematical models of total experimental metastatic burden growth, inter-patient variability of metastatic relapse risk and may guide optimal timing of treatments in neoadjuvant (presurgical) and adjuvant (postsurgical) settings to maximize patient benefit.

This study is the subject of the publications [Benzekry et al., 2016, Benzekry and Ebos, 2015].

2.2 Challenging the classical view of metastatic initiation and growth

The biology of the metastatic colonization process remains a poorly understood phenomenon. To improve our knowledge of its dynamics further than the previous study that only involved data from total metastatic burden, together with a PhD student that I co-supervised with Thierry Colin and Olivier Saut (Etienne Baratchart), and in collaboration with a team of biologists at the LAMC (Inserm, Bordeaux, France) and a team of magnetic resonance imaging specialists (RMSB, CNRS, Bordeaux, France), we conducted a modeling study based on **multi-modal data** from an orthotopic murine experimental system of metastatic renal cell carcinoma. These data allowed to have access, in addition to the mere total number of metastatic cells, to the dynamics of the size distribution of secondary lesions. The biological problem we addressed was:

Biological problem 3. *Is the "standard" view of metastatic initiation and growth – that secondary lesions once established grow without interactions with each other or with the primary tumor – quantitatively valid for description of the dynamics of the number and size of metastases?*

To quantitatively test this theory against the data, we used the same modeling framework as above (equations (1) and (3)). Critically, when calibrated on the growth of the primary tumor and total metastatic burden, the predicted theoretical size distributions were not in agreement with the MRI observations. Specifically, in the size distribution predicted by the model, with a similar total mass, there were **more but smaller** tumors than in the data. Moreover, tumor expansion only based on proliferation was not able to explain the volume increase of the metastatic lesions. These findings strongly suggested **rejection of the standard theory**, demonstrating that the time development of the size distribution of metastases could not be explained by independent growth of metastatic foci. This led us to propose **two possible explanatory hypotheses** that could reconcile the theory with the data: 1) merging of existing metastatic foci (which we retrospectively observed in our data) and 2) exchange of cells between established lesions (for instance, from the primary tumor to secondary colonies).

Together, these results have implications for theories of the metastatic process and suggest that global dynamics of metastasis development is dependent on interactions between metastatic lesions.

This study is the subject of the publication [Baratchart, 2016].

2.3 A theoretical model of "cancer without disease"

Autopsy studies of adults dying of non-cancer causes have shown that virtually all of us possess occult, cancerous lesions. This suggests that, for most individuals, cancer will become dormant and not progress, while only in some will it become symptomatic disease. Naming this phenomenon global dormancy, I investigated the following problem:

Biological problem 4. *What are the determinants of global dormancy of secondary tumors leading to what has been referred as "cancer without disease"? Can systemic inhibition of angiogenesis explain this phenomenon?*

To explain the autopsy findings in light of the preclinical research data, together with Philip Hahnfeldt (Center of Cancer and Systems Biology, Tufts University, Boston, USA) and Alberto Gandolfi (IASI, CNR, Roma, Italy), we used a mathematical model of cancer development at the organism scale describing a growing population of metastases, which, together with the primary tumor, can exert a progressively greater level of systemic angiogenesis-inhibitory influence that eventually overcomes local angiogenesis stimulation to suppress the growth of all lesions. The structure of the model was extended from the equations (1) and (3) in two ways: 1) consideration of a two-dimensional variable for characterization of a tumor's state (tumor size and carrying capacity) and 2) **growth interactions** between the tumors, which translated into a velocity that depended on ρ, thus making the transport equation **non linear**.

Based on parameters calibrated from literature data, this *in silico* study of the dynamics of the tumor/metastasis system **identified ranges of parameter values where mutual angio-inhibitory interactions within a population of tumor lesions could yield global dormancy**, i.e., an organism-level homeostatic steady state in total tumor burden.

Additionally, numerical investigations of the dynamics of the model revealed interesting, non-trivial patterns.

This study is the subject of the publications [Benzekry et al., 2014b, Benzekry et al., 2014a].

2.4 A combined in vivo/in silico study of tumor-tumor interactions

Interactions between different tumors within the same organism have major clinical implications, especially in the context of surgery and metastatic disease. Indeed, the suppressive effect of a primary tumor on secondary tumors' growth (experimentally observed since more than a century) might lead to post-surgery metastatic acceleration. **Three main explanatory theories** (competition, angiogenesis inhibition and proliferation inhibition) have been proposed but precise determinants of the phenomenon remain poorly understood. After the rather theoretical results from the previous study, I wanted to have a better quantitative understanding of this phenomenon and to address the following problem:

Biological problem 5. *Among existing theories of concomitant resistance (i.e. tumor-tumor cross inhibition of growth) all qualitatively valid for explanation of the phenomenon, which one(s) have to be quantitatively rejected and which one(s) are valid?*

To do so, I formalized these theories into mathematical models and designed biological experiments (together with Philip Hahnfeldt and Lynn Hlatky and conducted together with Clare Lamont) to test them with empirical data. The experimental findings were that in syngeneic mice bearing two simultaneously implanted tumors, **growth of only one of the tumors was significantly suppressed** (61% size reduction at day 15, $p < 0.05$ by Student's t-test).

Turning to the results inferred from the modeling analysis (that confronted in total more than 40 models to the data), the **competition theory had to be rejected while the angiogenesis**

inhibition and proliferation inhibition models were able to describe the data. Additional models including a theory based on distant cytotoxic log-kill effects were unable to fit the data. The model that I found more robust for description of the data – based on the proliferation inhibition theory – was **identifiable and minimal** (4 parameters), and its descriptive power was validated against the data, including consistency in predictions of single tumor growth when no secondary tumor was present. This model may also shed new light on single cancer growth insofar as it offers a biologically translatable picture of how local and global action may combine to control local tumor growth, and in particular, the role of tumor-tumor inhibition.

This model offers a depiction of concomitant resistance that provides an improved theoretical basis for tumor growth control and may also find utility in therapeutic planning to avoid post-surgery metastatic acceleration.

This study is the subject of the publications [Benzekry, 2017].

3 Treatments

Investigating the role of mathematical modeling in theoretical thinking of therapeutic oncology, I co-authored a review about historical theoretical concepts that were influential in the mode of administration of anti-cancer agents, with a particular emphasis on the concept of metronomic chemotherapies (frequent administration of low dose of cytotoxic agents with no prolonged drug-free breaks) [Benzekry et al., 2015b].

Together with Joseph Ciccolini (SMARTc, Inserm, Marseille, France) who is a clinical pharmacologist and biologist in experimental therapeutics in oncology, I studied a specific problem concerning the **combination** of an anti-angiogenic agent (the anti-VEGF[3] monoclonal antibody bevacizumab) and cytotoxics. Indeed, in the clinic, bevacizumab has only been approved in combination with these agents, which brings the questions of the **scheduling and sequence** of administration. Currently, bevacizumab is given concomitantly with the cytotoxics. However, several biological rationales lead to think that this might not be the best strategy (or not the best strategy for all the patients). Mathematical modeling could be of help in order to determine improved sequences of combination (delay between the administration of the drugs) and personalize the scheduling of the combination. This led us to define the following problem:

Therapeutic problem 1. *What is the optimal time gap between administration of an anti-angiogenic agent such as bevacizumab and cytotoxic chemotherapy?*

There are nontrivial interactions between anti-angiogenics and cytotoxics from the very nature of the functional role of the agents. Indeed, the drug delivery is ensured by the blood vasculature, which is the aimed target of anti-angiogenic therapy. However, another seemingly counter-intuitive effect of anti-VEGF therapy has been reported: **vascular normalization**. It consists in a transient improvement of the leaky, tortuous and functionally inefficient tumor vasculature following

[3]Vascular Endothelial Growth Factor

administration of bevacizumab. In a series of iterative rounds between modeling and experiments, we investigated who to capture the dynamics of this process in order to suggest an optimized delay between the administration of the drugs.

Departing from an initially purely theoretical model (i.e., not confronted to experimental data), I used experimental data from a breast cancer animal model obtained by the SMARTc team to design a model that **was able to reproduce the differences in tumor growth kinetics due to modulation of the scheduling**. This quantitative fit could generate interesting insights such as an estimation of a 5-fold improvement of the quality of the vasculature when giving bevacizumab and paclitaxel (a cytotoxic agent specific to the treatment of breast cancer) sequentially rather than concomitantly. This study is the subject of the publication [Mollard et al., 2017].

Further on, using data from a more clinically relevant experimental system of non-small cell lung carcinoma treated with bevacizumab and the cisplatin-pemetrexed doublet, I simplified the model (due to identifiability issues) and used nonlinear mixed effects for calibration of the parameters in order to **predict an optimal delay** between bevacizumab and chemotherapy. **This prediction (3 days) was subsequently confirmed experimentally**, with reduced tumor growth of 38% as compared to concomitant scheduling, and prolonged survival (70 vs. 74 days). Alternate sequencing of 8 days failed in achieving similar increase in efficacy, thus suggesting that modeling support is critical to identify optimal scheduling.

Together, this proof-of-concept study exemplified how mathematical modeling can help for the rational design of treatment protocols. In addition, the experimentally validated model that was established could reveal a precious tool for personalized adaptation of the scheduling of the combination between anti-angiogenics and cytotoxics.

This study is the subject of the publication [Imbs et al., 2017].

4 Studies that are not included in this document

For the sake of conciseness, several of other published works are not included in this document, either because I considered them of secondary relevance or because my contribution was minor as compared to others.

These include a study about the topological structure of protein-protein interaction networks across cancer types (performed together with Edward Rietman and Giannoula Klement from the Center of Cancer and Systems Biology at Tufts University, Boston, USA) [Benzekry et al., 2015c]. I found that quantification of the topology using persistent Betti numbers correlated with epidemiological survival, thus suggesting specific proteins to be prioritarily targeted in order to target the intracellular regulatory network.

Another recent study – in collaboration with Raphaël Serre, Dominique Barbolosi, Fabrice Barlési and Xavier Muracciole (SMARTc, Inserm UMR S_911, Marseille, France) – was devoted to the establishment of a mathematical model for the combination of radiotherapy and novel immune

checkpoint inhibitors (including both anti-CTLA-4 and anti-PD1/PDL1 agents) [Serre et al., 2016]. It also gave insights into the very interesting topic of the abscopal effect by which a *local* radiotherapeutic intervention has *distant* implications, possibly through immune-mediated mechanisms.

On the matter of radiotherapy, in collaboration with Araceli Henares-Molina, Alicia Martínez-González and Victor Pérez-García, we investigated how radiotherapy schemes impact on the time to malignant progression from low grade to high grade in gliomas.

Statistical prelude: models versus data and the population approach

When dealing with data in the natural sciences, it is necessary to invoke tools from statistics. Here, I briefly introduce the regression tools that have been constantly used to confront simulations from mathematical models to empirical data. The models I have considered are generally *dynamical models* and thus naturally require longitudinal data to be compared to. Given such data in a population of multiple subjects, three strategy are possible to identify the model's parameters that give the best fit to the data.

The first two consist in either considering the dynamics of each subject separately or the average across all subjects at each time point. These two tasks fall within the classical theory of nonlinear regression. The first approach is limited to situations where parameters of the model are identifiable given the dynamics of only one subject and does not offer a structural framework for description of the variability within the population. The second approach can take this last point into account but is biased by the fact that it might not make sense to associate the average trajectory to a trajectory itself, as soon as the model is nonlinear with respect to the parameters. For instance, if $\lambda_1 \neq \lambda_2$, then there is no λ such that $e^{\lambda t} = \frac{e^{\lambda_1 t}+e^{\lambda_2 t}}{2}$. In this context, a very powerful framework for model fitting and parameters estimation is the framework of *nonlinear mixed-effect modeling* [Lavielle, 2014]. This method revealed to be particularly well adapted in the context of our studies [Benzekry et al., 2014c, Benzekry et al., 2016, Mollard et al., 2016, Imbs et al., 2017, Baratchart et al., 2015].

In the general theory of nonlinear regression [Seber and Wild, 2003], fitting a model to experimental data is a problem that is often addressed by maximizing the likelihood of the data under the hypothesis that the data has been generated by the model plus some error resulting from the model misspecification (structural error) and the precision of the measures. More precisely, denoting by $(y_i^j)_{1\leq i\leq N^j}$ the measurements (in a subject j, $1 \leq j \leq J$) at the times t_i^j and $M(t_i^j;\theta^j)$ the corresponding values of the model function (dependent on a vector of parameters $\theta^j \in \mathbb{R}^p$), it is considered that the y_i^j's are realizations of random variables Y_i^j, with

$$Y_i^j = M(t_i^j;\theta^j) + \sigma_i^j \varepsilon_i^j, \quad \varepsilon_1^j, \ldots, \varepsilon_{N^j}^j \sim \mathcal{N}(0,1), \tag{3}$$

where $\mathcal{N}(0,1)$ denotes the standard gaussian probability law. The standard deviation of the Y_i^j's, denoted by σ_i^j is therefore of great importance in the definition of the regression problem and corresponds to the *measurement error model*. For instance, typical error models are the constant error model (the measurement error does not depend on the measure itself), $\sigma_i^j = \sigma, \forall i, j$, or the proportional error model $\sigma_i^j = \sigma M(t_i^j; \theta^j)$.

The mixed-effect approach consists in pooling all the subjects together and estimating a global *distribution* of the model parameters in the population. More precisely, the individual parameter vectors $\theta^1, \ldots, \theta^J$ are assumed to be realizations of a random variable θ following a (parametric) probability law that is then the object to be estimated (this law is often assumed to be log-normal to preserve the positivity of the parameters). The statistical representation is then formula (3), together with

$$\theta^j = \theta_{pop} + \eta^j, \quad \eta^j \sim \mathcal{N}(0, \Omega)$$

where $\theta_{pop} \in \mathbb{R}^p$ and $\Omega \in \mathbb{R}^{p \times p}$ are the new parameters to be estimated that characterize the *population*. The $\theta_{pop,k},\ k = 1 \ldots p$ are called the *fixed effects* and the η^j the *random effects*. Hence, instead of the J parameter sets in the individual approach, resulting in a total number of parameters of pJ, only $p + p^2$ parameters have to be estimated. Combined with an appropriate description of the error variance, a population likelihood of all the data pooled together can be defined. Usually, no explicit formula can be computed for its expression, making its maximization a more difficult task than the individual approach (which, provided the error model is fixed, reduces to least squares minization). This is implemented in several softwares such as Monolix [Lixoft, 2013], which maximizes the likelihood using the stochastic approximation expectation maximization (SAEM) algorithm [Kuhn and Lavielle, 2005]. This population approach, to the price of more structure on the description of the dispersion on the parameters within the population, gains in robustness of the estimation and potentiates the estimation by pooling all the data points of all subjects, thus potentially resolving identifiability issues when only few data are available per subject.

A great advantage of the statistical framework for estimation of the parameters, apart from giving a rational basis to the criterion to be minimized when fitting a model to data, is that it views the parameters estimates as random variables. As such, they have a distribution, which reflects the uncertainty in the estimated values, itself linked to the uncertainty of the data. From the combination of the error model and the sensitivity of the model to the parameters (i.e. the jacobian matrix of the model with respect to the parameters) one can compute an asymptotically[4] valid covariance matrix of this distribution [Seber and Wild, 2003]. This leads to the concept of *standard errors* on the parameters' estimates, defined as the squared roots of the diagonal entries of the covariance matrix. This concept is very useful to quantify the "practical" identifiability of the parameters from a model and some given data.

I have incorporated these concepts of statistical estimation of the parameters into a user-friendly software (termed CARCINOM[5]) dedicated to the modeling analysis of population longitudinal data arising in my research (mostly, tumor and metastatic burden growth curves), together with libraries

[4] when the number of data points goes to infinity

[5] for Computer-Assisted Research about Cancer growth and INsights on Oncological Mechanisms

of models for tumor growth, metastatic development and effect of therapies. From data provided in excel files and either pre-existing or user-defined models, the software performs the regression, computes several goodness-of-fit statistical metrics (such as the Akaike Information Criterion, the Root Mean Squared Error or statistical tests for the normality of residuals) as well as the linearized approximation of the standard errors of the parameters (from a finite-differences approximation of the model's jacobian matrix). Outputs from multiple models are exported as LaTeX tables for the model's fit performances and the parameters values. A population mixed-effects approach can also be performed[6], relying on the already existing `nlmefitsa` function. However, population estimations by Monolix are much less computationally expensive. I have developed two versions of the software: one in Matlab and one in python.

[6] only in the Matlab version

Chapter 1

Tumor growth

Contents

Abstract

In the intent to bridge the gap between mathematical models of increasing complexity and the reality of experimental observations in oncology, the first step was to question established models of macroscopic tumor growth. Indeed, the growth of a population of tumor cells is at the heart of a large body of studies in mathematical oncology. However, few of these actually confronted the models to experimental data, and even fewer compared several models among them. Therefore, we first asked: what are the relative descriptive properties of classical models of tumor growth? Of particular interest to us was the assessment of theoretical concepts and theories as able or not to describe quantitative tumor growth data. Then, we wondered about the utility of such models as predictive tools. Specifically, we investigated how bayesian estimation (i.e., combination of an *a priori* population distribution on the parameters' estimates and a small number of individual initial time points) could improve the accuracy of predictions.

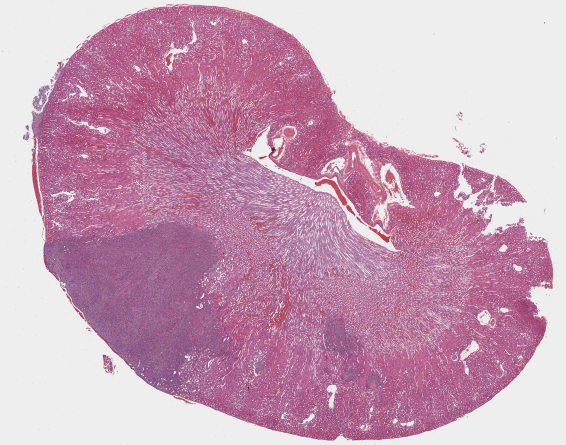

Figure 1.1 – Haematoxylin and eosin staining of a tumor-bearing mouse kidney (the area with higher density of nuclei on the left). Hematoxylin colors nuclei of cells in blue. Eosin stains cytoplasmic proteins, collagen and muscle fibers. Image courtesy of Dr John Ebos.

1.1 Introduction

1.1.1 Biological considerations

Tumor growth recapitulates several levels of complexity concerning not only the tumor cells themselves (at the genetic, molecular and inter-cellular signaling levels) but also intricate relationships with their environment through processes such as stromal recruitment, angiogenesis or escape from immune surveillance. This results in a possibly complex organization of the cells at the tissue level (Figure 1.1). However, a surprising regularity can be observed when looking at tumor growth from a macroscopic point of view, with relatively smooth tumor volume growth curves (see below).

The process of tumor growth can classically be observed in three classes of natural systems: 1) *in vitro* cultures (2D cell culture or more realistic 3D spheroid growth [Sutherland et al., 1971]), 2) experimental *in vivo* systems (tumor cells injected either subcutaneously or orthotopically[7] and using either isografts[8] or xenografts[9], or genetically engineered mouse models) or 3) clinical tumor growth, usually observed by means of non invasive imaging techniques. These three empirical ways have increasing level of measurement accuracy, inversely linked to their relevance for the study of human cancer.

Extensive biological studies have been devoted to tumor volume growth kinetics. We refer the reader to [Mayneord, 1932] and [Collins et al., 1956] for early studies on rodent and human data, respectively, to [Steel, 1977] for an extensive review of experimental research using various proliferation indices and to [Hart et al., 1998, Friberg and Mattson, 1997, Spratt et al., 1996, Heuser

[7] at the natural tumor site, e.g. the mammalian fat pad for a breast tumor
[8] graft from cells of the same species, therefore possible in immune-competent animals (mice)
[9] graft from cells of a different species (typically human cells), therefore only possible in immune-deprived animals (mice)

et al., 1979] for later work on human tumor growth. One of the most common findings for animal [Laird, 1965] and human [Steel and Lamerton, 1966, Spratt et al., 1993, Akanuma, 1978] tumors alike is that their relative growth rates decrease with time [Wheldon, 1988]; or equivalently, that their doubling times increase.

These observations suggest that principles of tumor growth might result from general growth laws, often amenable to expression as ordinary differential equations [Gerlee, 2013]. The utility of these models can be twofold: 1) testing growth hypotheses or theories by assessing their descriptive power against experimental data and 2) estimating the prior or future course of tumor progression [Laird, 1965, Norton et al., 1976] either as a personalized prognostic tool in a clinical context [Colin et al., 2010, Baldock et al., 2013, Wang et al., 2009, Portz et al., 2012], or in order to determine the efficacy of a therapy by determination of the deviation from the natural history of the disease either in a preclinical [Bernard et al., 2012, Simeoni et al., 2004] or clinical [Ribba et al., 2012] setting.

1.1.2 A brief state of the art of mathematical models of tumor growth

On the other hand, building on the tremendous amount of discoveries in cancer biology during the 20th century, numerous mathematical and computational models of tumor growth have flourished, trying to integrate more and more parts of an extremely complex process. Without aiming at any exhaustivity (a complete review of the field is far beyond the scope of this document), one could cite evolutionary (often stochastic) models of clonal evolution that elaborate on several (epi)-genetic alterations found to lead to carcinogenesis [Waclaw et al., 2015] (see the work of Franziska Michor [Michor, 2008, Chmielecki et al., 2011, Altrock et al., 2015]). Cell-cell interactions can be studied within the framework of cellular automata. For example, [Enderling et al., 2009] explores implications of the concept of cancer stem cells (first discovered in the context of leukemia, then also evidenced for solid tumors such as breast tumors [Al-Hajj et al., 2003]) and suggests to see tumors as conglomerates of self-metastases. The authors identified different emergent patterns of growth depending on values of cellular parameters (such as proliferation, death or migration). This framework is also well adapted to the study of mechanical cell-cell interactions [Drasdo and Höhme, 2005].

To describe spatial tumor growth at the tissue scale, models based on partial differential equations are more adapted, due to the computational limitations of agent-based models that require simulation of the behavior of each cell. In a landmark study, Greenspan used a diffusion-based model to offer insights on the development of a necrotic core within multicellular tumor spheroids experimental systems [Greenspan, 1972]. Later on, culminating in the 1990's with an important body of literature, investigators proposed to use principles of continuum mechanics and the theory of mixtures to model tumor growth. The populations of cells at play (for instance, tumor and healthy) are viewed as different phases, which can coexist within a given delimited region of space (in contrast with diffusion-limited models). This type of models allows for instance to account for the effect of growth-induced mechanical stresses. We refer the reader to existing extensive reviews

of these works for more information of all the processes that can be integrated in this approach (interactions with the extra-cellular matrix, mechanical properties of the different phases,...) [Byrne, 2010, Lowengrub et al., 2010, Bellomo et al., 2008, Araujo and McElwain, 2004]. See in particular [Araujo and McElwain, 2004] for an excellent review of the intermingled development of our understanding of tumor growth using both experimental and theoretical methods. Later examples of the use of such models can also be found in the work of Ribba et al. for investigation of the effect of radiotherapy schemes [Ribba et al., 2006a] or anti-invasive agents [Ribba et al., 2006b]. Another approach, initiated in the early 2000's by Kristin Swanson and James D Murray and intended for description of invasive brain tumors proposes to use a reaction-diffusion equation where the (logistic) reaction term corresponds to local proliferation and the diffusion term stands for the random motility of the cells [Swanson et al., 2002, Neal et al., 2013].

Going further in complexity, several mathematical models were designed to bring insights on the process of tumor neo-angiogenesis, which involves the coupling of dynamics of blood vessels formation (stimulated by the release of growth factors by hypoxic cancer cells) and tumor growth (dependent on the vasculature for the supply of nutrients). We refer the reader to [Anderson and Chaplain, 1998] for one of the most influential paper in this field and [Chaplain et al., 2006] for a review. Integration of the tumor vasculature and its dynamics into spatial models can also reveal very useful when studying intra-tumor drug delivery and transport [van de Ven et al., 2012, Welter and Rieger, 2013]. To cite one last illustrating example of the use of mathematical modeling to improve our biological understanding, Anderson et al. used a hybrid discrete-continuum model to investigate the role of the micro-environment on tumor growth. They observed distinct emergent patterns of invasion depending on the extra-cellular matrix structure [Anderson et al., 2006].

All these models allow, to some extent, integration of the tumor growth complexity but they have – to date – remained far from direct confrontation to empirical data. Indeed, the task is hard as data sets, even in controlled experimental conditions, rarely have the level of granularity of these spatial models (such as the spatial distribution of distinct clonal populations within the tumor). It is the subject of current active research to bridge the gap between continuum-mechanics based models of tumor growth and multi-dimensional data of tumor growth provided by clinical images [Baratchart, 2016, Lefebvre et al., 2016, Raman et al., 2016, Colin et al., 2015, Weis et al., 2015, Baratchart et al., 2015, Scribner et al., 2014, Cornelis et al., 2013, Yankeelov et al., 2013, Weis et al., 2013, Colin et al., 2012, Colin et al., 2010].

1.2 Theories of tumor growth

In this context, my first effort when I had the chance to have access to experimental data of (scalar) tumor volume growth was to take a step back and address the question of a *quantitative* comparison of classical scalar models of tumor growth in two experimental systems: a syngeneic animal model of Lewis Lung Carcinoma (LLC) cells grafted subcutaneously, and an exogenic animal model of human breast cancer cells (MDA-MB-231) grafted orthotopically.

The main variable of interest will be the tumor volume, denoted by $V(t)$ and assumed to be proportional to the number of tumor cells, according to the well-established conversion rule 1 mm^3 $\simeq 10^6$ cells [Spratt et al., 1995].

Exponential model The simplest conceivable theory of tumor growth is to consider proliferation only (with constant length of the cell cycle). However, as expressed above, non-constant doubling time have been reported in the literature. Accordingly, we also found in our data (for both animal systems) that the exponential model was not able to fit the data (Figure 1.2).

Remark 1.1 (Measurement error)**.** *In our case, examination of the distribution of the measurement error as a function of the caliper-measured volumes of subcutaneous tumors from 133 measurements performed twice spanning a wide range of values (20.7 - 1429 mm^3) led to the following model for the standard deviation of the error (where $M(t_i^j;\theta^j)$ stands for the values of the model M at times t_i^j for the parameter set θ^j):*

$$\sigma_i^j = \begin{cases} \sigma M(t_i^j;\theta^j)^\alpha, & \text{if } M(t_i^j;\theta^j) \geq V_m \\ \sigma V_m^\alpha, & \text{if } M(t_i^j;\theta^j) < V_m \end{cases}$$

with $\alpha = 0.84$, $V_m = 83$ mm^3 and $\sigma = 0.21$ (see [Benzekry et al., 2014c] for details). This model means that, above a given threshold V_m, the measurement error is sub-proportional and, below this threshold, the error made is the same as when measuring V_m.

Once the measurement error model fixed and provided that σ is known, likelihood maximization reduced to minimization of the sum of the weighted least squares.

Generally, we found that considerations of the measurement error model had an important impact on model fits and therefore acceptance or rejection of theories as able or not to describe the data.

In all graphical representations of tumor volume within this chapter, the data presented are individual measurements and the error bar represents one standard deviation according to the measurement error model described above.

Logistic model Going one parameter further than the exponential model, we considered a very classical model in population dynamics that does exhibit a growth slowdown due to competition among the individuals (for space, or food): the logistic model. Interestingly, this additional assumption was not able to recapitulate tumor growth, in neither of the two experimental systems, see Figure 1.3, nor additional *in vivo* tumor growth data that we were given to analyze, including experimental melanoma and renal cell carcinoma tumor growth (data not shown). Even though among the volume range studied the fits were visually not so inaccurate (but still less accurate than other models), the value inferred for the maximally reachable volume was systemically biologically unrealistically small (medians of 1297 mm^3 for the lung system and 1221 mm^3 for the breast system). Indeed, for the LLC system for instance, much larger volumes are obtained when tumors are allowed to grow larger (up to at least 10 000 mm^3 in [Hahnfeldt et al., 1999] for in-

Model	Interpretation	Equations
Exponential	Proliferation of a constant fraction of the tumor volume (growth fraction) with constant cell cycle length	$\begin{cases} \frac{dV}{dt} = aV \\ V(t=0) = 1 \end{cases}$
Exponential - linear	Biologically agnostic. Can be approximated by a model with competition between proliferative cells and presence of a non-proliferative compartment (section 1.3)	$\begin{cases} \frac{dV}{dt} = \begin{cases} a_0 V, & t <= \tau \\ a_1, & t < \tau \end{cases} \\ V(t=0) = 1 \\ \tau = \frac{1}{a_0} \ln\left(\frac{a_1}{a_0 V_0}\right) (\Leftrightarrow V'(\tau^-) = V'(\tau^+)) \end{cases}$
Logistic	Competition only	$\begin{cases} \frac{dV}{dt} = aV\left(1 - \frac{V}{K}\right) \\ V(t=0) = 1 \end{cases}$
Gompertz	Biologically agnostic. Exponential decrease in time of the growth fraction. V_c = volume of one cell.	$\begin{cases} \frac{dV}{dt} = \left(\alpha_0 - \beta \ln\left(\frac{V}{V_c}\right)\right) V \\ V(t=0) = 1 \end{cases}$
Power law	Fractional (Hausdorff) dimension of the proliferative tissue	$\begin{cases} \frac{dV}{dt} = aV^\gamma \\ V(t=0) = 1 \end{cases}$
Generalized logistic	Biologically agnostic	$\begin{cases} \frac{dV}{dt} = aV\left(1 - \left(\frac{V}{K}\right)^\alpha\right) \\ V(t=0) = 1 \end{cases}$

Table 1.1 – Classical models for single tumor growth.

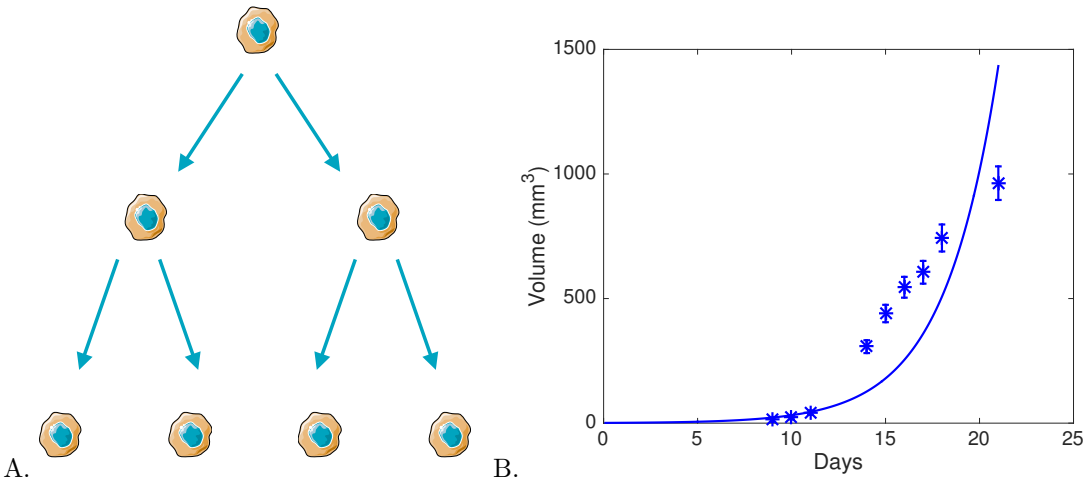

$$\begin{cases} \frac{dV}{dt} = aV \\ V(t=0) = 1 \text{ mm}^3 \end{cases}$$

Figure 1.2 – Exponential growth. A. Scheme of tumor growth under proliferation only. B. Representative fit of an exponential model (starting from the initial number of injected cells – 10^6 cells $\simeq$ 1 mm^3 – at the time of injection) to experimental data of LLC tumor growth.

stance). Attempts of fitting the logistic model to data sets with volumes spanning ranges up to larger volumes resulted in important visual inaccuracy of the fits (results not shown). Finally, statistical goodness-of-fit metrics confirmed rejection of the logistic model in favor of others such as the Gompertz or the power law model (Table 1.2).

Gompertz model While this model emerged first as a “survival" function describing the number of living people as a function of age [Gompertz, 1825], as expressed above, the Gompertz function (or more precisely an expression with parameters generating an increasing curve) has experienced considerable success as a growth function, and specifically in the field of clinical oncology under the impulsion of Larry Norton who employed this model to revisit the log-kill concept of Skipper, Schabel and Wilcox for the effect of chemotherapies [Skipper, 1965] into the so-called Norton-Simon hypothesis [Norton, 1988, Norton et al., 1976, Norton and Simon, 1977, Norton and Simon, 1986, Simon and Norton, 2006]. These ideas played then an important role in the design of a pivotal large phase III trial for investigating densification of adjuvant chemotherapy protocols for the treatment of breast cancer [Citron et al., 2003].

Consistently with previous studies in experimental *in vivo* systems [Laird, 1964, Laird, 1965, Demicheli et al., 1989, Michelson et al., 1987], we also found excellent descriptive properties of the Gompertz model (see Table 1.1 for its expression) in our data , for both experimental systems (Figure 1.4 and Table 1.2). While still not fully explained up to our knowledge (despite several at-

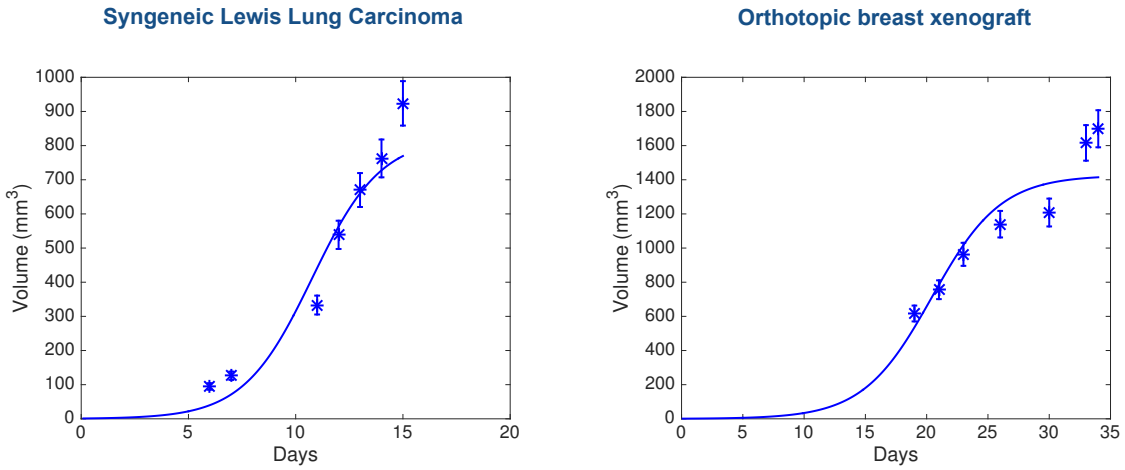

$$\begin{cases} \frac{dV}{dt} = aV\left(1 - \frac{V}{K}\right) \\ V(t=0) = 1 \text{ mm}^3 \end{cases}$$

Figure 1.3 – Best-fit of the logistic model on two representative growth curves from the two experimental systems.

tempts that recover approximative Gompertz growth from more fundamental principles of growth such as the assumption of a maturation velocity that decreases as a function of the global size of the cell population [Frenzen and Murray, 1986]), the dynamics of gompertzian growth state that the growth fraction of the tumor volume (i.e. the portion of cycling tumor cells) is a decreasing function of time. Parameters of the model were highly identifiable when the model is written in the form considered here and reported in Table 1.1 (lower identifiability was obtained when considering the common parameterization $\frac{dV}{dt} = aV \ln\left(\frac{K}{V}\right)$), with median normalized standard errors inferior to 12% (Table 1.3). In contrast to the logistic model, inferred values for the maximal tumor volume were biologically consistent (median 12195 mm^3 and 2987 mm^3 for the lung and breast data, respectively).

Of note, several studies also found good agreement between the Gompertz model and empirical data of clinical tumor growth (bening thyroid tumors [Parfitt and Fyhrie, 1997], lung metastases from testicular tumors [Demicheli, 1980], IgG multiple myeloma [Sullivan and Salmon, 1972] or breast tumors [Norton, 1988]).

Metabolic considerations and the power law model Von Bertalanffy [Bertalanffy, 1957], followed later on by others [West et al., 2001], proposed to derive general laws of organic growth from basic energetics principles. Stating that the net growth rate should result from the balance of synthesis and destruction, observing that metabolic rates very often follow the law of allometry (i.e. that they scale with a power of the total size) and assuming that catabolic rates are in proportion

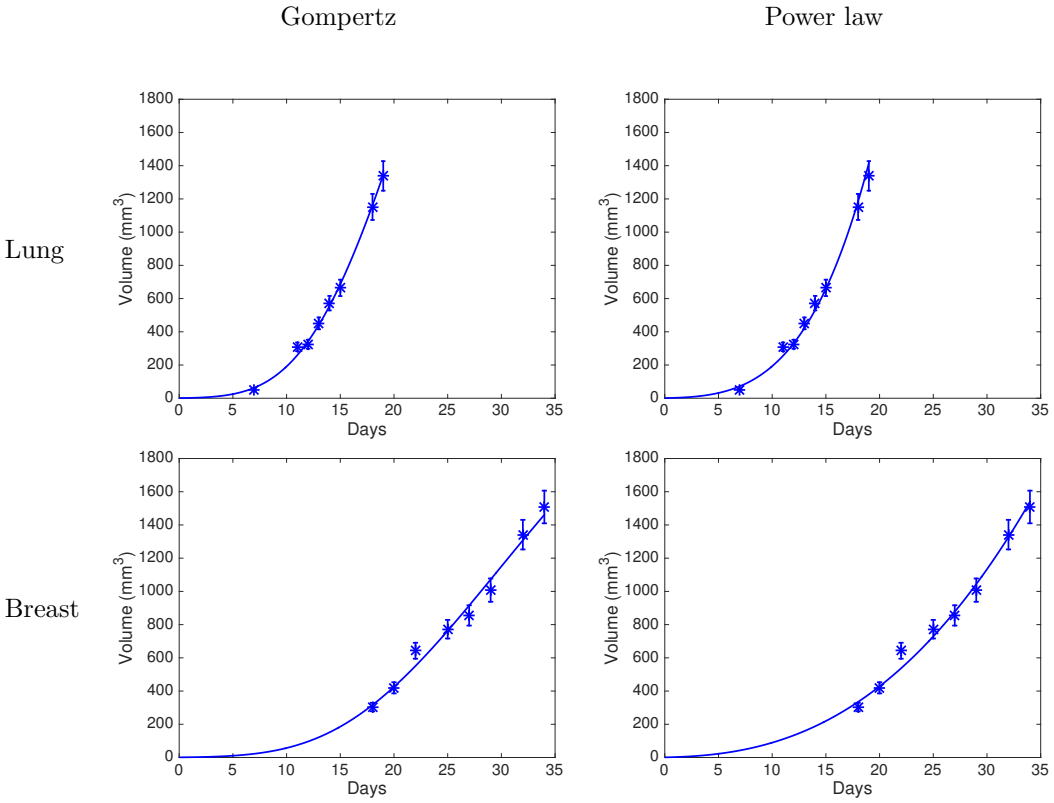

Figure 1.4 – Representative fits of the Gompertz and power law models for tumor growth curves in the lung and breast experimental systems

to the total volume, he derived the following model for growth of biological processes:

$$\frac{dV}{dt} = aV^{\gamma} - bV, \tag{1}$$

which has already been successfully applied to describe tumor growth [Guiot et al., 2003, Herman et al., 2011]. More elaborate considerations linking tumor growth, metabolic rate and vascularization leading to equation (1) can be found in [Herman et al., 2011]. This study also provides expressions of the coefficients in terms of measurable energetic quantities. From the observation that our data does not exhibit a clear saturation phase, a qualitative feature of equation (1), we also considered another model, derived from (1), by neglecting the loss term, i.e. taking $b = 0$. This model will be termed the power law model. As can be seen in Figure 1.4 and Table 1.2, it was able to give a very good description of our data.

Pushing further the reasoning of [Bertalanffy, 1957] and arguing that the rate of synthesis of new material, in the context of tumor growth, should be proportional to the number of proliferative cells (under the assumption of a constant cell cycle length), this model assumes that the proliferative tissue is proportional to V^{γ}. This could be further interpreted as a possible fractional Hausdorff

dimension of the proliferative tissue, when viewed as a metric subspace of the full tumor volume (itself a three-dimensional subset of the three-dimensional Euclidean space). This dimension would be equal to $3\,\gamma$ and could be less than 3 when $\gamma < 1$. In this interpretation, the case $\gamma = 2/3$ (i.e. dimension equal to 2) could correspond to a proliferative rim limited to the surface of the tumor, a very well known phenomenon observed in tumor growth [Mayneord, 1932]. This implies that the tumor radius — proportional to $V^{1/3}$ — grows linearly in time. Such linear growth of the tumor radius has been reported for tumor growth, for instance in the case of gliomas, thus confirming this model prediction [Baldock et al., 2013]. At the other extreme, a three-dimensional proliferative tissue ($\gamma = 1$) represents proliferative cells uniformly distributed within the tumor and leads to exponential growth. Any power $0 < \gamma < 1$ gives a tumor growth with decreasing growth fraction (and thus decreasing relative growth rate), for which the power law model provides a description in terms of a geometrical feature of the proliferative tissue. Interestingly, the values of γ that we inferred from fitting the tumor growth curves were highly identifiable and found to have small inter-animal variability (especially in the LLC case). They suggested values of 2.37 and 1.74 for the fractal dimensions of the proliferative tissues for the lung and breast tumors, respectively.

This model was first used (though without mention of the previous interpretation) for murine tumor growth in [Dethlefsen et al., 1968] and was also applied to human data in [Hart et al., 1998].

Other growth models with more parameters We also tried to fit several other models with more than two free parameters, including the generalized logistic model or a model with dynamic carrying capacity. Descriptive properties were found excellent (Table 1.2). However, the major drawback of these models was the lack of identifiability of their parameters, as can be observed in the Table 1.3. This translated into poor utility in terms of predictive power (see below).

Lung data

Model	SSE	AIC	RMSE	R2	p > 0.05	#
Generalized logistic	**0.12(0.019 - 0.416)[1]**	**-13(-30.4 - 0.978)[1]**	0.398(0.174 - 0.816)[3]	**0.982(0.94 - 0.997)[1]**	100	3
Power law	0.155(0.0158 - 0.713)[2]	-13.4(-34.5 - 2.95)[2]	0.409(0.145 - 0.957)[2]	0.962(0.784 - 0.998)[3]	100	2
Gompertz	0.155(0.019 - 0.67)[3]	-13.4(-32.4 - 2.39)[3]	**0.407(0.159 - 0.928)[1]**	0.97(0.815 - 0.997)[2]	100	2
Logistic	0.232(0.0498 - 0.726)[4]	-8.34(-18.4 - 3.44)[4]	0.518(0.273 - 0.984)[4]	0.964(0.92 - 0.989)[4]	100	2
Exponential-linear	0.22(0.0481 - 0.76)[5]	-8.51(-17.1 - 3.8)[5]	0.507(0.268 - 1.01)[5]	0.96(0.911 - 0.988)[5]	100	2
Exponential	1.36(0.31 - 2.36)[6]	6.01(-5.38 - 13.4)[6]	1.22(0.595 - 1.61)[6]	0.64(0.281 - 0.944)[6]	15	1

Table 1.2 – Fit performances of growth models. Models were ranked in ascending order of the means of the Root Mean Squared Error (RMSE), defined from the sum of squared errors (SSE) by (for an animal j)

$$SSE^j = \sum_{i=1}^{N^j} \left(\frac{y_i^j - M(t_i^j; \hat{\theta}^j)}{\frac{\sigma_i^j}{\sigma}} \right)^2, \quad RMSE^j = \sqrt{\frac{1}{N^j - p} SSE^j}$$

with $\hat{\theta}^j$ the maximum likelihood estimate of the parameter vector for animal j (i.e., minimizer of SSE^j) and p the number of free parameters in the model. For each metric, indicated are the median values (among all animals) and in parenthesis the minimal and maximal values. When reported, value inside brackets is the rank of the model for the underlying metric. The model ranking first is highlighted in bold. The Akaike Information Criterion (AIC) is defined by [Burnham and Anderson, 2003]

$$AIC^j = N^j \ln \left(\frac{SSE^j}{N^j} \right) + 2p$$

(caption continued on next page).

Breast data

Model	SSE	AIC	RMSE	R2	p > 0.05	#
Gompertz	0.0976(0.0147 - 0.328)[3]	**-11.3(-27.8 - -0.848)[1]**	0.348(0.14 - 0.677)[2]	0.922(0.674 - 0.985)[3]	100	2
Exponential-linear	**0.0919(0.0159 - 0.49)[1]**	-11.7(-24.9 - 1.01)[2]	**0.336(0.163 - 0.828)[1]**	0.915(0.664 - 0.989)[4]	100	2
Generalized logistic	0.0814(0.00366 - 0.328)[2]	-10.7(-26.4 - 0.19)[3]	0.355(0.0956 - 0.757)[3]	**0.94(0.803 - 0.988)[1]**	100	3
Power law	0.102(0.0159 - 0.323)[4]	-10.9(-21.7 - -0.0172)[4]	0.356(0.163 - 0.707)[4]	0.917(0.613 - 0.986)[2]	100	2
Logistic	0.145(0.00367 - 0.417)[5]	-8.1(-22 - -0.129)[5]	0.429(0.0782 - 0.764)[5]	0.863(0.648 - 0.988)[5]	100	2
Exponential	2.19(0.617 - 3.44)[6]	8.77(0.616 - 13.5)[6]	1.59(0.848 - 2)[6]	-0.907(-5.94 - 0.875)[6]	53	1

Table 1.2 – (continued caption). The R^2 is informative of how good is the model fit compared to a completely agnostic one that would result from assuming just the mean of the data and is defined by:

$$R^{2,j} = 1 - \frac{\sum_{i=1}^{N^j} \left(y_i^j - M(t_i^j; \hat{\theta}^j \right)}{\sum_{i=1}^{N^j} \left(y_i^j - \overline{y}^j \right)}, \quad \overline{y}^j = \frac{1}{N^j} \sum_{i=1}^{N^j} y_i^j$$

the resulting from the mixed-effect estimation (see Materials and Methods) and is defined in (14). Values reported in the column are percentages of animals for which Kolmogorov-Smirnov test for normality of residuals was not rejected at the significance level of 0.05. # = number of parameters.

Lung data

Model	**Par.**	**Unit**	**Median value (CV)**	**NSE (%) (CV)**
Generalized logistic	a	-	2.55e+03 (810)	4e+04 (162)
	K	-	4.38e+03 (7.37e+03)	57.9 (626)
	α	-	0.000141 (4.29e+05)	4e+04 (162)
Power law	α	$\text{mm}^{3(1-\gamma)}\cdot\text{day}^{-1}$	0.921 (41.9)	10.6 (55)
	γ	-	0.788 (9.35)	3.42 (62.4)
Gompertz	α_0	day^{-1}	1.84 (35.7)	9.28 (65.3)
	β	day^{-1}	0.0792 (43)	12 (74.4)
Logistic	a	day^{-1}	0.502 (17.5)	2.74 (54.1)
	K	mm^3	1.3e+03 (23.3)	15.3 (49)
Exponential-linear	a_0	$[day^{-1}]$	0.49 (19.5)	4.17 (58.1)
	a_1	$[mm^3 \cdot day^{-1}]$	116 (24)	15.4 (63.3)
Exponential	a	day^{-1}	0.399 (14.1)	2.95 (23.8)

Breast data

Model	**Par.**	**Unit**	**Median value (CV)**	**NSE (%) (CV)**
Gompertz	α_0	day^{-1}	1.55 (22.5)	8.52 (66.2)
	β	day^{-1}	0.0719 (25)	9.73 (84.4)
Exponential-linear	a_0	$[day^{-1}]$	0.31 (16.9)	5.61 (72.2)
	a_1	$[mm^3 \cdot day^{-1}]$	67.8 (34.8)	11.8 (87.4)
Generalized logistic	a	-	2.75e+03 (264)	6.26e+04 (567)
	K	-	1.96e+03 (1.5e+04)	25.2 (1.32e+03)
	α	-	2.67e-05 (2.16e+06)	6.26e+04 (567)
Power law	α	$\text{mm}^{3(1-\gamma)}\cdot\text{day}^{-1}$	1.32 (92.2)	29.4 (51.7)
	γ	-	0.58 (23.4)	9.73 (77.5)
Logistic	a	day^{-1}	0.305 (10.1)	3.18 (34.8)
	K	mm^3	1.22e+03 (34)	10.9 (79.6)
Exponential	a	day^{-1}	0.223 (5.88)	3.75 (21.1)

Table 1.3 – Values of the parameters estimates, associated inter-animal variability and standard errors. CV = Coefficient of Variation = $\frac{\text{standard deviation}}{\text{mean}} \times 100$. NSE = Normalized Standard Error = $\frac{\text{standard error on the parameter estimate}}{\text{estimate}}$. See [Benzekry et al., 2014c] or [Seber and Wild, 2003] for methods of computation of the standard errors.

1.3 A modeling-based explanation of biphasic exponential-linear growth using bioluminescence data quantifying the dynamics of proliferative cells

The human breast tumor experimental system consisted of MDA-MB-231 cells [Ebos et al., 2008] orthotopically injected into the right inguinal mammary fat pads of severe combined immunodeficient mice. For description, of this data, a model with initial exponential phase followed by a linear phase (see Table 1.1 for its mathematical expression) was particularly adapted, both at the individual [Benzekry et al., 2014c] and population [Mollard et al., 2016] levels (Figure 1.5), as previously introduced by others, although on data from ovarian and colorectal cancer [Simeoni et al., 2004]. In collaboration with experimentalists, I have had access to additional data about tumor growth

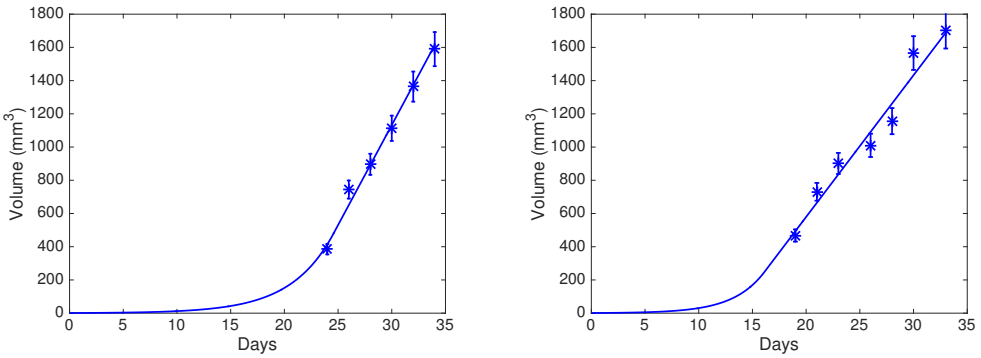

Figure 1.5 – Examples of fits of the Exponential-linear model to orthotopically implanted breast tumor growth

in the same experimental system. These consisted in quantification of bioluminescence emission from tumor cells previously transfected with firefly luciferase (an enzyme capable of generating light in the presence of luciferin). The particularity of this tumor growth assay is that it allowed to distinguish the concurrently measured total tumor volume from the number of living tumor cells. Indeed, only the latter is responsible for the bioluminescence signal (see [Mollard et al., 2016] for materials and methods). As a general observation, it was found a saturation of this signal with time, while tumor volume was keeping increasing.

To inform on the volume and bioluminescence combined kinetics, we investigated mathematical models that would be able to reproduced the data and proposed a biologically-based model that would both reproduce the data and explain the exponential-linear growth pattern previously observed. We divided the total volume into a proliferative compartment (as recorded by the bioluminescence and denoted $P(t)$) and another compartment (possibly composed of necrotic debris and thus denoted by $N(t)$) that would not be proliferatively active but nevertheless contribute to the caliper-measured volume while stopping to emit light signal (Figure 1.6.a). Growth of the proliferative cells is assumed to be logistic, i.e. proliferation limited by competition (for space or

nutrients). Assuming a micro-environment carrying capacity K and a proliferation rate $a\left(=\frac{\ln 2}{\tau}\right)$, with τ the cell cycle length, the probability of cell division during a small time interval of length dt is $a\left(1-\frac{P(t)}{K}\right)dt$ and we have $\frac{dP}{dt}=aP\left(1-\frac{P(t)}{K}\right)=aP-\frac{a}{K}P^2$. When tumor cells are unable to proliferate, we assume that they enter the necrotic compartment. Writing a law of mass conservation we have

$$\begin{cases} \frac{dP}{dt}=aP\left(1-\frac{P(t)}{K}\right)=aP-\frac{a}{K}P^2 & P(t=0)=P_0 \\ \frac{dN}{dt}=\frac{a}{K}P^2 & N(t=0)=0 \\ V=P+N & \end{cases}$$

where P_0 is the number of cells injected, converted into a bioluminescence signal using a predetermined cell-to-light ratio.

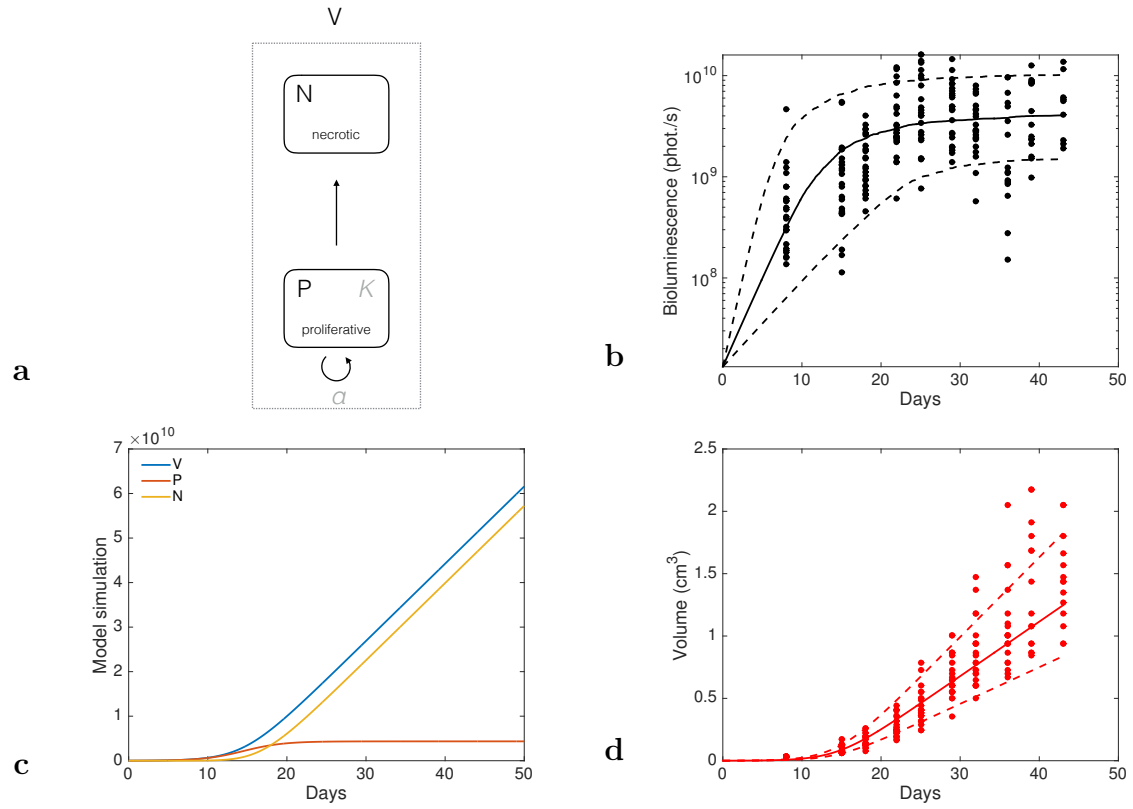

Figure 1.6 – Combined quantitative mathematical modeling of the bioluminescence emission and the caliper-measured volume kinetics. (a) Model scheme. (b) Model fit of the proliferative compartment to the 3D bioluminescence signal, using a population approach (mixed-effects) for inter-animal variability. Solid line = median. Dashed lines = 10th and 90th percentiles. Log scale. (c) Resulting model prediction of the total tumor volume, up to a proportionality constant λ and to appropriate conversion into cm^3 (see text). (d) Simulation of the model dynamics with P = proliferative tissue, N = necrotic tissue, V = total volume.

The model was fit to the data using the nonlinear mixed-effects statistical framework for dealing with the non-negligible inter-animal variability. It was fully able to describe the bioluminescence data and quantified a plateau reached at $4.35 \times 10^9 \pm 2.40 \times 10^9$ photons/second (Figure 1.6.b). Identifiability of the parameters was excellent, as revealed by low standard errors [Mollard et al., 2016]. Based on these parameters retrieved from the bioluminescence data, simulation of the full model kinetics predicted a biphasic pattern for the tumor volume growth curve: first an exponential phase, followed by a linear phase (Figure 1.6.c). Interestingly, this prediction was both qualitatively and quantitatively in agreement with the caliper-measured volume experimental data (Figure 1.6.d). Indeed, the model was able to accurately predict the volume growth kinetics up to a proportionality constant λ that was estimated to 2.25 ± 0.23, after renormalization of the signal into a cm^3 unit using the cell-to-signal ratio determined above. We hypothesize that this constant λ is associated to the reported fact that not the entire tumor volume is composed of tumor tissue (i.e., alive plus necrotic) as it also comprises a non-negligible part of stroma (estimated here to 56% of the total volume). Taken together, our results show that our simple mathematical model was able to describe the dynamics of both the proliferative component and the entire tumor volume. In doing so, it also provides a valid explanation of the exponential-linear pattern of the tumor volume kinetics. In our theoretical framework, when the proliferative tissue reaches saturation, this generates a constant growth rate of the volume (because $\frac{dV}{dt} = aP$), which in turn provokes the transition to the linear phase.

1.4 Predictive power of classical models of tumor growth

1.4.1 Using individual data points only

We then addressed the problem of forecasting future tumor growth using a given number of initial data points. As can be seen in a representative example in Figure 1.7 using $n = 5$ data points, the predictive power of all the models was rather limited. Quantitatively, variable prediction error was observed across the two tumor types and across the mice. Using $n = 5$ data points and predicting at a depth of $d = 2$ days, the mean relative errors ranged 21 - 28 % for the LLC system and 13 - 18 % for the breast tumors (Table 1.4). As could have been expected, when using less data points, the predictive power decreased. Using only three time points and predicting either the next data point (LLC data) or at a depth of $d = 2$ days (breast data), the mean relative error was 29 - 31 % for the LLC system (with the notable exception of the exponential-linear model at 21%) and 27 - 33% for the breast system (Table 1.4). Interestingly, the same setting (using three data points to predict at depth $d = 1$ for the LLC data or $d = 2$ for the breast data) but in a different part of the growth curve, namely in the last phase (starting volumes of 1245 ± 254 mm^3 and 1383 ± 211 mm^3 for the LLC and breast data, respectively), led to improved predictive power, with relative errors ranging 8- 14% (LLC data) and 14 - 17% (breast data), see Table 1.4. This last setting might be the most clinically relevant since in this setting, diagnosis might occur when the tumor is already quite large (typically, 1 g $\simeq 10^9$ cells for a breast tumor). Notably, the exponential-linear model

exhibited excellent predictive power for the breast data, in line with the previous findings of its accurate descriptive power for this experimental model. In particular, even when using only one data point (plus the initial condition $V(t=0) = 1$ mm^3), the predictive power was excellent, even at a depth of more than 10 days.

We refer the interested reader to [Benzekry et al., 2014c] for more details, including the descriptive power of the models at larger depths.

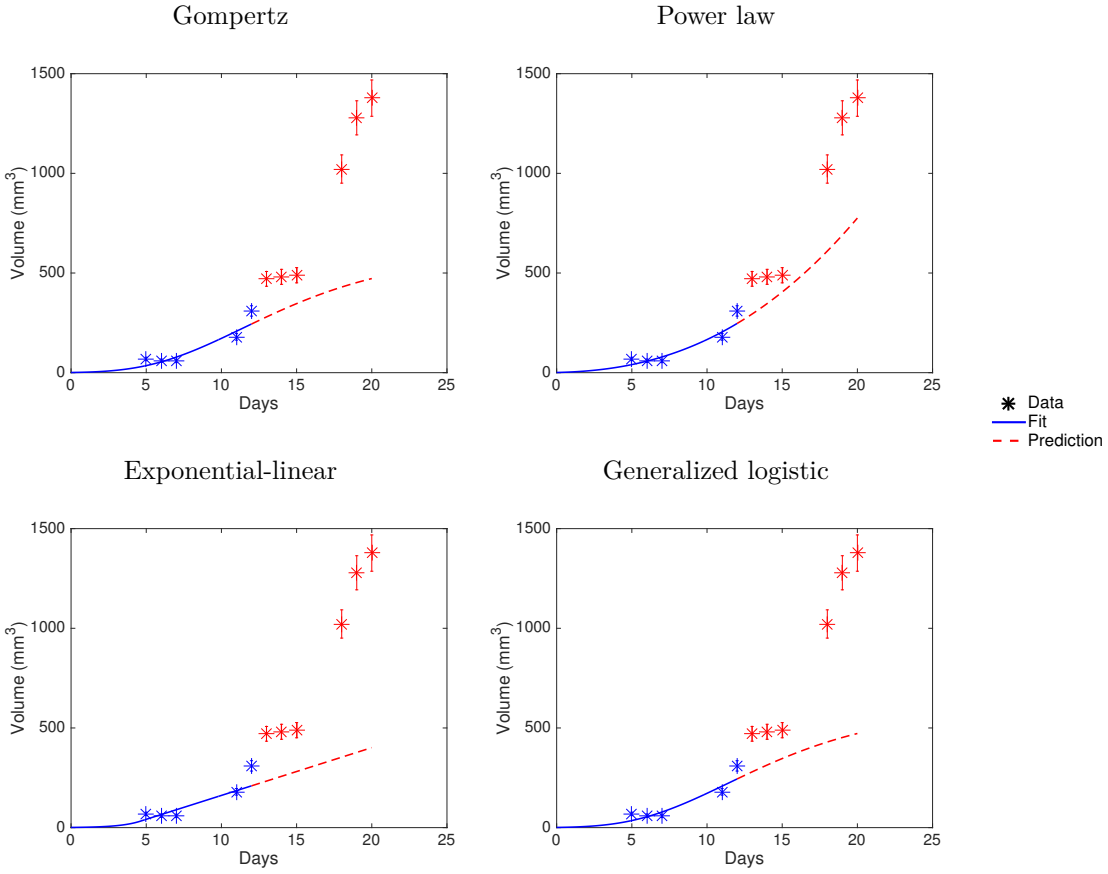

Figure 1.7 – Representative examples of the predictive power of 4 models of tumor growth when using 5 data points (plus a fixed initial condition $V(t=0) = 1$ mm^3). LLC data.

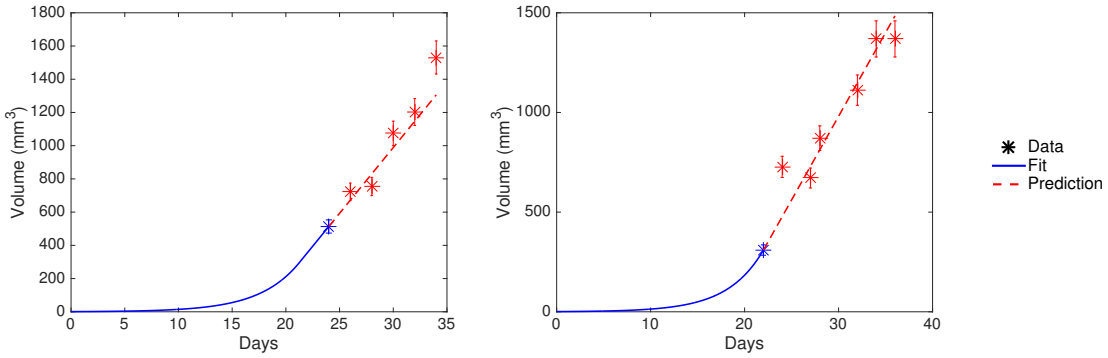

Figure 1.8 – Representative examples of the predictive power of the exponential-linear model when using 1 data point (plus a fixed initial condition $V(t = 0) = 1$ mm^3). Breast data.

	Lung data			**Breast data**		
Model	$\mathbf{RE_{5,2}}$	$\mathbf{RE_{3,1}}$	$\mathbf{RE^f_{3,1}}$	$\mathbf{RE_{5,2}}$	$\mathbf{RE_{3,2}}$	$\mathbf{RE^f_{3,2}}$
Power law	0.21 (0.02 - 0.52)	0.29 (0.01 - 1.08)	0.08 (0.01 - 0.29)	0.15 (0.03 - 0.57)	0.33 (0.09 - 0.97)	0.14 (0.00 - 0.41)
Gompertz	0.25 (0.07 - 0.57)	0.30 (0.03 - 1.08)	0.10 (0.00 - 0.30)	0.15 (0.00 - 0.54)	0.33 (0.08 - 0.97)	0.17 (0.00 - 0.61)
Exponential linear	0.22 (0.04 - 0.43)	0.21 (0.03 - 0.99)	0.10 (0.01 - 0.33)	0.13 (0.01 - 0.36)	0.27 (0.08 - 0.84)	0.10 (0.00 - 0.32)
Generalized logistic	0.28 (0.07 - 0.57)	0.31 (0.03 - 1.08)	0.14 (0.01 - 0.30)	0.18 (0.00 - 0.54)	0.27 (0.10 - 0.73)	0.15 (0.00 - 0.41)

Table 1.4 – Predictive power of selected models. $RE_{n,d}$= relative error of the prediction using n data points and predicting d days in the future. RE^f = final portion of the growth curve. Reported are the mean (min - max).

1.4.2 Predictions improvement when employing bayesian estimation

When relatively fewer data points were used, for example with only three, individual predictions based on individual fits were found to be globally limited for the lung tumor data, especially over a large time frame. However, this situation is likely to be the clinically relevant since few clinical examinations are performed before the beginning of therapy. On the other hand, large databases might be available from previous examinations of other patients and this information could be useful to predict future tumor growth in a particular patient. In a preclinical setting of drug investigation, tumor growth curves of animals from a control group could be available and usable when inferring information on the individual time course of one particular treated animal.

An interesting statistical method that could potentiate this is *bayesian estimation*. It consists in using *a priori* information, i.e. learning the population distribution of the model parameters from a given pre-established database and to combine it with the individual parameter estimation from the available restricted data points on a given animal. We investigated this method in order to determine if it could improve the predictive performances of the models. Each dataset was randomly divided into two groups. One was used to learn the parameter distribution (based on the full time curves), while the other was dedicated to predictions (limited number of data points). For a given animal of this last group, no information from his growth curve was used to estimate the a priori distributions. The full procedure was replicated 100 times to ensure statistical significance, resulting in respectively 2000 and 3400 fits performed for each model.

Let a dataset and a model M be given. Individual fits for the first group (the “learning" group) were performed using all the available data, generating mean values $(\overline{\theta_1}, \ldots, \overline{\theta_p})$ and standard deviations $(\omega_1, \ldots, \omega_p)$ of the parameters within the population. This information was subsequently used when estimating the individual parameter set of a given animal from the second group (the “forecast" group). Indeed, assuming a gaussian distribution of each parameter within the population and using Baye's formula, the new likelihood of the data points $y_1^j, \ldots, y_{N^j}^j$ in animal j writes:

$$p\left(y_1^j, \ldots, y_{N^j}^j, \theta^j\right) = p(y_1^j, \ldots, y_{N^j}^j | \theta^j) p(\theta^j)$$

which leads to minimization of the following objective function for the log-likelihood:

$$J(\theta^j) = \sum_{i=1}^{N^j} \left(\frac{y_i^j - M(t_i^j; \hat{\theta}^j)}{\sigma_i^j} \right)^2 + \sum_{k=1}^{p} \left(\frac{\theta_k^j - \overline{\theta_k}}{\omega_k} \right)^2 \tag{2}$$

Predictions obtained using this technique were significantly improved for the LLC subcutaneous tumors. Prediction improvement was particularly high for models exhibiting a small dispersion of the parameters within the population distribution, such as the power law model (see Figure 1.9). Indeed, when using formula (2) above for estimation of the parameters, we see that adjunction of the *a priori* information is only useful if the standard deviation of the parameters within the population is not too important. This was indeed the case for the power law model with coefficients of variation of 9% and 42 % for the parameters γ and a, respectively. According to a success

metrics defined (using the measurement error model established above) as the error being within three standard deviations [Benzekry et al., 2014c], the average prediction successes reached 90% using the power law model at depth $d = 1$ day, it was only 57.1% using an individual approach. Prediction success rates were improved even at large future depths. For instance, for $d = 7$ days, the average success rate was 50.6% versus 6.07% using individual prediction. For the breast data, due to already high prediction scores without adjunction of *a priori* information, the exponential-linear model did not benefit from the method. For the next day data point of the breast tumor growth curves, predictability was already almost maximal without adjunction of a priori information and thus no important impact was observed.

Taken together, our results demonstrated that, for each experimental system, a prediction method could be applied that ensures good predictions of future tumor growth using a minimal number of data points.

For the orthotopic breast xenografts, the exponential-linear model generated excellent predictions, even without the addition of population information. For the LLC ectopic subcutaneous tumors, combination of bayesian estimation (*a priori* on the population distribution) and the power law model was the best strategy. While encouraging, this last result however highly depends on the large degree of homogeneity across the tumor growth curves in this animal model, which is well captured by parameters with small population coefficients of variation. This feature comes from the fact that the experimental conditions were actually controlled to ensure maximal reproducibility and thus minimal heterogeneity. The tumor cells all come from the same cell line. They were injected in mice from an inbred strain (C57BL/6) and thus the hosts are nearly all identical to each other in genotype.

This makes the situation very different from clinical human cancers, which much more heterogenous in their growth patterns, even within the same tumor type and histology. Indeed, when we applied this bayesian methodology to a dataset meningiomas growth in 24 patients, no prediction improvement was obtained (unpublished results). It is the subject of current active research to bridge the gap between continuum-mechanics based models of tumor growth and multi-dimensional data of tumor growth provided by clinical images [Colin et al., 2015, Colin et al., 2010, Colin et al., 2012, Cornelis et al., 2013, Raman et al., 2016, Scribner et al., 2014, Baratchart et al., 2015, Baratchart, 2016, Lefebvre et al., 2016, Yankeelov et al., 2013, Weis et al., 2013, Weis et al., 2015].

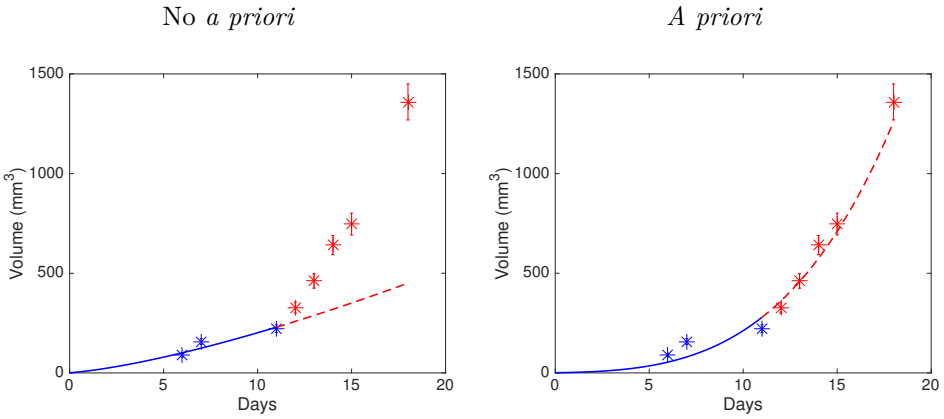

Figure 1.9 – Example of improvement of the predictive power using bayesian estimation and the power law model.

Chapter 2

Metastasis: biological dynamics at the organism scale

Contents

Abstract

While a large zoology of mathematical models exist for tumor growth as seen in the previous chapter, few have been developed for description of the metastatic process, despite its fundamental clinical importance. Furthermore, mathematical models of invasion and metastasis are most often confined to *local* determinants of these processes and seldom consider the *systemic* nature of metastatic dynamics. Nevertheless, recent findings in cancer biology have uncovered nontrivial dynamics occurring at the organism scale. In the studies of this chapter, in collaboration with several teams of biologists, we attached ourselves to gather experimental data obtainable for quantification of the metastatic process and used a unified mathematical framework to interrogate several biological questions.

First, in collaboration with John Ebos at the Roswell Park Cancer Institute (Buffalo, USA), we investigated the relevance of quantitative laws of metastatic dissemination and growth for description of pre-surgical primary tumor and post-surgical metastatic burden data (quantified by bioluminescence), in two clinically relevant "ortho-surgical" animal models of metastasis (section 2.3 and [Benzekry et al., 2016]).

The second study was performed in the framework of the PhD thesis of Etienne Baratchart that I co-supervised with Thierry Colin and Olivier Saut. It has been performed in collaboration with a team of biologists led by Andreas Bikfalvi and composed also of Lin Cooley and Wilfried Souleyreau (Laboratoire de l'Angiogénèse et du Micro-Environnement des Cancers, Inserm U1029, Bordeaux, FR) and a team specialized in *in vivo* animal magnetic resonance imaging led by Sylvain Miraux with MRI observations performed by Emeline Ribot (Centre de Résonance Magnétique des Systèmes Biologiques, CNRS, Bordeaux, FR). It consisted in quantitatively challenging the "classical" model of metastatic development where no interactions occur between established lesions against the experimental data (section 2.4 and [Baratchart et al., 2015]).

During my postdoctoral stay at the Center of Cancer and Systems Biology (CCSB, Tufts University, Boston, USA), in collaboration with Philip Hahnfeldt (CCSB) and Alberto Gandolfi (Istituto di Analisi dei Sistemi ed Informatica "Antonio Ruberti", Roma, IT), we investigated systemic tumor-tumor interactions from a theoretical perspective to shed light on global metastatic dormancy (section 2.5 and [Benzekry et al., 2014b, Benzekry et al., 2014a]). Finally, using a combined experimental and modeling approach to address theories of tumor-tumor distant interactions (section 2.6 and [Benzekry et al., 2017]). The experiments were designed by myself in concertation with Lynn Hlatky and Philip Hahnfeldt but were mostly performed by Clare Lamont.

2.1 Introduction

Metastasis (from the greek $\mu\varepsilon\tau\acute{\alpha}$ = beyond and $\sigma\tau\acute{\alpha}\sigma\iota\zeta$ = place) is the colonization of one or multiple distant site(s) from the primary tumor location. A wide heterogeneity of distant metastatic locations is observed across cancer types, some of them not generating any metastasis at all (such as gliomas), and others exhibiting preferential distant sites for establishment of secondary colonies [Valastyan and Weinberg, 2011]. For instance, prostate cancer almost exclusively metastasizes to the bones. While some locations have a natural explanation (the lungs are typical sites of metastasis due to the small size of capillaries there, the liver as well due to its filtering role and the portal vein directly effluxing into it), elucidating precise determinants of metastatic tropism remains an open biological question in cancer biology. However, this is mentioned here just for the curiosity of the reader as this problem cannot be addressed within the formalism developed here.

The metastatic process is complex and results from a cascade of several events (Figure 2.1). Briefly, several bottlenecks have to be overcome before establishment of a distant metastasis. These include: detachment from the primary tumor, migration and invasion in the local micro-environment (involving phenotypical changes of the tumor cell such as the epithelial-to-mesenchymal transition), intravasation into blood vessels, survival in transit, extravasation at a distant site, possibly a dormancy phase either as an isolated cell or as a micro-tumor [Chambers et al., 2002] for periods lasting from months to decades [Nguyen et al., 2009], stromal recruitment at the distant site, angiogenesis and growth to a macroscopic size. In addition, new findings in the last three decades about organism-scale phenomena rendered the picture even more complex and the relationship between primary tumor growth and eventual metastasis remains enigmatic [Klein, 2009]. Metastatic seeding was initially thought to occur only during late stages of primary tumor growth and invasion [Hanahan and Weinberg, 2000]; however, recent evidence suggests systemic dissemination is a much earlier event [Hanahan and Weinberg, 2011]. Indeed, even the direction of tumor spread, initially thought to occur unidirectionally from primary to secondary sites, has been replaced by more complex and dynamic theories of interaction. These include models where primary and secondary lesions grow (and evolve) in parallel [Klein, 2009] and the possibility that cell seeding can be bidirectional, with metastasis potentially "re-seeding" back to original primary location [Norton and Massagué, 2006, Comen et al., 2011, Kim et al., 2009]. Other examples of nonlinear interactions at the systemic scale include: distant inhibition of angiogenesis, possibly leading to post-surgical acceleration [O'Reilly et al., 1994, Demicheli et al., 2008], distant preparation of the pre-metastatic niche through recruiting of bone marrow-derived hematopoietic progenitors [Kaplan et al., 2005]. We refer the reader to [Valastyan and Weinberg, 2011] for an excellent review of the current knowledge of metastatic biology, including details about the molecular players involved in different steps of the metastatic cascade, as well as the estalished roles of several stromal cells. This paper also reviews the current theoretical models of metastasis formation. For more historical considerations of the study of cancer metastasis, see [Talmadge and Fidler, 2010].

To assist in understanding this complexity, mathematical modeling has been used to determine the relationship between primary (localized) and secondary (metastatic) tumor dissemination and

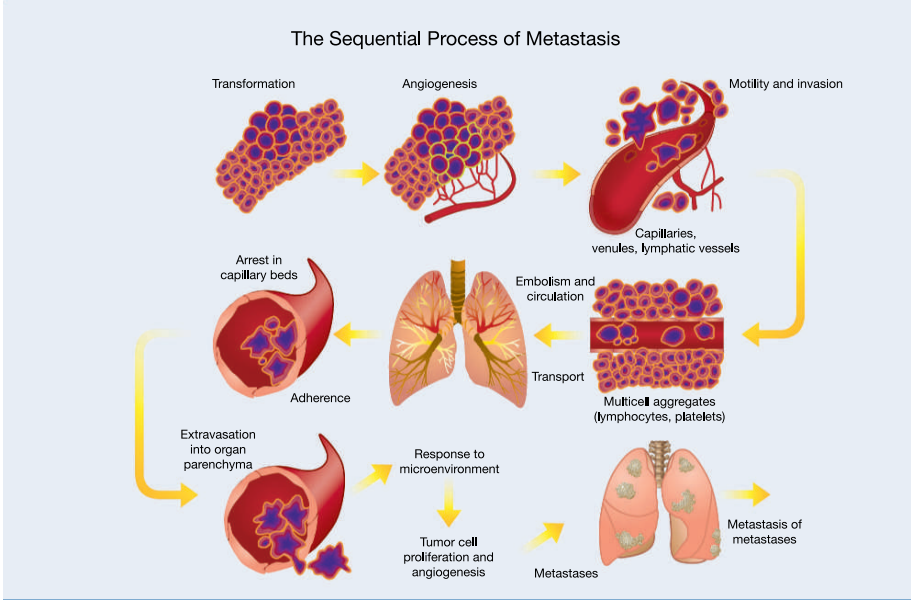

Figure 2.1 – The metastatic cascade. Reproduced from [Talmadge and Fidler, 2010]

growth. A detailed review of all the mathematical modeling studies that addressed the questions of metastatic dissemination and growth is beyond the scope of the present document (and can be found, in part, elsewhere [Scott et al., 2013b, Clare et al., 2000]) but a few publications of biological or clinical interest that the curious reader can consult are: [Slack et al., 1969, Liotta et al., 1976a, Saidel et al., 1976, Guiguet et al., 1982, Koscielny et al., 1985, Klein and Bartoszyński, 1991, Kimmel and Flehinger, 1991, Yorke et al., 1993, Retsky et al., 1997, Koscielny and Tubiana, 1999, Iwata et al., 2000, Michor et al., 2006, Hanin et al., 2006, Barbolosi et al., 2009, Bethge et al., 2012, Haeno et al., 2012, Newton et al., 2012, Newton et al., 2013, Scott et al., 2014, Scott et al., 2013a, Mehrara et al., 2013, Coumans et al., 2013, Araujo et al., 2014, Bazhenova et al., 2014, Brodbeck et al., 2014, Hanin and Bunimovich-Mendrazitsky, 2014, Hanin et al., 2015, Hanin and Rose, 2016, Poleszczuk et al., 2016].

The mathematical formalism that we develop below has been employed to address the following biological questions about metastasis, which have the common characteristic of concerning dynamics of the disease at the organism scale.

Biological problem 2. *What are the qualitative and quantitative differences among experimental models of metastasis for different cancer types? Is the growth of secondary tumors identical to the growth of the primary tumor, in a given experimental system? How does the dissemination process depend on the size of the primary tumor? What is the impact of surgery on metastatic growth and dissemination?*

Biological problem 3. *Is the "standard" view of metastatic initiation and growth – that secondary lesions once established grow without interactions with each other or with the primary tumor – quantitatively valid for description of the dynamics of the number and size of metastases?*

Biological problem 4. *What are the determinants of global dormancy of secondary tumors leading to what has been referred as "cancer without disease" [Folkman and Kalluri, 2004]? Can systemic inhibition of angiogenesis explain this phenomenon?*

Biological problem 5. *Among existing theories of concomitant resistance (i.e. tumor-tumor cross inhibition of growth) all qualitatively valid for explanation of the phenomenon, which one(s) have to be quantitatively rejected and which one(s) are valid?*

We refer the reader to the introduction of each section for more precise biological background on each of these questions.

2.2 A general mathematical formalism for metastatic development

As in every modeling process, simplifications of the reality have to be made following ion order to address the problematic for which the model is built or fit the type of data that is experimentally or clinically obtainable. In our case, in accordance with the biological literature, we chose to divide the metastatic process into two main phenomena: dissemination and colonization [Valastyan and Weinberg, 2011, Chaffer and Weinberg, 2011, Nguyen et al., 2009]. This is also in line with the clinically observable quantities (for stage IV disease, see Figure 2.2) and clinically relevant variables of interest for the clinical problem (number and size of secondary tumors).

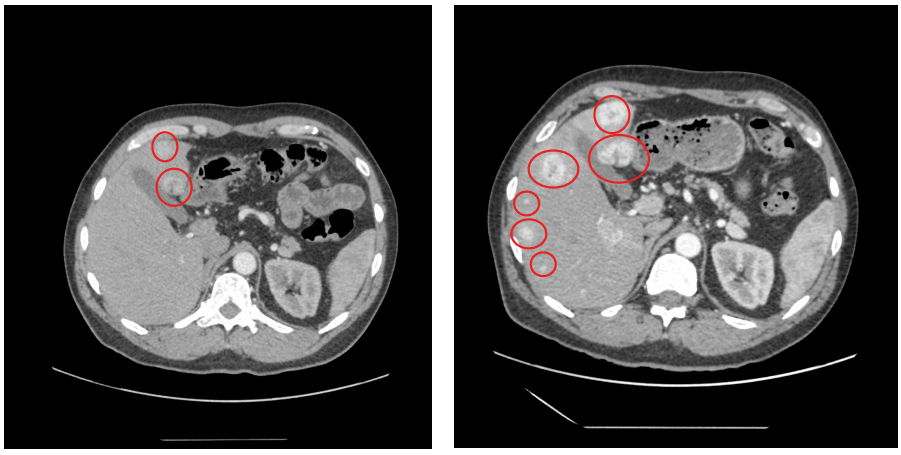

Figure 2.2 – Enhanced CT scan of the liver of a kidney cancer patient with multiple metastatic tumors showing progression of the disease characterized by apparition of new lesions and growth of existing ones. Images courtesy of Dr F. Cornelis (radiology unit, CHU Bordeaux)

The metastatic modeling approach we used mostly follows a formalism initiated by Iwata, Kawasaki and Shigesada [Iwata et al., 2000]. The main idea is to describe the population of secondary tumors

by means of a physiologically structured density $\rho(t, v)$ where t is the time and v is the volume of the lesions. This means that for a small dv, the number of metastases having size comprised in the interval $(v, v + dv)$ is given by $\int_v^{v+dv} \rho(t, u)du \simeq \rho(t, v)dv$. The original model of Iwata et al. was further expanded in three ways by our and others' work: (i) effect of systemic therapies [Benzekry et al., 2012a, Benzekry, 2012a], (ii) systemic growth interactions between established lesions [Benzekry et al., 2014b, Benzekry et al., 2014a] and (iii) use in in vivo human xenograft models involving orthotopic primary tumors (primary tumor) and metastasis both in nonsurgical [Hartung et al., 2014] and surgical [Benzekry et al., 2016] systems. The two main components (growth and dissemination) are modeled by:

1. Presurgical primary (g_p) and secondary (g) tumor growth rates, defined as the infinitesimal tumor size increase per time unit (expressed in [size] $\times$ [time]$^{-1}$)
2. A dissemination rate (d), defined as the infinitesimal number of new metastases per time unit (expressed in [time]$^{-1}$).

A schematic description of the model is depicted in Figure 2.3.

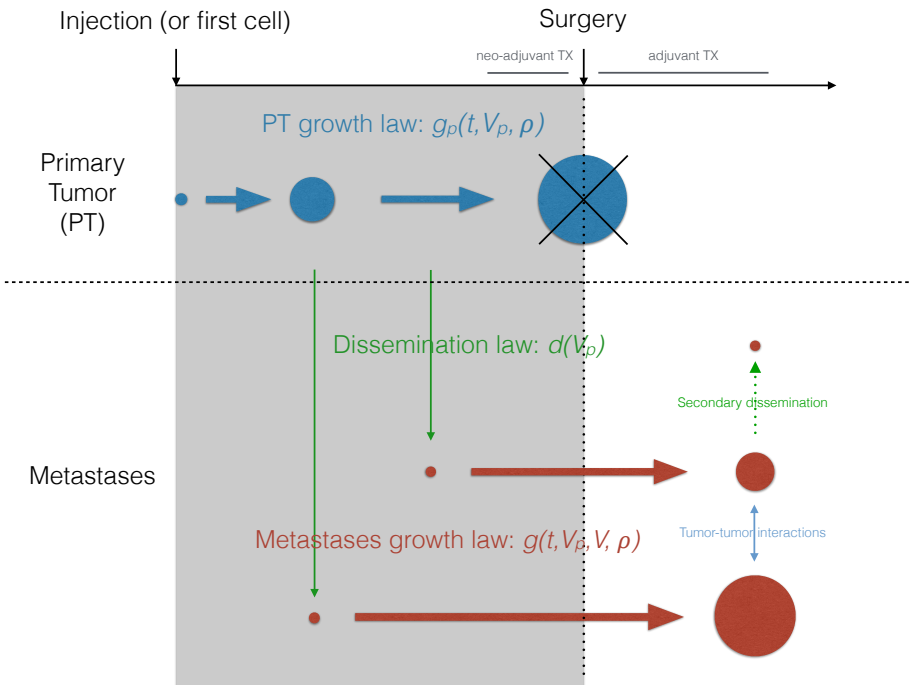

Figure 2.3 – Model scheme for metastatic dynamics divided into growth and dissemination. The grey area represents the pre-surgical phase, often equal to the indolent pre-diagnosis period. The green dotted-line represents the possibility of metastases from metastases. TX = treatment.

Growth Dynamics As in chapter 1, the primary tumor volume $V_p(t)$ solves the following equations

$$\begin{cases} \frac{dV_p}{dt} = g_p(t, V_p, \rho) \\ V_p(t=0) = V_i \end{cases} \tag{1}$$

The initial condition for the primary tumor, denoted by V_i, was determined either by the number of injected cells (for confrontation to *in vivo* experiments) or the initial tumor size at inception (clinical cases, $V_i = 1$ cell). Metastases were assumed to start from one cell (size denoted V_0). When treatment is taken into account, this problem can become non-autonomous [Benzekry, 2012a]. We also included a possible dependency of g_p on ρ to account for possible non-trivial growth interactions between the primary tumor and the mets [Benzekry et al., 2014b, Benzekry et al., 2017]. Note also that for simplicity of the exposition here we considered a tumor state as represented by its volume v only but this can be extended to a multi-dimensional state (such as volume and carrying capacity, see section 2.5 and [Benzekry et al., 2012b, Benzekry, 2011a, Benzekry, 2012a, Benzekry et al., 2014b, Benzekry et al., 2014a, Benzekry, 2012b]).

From our previous study quantifying the descriptive power of several growth kinetics models using data from the same breast animal model (chapter 1), the Gompertz model accurately described primary tumor growth curves. However, a limitation of this model is that the tumor doubling time could become arbitrarily small for small volumes, a feature that we considered biologically irrelevant for volumes at metastatic initiation (of the order of the cell). A lower bound to this doubling time might be expressed by the in vitro doubling time of the cell line, which can be experimentally determined. Consequently, we adopted the Gomp-Exp model [Wheldon, 1988], defined by

$$g_p(v) = g(v) = \min\left(\lambda v, \left(\alpha_0 - \beta \ln\left(\frac{v}{V_0}\right)\right)\right)$$

Under this model, growth is divided between two phases: an initial exponential phase, followed by a Gompertz growth phase. Parameter λ is the maximal proliferation rate that can be comouted from in vitro proliferation assays. The second term in the min function is the Gompertz growth rate, defined by two parameters. Parameter α_0 is the intrinsic relative (also termed specific) growth rate at the size V_0 of one cell. Parameter β is the exponential decay rate of the relative growth rate.

Metastatic dissemination The formation of new metastases was assumed to occur at a volume-dependent rate $d(v)$ having the following parametric expression [Iwata et al., 2000]:

$$d(v) = \mu v^{\gamma} \tag{2}$$

where parameter μ is an intrinsic parameter of metastatic aggressiveness. This critical coefficient is the daily probability for a given tumor cell to successfully establish a metastasis. Therefore, it is the product of several probabilities: (i) the probability of having evolved the necessary genetic mutations to ensure the phenotypic abilities required at each step of the metastatic process, (ii)

the probability of surviving all adverse events occurring in transit including survival in the blood or immune escape, among others, and (iii) the probability to generate a functional colony at the distant site. Following reported observations [Steel and Lamerton, 1966], we assumed that all the metastases were growing at the same volume-dependent rate g and that they all started from the same volume corresponding to the volume of one cell. As for the primary tumor growth, we also allowed g to depend on ρ to account for metastases-metastases growth interactions (note that this transforms the transport equation into a nonlinear one).

$$\begin{cases} \partial_t \rho(t,v) + \partial_v(g(t,v,\rho)\rho(t,v)) = 0 &]0,T[\times]V_0,+\infty[\\ g(t,V_0,\rho)\rho(t,V_0) = d(V_p(t)) + \int_{V_0}^{+\infty} d(v)\rho(t,v)dv &]0,T[\\ \rho(0,v) = 0 &]V_0,+\infty[\end{cases} \tag{3}$$

where T is the final time. The first equation is a continuity equation expressing conservation of the number of metastases when they grow (equivalent to the transport in size). The second equation is a Neumann boundary condition on the flux of entering metastases at size $v = V_0$. Its right hand side is composed of two terms. The first one is the rate of birth of new metastases from the primary tumor. The second (integral term) represents the birth of metastases from metastases themselves, a feature for which there is no clear consensus in the literature [Tait et al., 2004, Sugarbaker et al., 1971, Bethge et al., 2012] and that was not always relevant to our studies but is included here for generality. The third equation describes the initial condition (no metastases at the initial time). From the solution of this problem, two main macroscopic quantities of interest can be derived, the metastatic burden $M(t)$ and the number of metastases $N(t)$. Of note, these have simple expressions when secondary dissemination and tumor-tumor interactions are neglected:

$$N(t) = \int_{V_0}^{+\infty} \rho(t,v)dv = \int_0^t d(V_p(s))ds = \mu \int_0^t V_p(s)^\gamma ds$$

$$M(t) = \int_{V_0}^{+\infty} \rho(t,v)dv = \int_0^t d(V_p(t-s)V(s))ds$$

In the convolution formula for $M(t)$, $V(s)$ represents a solution to the Cauchy problem (1), with g instead of g_p and V_0 as initial condition. This formula allows fast simulation of the model using the fast Fourier transform algorithm [Hartung, 2015], which is essential for estimation of the parameters that requires a very large number of model evaluations.

Discrete and stochastic dynamics Although the formalism described above is very convenient for confrontation to data of the total metastatic burden because of its fast computation formula, a continuous rate of shedding of metastases (and thus, a continuous size distribution ρ) might be debatable. Indeed, metastasis is a discrete event and we are not in the limit of a large number of events that would justify approximation by a continuous rate. Moreover, typical clinical observations typically consist in a finite number of lesions, primarily characterized by their size (Figure 2.2).

Therefore, we also implemented a discrete and stochastic framework of the model (in the case of

negligible secondary dissemination and tumor-tumor interactions). The stochasticity here refers to intra-individual randomness in the metastatic dissemination. The formation of new metastatic foci is assumed to be a sequence of random events exponentially distributed with rate $d(V_p(t))$. The number of metastases follows then a Poisson process $\mathcal{N}(t)$ with intensity $d(V_p(t))$. The appearance time of the i-th metastasis is defined by

$$T_i = \inf \{t \geq 0;\ \mathcal{N}(t) \geq i\}$$

Adapting the previous methodology to the case of randomly distributed dissemination times and denoting $\tilde{\rho}$ the resulting random size distribution of metastases, $\tilde{\rho}$ is a sum of Dirac masses solving the following problem:

$$\begin{cases} \partial_t \tilde{\rho}(t,v) + \partial_v(\tilde{\rho}(t,v)g(v)) = 0 & t \in]0,+\infty[,\ v \in]V_0,+\infty[\\ g(V_0)\tilde{\rho}(t,V_0) = \sum_{i=1}^{+\infty} \delta\left(t = T_i\right) & t \in]0,+\infty[\\ \tilde{\rho}(0,v) = 0 & v \in]V_0,+\infty[\end{cases} .$$

Equivalently, denoting by V_i the volume of the i-th metastasis, we have

$$\begin{cases} \frac{dV_i}{dt} = g(V_i(t)) \\ V_i(T_i) = V_0, \quad V_i(t) = 0, \text{ for } t \leq T_i \end{cases}$$

thus transforming the partial differential equation (3) into a set of differential equations. From these considerations the stochastic total metastatic burden at time t, denoted by $\mathcal{M}(t)$ is defined by the following expression

$$\mathcal{M}(t) = \int_{V_0}^{+\infty} v\tilde{\rho}(t,v)dv = \sum_{i=1}^{+\infty} V_i(t)$$

The two approaches (deterministic and stochastic) are in fact closely and consistently linked. Indeed, it can be shown [Hartung and Christophe, 2014] that the quantities $M(t)$ and $N(t)$ defined above in the deterministic framework are the respective expectations of $\mathcal{M}(t)$ and $\mathcal{N}(t)$.

2.3 Spontaneous metastasis following surgery in clinically relevant animal systems

Introduction

The dearth in experimental metastatic data stems largely from the complexity of studying metastasis itself. While clinical (retrospective) data have value [Klein, 2009, Slack et al., 1969, Yorke et al., 1993, Coumans et al., 2013, Koscielny et al., 1984], mouse tumor models have typically aimed to mimic (and distinguish between) several stages of the metastatic process. In certain mouse models, metastasis can derive from a tumor that is implanted ectopically or orthotopically into a primary or metastatic site ("ectopic", "orthotopic", or "ortho-metastatic" models, respectively [McMillin et al., 2013]) and can involve various immune states (i.e., human xenograft or mouse isograft). Although more rarely performed, models can also include surgical resection of the primary tumor, which allows for progression of clinically relevant spontaneous metastatic disease. These can include surgery following ectopic implantation (i.e., "ecto-surgical", such as tumors grown in the ear or limb that are later amputated), or orthotopic implantation and resection (i.e., "ortho-surgical"), which more faithfully represent patient disease. To date, no studies have utilized data from ortho-surgical metastasis models for mathematical analysis.

Results

The data used in this study were obtained by the laboratory of J. Ebos at the Roswell Park Cancer Institute by M. Mastri and A. Tracz. They are derived from two ortho-surgical metastasis models representing competent and incompetent immune systems with luciferase-tagged human breast (LM2-4$^{\mathrm{LUC+}}$) and mouse kidney (RENCA$^{\mathrm{LUC+}}$) cell lines (Figure 2.4A). The luciferase tagging of the cells allowed to longitudinally track the post-surgical growth of the total number of metastatic cells within the mice organisms, together with the pre-surgical primary tumor size.

The objective was to confront the mathematical formalism from the previous section to experiment in order to establish parsimonious[10] models of the metastatic dynamics for each experimental system. To do so, we combined our mechanistic model of metastatic development with the nonlinear mixed effects framework for parameters estimation (see the statistical prelude). A lognormal distribution of the parameters and a proportional error model were assumed. This allowed us to test different model assumptions, such as the functional expression of the primary tumor and metastases growth laws (exponential or Gomp-Exp) and the relationships between them (same or different growth law, same or different growth parameters). For each case, the optimal structure resulting from our investigations was to assume the same structural growth law for the primary tumor and the metastases, although with possibly different parameter values.

For the human breast (LM2-4$^{\mathrm{LUC+}}$) metastasis system, the best identifiable[11] description model

[10] i.e., minimally parameterized
[11] in the sense of "acceptable" standard errors on the parameters estimation, i.e. inferior to 50%

included growth dynamics defined by the Gomp-Exp growth model and growth parameters for primary tumor and metastases treated identically ($g = g_p$).

For the kidney (RENCA$^{\mathrm{LUC+}}$) metastasis system, the optimal model considered growth dynamics defined by an exponential growth model and growth parameters for primary tumor and metastases treated differently.

In each case, we could fit our data equally well with various values of the parameter γ from the dissemination coefficient (2), and thus concluded that it cannot be identified from combined primary tumor growth and metastatic burden dynamics data alone [Benzekry et al., 2016]. Future studies would require more data, especially on the number and size distribution of the secondary lesions, to precisely determine the shape of the dissemination coefficient. Adopting thus the simplest theory, we assumed that all the cells within the tumor had equal metastatic potential and took $\gamma = 1$.

Importantly, combinations of the mechanistic model and the mixed-effects framework could quantify the dynamics of the process as well as the inter-animal variability. The latter was better characterized by the metastatic potential parameter μ (large coefficients of variation [Benzekry et al., 2016]). Resulting population and individual fits of the best models to the data are shown in Figure 2.4B and C, and Figure 2.5, respectively. Notably, the models were able to accurately predict metastatic dynamics in independent data sets where surgery was performed on a different day, and that were not used during the parameters estimation process (Figures 2.4.C and E).

Our quantitative modeling study allowed us to better understand the metastatic process and identify differences between the two experimental systems. For the breast model, inference of μ revealed small metastatic potential (median value 4.43×10^{-11} cell$^{-1}\cdot$ day^{-1} with considerable inter-animal variability (coefficient of variation of 176%)), which translated into late development of metastases following xenograft and growth of the metastatic burden mostly dominated by proliferation (Figures 2.4B and 2.5A–C). In contrast, the kidney model metastatic burden growth curves exhibited a different behavior, with a marked change of regimen at the time of surgery. In the context of the model, this means that most of the presurgical increase was driven by the dissemination process, and not by proliferation of the metastases themselves. This was reflected by a very large value of μ (median value 4.15×10^{-2} cell$^{-1}\cdot$ day^{-1}), with nine orders of magnitude of difference compared with the breast model. This feature was not directly visible, nor quantifiable, by direct examination of the data, and reflects the large metastatic aggressiveness of isograft spontaneous metastasis animal models, because overpassing the immune surveillance is a major challenge in the metastatic process [Hanahan and Weinberg, 2011]. When the primary tumor was removed, dissemination stopped and only proliferation remained for further metastatic growth, which happened at a slower rate than at the primary site (Figures 2.4C and 2.5D–F). In some cases, growth of the metastatic burden remained constant or even decreased after surgery. This result reflects the fact that the competent immune status of the mice might have an important impact on the establishment of durable, fast-growing metastatic colonies at the secondary sites [Milsom et al., 2013].

Together, our data-based quantitative modeling analysis of presurgical primary tumor and postsur-

gical metastatic burden growth kinetics demonstrated the ***descriptive and predictive power of the models****, unraveled* ***distinct growth patterns*** *between the two animal models, and emphasized the critical role of the parameter* μ *for* ***quantification of the inter-animal variability in metastatic aggressiveness****.*

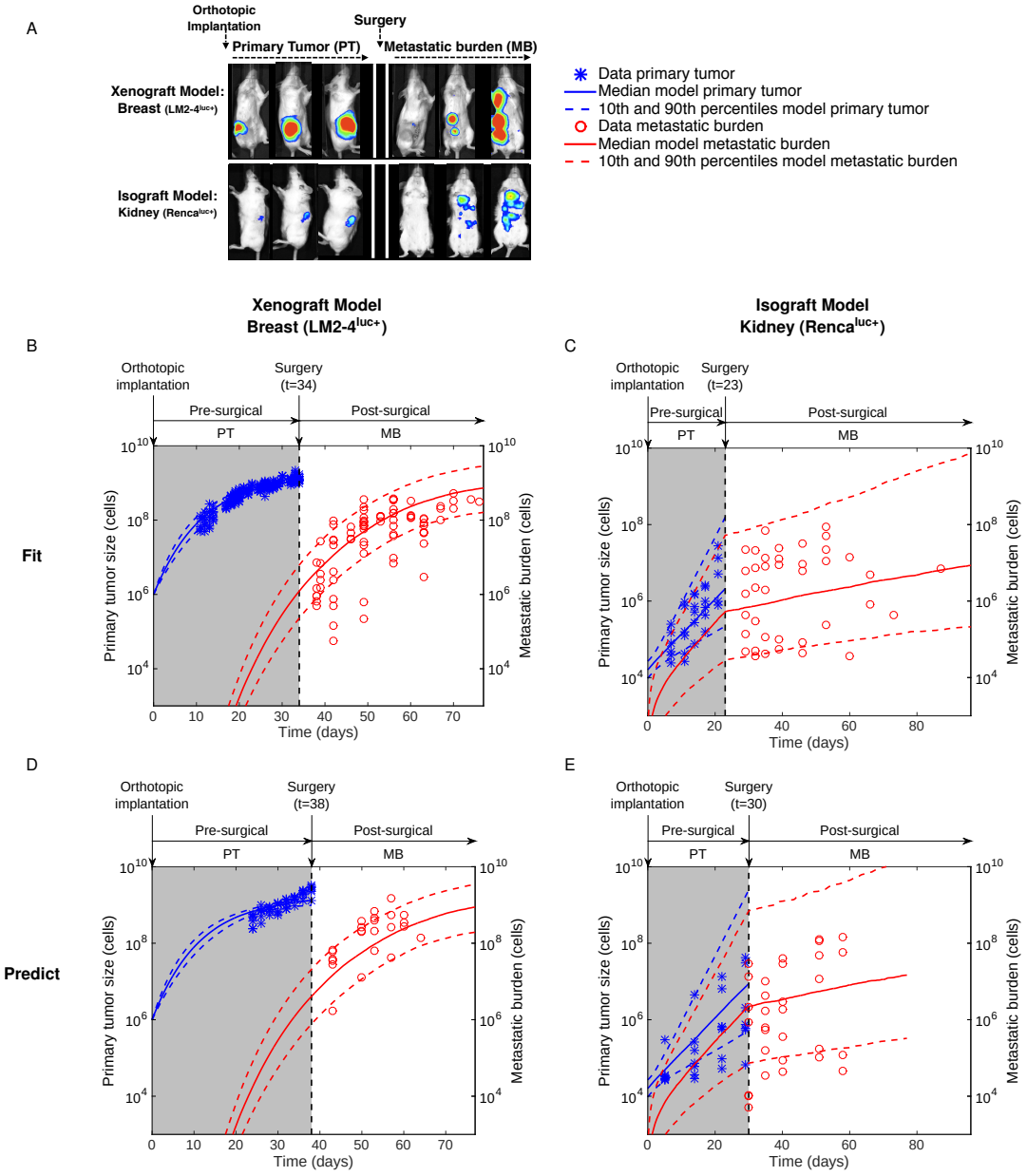

Figure 2.4 – Population fits and predictive power using perioperative data from ortho-surgical metastasis models. A, spontaneous metastasis were generated following orthotopic tumor cell implantation and then primary tumor resection ("ortho-surgical") in two models: (i) human xenograft model: intramammary fat pad implantation of 1×10^6 LM2-$4^{\mathrm{LUC+}}$ human metastatic breast carcinoma cells followed by surgical excision after 34 and 38 days (two separate experiments, N = 22 mice total) and (ii) mouse isograft model: subcapsular implantation of 4×10^4 $\mathrm{RENCA}^{\mathrm{LUC+}}$ mouse kidney carcinoma cells followed by full surgical nephrectomy 23, 26, and 30 days after implantation (N = 19 mice total). Representative examples of presurgical (primary tumor) and postsurgical (MB) bioluminescence. B and C, using a nonlinear mixed-effects modeling approach, a distribution of the parameters was estimated from the data, which, in turn, generated a distribution of model outputs (pre- and postsurgical growth curves). The solid lines depict the median of these distributions and the dashed lines the 10th and 90th percentiles. The population fit of the kidney data was established using two datasets with two resection times, only one of which is presented here for the sake of clarity. D and E, from the population fits obtained, the predictive power of the models was assessed against independent datasets with different resection times.

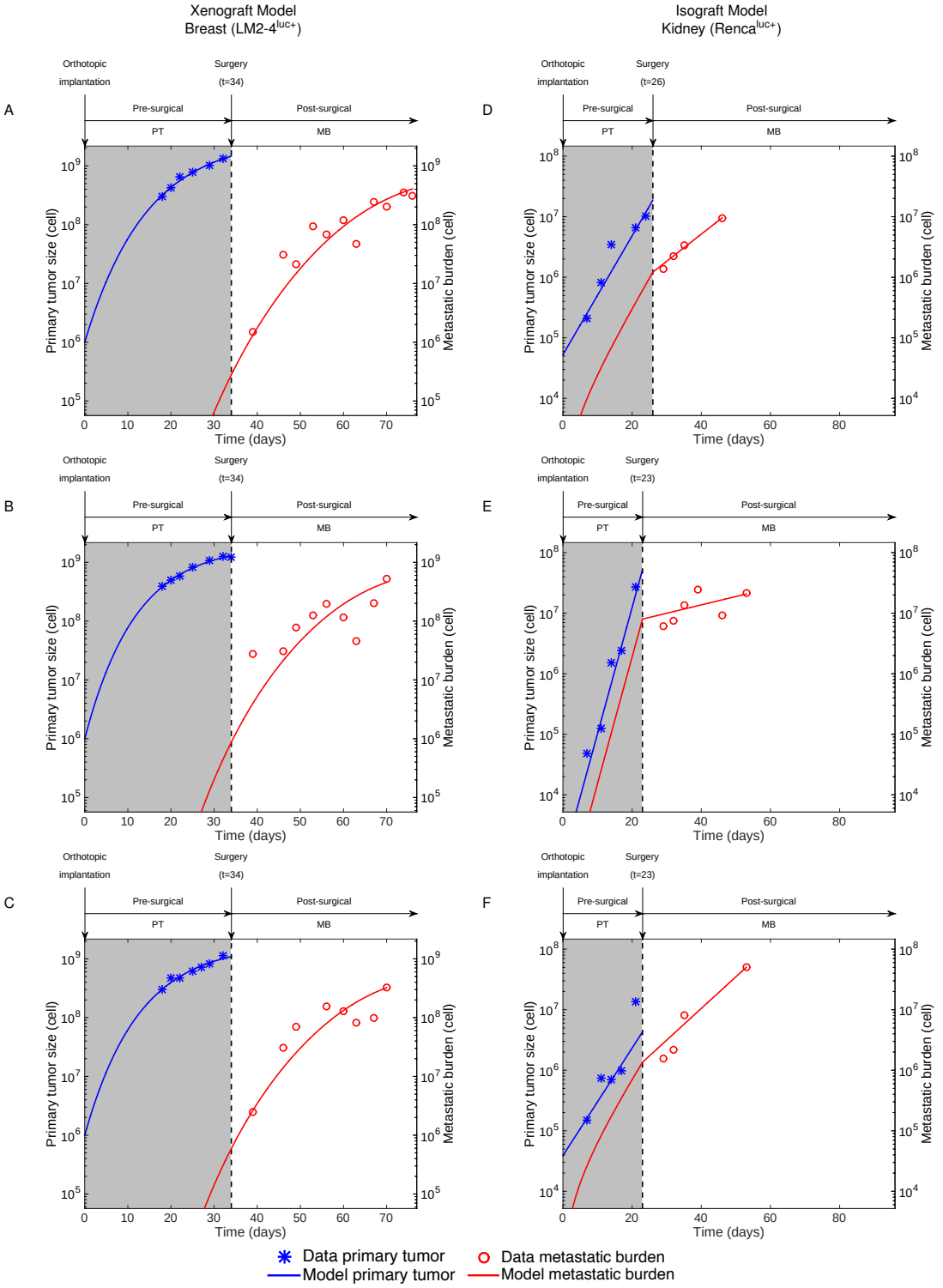

Figure 2.5 – Individual fits of perioperative primary and secondary disease in breast and kidney ortho-surgical metastasis systems. A–C, xenograft breast case. Gomp-Exp growth model for both primary and secondary tumors, with same growth parameters (3 degrees of freedom in total). D–F, isograft kidney case. Exponential growth for both primary and secondary tumors with different growth parameters (3 degrees of freedom total). For each animal, the fit was performed on the primary tumor first and then the metastatic burden. We only show here three representative examples for each dataset. All the individual fits can be found in the supplementary material of [Benzekry et al., 2016]

2.4 Challenging the classical view of metastatic initiation and growth

In a subsequent biological study of the metastatic process usin the same kidney cancer animal model as above (renal adenocarcinoma cell line RENCA orthotopically injected in the subcapsular space of Balb/c mice), although without surgery of the primary tumor, we had access to more precise multi-modal data about the metastatic development, including magnetic resonance images (MRI) quantifying the number and size of macroscopic vascularized lesions in a non-invasive and longitudinal fashion. This allowed to question the "standard" model of metastatic dissemination and growth as classically considered in the literature and so far in our mathematical modeling framework, formulated in the biological problem 3 that we recall here:

Biological problem 3. *Is the "standard" view of metastatic initiation and growth – that secondary lesions once established grow without interactions with each other or with the primary tumor – valid for description of the dynamics of the number and size of metastases?*

This study was performed in collaboration with a team of biologists at the "Laboratoire de l'Angiogénèse et du Micro-environnement des Cancers" led by A. Bikfalvi (Inserm, Bordeaux, FR) and composed of W. Souleyreau and L. Cooley on one hand, and a team specialized in magnetic resonance imaging for *in vivo* experiments in small animals (E. Ribot and S. Miraux, magnetic resonance of biological systems center, Bordeaux, FR). The modeling work was performed in the framework of E. Baratchart's PhD that I co-supervised with T. Colin and O. Saut [Baratchart, 2016].

Two sources of quantitative data were available for analysis. First, cells were tagged with a green fluorescent protein (GFP), which allowed quantification of the number of cells in a given sample by means of quantitative real-time polymerase chain reaction (see [Baratchart et al., 2015] for experimental details). This also permitted detection of single cells in a lung tissue slice through optical microscopy, thus estimating the appearance of the first metastatic cells in the lungs approximately 14 days after inoculation of the RENCA cells in the kidney (Figure 2.6). However, a drawback of this experimental technique was that sacrifice of the animal was required for quantifications and thus no longitudinal data within the same animal could be extracted. Therefore, GFP data points presented here represent each a given animal ($n = 31$ animals in total). Second, MRI data allowed detection of metastases but only when larger than a visibility threshold (of the order of 0.05 mm^3). A great advantage of this technique was its non-invasiveness, thus allowing longitudinal observations in the same animal ($n = 6$ mice in total were repeatedly imaged). At MRI, the first macro-metastases were observed at day 18-19 (Figure 2.6).

2.4.1 Data-driven modeling of metastatic development

Growth rates of individual metastatic tumours Assuming that each metastasis originates from one cell would imply that some metastases grow from the volume of one cell ($\simeq 10^{-6}$ mm^3), to

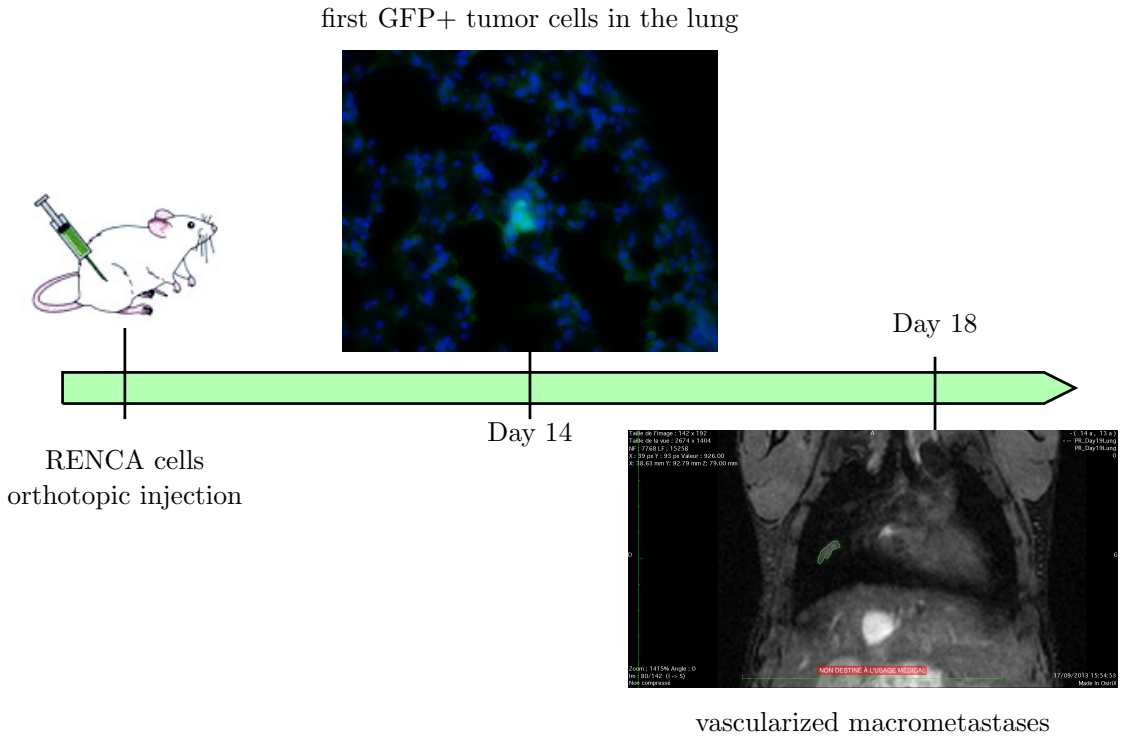

Figure 2.6 – The animal model. At day 14 after GFP+ RENCA cells injection, the first tumor cells were observed in the lungs (in green). At days 18-19, the first macro-metastases were observed by MRI.

a volume of few mm^3 (between 0.022 and 12 mm^3 in our measurements) in five days at most. This would give tumor doubling times comprised between 5 and 8 hours, which represents less than one third of the doubling time observed in vitro (24.5 hours [Miyake et al., 1999]). Even if considering that the metastases arose from a few cells (2–50) instead of one [Liotta et al., 1976b, Aceto et al., 2014], this would imply doubling times between 5.5 and 13.5 hours. These would also have to remain constant during 5 days. Such a fast growth is highly improbable since no mammalian cell has a cell cycle length smaller than 10 hours [Steel and Lamerton, 1966]. Moreover, as expressed in chapter 1 the doubling time has been reported to be non-constant and to increase during in vivo growth. Hence, growth at initiation would have to be even faster in order to fit the data. Therefore, the theory consisting in describing each metastasis with a tumour expansion only based on cell proliferation seemed unlikely.

Primary kidney tumor and the dynamics of lung metastasis The standard theory of metastatic development assumes that secondary tumors are seeded from the primary tumor and that, once established at the distant sites (the lungs in our case), they grow independently from each other and from the rest of the organism [Gupta and Massagué, 2006, Talmadge and Fidler, 2010, Fidler and Paget, 2003, Talmadge et al., 1982, Fidler and Talmadge, 1986, Klein, 2009], as distinct foci initiated by single or few cells. To test this theory, we used our mathematical

formalism as described above, and the following strategy. First the model was fitted to the GFP data quantifying primary tumor and total metastatic burden growths, thus allowing inference of the growth and dissemination parameters (with quantification of their inter-animal variability and estimation uncertainty). Second, the resulting predictions in terms of number and size of macroscopic metastases were compared to the MRI data. In contrast to the previous findings, for this non-surgical experimental study, we found that the model best adapted was a Gomp-Exp growth model for both the primary and secondary tumors, with same growth parameters (see [Baratchart et al., 2015] for details).

Data from the primary tumour and the metastatic burden were fitted together, and the model demonstrated satisfactorily descriptive power for the total metastatic burden (Figure 2.7).

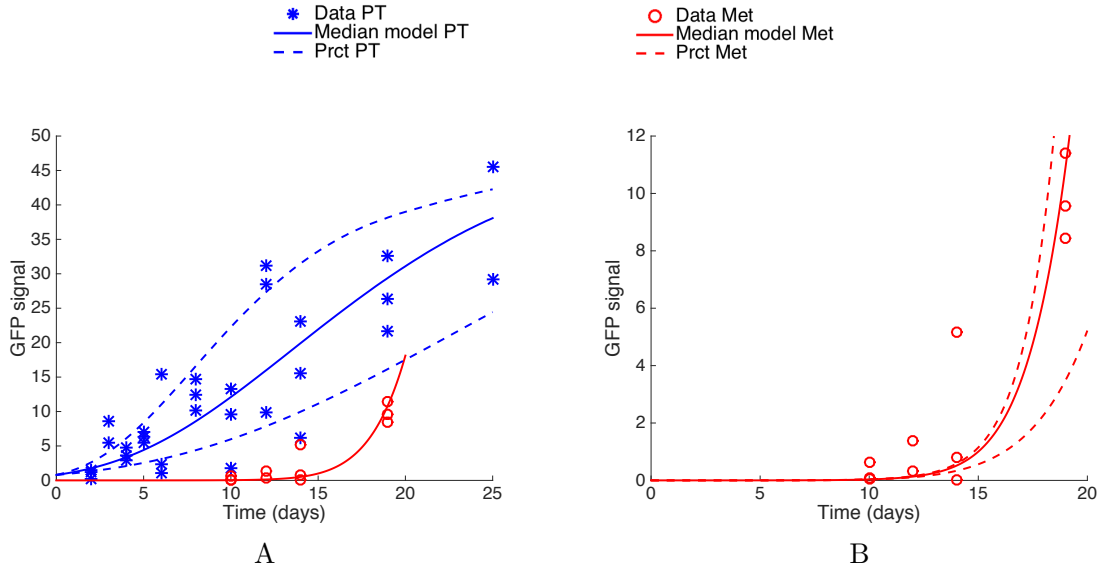

Figure 2.7 – The standard theory: Primary tumor and metastatic burden dynamics fit. (A) Fits of the primary tumor and metastatic burden dynamics, under a mathematical model assuming independent growth of each secondary tumour and using mixed-effects modeling for statistical representation of the population distribution of the parameters and measurement error. (B) Fit on the metastatic burden. In panels (A) and (B), each data point corresponds to one distinct mouse (n = 31 animals in total). PT = Primary Tumor. Met = Metastatic burden. Prct = 10% and 90% percentiles

The calibrated model was further used to predict the distribution of macro-metastases visible in the MRI images, and to confront this prediction to the observations. Among the MRI data, images of only one mouse (over 6) were eligible for reliable assessment of the complete size distribution of macro-metastases, which was performed by manual segmentation of metastatic lesions in each of the 142 coronal slices of the MRI (resolution 156 µm x 155 µm x 155 µm), for each time point. In the other mice, the images had no sufficiently defined contours to properly establish a complete size distribution of the metastases. In the mouse where number and size of the lesions could properly be assessed, the smallest detectable metastasis had a volume of 0.05 mm^3, which was taken as the

minimal visibility threshold. Results of the model simulation for the metastatic size distribution are reported in Figure 2.8A, together with the experimental data. Inter-animal variability was simulated using the population (lognormal) distribution of the parameters distribution retrieved from the population mixed-effects fit. The maximal volumes predicted by the model/standard theory were considerably smaller than those observed by MRI. For example, at T = 19 days, while the total metastatic burden was similar in the data and in the model (Figure 2.7), the macro-metastatic burden was three-fold larger in the data than in the model's average prediction (Figure 2.8B), and the largest metastasis five-fold larger. At T = 26 days, although macro-metastatic burdens were similar in the data and in the model, the standard theory predicted that the largest tumor would have a volume of only 1.14 mm^3 in average (standard deviation = 0.755 mm^3), while the largest observed metastasis had a volume more than 10 fold larger (13.6 mm^3). This was compensated by a considerably larger number of metastatic lesions in the model (95.4 ± 47 versus 11 in the data). For each of these quantities, the p-value (probability to obtain the data value – or larger – under the null hypothesis that the data would have been generated by the model, evaluated numerically) was statistically significant ($p < 10^{-5}$).

A

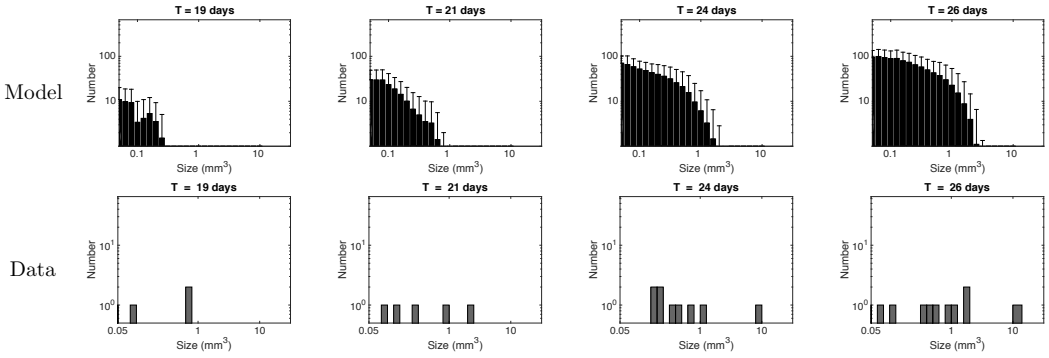

B

T	19		21		24		26	
	Data	Model	Data	Model	Data	Model	Data	Model
Number	4	4.8 (2.7)	5	17.6 (9.52)	9	52.9 (27.5)	11	95.4 (47)
Macro-burden (mm^3)	1.58	0.524 (0.361)	3.55	2.47 (1.8)	11.5	12.2 (9.94)	21.2	28.6 (24.4)
Size of largest met (mm^3)	0.78	0.143 (0.089)	2.19	0.326 (0.221)	8.17	0.766 (0.535)	13.6	1.14 (0.755)

Figure 2.8 – Time course of the macro-metastases size distribution: standard model versus observations. (A) Top row: Simulation of the mathematical formalism of the standard theory (i.e. dissemination and independent growth of the resulting tumour foci), using the parameter values inferred from the data of the total metastatic burden (total GFP signal in the lungs). Only tumors larger than the visible threshold at MRI (0.05 mm3) are plotted. Shown are the results of 1000 simulations, mean + standard deviation. Bottom row: Observations of macro-metastases numbers and sizes in one mouse on MRI data. (B) Comparison of several metrics derived from the metastatic size distributions. For the model, numbers are represented as mean value and standard deviation in parenthesis. The data corresponds to the mouse presented in the upper histogram.

These conclusions were limited by the fact that the entire time course of metastatic size distribution

of only one mouse was available for reliable comparison with the model. However, in all the 6 mice, the size of the largest metastasis at day 19 could be measured and ranged 0.45 - 12 mm^3, which was significantly larger than the model predictions ($p < 10^{-5}$, z- test). The largest metastases predicted by the model ranged $9.5 \times 10^{-4} - 0.3$ mm^3. This strongly suggested that the standard theory was not able to describe the volumes of individual foci. Moreover, even without statistical comparison of the model's predictions to the empirical data, the numbers predicted by the model (in particular the number of macro-metastatic lesions at day 26) seem highly unrealistic. To assess the robustness of our results regarding several assumptions of the model, we investigated varying several parameters, including the initial size of metastatic foci and the power in the dissemination coefficient (see [Baratchart et al., 2015] for details). The results confirmed our conclusions.

Our findings strongly indicated that the standard theory of metastatic progression, as described by the model employed here (i.e., dissemination and independent growth), when calibrated to data of total metastatic burden, was in contradiction with experimental observations of number of metastatic foci and their size distributions.

For the same total metastatic burden, the model predicted much more lesions with smaller size than present in the data. It was beyond the scope of our study to elaborate (and validate) a unified model able to recapitulate the behavior of metastatic tumors during the colonization process. However, as a first step toward this objective, we put forward two possible hypotheses to correct the inconsistency of the standard theory: 1) non-trivial interactions between metastases and 2) interactions between the metastatic foci and the circulating tumor cells (cells attraction). The plausibility of the first point was actually retrospectively demonstrated by observations of two metastases merging in our data (between days 21 and 24, see Figure 2.9) and therefore decided to investigate this further. More specifically, we wanted to address the following questions: do spatial interactions have an impact on the dynamics of the total metastatic burden? To what extent could this correct the theoretical predictions of the unlikely fast growth rates? Answers to these questions have implications on future theoretical models of metastatic development.

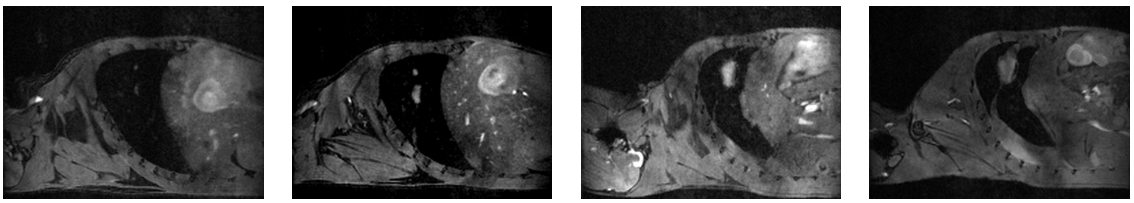

Day 19 Day 21 Day 24 Day 26

Figure 2.9 – Metastases merging. From left to right: Sagittal slices of the lungs from day 19 until day 26 for the same mouse. Two tumors are growing close to each other and merge between days 21 and 24.

2.4.2 Spatial interactions between metastatic tumors

The possibility of merging for two neighboring metastases introduces a spatial aspect of metastatic colonization and, therefore, requires a spatial modeling approach. During his PhD work, E. Baratchart derived such a model which had to full-fill the following requirements: 1) it should be based on biological knowledge of macroscopic tumor growth (retrieved from the literature), 2) it should remain as parsimonious as possible (minimal number of parameters) and 3) it should be able to fit our spatial growth data.

The model that was developed belongs to the class of continuum mechanics-based mixture models. It describes a saturated flow in a porous medium comprising two entities, the tumor tissue and the healthy tissue, with P denoting the tumor cell density and S the healthy cell density. The third variable is a pressure field Π. The model describes, on a domain Ω, the passive motion of the tissues due to the increase in volume caused by proliferation. Following others [Ambrosi and Preziosi, 2002] in using Darcy's law for description of the velocity field v and writing mass-balance equations for the tissue densities, we have:

$$\begin{cases} \partial_t P + \operatorname{div}(vP) = \gamma P \\ \partial_t S + \operatorname{div}(vS) = S \\ v = -k\nabla\Pi \end{cases}$$

Writing the saturation condition $P + S = 1$, summing the two first equations leads and using the third one leads to

$$\begin{cases} -k\Delta\Pi = \gamma P \\ \Pi_{|\partial\Omega} = \Pi_{\text{eq}} \end{cases}$$

where Dirichlet boundary conditions were considered to represent the homeostatic pressure of the body Π_{eq}. The main characteristic of the model was to consider, following works of others on tumor tissue biophysical properties [Montel et al., 2012, Stylianopoulos et al., 2013, Stylianopoulos et al., 2012], that the growth rate γ was a decreasing function of Π. This was modeled by a decreasing exponential law [Montel et al., 2012]:

$$\gamma(\Pi) = \gamma_0 \exp\left(-\frac{\Pi}{\Pi_0}\right).$$

Under the assumption of a constant porosity, the value of k has no impact. Indeed, as long as the product $k\Pi_0$ remains constant, the solution remains unchanged. That is why we fixed $k = 1$. Moreover, the boundary condition was taken homogeneous: $\Pi_{\text{eq}} = 0$. Therefore, *in fine*, the model depended only on two parameters, consistently with our previous results that demonstrated (chapter 1) that two degrees of freedom are sufficient to describe tumor growth curves. Indeed, the

model was able to fit longitudinal growth of four metastases observed by MRI (Figure 2.10[12]). The fits were performed on the volume only and considering the metastases as spherical, which allowed to derive explicit formula useful to establish bounds on the parameter space (see [Baratchart, 2016] for details).

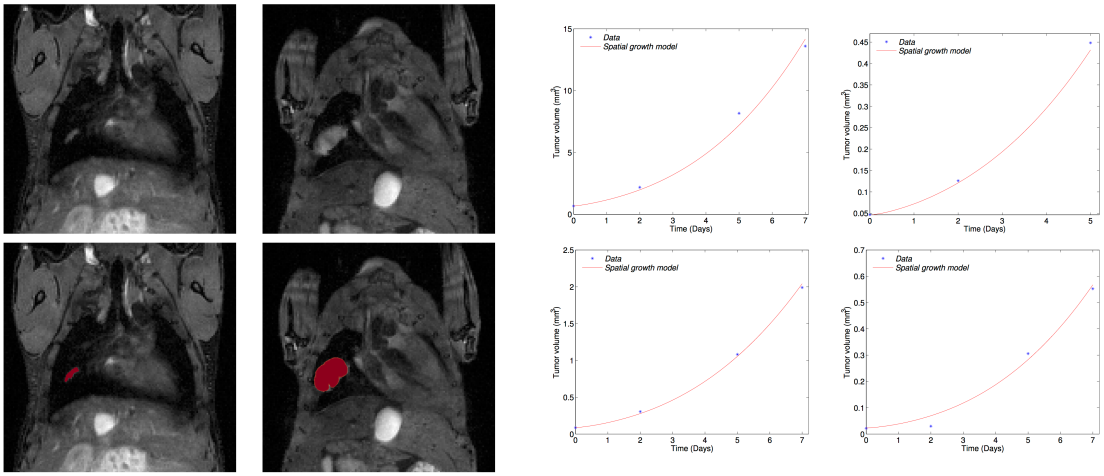

A B

Figure 2.10 – Spatial model fitting. (A) Top: Coronal MRI data of the lungs at days 19 and 26. Bottom: the simulated growth by the model using the fitted parameters and starting from the real shape of the observed metastasis at day 19 on the coronal MRI slice. (B) Volumes compared to simulations by the fitted model for the growth of four individual metastasis.

Endowed with this calibrated model of pressure-mediated tumor growth, we studied the quantitative impact of tumor merging on growth and found in simulations that the growth of two close tumors (initial distance of 0.2 mm) would result in a 31% ± 1.5% smaller total size after 7 days compared with a situation with two independent, non-merging tumors [Baratchart et al., 2015] (see also `https://www.youtube.com/watch?v=hTEy-O-oMMU` for a movie of the spatial growth of two mechanically interacting tumors). We also investigated whether the merging of metastatic foci could have generated the formation of macro-metastases in the observed timeframe (from one cell at day 14 to a macroscopic size at day 19) with biologically realistic growth rates. We investigated the two situations: without spatial interactions (i.e., assuming the volume resulting from the merging as equal to the sum of the metastatic foci volumes), and with spatial interactions. To do so, we performed four simulations with the four fitted parameter sets, starting from one cell, to estimate the number of merging metastatic foci required to obtain the respective observed volumes (of 0.022, 0.046, 0.085 and 0.67 mm^3) seven days after initiation (day nineteen). Indeed, we chose day twelve and not day fourteen (which was the time at which the first metastatic cells were observed by direct examination of lung tissues) as the starting day because the GFP signal started to rise at day twelve (Figure 2.7). As can be seen in Table 2.1, since spatial interactions reduce the growth velocity, the number of metastases was higher when interactions were taken into account.

[12]See also a movie of the simulation at the following url: `https://www.youtube.com/watch?v=FbATGHFjj3s`

Because of potential variability (error measurements during the segmentation, differences between the MRI signal and the real lesion, especially for the small metastases, modeling assumptions), the estimated numbers of required metastatic foci may give only a rough estimate. For two of the metastases (Meta 2 and Meta 4), the estimated numbers appear to be reasonable. On the other hand, for the two other ones, the required number ranged respectively between 301 and 375 and between 1300 and 2100, which were probably too large to be biologically realistic.

	Without spatial interactions	With spatial interactions
Meta 1	1337	2127
Meta 2	20	65
Meta 3	301	375
Meta 4	40	70

Table 2.1 – Number of required merging foci to grow from one cell to a macro-metastasis in 7 days

The inability of the merging theory to fully explain all of the observed volumes may indicate that besides merging by passive motion due to proliferation, other mechanisms such as chemokine-mediated cells attraction occur [Kaplan et al., 2005, Hiratsuka et al., 2006]. Circulating tumor cells may be attracted by some established niches and explain the abnormally fast volume expansions that we observed. Indeed, such chemokine-mediated attractions are presumed to play an important role for the pre-metastatic and metastatic niches establishment, in mediating myeloid and tumor cells attraction [Kaplan et al., 2005, Hiratsuka et al., 2006, Psaila and Lyden, 2009]. Moreover, chemo-attractants may play a role in tissue tropism of metastatic cells [Joyce and Pollard, 2009]. Chemotactic gradients can attract metastatic cells that express the chemokine receptor to specific locations. In subsequent work, additional phenomena such as aggregation and recruitment of cells during the metastatic process from the circulation have been integrated in a more elaborate mathematical model [Baratchart, 2016]. Another phenomenon that could possibly explain the observed volumes would be the presence of circulating tumour cell clusters that would give rise to metastases [Aceto et al., 2014]. Indeed, the authors of this study recently showed in a breast cancer animal model that metastases do not originate from single cells only but also from tumor cells clusters that have a higher metastatic potential than single cells. However, they did not show evidence of this phenomenon for kidney cancer and in their experiments, clusters were formed by at most 50 cells. As shown in our study [Baratchart et al., 2015], this order of magnitude of the initial cell numbers that colonizes the lung was not able to describe the dynamics of metastasis formation in our model and experimental data.

Taken together, although spatial interactions might play an important role for the dynamics of metastasis development in the lung and probably also in other organs., it is unlikely that they alone control metastasis expansion. Other mechanisms are probably also involved such as recruitment of additional cells from the blood stream and micro-environmental cues such as nutrient depletion or responses to environmental stress.

2.5 A theoretical model of "cancer without disease"

While we studied contact interactions between two tumors in close vicinity in the previous section, distant systemic interactions between tumors possibly in distinct organs have also been evidenced since more than one century [Demicheli et al., 2008]. From a modeling point of view, we published two studies on these phenomena [Benzekry et al., 2014b, Benzekry et al., 2017]. The first was focused on secondary tumors dormancy and investigated the possibility of global dormancy (also called "cancer without disease" [Folkman and Kalluri, 2004]). The second took a step back and –instead of directly considering a primary tumor and a population of metastases – focused as a first step on the dynamics of two tumors growing simultaneously in the same organism, with the objectives of quantitatively interrogating classical theories of concomitant resistance and validate a mathematical model of tumor-tumor growth interactions.

2.5.1 Introduction

Almost all of us carry small tumor lesions that for many will not progress to symptomatic disease. Indeed, as evidenced in autopsy studies for adults without pre-established cancer such as [Welch and Black, 2010, Black and Welch, 1993], occult lesions are present in most healthy adults. Nielsen et al. [Nielsen et al., 1987] found that, out of 110 women cases, among which only one had been previously treated for breast cancer, 22% had at least one malignant lesion. Moreover, 45% of these had multicentric lesions. Similar results have been reported for prostate cancer in men [Sánchez-Chapado et al., 2003]. For thyroid cancer, autopsy results [Black and Welch, 1993] showed a prevalence rate of 99.9% for occult carcinomas, while incidence of thyroid cancer is only 0.1% [Folkman and Kalluri, 2004].

To explain these results, it is necessary to understand the tumor dormancy phenomenon. Tumor dormancy [Aguirre-Ghiso, 2007, Almog, 2010] is defined by stable or very slow tumor growth. It can happen at the cellular level as a malignant cell remaining quiescent for a long period before awakening, but here we focused on the mm-scale lesions such as have surfaced in the several remarkable autopsy studies discussed, i.e., tissue-level tumor dormancy. Although the sizes of these dormant tumors remain almost constant, it is not due to a cessation in cell proliferation, but rather to increased apoptosis that leads to a near zero net growth rate [Holmgren et al., 1995]. Clinically, tumor dormancy has been observed in breast cancer [Nielsen et al., 1987, Retsky et al., 2008, Retsky et al., 2010, Brackstone et al., 2007], melanoma [Ossowski et al., 2010] and prostate cancer [Sánchez-Chapado et al., 2003], among many others [Aguirre-Ghiso, 2007]. Dormancy is particularly relevant to the situation where secondary tumors (metastases) remain small and undetectable for extended periods.

Various explanations have been proposed for tumor dormancy, among these being the achievement of a balance between stimulation and inhibition of angiogenesis [Almog et al., 2006, Almog, 2010, Hahnfeldt et al., 1999]. This mechanism offers one explanation for how secondary tumors may be suppressed to a near-dormant state by the primary; a phenomenon known as 'concomitant

resistance' [Prehn, 1993, Chiarella et al., 2012]. In fact, a number of explanations for the concomitant resistance phenomenon have been suggested, and were investigated in a subsequent study (see below). Because of evidence that concomitant resistance happens in immune-deficient mice [Gorelik, 1983] and considering the large and unequivocal body of support for the role angiogenesis inhibition plays in the maintenance of tumor dormancy [Holmgren et al., 1995, O'Reilly et al., 1994, O'Reilly et al., 1997, Rofstad and Graff, 2001, Volpert et al., 1998, Sckell et al., 1998] and the "angiogenic switch" [Hanahan and Folkman, 1996] in escape from dormancy, our focus here will be on the last theory. Angiogenesis, the process of creating new blood vessels and developing a supporting vascular network, was put forward by J. Folkman [Folkman, 1971] to be critical for tumor growth. Indeed, without development of new blood vessels, a malignant neoplasm cannot grow further than about 2 to 3 mm in diameter, due to nutrient supply limitations [Folkman, 1971]. This process is regulated by the release from cancer cells of stimulatory growth factors, such as vascular endothelial growth factor (VEGF), that induce proliferation, migration and maturation of surrounding endothelial cells, as well as the production of angiogenesis inhibitory factors that act to curtail endothelial expansion [Folkman, 2007]. As an example, in 1994 when examining the growth of Lewis lung carcinoma in a syngeneic murine tumor model, O'Reilly et al. [O'Reilly et al., 1994] discovered an endogenous molecule having an inhibitory effect on angiogenesis, which they called 'angiostatin', followed soon by the discovery of 'endostatin' [O'Reilly et al., 1997]. Endogenous anti-angiogenic molecules were also evidenced in human cancer, an example being thrombospondin-1 [Volpert et al., 1998]. Overlaying the ability of tumors to stimulate vasculature, the discovery of their ability to also inhibit it [Folkman, 1995b] allows for the possibility that tumors may indirectly control their own growth [Hahnfeldt et al., 1999, Folkman, 2007, Folkman, 1995a], perhaps as a vestige of normal organ growth control. Further, inherent to this self-control notion, if the inhibitors were longer-lived and thus more persistent in the circulation, they could have the collateral effect of suppressing angiogenesis and growth at distant metastatic sites as the tumor mass gets large [Hahnfeldt et al., 1999]. Indeed, the half-life of angiogenesis stimulators has been reported to be on the order of minutes for VEGF [Folkman, 1995a], while that for angiogenesis inhibitors is on the order of hours [O'Reilly et al., 1994, Volpert et al., 1998].

2.5.2 Mathematics of systemic inhibition of angiogenesis

To describe the time dynamics of a metastatic population under systemic inhibition of angiogenesis (SIA), we employed a similar framework as previously introduced (section 2.2), although extended to a bi-dimensional "trait" for the state of a tumor. Tracking of tumors not only through their size/volume (one-dimensional model) but also with their vascular-dependent carrying capacity K (two-dimensional) had been previously developed by us to extend the initial Iwata, Kawasaki and Shigesada model [Iwata et al., 2000] in order to account for the angiogenic process in tumor growth [Benzekry, 2011b, Benzekry et al., 2014a, Benzekry, 2011a, Benzekry, 2012b]. The density ρ is now a function $\rho(t, V, K)$, the physiologically structured density of metastases having volume V and carrying capacity K at time t. Denoting by $G(V, K, V_p, \rho)$ the tumors' growth rate, the model

writes:

$$\begin{cases} \partial_t \rho + \mathrm{div}(G\rho) = 0 &]0,T[\times\Omega \\ G(V_0,K_0,V_p,\rho)\rho(t,V_0,K_0) = \delta_{(V,K)=(V_0,K_0)}\left(d(V_p(t)) + \int_\Omega d(v)\rho(t,v,k)dvdk\right) &]0,T[\times\partial\Omega^+ \\ \rho(0,V,K) = 0 & \Omega \end{cases} \tag{4}$$

where $\Omega = (V_0,+\infty)\times(0,+\infty)$ is the physiological domain of possible sizes and carrying capacities, δ is the Dirac mass (see [Benzekry, 2012b] for details about the measure nature of the solution of this equation, in the linear case) and $\partial\Omega^+$ stands for the subset of the boundary where the flux is pointing inward.

The main modeling effort consisted then in defining a biologically relevant value of the growth rate G. Following the approach of [Hahnfeldt et al., 1999] we assumed

$$G(V,K,V_p,\rho) = \begin{pmatrix} aV\ln\left(\frac{K}{V}\right) \\ Stim(V,K) - Inhib(V,K,V_p,\rho) \end{pmatrix}$$

In the previous expression, the first line is the rate of change of the tumor volume V (where a is a constant parameter driving the proliferation kinetics of the cancer tissue) and the second line is the rate of change of the carrying capacity K. The main idea of this tumor growth model was to start from a gompertzian growth of the tumor volume (or any carrying capacity-like growth model [d'Onofrio and Gandolfi, 2004]) and to assume that the carrying capacity K is a dynamical variable representing the tumor environment limitations (here limited to the vascular support) changing over time. The balance between a stimulation term $Stim(V,K)$ and an inhibition term $Inhib(V,K,V_p(t),\rho(t,V,K))$ governs the dynamics of the carrying capacity. For the stimulation term we followed [Hahnfeldt et al., 1999] and assumed

$$Stim(V,K) = bV$$

where the parameter b is related to the concentration of angiogenic stimulating factors such as VEGF. This last quantity was derived to be constant in [Hahnfeldt et al., 1999] from the consideration of very fast clearance of angiogenic stimulators [Folkman, 1995a].

For the inhibition term, Hahnfeldt et al. [Hahnfeldt et al., 1999] only considered a local inhibition coming from the tumor itself. Our main modeling novelty was to consider in addition a global inhibition coming from the release in the circulation of angiogenic inhibitors by the total (primary + secondary) population of tumors. Writing a diffusion equation for the local production of inhibitors, solving it and computing the average spatial amount of these factors, we finally obtained (see [Benzekry et al., 2014b] for details of the calculations)

$$G(V,K,V_p,\rho) = \begin{pmatrix} aV\ln\left(\frac{K}{V}\right) \\ bV - dV^{2/3}K - eIK \end{pmatrix}$$

where e is an inhibition efficacy coefficient and I is the amount of circulating inhibitors, given by

$$\begin{cases} \frac{dI}{dt} = pV_p + \int_\Omega pv\rho(t,v,k)dvdk - kI \\ I(t=0) = 0 \end{cases} \tag{5}$$

with p the inhibitor production rate and k an elimination rate. The expression of d was also established to depend on the diffusion coefficient of inhibitors D, pharmacokinetics volume of distribution V_d, e and p:

$$d = eV_d \frac{p}{15D^2} \left(\frac{3}{4\pi}\right)^{2/3} \tag{6}$$

For the primary tumor, we assumed the same structural growth model. The dynamics of (V_p, K_p) was thus given by

$$\frac{d}{dt}\begin{pmatrix} V_p \\ K_p \end{pmatrix} = G_p(V_p, K_p, V_p, \rho)$$

where G_p had the same expression as G, except that the parameters a_p and b_p (the values of a and b that are associated with the function G for the primary) may be different from a and b associated with metastases. The inhibitor production rate p and effect of the inhibitor e were assumed to be the same for the primary and secondary tumors, which implied same value also for d in view of formula (6).

2.5.3 Biological results

At the time of this study, we did not dispose of quantitative experimental data sets about metastatic development allowing the inference of biologically relevant parameters. Therefore, for estimation of the growth and dissemination parameters, we employed published data on primary tumor growth as well as number and mean size of metastases [Huang et al., 2002]. For the determinant parameter p of inhibitor production, we derived its value from observations of [O'Reilly et al., 1994] that demonstrated that injection of 12.5 µg per day of recombinant human angiostatin reproduced the systemic inhibition due to the presence of a primary tumor removed when it reached the size of 1500 mm^3. We refer the interested reader to [Benzekry et al., 2014b] for methodological details.

Simulation of the cancer history from the first cancer cell predicted uncontrolled metastatic burden

Using our model and based on the parameters estimated from literature data, we were able to extrapolate to a totally new setting where the primary tumor starts with one cell instead of an already large number of cells (approximately 10^5). In so doing, we were able to simulate the whole cancer natural history, starting from one initial cancerous cell (and initial carrying capacity of 1 mm^3) until the metastatic burden reached 5000 mm^3, a burden we considered potentially lethal for a mouse. The simulation predicted this would happen 62.7 days after the first primary tumor

cancer cell. Time development of the primary tumor volume, metastatic burden, total number and mean size of metastases as well as inhibitor amount in the host are plotted in Figure 2.11.

Interestingly, the model simulation predicted that the metastatic burden would overcome the primary tumor mass, implying that the mouse would probably die from growth of its secondary lesions rather than from the initial tumor. This is consistent with the metastatically aggressive phenotype of the 4T1 cell line. Quantification of the number of metastases revealed a final number of about 217 tumors, lots of them being small (Figure 2.11A) and probably undetectable in an experimental setting. Simulation with the same set of parameters but neglecting the effect of SIA ($I = 0$) showed no detectable difference on this time frame. Significant changes were observed later on, for volumes that were not considered to be physiologically relevant. This confirms that for the 4T1 cell line, metastases do develop and do not exhibit global dormancy, even when SIA is present with the inhibitor production parameter value extracted from [O'Reilly et al., 1994].

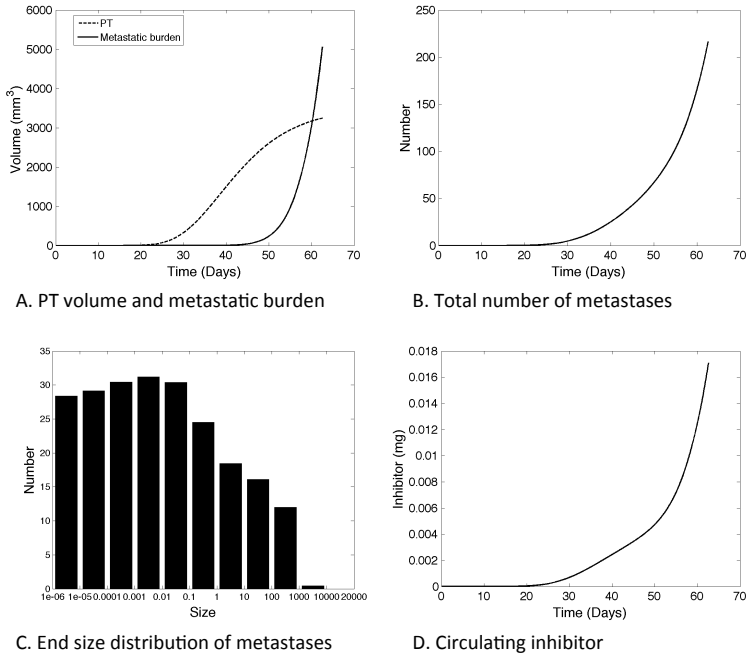

Figure 2.11 – Simulation of the natural cancer history from the first cancer cell. Size expressed in mm^3.

Higher production of systemic angiogenesis inhibitor could result in long-term stable global dormancy in a population of self-inhibiting metastases

The previous simulations used parameter values derived from experimental data of a situation were metastases do develop and grow, because this is the only case where metastases are measurable and data are available. However we are interested here in global dormancy and situations where the

metastatic population could remain ultimately small. We postulated that this could happen when production of the angiogenesis inhibitor, represented by parameter p in our model, is significantly higher. Simulation results plotted in Figure 2.12 were obtained using a value of p a value about 30 times that extracted from [O'Reilly et al., 1994]. In this context, the first cancer cell initiated the disease by growing and generating a first pool of metastases, but the metastatic burden then quickly overshadowed the growth of the primary lesion (Figure 2.12A). The primary tumor reaches a small maximal size of $21.2\,\mathrm{mm}^3$ at time 82.9 days (Figure 2.12A) and then shrunk due to inhibition of angiogenesis provoked by the distant metastases. There was a slowdown and eventual stabilization of the metastatic burden, with a plateau value of about $2200\,\mathrm{mm}^3$. The burden was composed of a large number of metastases (Figure 2.12B), most of them being occult micro-metastases as can be seen in the final size distribution (Figure 2.12C). This interesting feature of the model simulation could be an in silico replicate of the aforementioned situations of cancer without disease [Folkman and Kalluri, 2004]. In our model it translates into an asymptotical steady state for the metastatic burden while still composed of small lesions. The general dynamics of the metastatic burden results from the balance of two stimulating forces; growth and spread of new individuals, competing with systemic inhibition of angiogenesis. Stimulation depends on the parameters a and b, which capture the growth process, and μ and γ, which capture spreading. Inhibition depends on e and k, as well as on p, which controls the value of d. The present values of the parameters generated long-term stabilization of the mass. The size distribution of the population of secondary tumors at time $T = 350$ days was revealed to be non trivial, with different numbers in the various size ranges. By this time, all the metastases had volume lower than 10 mm^3.

In sum, assuming substantial systemic inhibition of angiogenesis, we theoretically obtained an *in silico* replicate of a situation in which an important population of dormant micro-metastases inhibiting each others' growths is present, with a possibly non-lethal final total metastatic burden. This situation was seen to result when a 30-fold higher value for the inhibitor production compared to the case of growth of a breast cancer line 4T1 extracted from the literature, where unlimited expansion of the total metastatic burden was forecast. Our analysis showed that SIA could conceivably create such a situation, although it would require a very high value of the inhibitor production rate, which does not appear to be physiological. This suggests that SIA alone is probably not sufficient to induce spontaneous global dormancy and that other processes (such as immune effects) are probably significantly involved. This motivated us to study this phenomenon further and design a study of interactions among multiple tumor implants in controlled immune contexts (see below and [Benzekry et al., 2017]).

2.5.4 Mathematically intriguing nonlinear dynamics

In a subsequent study, we focused on the variety of dynamical behaviors possibly generated by the model [Benzekry et al., 2014a]. After nondimensionalization, we explored the growth/dissemination/inhibition balance by varying the values of parameters b (for growth), μ (for dissemination) and e (for inhibition). Simulation results of individual increase of each parameter from a baseline value are reported in Figure 2.13. As appears, disruption of the base regime of parameters (where

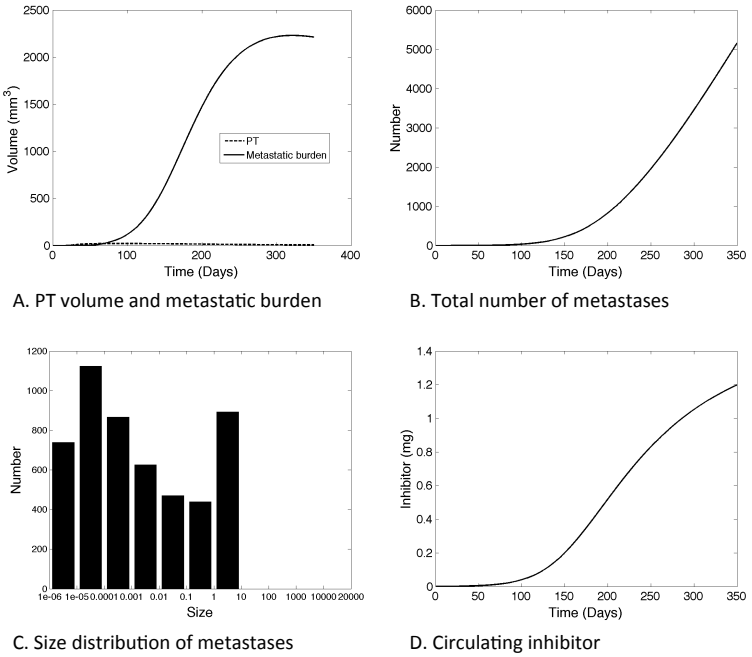

Figure 2.12 – Simulation of the cancer history from the first cancer cell.

all the forces in presence were in relative equilibrium, generating a bounded oscillatory regime for the total metastatic burden) towards more pronounced impact of either of the constitutive processes of our model generated more complex dynamics. Different parameters had different impacts on the global behavior. Potentiation of the growth velocity (as well as resistance to the inhibition pressure) through increase of b resulted in an asymptotic behavior of the global metastatic burden which, while still being periodic, repeated a much more complex pattern, revealing interesting underlying dynamics. In particular, observation that the same value of the metastatic burden did not always yield the same future evolution implies that no autonomous ordinary differential equation can be derived for the dynamics of $M(t)$, since same values of M at different times lead to different future evolutions. Indeed, when $M(t)$ returns to a previous value, the state of the global dynamical system is different because the composition of the tumors population (represented by ρ) itself is not the same. Interestingly, this happens despite the fact that the growth rate depends on ρ only through M.

Increase of μ resulted in densification of the oscillations and amplitude increase, yielding sharp repeated peaks of metastatic growth. Violent increases of the total metastatic burden were followed by similarly violent decreases that made the system reach almost-zero values. Stronger inhibition pressure delayed the stabilization of the system to an oscillatory regimen, intensified the oscillations frequency and lowered their amplitude. Note that in this situation, as well as in the base situation, the total metastatic volume remained away from zero, suggesting a non-negligible amount of long-lasting residual disease.

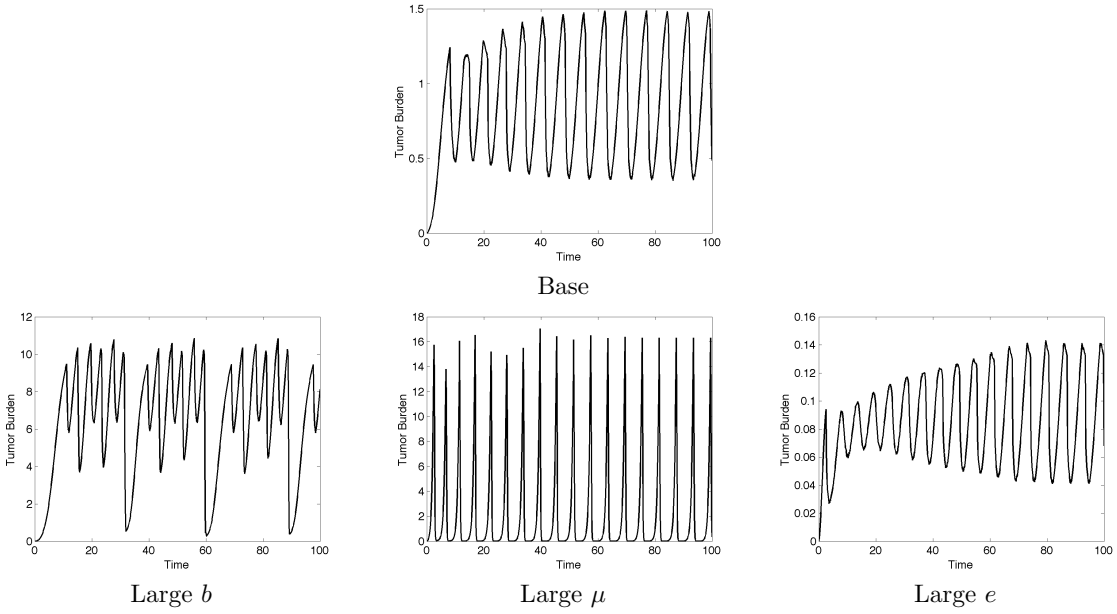

Figure 2.13 – Dynamics of the metastatic burden under 10 fold increase of representative parameters. Size expressed in mm^3.

Turning our interest to the opposite situation, i.e. 10 fold decrease of the individual parameters, showed yet other interesting behaviors, for which we refer the interested reader to [Benzekry et al., 2014a]. These included the possibility of an homeostatic state of the system where all the forces in presence equilibrate to give a stable state where metastases don't grow while still remaining present in the organism, possibly with small volumes that would make the micro-metastases undetectable. We also observed bounded non-periodic dynamics as well as periodic but tormented patterns, underlining the complexity of the dynamics of the density (Figure 2.14). On the opposite to this widely varying behavior, the model numerically exhibited convergence to a steady state for the total metastatic burden when initial conditions (for both primary tumor and metastases) were set to $(V_0, K_0) = (10^{-4}, 10^{-3})$. Same apparent convergence also occured for the number of metastases $N(t)$ and the amount of inhibitor $I(t)$. Looking closer to the volume distribution of metastases at the end of the simulation revealed concentration of the density to the smallest possible volume, suggesting convergence to a Dirac mass located in (V_0, K_0).

2.6 A combined *in vivo/in silico* study of tumor-tumor interactions

Motivated by the previous theoretical considerations and by the clinical problem of post-surgical metastatic acceleration due to an inhibitory growth pressure from the primary tumor, we decided to

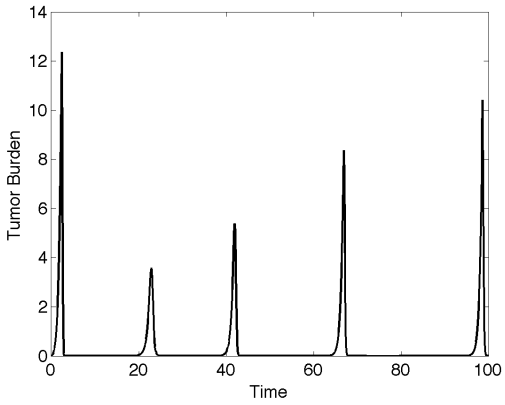

$\mu = 10$, $k = 0.1$

Increasing sharp relapses

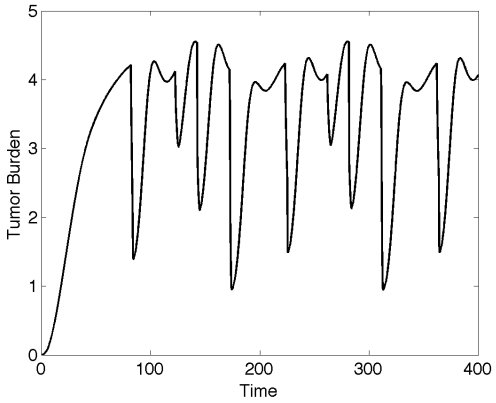

$\mu = 0.1$, $k = 0.1$, $e = 0.02$

Complex periodic behavior

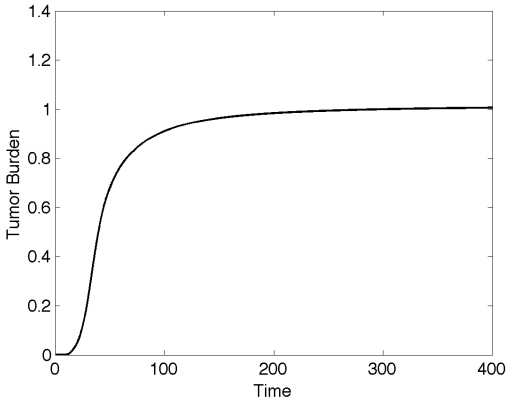

$V_0 = 10^{-4}, \quad K_0 = 10^{-3}$

Possible convergence to a stable equilibrium

Figure 2.14 – Examples of other interesting dynamics.

conduct an experimental study of the phenomenon of tumor-tumor interactions [Benzekry et al., 2017]. To build on solid ground, instead of directly studying the tumor-metastases system, we decided to investigate first the interactions of two tumors growing distantly in the same organism (a phenomenon also termed "concomitant resistance"). The objectives were to: 1) investigate the relative likelihood of existing theories of this phenomenon (retrieved from a thorough review of the literature) and 2) establish and validate a minimal mathematical model, biologically grounded and with identifiable parameters.

2.6.1 Introduction

Concomitant tumor resistance (CR) is a phenomenon by which the presence of a tumor in an organism negatively influences the appearance and growth of another implant (see [Chiarella et al., 2012] for a review). It has been reported in numerous experimental studies spanning over a century, and implementing a large variety of animal models [Marie and Clunet, 1910, Gershon et al., 1967, Dewys, 1972, Gunduz et al., 1979, Gorelik et al., 1981, Gorelik, 1983, Ruggiero et al., 1985, Fisher et al., 1983, Sckell et al., 1998, Li et al., 2001, Demicheli et al., 2008]. These studies investigated either the concomitant or subsequent implantation of a second graft after a primary injection [Gershon et al., 1967, Simpson-Herren et al., 1976, Gunduz et al., 1979, Gorelik, 1983, Ruggiero et al., 1985, Li et al., 2001], or the inhibition of secondary tumors arising from the primary (metastases) [Marie and Clunet, 1910, Dewys, 1972, Gorelik et al., 1978, O'Reilly et al., 1994, Rofstad and Graff, 2001]. They consistently evidenced a systemic growth suppression effect, demonstrated by the occurrence of post-removal growth acceleration [Marie and Clunet, 1910, Ketcham et al., 1961, Simpson-Herren et al., 1976, Gorelik et al., 1978, Gunduz et al., 1979, Fisher et al., 1983, Fisher et al., 1989, O'Reilly et al., 1994, Peeters et al., 2008]. In the clinic, suppression of the growth of metastases by the presence of the primary tumor has yet to be appreciated in general therapeutic planning, although it has been reported in patients [Coffey et al., 2003, Peeters et al., 2006, Peeters et al., 2008, Ceelen et al., 2014]. However, despite the abundance of reports of this phenomenon, the precise determinants of CR remain poorly understood and only qualitative theories have been advanced.

CR is of direct clinical relevance insofar as it implies that removal of a primary tumor, with the resultant release of its inhibitory pressure on occult secondary sites, could be followed by post-surgery metastatic acceleration (PSMA). PSMA has been demonstrated to occur in numerous animal experiments [Marie and Clunet, 1910, Simpson-Herren et al., 1976, Gorelik et al., 1978, Gunduz et al., 1979, Fisher et al., 1989], as well as in clinical case reports [Coffey et al., 2003, Peeters et al., 2006, Ceelen et al., 2014]. Further support for the occurrence of PSMA in a notable fraction of patients was also provided by the observation of two peaks in the hazard relapse rate of a large cohort of breast cancer patients [Demicheli et al., 1996, Coffey et al., 2003, Demicheli et al., 2007, Retsky and Demicheli, 2014].

Several hypotheses have historically been proposed for the explanation of the underlying mechanism of CR. The first was due to P. Ehrlich and consisted in athrepsia, i.e. that two (or more) tumors in the same organism would compete for nutrients and that the growth of one tumor would leave less nutrients available for the other ([Ehrlich, 1906], cited by [Gorelik et al., 1981]). However, this was challenged by the observations that CR was decreased when the number of inoculated cells was increased [Ruggiero et al., 1985]. Another popular theory, first introduced by Bashford in 1908, was based on immunologic mechanisms and stipulated that the presence of a first tumor would activate an immune response preventing the second graft to take or grow [Gershon et al., 1967, Gorelik et al., 1981]. However, several studies demonstrated the occurrence of CR in tumor models with no or weak immunogenicity, or in immune-deprived mice, thus challenging this explanation [Dewys,

1972, Gorelik et al., 1981, Gorelik, 1983, Ruggiero et al., 1985]. This implies that, although immunologic factors might contribute to CR, they cannot explain it entirely.

As explained previously, in the 1990's, a team led by J. Folkman discovered endogenous inhibitors of angiogenesis by demonstrating that injection of these factors could substitute for the suppressive effect on lung metastases exerted by the primary tumor [O'Reilly et al., 1994, O'Reilly et al., 1997]. This led the investigators to link CR to distant systemic inhibition of angiogenesis.

The idea of circulating inhibiting factors due to the presence of a primary tumor had been proposed and confirmed in earlier studies [Dewys, 1972, Gorelik et al., 1981], but their precise mode of action has remained elusive. Distinct from the angiogenesis inhibitors previously mentioned, another research group identified other blood-borne factors with direct anti-proliferative action, namely meta- and ortho-tyrosine, that would reduce proliferation by driving tumor cells into a G0-phase state of dormancy or induce an S-phase arrest [Ruggiero et al., 2011, Ruggiero et al., 2012].

So far, arguments and theories about CR have remained qualitative in nature. In the study published in [Benzekry et al., 2017], comparing alternative mathematical formalisms, we demonstrated that a simplified model with well-motivated parameters that addresses concomitant resistance specifically was able to capture features of coupled tumor growth and may shed more light on the understudied subject of systemic controls in cancer, a potentially critical step toward eventually understanding metastatic control.

2.6.2 Mathematical modeling of concomitant resistance

More than 40 models in total were constructed and tested against our data. They were based on different structural expressions formalizing the three main theories of CR considered here: distant inhibition of proliferation, distant inhibition of angiogenesis and competition.

Volumes of the two tumors at time t were denoted $V_1(t)$ and $V_2(t)$ and differential equations were derived for the rate of change of these quantities. For biological relevance, we required that the models comply with the following conditions: 1) in the absence of a second tumor, the models had to be able to fit single-tumor growth curves, 2) the shape of the inhibition effect had to be identical from tumor 1 on tumor 2 as from tumor 2 to tumor 1 (structural symmetry) and 3) the parameters had to be identical for the two tumors (parametrical symmetry).

The source of the observed difference between the two growing tumors was assumed to result from an initial (small) discrepancy in the number of cells that took during the tumors grafts, respectively denoted $V_{0,1}$ and $V_{0,2}$. After investigation of the sensitivity of several models to these quantities and their ratio, we considered more relevant for robustness of the results to fix their ratio for all the animals (25% percent higher cell loss in the inhibited tumor as compared to the non-inhibited one).

The model that was ultimately considered as giving the most robust and identifiable description of our data was based on the proliferation-inhibition theory and relied on experimental evidence from [Ruggiero et al., 2011, Ruggiero et al., 2012] demonstrating that a tumor produces inhibitory

factors (IF), such as meta- and ortho-tyrosines, that induce a cell cycle arrest (Figure 2.15).

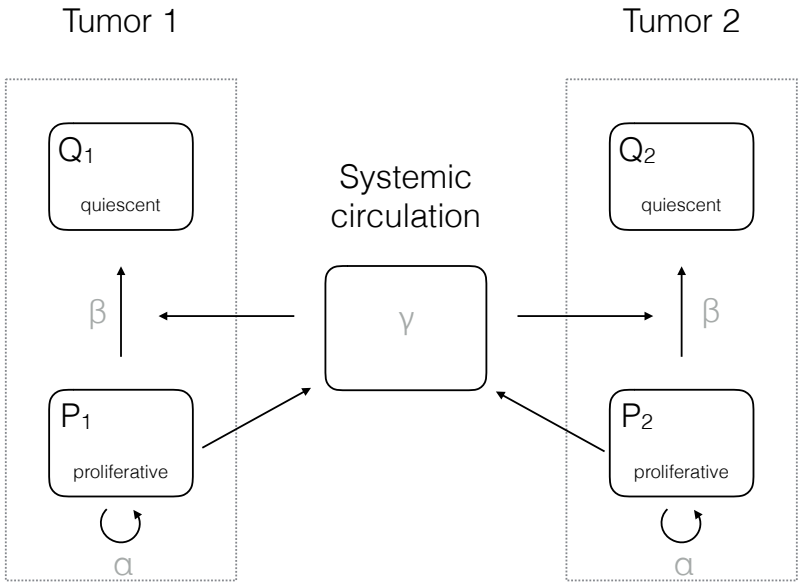

Figure 2.15 – Scheme of the proliferation-inhibition model

The model assumptions are:

- Proportionality between volume and number of cells, using the conversion rule $1\,\mathrm{mm}^3 \simeq 10^6$ cells.
- Each tumor volume is divided into two compartments: proliferative cells (P_i with i the tumor index) and non-proliferative tissue (Q_i).
- Proliferative cells have a constant length of the cell cycle τ. The proliferation rate $\left(= \frac{\ln(2)}{\tau}\right)$ is denoted α (day^{-1}).
- Proliferative cells release IFs with a rate proportional to their number. The proportionality coefficient is denoted β_0 and is expressed in $\mathrm{mol{\cdot}mm^{-3}{\cdot}day^{-1}}$. There is a local elimination of IFs with rate k_{loc} (day^{-1}) and the concentration is assumed to be at steady state.
- A fraction ϕ of these factors is released into the systemic circulation.
- In the blood, IFs are subject to a first order elimination process with rate k (day^{-1}). We assume that the time scale of the blood distribution is faster than the tumor growth and thus consider the blood concentration at steady-state. Assuming that a fraction ψ reaches the distant site, the concentration of IFs at the distant site is therefore $\psi \frac{\beta_0 \phi}{k} P_i$. At the local site it is $\frac{\beta_0(1-\phi)}{k_{loc}} P_i$.
- At each local site, the IFs induce a proliferation arrest, making cells go from a proliferative state to a quiescent state. A given amount of these molecules provokes cell cycle arrest of

a constant *number* of proliferative cells (in contrast to a constant *fraction* usually employed log-kill law valid for cytotoxic agents on leukemic cells [Skipper, 1965]), with rate β_1 ($\text{mol}^{-1}\cdot \text{mm}^3\cdot \text{day}^{-1}$). Denoting $\beta = \frac{\beta_0(1-\phi)}{k_{loc}}\beta_1$ (day^{-1}) and $\gamma = \psi\frac{\beta_0\phi}{k}\beta_1$ ($\text{day}^{-}1$) the number of cells going from a proliferative state to a quiescent state within the tumor i is thus $\beta P_i + \gamma(P_i + P_j)$. Note that this includes both local inhibition and global inhibition, which accounts for factors released by the other tumor (tumor j) but also tumor i itself.

The model then writes:

$$\begin{cases} \frac{dP_1}{dt} = \alpha P_1 - (\beta P_1 + \gamma\,(P_1 + P_2))\,\mathbb{1}_{P_1>0} & P_1(t=0) = V_{0,1} \\ \frac{dQ_1}{dt} = (\beta P_1 + \gamma\,(P_1 + P_2))\,\mathbb{1}_{P_1>0} & Q_1(t=0) = 0 \\ V_1 = P_1 + Q_1 & \\ \frac{dP_2}{dt} = \alpha P_2 - (\beta P_2 + \gamma\,(P_1 + P_2))\,\mathbb{1}_{P_2>0} & P_2(t=0) = V_{0,2} \\ \frac{dQ_2}{dt} = (\beta P_2 + \gamma\,(P_1 + P_2))\,\mathbb{1}_{P_2>0} & Q_2(t=0) = 0 \\ V_2 = P_2 + Q_2 & \end{cases} \tag{7}$$

The Heaviside functions $\mathbb{1}_{P_i>0}$ (equal to one if $P_i > 0$ and zero elsewhere) stand for the fact that when factors are present but no proliferative cells exist, no cells go to quiescence. In particular, they ensure that the solutions (understood in the weak sense due to the discontinuous nature of the Heaviside function) remain positive.

The equations of the other 4 models reported in our study, including those formalizing competition for nutrients and distant inhibition of angiogenesis, are shown in the Table 2.2.

2.6.3 Results

We studied the phenomenon of CR by combining experiments and mathematical modeling, informed by pre-existing theories in the literature. For the experiments, two groups were considered. The first group (control) consisted of twenty mice in which single implants were performed. In the second group (double tumors, abbreviated as DT) consisting of ten mice, two grafts with identical load (10^6 cells) were performed on day 0, at the same locations on opposite flanks of the mice. We refer the reader to [Benzekry et al., 2017] for a complete description of the materials and methods.

In a mouse bearing two tumors, one has normal kinetics and the growth of the other is suppressed

We first performed a direct (i.e., not model-based) statistical analysis of the data. We compared control tumor growth kinetics in mice bearing single implants with the growth curves of tumors in a double-tumor bearing host (Figure 2.16). Observations of the kinetics of each tumor in the

DT group suggested that in each mouse, one tumor was growing faster than the other, possibly inhibiting the second one (Figure 2.16A). This behavior was observed consistently in all the animals of the DT group except in two of them (animals 2 and 9 in Figure 2.16A), and did not seem to result from the lateral location (left or right) of the tumors. Intriguingly, the two mice where the phenomenon was not observable were found to have a connecting blood vessel joining the two tumors and were the only ones to exhibit this macroscopic vascular structure. Direct sharing of same vasculature seemed to equilibrate tumor expansions. One possible explanation for the absence of cross growth suppression in these mice could be that the production of inhibitors was negligible in these tumor-host systems. This could also explain the formation of the connecting blood vessel due to increased neo-angiogenesis (under the theory of angiogenesis inhibition-driven growth suppression).

In order to statistically confirm that this observation was not purely due to intrinsic randomness in experimental conditions (such as the number of initial cells that "take" from the injection) that would by themselves generate different growth curves for the two implants in the same mice, we performed a statistical analysis. It aimed at testing the null hypothesis that both tumors would be identically and independently growing (i.i.g.). We artificially generated 10 couples of i.i.g. tumors by subdividing the control group of 20 animals into two groups of 10, randomly picking tumors from each subgroup and pairing them together. We then picked each small tumor from these pairs (and similarly, each large tumor), by choosing the one with smallest final volume. This yielded two samples of 10 "control small" and "control large" tumors that can be considered as what would have emerged from randomness only in initiation and growth. These two samples could then be statistically compared to the experimental samples of small and large tumors from the DT group. We observed significant differences between the small tumors from the DT group and the "control small" tumors from day 12 until the end, with the exception of days 18 and 19 where differences were not significant due to large variability (Figures 2.16B and 2.16C). On the other hand, no statistical difference was observed between the large tumors from the DT group and their control counterparts.

These results demonstrated that in a mouse where two tumors were simultaneously growing, the larger tumor was growing at the same speed as would a single tumor, while the other had significantly slower kinetics.

A dynamical benchmark of models of concomitant resistance

After studying what could be extracted from single tumor growth models [Benzekry et al., 2017], we investigated models of simultaneous growth of two tumors in the same organisms in order to study and quantify the possible underlying mechanisms of tumor-tumor interactions leading to the observed growth kinetics differences that were observed. A virtually infinite number of models can be conceived for description of CR, both in terms of structural shape (equations) and values of the parameters. We report here only on the results from analysis of 5 informative models (Table 2.2). Interestingly, several models were found unable to fit the data, suggesting rejection of (at least one

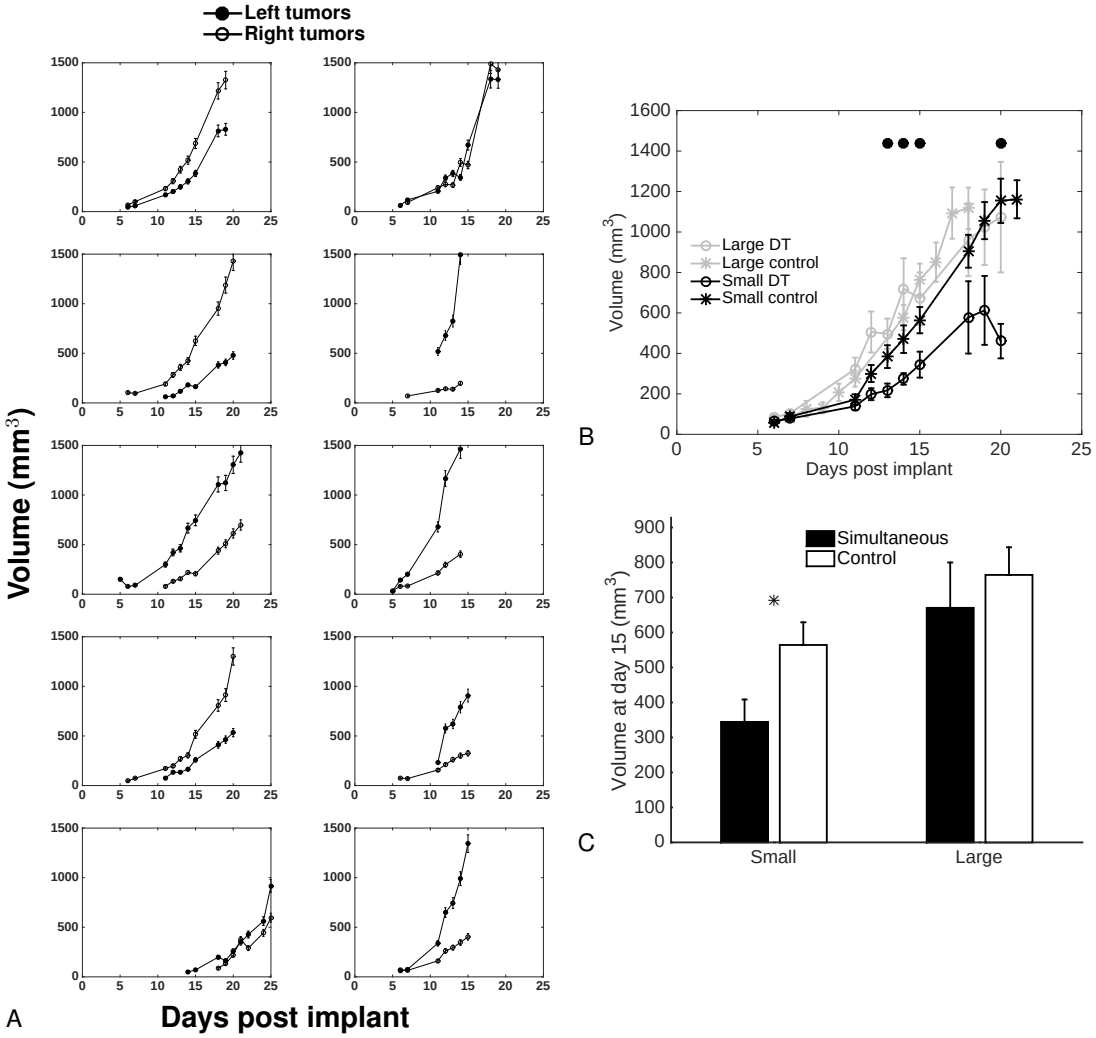

Figure 2.16 – Data of dynamics of simultaneous tumor growth. A. Dynamics of the left and right tumors from mice inoculated with 1×10^6 LLC cells on the two lateral sides at day 0. B. Comparison of large and small tumors with large and small tumors extracted from artificially paired control tumor growth curves (see text for details). Mean ± standard error. Circles indicate statistically significant differences between the small tumors from the simultaneous group and the small control tumors (Student's t-test with unequal variance, $p < 0.05$). C. Tumor sizes at day 15. Mean ± standard error. * = $p < 0.05$, Student's t-test with equal variance.

of) the hypotheses that they rely on. These include a model for the athrepsis theory (competition for nutrients) [Benzekry et al., 2017]. The other models were based on either systemic inhibition of angiogenesis (SIA) – formalized using a model of interaction between tumor growth and vascular support [d'Onofrio and Gandolfi, 2004] – or induction of quiescence due to a cytostatic seric factor. We termed the models based on this last theory proliferation inhibition (PI) models. The SIA model was able to give a reasonably accurate description of our data. For PI models, which have

similar structures as equation (7), three hypotheses were investigated: 1) direct effect (a given quantity of IFs induces a given number of cells going to quiescence) (equation (7)), 2) log-kill effect (a given quantity of IFs induces a given fraction of cells going to quiescence) and 3) total number of cells ($P_i + Q_i$) as a source of IFs. Notably, models 2) and 3) were unable to fit the data and had to be rejected [Benzekry et al., 2017]. On the other hand, the model 1) gave a particularly good fit to the data (Figures 2.17A and B). Table 2.3 summarizes statistical quantitative metrics of goodness-of-fit the models that allow comparison of their descriptive power, while Figure 2.17C shows the distribution of the residuals. Table 2.4 reports the parameter values of all the models estimated from the best fits, together with their inter-animal variability (parameters were individually fitted for each mouse) and standard errors for the estimates. These tables were obtained using the software Carcinom that we developed for fitting models to data.

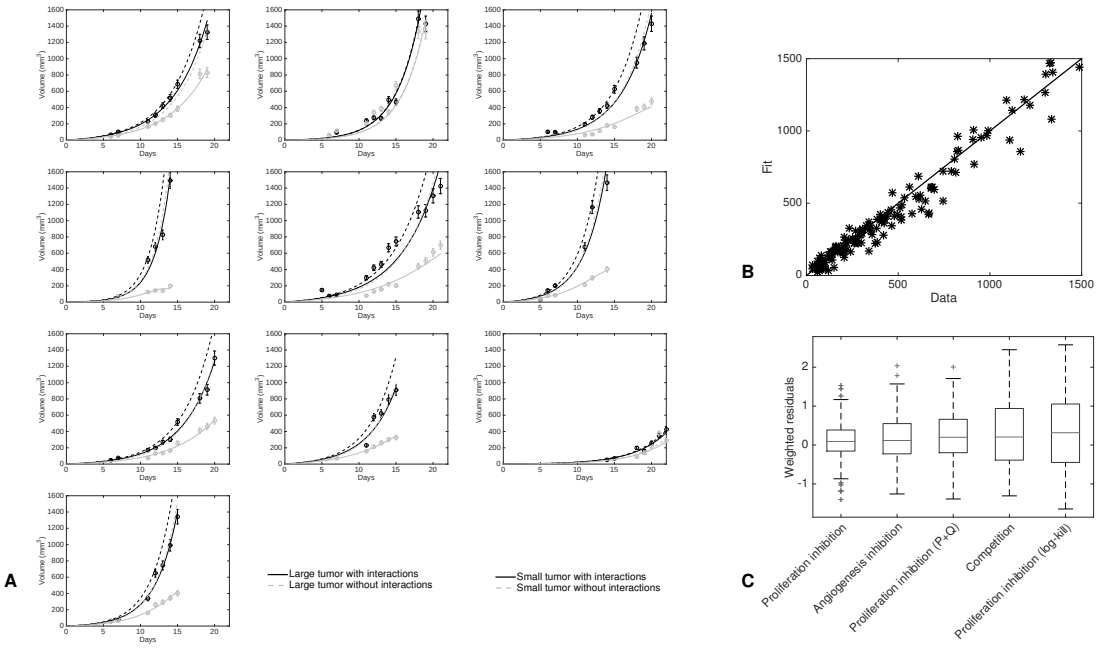

Figure 2.17 – Individual fits of the two-tumors proliferation-inhibition model. A. Fits of all the animals. In each mouse the only difference between the two tumors lies in the number of tumor cells that take, i.e. parameter $V_{0,2}$. Dashed lines are simulations of the model with no interactions between the two tumors (i.e. without terms containing P_j in the equations on P_i ($i \neq j$). B. Fitted values versus data points for all the two-tumors growth curves of A. The solid line is the identity function. C. Distribution of the residuals for the best-fits of the three two-tumors models.

Model name	Equations
Competition	$\begin{cases} \frac{dV_1}{dt} = aV_1 \ln\left(\frac{K}{V_1+V_2}\right) & V_1(t=0) = V_{0,1} \\ \frac{dV_2}{dt} = aV_2 \ln\left(\frac{K}{V_1+V_2}\right) & V_2(t=0) = V_{0,2} \end{cases}$
Angiogenesis inhibition	$\begin{cases} \frac{dV_1}{dt} = aV_1 \ln\left(\frac{K_1}{V_1}\right) & V_1(t=0) = V_{0,1} \\ \frac{dK_1}{dt} = bK_1 - dV_1^{2/3}K_1 - eV_2\mathbb{1}_{K_1>K_0} & K_1(t=0) = K_0 \\ \frac{dV_2}{dt} = aV_2 \ln\left(\frac{K_2}{V_2}\right) & V_2(t=0) = V_{0,2} \\ \frac{dK_2}{dt} = bK_2 - dV_2^{2/3}K_2 - eV_1\mathbb{1}_{K_2>K_0} & K_1(t=0) = K_0 \end{cases}$
Proliferation inhibition	$\begin{cases} \frac{dP_1}{dt} = \alpha P_1 - (\beta P_1 + \gamma(P_1+P_2))\mathbb{1}_{P_1>0} & P_1(t=0) = V_{0,1} \\ \frac{dQ_1}{dt} = (\beta P_1 + \gamma(P_1+P_2))\mathbb{1}_{P_1>0} & Q_1(t=0) = 0 \\ V_1 = P_1 + Q_1 \\ \frac{dP_2}{dt} = \alpha P_2 - (\beta P_2 + \gamma(P_1+P_2))\mathbb{1}_{P_2>0} & P_2(t=0) = V_{0,2} \\ \frac{dQ_2}{dt} = (\beta P_2 + \gamma(P_1+P_2))\mathbb{1}_{P_2>0} & Q_2(t=0) = 0 \\ V_2 = P_2 + Q_2 \end{cases}$
Proliferation inhibition (log-kill)	$\begin{cases} \frac{dP_1}{dt} = \alpha P_1 - (\beta P_1 + \gamma(P_1+P_2))P_1 & P_1(t=0) = V_{0,1} \\ \frac{dQ_1}{dt} = (\beta P_1 + \gamma(P_1+P_2)) & Q_1(t=0) = 0 \\ V_1 = P_1 + Q_1 \\ \frac{dP_2}{dt} = \alpha P_2 - (\beta P_2 + \gamma(P_1+P_2))P_2 & P_2(t=0) = V_{0,2} \\ \frac{dQ_2}{dt} = (\beta P_2 + \gamma(P_1+P_2)) & Q_2(t=0) = 0 \\ V_2 = P_2 + Q_2 \end{cases}$
Proliferation inhibition (P+Q)	$\begin{cases} \frac{dP_1}{dt} = \alpha P_1 - (\beta V_1 + \gamma(V_1+V_2))\mathbb{1}_{P_1>0} & P_1(t=0) = V_{0,1} \\ \frac{dQ_1}{dt} = (\beta V_1 + \gamma(V_1+V_2))\mathbb{1}_{P_1>0} & Q_1(t=0) = 0 \\ V_1 = P_1 + Q_1 \\ \frac{dP_2}{dt} = \alpha P_2 - (\beta V_2 + \gamma(V_1+V_2))\mathbb{1}_{P_2>0} & P_2(t=0) = V_{0,2} \\ \frac{dQ_2}{dt} = (\beta V_2 + \gamma(V_1+V_2))\mathbb{1}_{P_2>0} & Q_2(t=0) = 0 \\ V_2 = P_2 + Q_2 \end{cases}$

Table 2.2 – Two-tumors models' equations

Model	**SSE**	**AIC**	**RMSE**	**R2**	**p < 0.05**	**#**
Proliferation inhibition	**0.194(0.0319 - 0.713)[1]**	**-12(-54 - 2.26)[1]**	**0.453(0.182 - 0.845)[1]**	0.964(0.87 - 0.987)[2]	1/10	3
Angiogenesis inhibition	0.296(0.121 - 0.693)[2]	-4.28(-32.2 - 2.31)[2]	0.557(0.355 - 0.844)[2]	**0.965(0.924 - 0.985)[1]**	1/10	4
Proliferation inhibition (P+Q)	0.328(0.144 - 0.822)[3]	-3.86(-30.8 - 5.4)[3]	0.59(0.388 - 0.909)[3]	0.956(0.72 - 0.987)[3]	5/10	3
Competition	0.666(0.141 - 2.2)[4]	0.71(-33.2 - 13.1)[4]	0.828(0.383 - 1.5)[4]	0.694(-0.0757 - 0.964)[4]	9/10	2
Proliferation inhibition (log-kill)	0.721(0.308 - 2.04)[5]	2.92(-13.2 - 14.4)[5]	0.863(0.558 - 1.45)[5]	0.594(-0.135 - 0.937)[5]	9/10	3

Table 2.3 – SSE = Sum of Square Errors, AIC = Akaike Information Criterion, BIC = Bayesian Information Criterion, R2 = coefficient of determination. # = number of parameters. The numbers in parentheses indicate the (min - max) range of the values and the numbers inside the brackets are ranks of the models relatively to the criterion. The "p<0.05" column contains number of animals for which the null hypothesis of a gaussian distribution of the residuals was rejected for either the large or the small tumor (Kolmogorov-Smirnov goodness-of-fit test).

Model	Par.	Unit	Median value (CV)	RSE (%)
Proliferation inhibition	α	day^{-1}	3.63 (58)	21.7
	β	day^{-1}	3.29 (64.6)	25.9
	γ	day^{-1}	0.0405 (61.2)	3.94
Angiogenesis inhibition	a	day^{-1}	3.06 (1.06e+03)	47.4
	b	day^{-1}	0.57 (24.8)	3.02
	d	$mm^{-2} \cdot day^{-1}$	0.00368 (35.3)	20.4
	e	day^{-1}	0.119 (43.5)	1.72
Proliferation inhibition (P+Q)	α	day^{-1}	0.701 (26.9)	3.61
	β	day^{-1}	0.187 (50.1)	5.31
	γ	day^{-1}	0.00754 (253)	9.45
Competition	a	day^{-1}	0.085 (30.9)	3.45
	K	mm^3	8.36e+03 (2.17e+06)	15
Proliferation inhibition (log-kill)	α	day^{-1}	0.531 (33.8)	7.45
	β	day^{-1}	7.72e-09 (1.1e+07)	9.41e+07
	γ	day^{-1}	0.00168 (254)	13.4

Table 2.4 – Two-tumors models' inferred parameters from fits to the data. CV = coefficient of variation. RSE = relative standard error.

These results demonstrate that a mathematical modeling approach was able, by confrontation of the best-fits of the model, to discriminate among qualitatively equally likely theories of CR and suggest a PI model, having attributes that may explain (or at least describe) this particular phenomenon.

Validation of a simple and biologically-based mathematical model of CR

Double tumor growth The PI model 1), formalized by equations (7), consists in assuming a direct and mutual growth rate decrease between the two tumors, due to passage to quiescence (Figure 2.15). Goodness of fit was found excellent (Figure 2.17), as well as identifiability of the parameters (see standard errors in Table 2.4). Notably, while being fitted directly on the two tumors growths, the predicted behavior when simulating no interactions was in full agreement with the control growth curves. Indeed, the dashed lines in Figure 2.17A are close to the growth curves of the large tumors, which were found to be not significantly different from "naturally happening" large tumors. Hence the model was able to learn and identify the unaltered growth part from altered growth curves, highlighting its reliability.

In mouse number two (second plot in the top row of Figure 2.17A), consistently with the observation of identical growth kinetics between the two tumors, the model identified a value of parameter γ not significantly different from zero. On the other hand, the model did identify interactions between the two tumors in the other animals, as emphasized by 95% confidence intervals of parameter γ inferred from the parameter estimation process that did not contain 0 ($(0.0374, 0.0436)$ in our estimation). In turn, this translated into substantial differences in the kinetics (see Figure 2.17A where growth curves are plotted with or without interactions). Of important note, these differences in the kinetics were mostly due to the interaction between the two tumors, rather than the initial difference in cell loss. This is demonstrated in Figure 2.17A where it can be observed that the growth curves of the small tumors with only a different initial volume (dashed curves) were considerably higher than the curves where interaction was taken into account. Moreover, these curves were both close to the large tumor growth curves, indicating that the difference in V_0 had only a negligible impact on the difference between the two growth curves, the major determinant being the tumor-tumor cross inhibition effect. Critically, the differences for the large tumor curves were much smaller than for the small tumor curves (while the interaction parameter was the same for both tumors), indicating that the model gives a valid quantitative theory of why only one tumor was affected by CR.

Together, our results provide a biologically-based and minimally parameterized mathematical model for tumor growth kinetics interactions in a two-tumors bearing host. The model confirmed a significative non-zero value for the interaction parameter in 9/10 mice, which gave a quantitative measure of the phenomenon. Asymmetry between the two tumors was explained by an initial difference in the take between the two implants.

Single tumor growth In addition to being able to describe double tumor growth and CR, the elementary model that we proposed also offered a simple formalism for single tumor volume growth. The model consists in the division of the cancer cells into two sub-populations: proliferative and quiescent cells (which could also account for necrotic tissue still present in the total volume measurement). In the absence of a secondary tumor, the model (7) becomes:

$$\begin{cases} \frac{dP}{dt} = (\alpha - \beta - \gamma)P, & P(t=0) = V_0 \\ \frac{dQ}{dt} = (\beta + \gamma)P, & Q(t=0) = 0 \end{cases}$$

This provides a valid and simple linear mathematical construct able to describe the growth of single tumors [Benzekry et al., 2017]. It sheds new lights on general tumor growth laws as it demonstrates that classical Gompertzian growth – which is able to describe accurately Lewis Lung tumor growth curves (chapter 1 and [Benzekry et al., 2014c]) – can be reproduced by these equations, with no significant differences (i.e. a difference in Akaike Information Criterion less than 2, see [Benzekry et al., 2017]). Indeed, it had remained elusive why the Gompertzian curve, which was originally designed not even for growth processes [Gompertz, 1825], describes tumor growth curves and their consistent relative growth rate decrease with such important accuracy, while being only phenomenological and not biologically grounded. Interestingly, we obtained that a model where growth deceleration was assumed to result (only) from passage to quiescence due

to the production of factors by the proliferative tumor cells themselves was able to explain single tumor growth curves as accurately as the Gompertz model, or other models such as the power law. Parameters identifiability of this new model was also excellent.

2.6.4 Discussion

Arguments disregarding the competition theory had already been put forward by others [Gershon et al., 1967, Gorelik et al., 1981, Prehn, 1993]. For example, Gorelik had argued that under this theory, the intensity of CR should be an increasing function of the amount of cells implanted in a subsequent graft, in contradiction with experimental findings, thus disqualifying the theory [Gorelik et al., 1981]. However, these arguments had remained qualitative. Our formal study adds a quantitative basis to these considerations by showing that, under the modeling assumptions we operated, this theory was unable to accurately describe our data [Benzekry et al., 2017].

More elusive in the literature had remained the question to discriminate between angiogenesis inhibition, as evidenced by the work of Folkman and colleagues [Holmgren et al., 1995, O'Reilly et al., 1994], and direct induction of quiescence by seric factors, as proposed by Ruggiero and colleagues [Ruggiero et al., 1985, Ruggiero et al., 2011, Ruggiero et al., 2012]. Our results suggested that the latter theory, when considered alone, could be sufficient to drive CR, insofar as it exhibited good match to the data. However, this does not preclude systemic inhibition of angiogenesis (SIA) to occur, since an SIA-based model was able to describe the data almost as well. Furthermore, the two theories are not mutually exclusive. This last remark also applies to the competition theory: it cannot be completely disregarded that a combination of the three phenomena happens in the occurrence of CR. However, it was beyond the scope of this study to be able to disentangle between a combination of the phenomena and one phenomenon alone.

Our findings not only shed light on the dynamics of CR but also proposed a simple and biologically-based model of (double and) single tumor growth able to describe the ubiquitously observed growth retardation with larger volumes already mentioned in the first chapter of this thesis and usually modeled by means of the Gompertz equation [Laird, 1964, Norton, 1988]. Although several attempts of deriving the Gompertz equation from basic principles have been performed in the literature [Bajzer and Vuk-Pavlović, 2000, Frenzen and Murray, 1986], the model we propose here benefits from its simplicity. It has only two (aggregated) parameters, which quantify two phenomena: 1) proliferation of the active cancer cells and 2) production by these active cells themselves of factors that drive them to quiescence. Interestingly, this model brings new light on the so-called paradox of CR [Prehn, 1993], which can be expressed as follows: if distant inhibition occurs, potentially driving other tumors to dormancy, then why does the primary tumor continue growing? Our general model gives a way to quantitatively formalize this. Indeed, the same factors act as local and distant inhibitors and we showed that, under appropriate values of the parameters (but identical for the two tumors), one could obtain at the same time almost unaltered growth of the large (primary) tumor and significant suppression of the growth of the small (secondary) tumor. The presence of endogenous molecules with inhibitory activity thus challenges a naïve view where

growth retardation would only be due to interactions dictated by competition (for space or nutrients). Consistently, such a model (logistic growth), had already been shown unable to adequately fit experimental tumor growth curves in the first part of this thesis. Considering the implications, the mere fact a tumor would produce both angiogenesis stimulators and inhibitors at the same time, with near and far ranges, does not readily reconcile with a purely localized purpose, but instead speaks to tumor control being manifestly a systemic phenomenon, quite distinct from the naïve concept of an entity governed by local conditions alone, independent of other tumor sites. Implicit in this, and as proposed by others [Prehn, 1991, Prehn, 1993], a vision of tumor growth as an integrated, organ-like development could bring sense to this seeming paradox.

Chapter 3

Metastasis: clinical data

Contents

Abstract

While experimental data on the natural course of metastasis are hard to obtain, it is even harder to get access to clinical data, mainly because: 1) metastasis can only be diagnosed and measured once they have reached a substantial size (diameter of about 5-10 mm on clinical images, which corresponds to approximately 10^8 cells) and 2) when patients are diagnosed with advanced stage they usually benefit from therapy with a systemic drug. Nevertheless, for the cases of breast and lung cancers, we could find in the literature two useful data sets of the probability of metastatic relapse as a function of the size of the primary tumor [Koscielny et al., 1984, Mujoomdar et al., 2007], which were used to test our modeling framework in a clinical setting. For the breast data set, we demonstrated the ability of our mathematical model to describe the inter-individual variability in the probability of metastatic relapse in terms of the only parameter μ (additionally to the primary tumor size), thus emphasizing its critical role and clinical usefulness. Further on, leveraging this quantitative calibration for description of metastatic aggressiveness, we conducted a simulation study that was able to simulate relevant survival curves and revealed a nonlinear dependence between the size of the primary tumor at diagnosis and the survival benefit from surgery. These results were published in [Benzekry et al., 2016].

In parallel, we had access to clinical images of a patient with apparition and longitudinal follow up of cerebral metastases from an EGFR-mutated lung adenocarcinoma (6 time points and 47 metastatic size measurements, data from the Bergonié Institute (Dr F. Chomy)), which provided a unique opportunity to further study the kinetics of metastatic dynamics in a human cancer disease. We found that the model was able to describe accurately the data with only three free parameters, thus bringing hope to a clinical identification of these from data at diagnosis. Moreover, the model made interesting predictions such as the time of initiation of the first brain metastasis (predicted here to have occurred before diagnosis).

Finally, conclusions and perspectives of future work are drawn.

3.1 Introduction

Metastasis remains a major challenge as 90% of solid cancer patients die from this process and associated complications [Steeg, 2016, Chaffer and Weinberg, 2011]. Five-year survival rates drastically drop when the disease has spread to other sites of the organism (Figure 3.1). For instance, the 5-year survival rate of kidney cancer goes from 91.8% for a localized disease to 12.1% when metastases are present at diagnosis [Howlader et al., 2014]. Surgical removal of an early-stage localized tumor remains one of the most effective strategies in reducing the probability of systemic metastatic disease spread [Gupta and Massagué, 2006]. Improved technologies of early cancer detection aim to classify primary tumor stage to identify whether potential treatment modalities — such as presurgical "neoadjuvant" or postsurgical "adjuvant"—should be considered to complement surgery and reduce metastatic potential.

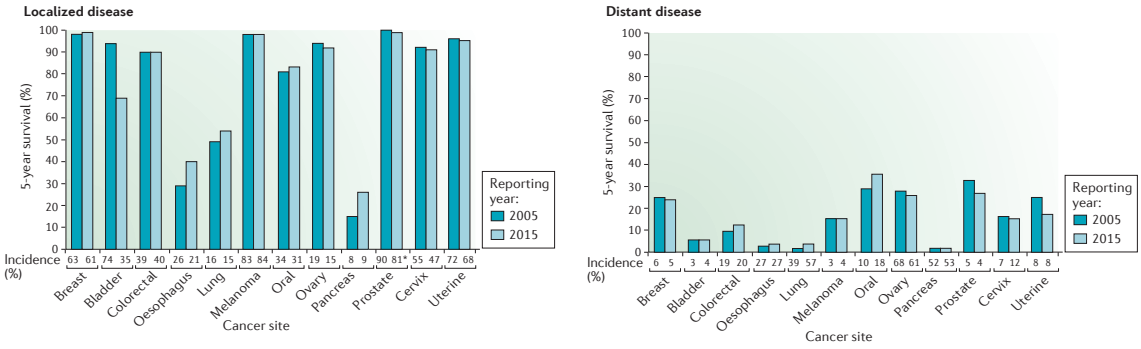

Figure 3.1 – Five-year survival rates of several cancer types according to the disease's state (local, regional or distant). Adapted from [Steeg, 2016]

In this context, several clinical problems can be addressed by mathematical methods. The first that we identified is the following.

Clinical problem 1. *Estimate the amount of occult distant metastases at diagnosis*

This problem is of critical relevance to better personalize adjuvant (i.e. post-surgical) chemotherapy, which is particularly salient for breast cancer. In this disease, the 5-year survival rate is 88% [Howlader et al., 2014] but the 20-year overall survival rate is not as good (39-45% reported in [Litière et al., 2012]). Indeed, while 93% of breast cancers are diagnosed with a local or regional disease [Howlader et al., 2014], metastasis is now thought to be an early event and it has been estimated that 90% of these early stage patients have already undergone distant dissemination, although still at the indolent and invisible stage [Fisher, 1980, Retsky et al., 2010]. This realization in the 1970's opened the era of adjuvant chemotherapy in the clinic in the 1980's, but still metastatic relapse occurs in approximately 30% of patients diagnosed with localized disease [Pollard, 2016]. This observation as well as the severe toxicities associated with cytotoxic drugs call for a better classification of patients at diagnosis, predictive of the benefit from adjuvant therapy.

The standard WHO classification for breast cancer is based on morphological features [Lakhani et al., 2012], but molecular markers (such as hormonal receptors and HER2 status or Ki67 level) have also fundamental and increasing importance. Indeed, the hormonal receptors status are critical to determine the suitability of patients to hormonal therapy (Tamoxifen or aromatase inhibitors), and the HER2 status to targeted therapy (trastuzumab). These have generated a new classification of breast tumors that includes the following groups: luminal A (hormone-receptor positive, HER2-, low Ki-67 with good prognosis), luminal B (hormone-receptor positive, HER2+ or HER2-, high Ki-67, slightly worse prognosis), HER2 enriched (hormone-receptors negative, HER2+) and triple negative (also called basal-like, hormone-receptors negative, HER2-, bad prognosis). Going further in using methods from molecular biology – shown to be related to the receptors expression [Perou et al., 2000] – gene expression signatures comprising either 70 genes [van 't Veer et al., 2002, van de Vijver et al., 2002] or 21 genes [Paik et al., 2004] have been established as prognostic of 5-years metastatic relapse [Chibon, 2013]. These have yielded DNA-microarray-based diagnostic tests such as Oncotype DX or Mammaprint with predictive value of the response to adjuvant chemotherapy and/or hormonotherapy. A prospective trial validated the usefulness of the Oncotype DX 21 genes expression signature for identification of patients to treat with hormonotherapy only (as opposed to combination with chemotherapy) and thus reducing the burden of unnecessary toxicities. In addition, factors derived from immuno-histochemistry more easily available at diagnosis in clinical routine from tissue micro-arrays – including for instance levels of adhesion proteins such as cadherins – have been reported as impacting the chance of metastatic relapse [de Mascarel et al., 2015].

However, there is a lack of a comprehensive framework to potentiate theses factors into personalized predictions of the risk of and time to metastatic relapse. Statistical softwares such as the Adjuvant! online[13] (based on US cohorts) [Ravdin et al., 2001] and Predict[14] tools (for british patients and which additionally considers HER2 and Ki67 status) [Wishart et al., 2010] provide estimates for the 5 and 10-year survival rates as well as benefits from adjuvant therapy given particular entries. However, they do not consider any biological mechanism and are based on classical survival statistical analysis. As such, they might not take the best advantage of the increasing number of routinely available biological markers such as the aforementioned Ki67 level (linked to proliferation and growth fraction), E-cadherin or TRIO levels (adhesion proteins), or stem cells markers. In this context, a mathematical model of metastasis that would account for the biology of the process might yield more accurate estimations and personalized predictions of clinically relevant quantities such as the time to relapse or the amount of occult disease (number and size of distant lesions) present at diagnosis.

The other cancer that we focused on in clinical results reported in this manuscript is lung cancer, and more precisely non-small cell lung cancer (NSCLC). Lung cancer is still a rising concern in oncology as it is the first leading cause of death by cancer, with more than 1.5 million deaths in 2012 worldwide (World Health Organization). Nearly 80% of lung cancers are of the NSCLC type, and, in contrast with breast cancer, 50% of them are diagnosed at the metastatic stage. Brain

[13] `https://www.adjuvantonline.com/#`
[14] `http://www.predict.nhs.uk/index.html`

metastases (BM) affect more than 20% of patients with NSCLC [Barnholtz-Sloan et al., 2004]. Despite recent advances in this field, BMs remain a major concern as they are associated with a poor prognosis [Oh et al., 2009]. In addition, BMs are responsible for debilitating symptoms (asthenia, nausea, etc...) decreasing the patients' quality of life. Lung cancer is known to be the most deleterious in terms of brain metastases [Barlesi et al., 2013, Métellus et al., 2013, Tabouret et al., 2013]. In addition to the clinical problem 1, also relevant for early stage NSCLC (i.e. locally diagnosed disease), another one might be stated.

Clinical problem 2. *For patients with a limited number (typically, one to three) of BMs, decide what therapeutic strategy to follow, in particular regarding the use of whole-brain radiotherapy (WBRT).*

Indeed, as of today, the utility of WBRT in the management of BMs from NSCLC is still controversial, in particular due to important neuro-cognitive toxicities [Barlesi et al., 2013, Owonikoko et al., 2014, Tallet et al., 2012]. Several phase III trials were conducted but no firm conclusion that would be valid for all patients could be drawn [Mulvenna et al., 2016, Pechoux et al., 2016]. This points to the need of rational tools to decide therapeutic action in a patient-specific way. Similarly, the clinical follow-up and planning of cerebral MRI could highly benefit from individualized predictions of the probability of relapse.

3.2 Primary tumor size-dependent probability of metastatic relapse

Our methodology for fitting clinical data of metastatic relapse probability followed the same format as in [Barbolosi et al., 2011]. For the two datasets that we considered, we made the assumption that the probability of developing a metastasis in the future was to have already one present (but possibly invisible) at diagnosis. This assumption is particularly relevant for breast cancer where, following diagnosis, surgery was performed, thus leaving no possibility for the origin of the metastases than before diagnosis. It is more debatable for lung adenocarcinomas but we considered it reasonable as a first attempt.

To avoid over-parameterization, parameters for the growth of the primary and secondary tumors were fixed (not subject to optimization) and corresponded to a maximal volume of 10^{12} cells ($\simeq 1$ kg) [Retsky et al., 1997] and doubling times taken from the literature (7.5 months at 1 gram for breast cancer [Koscielny et al., 1985, Coumans et al., 2013] and 169 days for lung ADK [Detterbeck and Gibson, 2008]). The parameter γ was considered identical for all the patients. For the breast study, following our preclinical findings where $\gamma = 1$ was able to describe the data, we kept also this value in the clinical case. For the lung study, several values were investigated (see below).

We considered thus that the parameter μ alone was responsible for inter-patient variability in metastatic relapse, and assumed that it followed a lognormal distribution with mean μ^m and standard deviation μ^σ. From a given size V_p^1 at diagnosis, the unobserved time period $T_1(V_p^1)$ can

be computed by:

$$T_1(V_p^1) = -\frac{1}{\beta}\ln\left(1 - \frac{\beta}{\alpha_0}\ln(V_p^1)\right)$$

where α_0 and β are the two Gompertz parameters. The probability of having at least one metastasis at diagnosis was then given by

$$\mathbb{P}\left(\text{Mets}\right) = \mathbb{P}\left(N\left(T_1\left(V_p^1\right)\right) \geq 1\right) = \mathbb{P}\left(\mu \int_0^{T_1(V_p^1)} V_p(t)^\gamma dt \geq 1\right).$$

This last quantity can be computed by Monte Carlo simulations for a given (μ^m, μ^σ). Additionally, when the data was given as a range of primary tumor sizes, we considered a uniform distribution within each range for the size at diagnosis (see [Benzekry et al., 2016] for details).

3.3 Breast cancer

3.3.1 Clinical data of metastatic relapse probability

Before the generalization of adjuvant therapy for breast cancer, Koscielny and colleagues [Koscielny et al., 1984] reported data from a cohort of 2 648 patients followed for 20 years after surgery of the primary tumor, without additional treatment. Their data (reproduced in Table 3.1) demonstrated that, despite a clear association between primary tumor size at diagnosis and the probability of metastatic relapse, not all the patients having a given primary tumor size were relapsing. For instance, only 42% of patients with a primary tumor diameter at diagnosis between 2.5 and 3.5 cm developed metastasis. Using a lognormal population distribution of parameter μ, we were able to obtain a good fit to the data of metastatic relapse for all size ranges (Table 3.1). These results demonstrated that, within our semi-mechanistic modeling approach, parameter μ was able to capture the inter-individual metastatic variability, not only in animal models but also for patient data.

Diameter of primary tumor at diagnosis (cm)	**Number of patients**	**Proportion of patients developing metastasis (%)**	**Model fit**
$1 \leq D \leq 2.5$	317	27.1	25.5
$2.5 < D \leq 3.5$	496	42.0	42.4
$3.5 < D \leq 4.5$	544	56.7	56.3
$4.5 < D \leq 5.5$	422	66.5	65.9
$5.5 < D \leq 6.5$	329	72.8	74.3
$6.5 < D \leq 7.5$	192	83.8	80.8
$7.5 < D \leq 8.5$	136	81.3	85.7

Table 3.1 – Fit of clinical data of metastatic relapse probability in breast cancer (data from [Koscielny et al., 1984])

3.3.2 Assessing the impact of surgery on metastasis and survival

When diagnosis detects only a localized primary tumor, distant occult disease might already be present. In our model, the extent of this invisible metastatic burden depends on: (i) the primary tumor size at diagnosis and (ii) the patient's metastatic potential μ. For instance, if the primary tumor size (or μ) is small, then the occult metastatic burden might be negligible and surgery would substantially benefit to the patient in terms of metastatic reduction, by stopping further spread of new foci. Conversely, if the primary tumor size (or μ) is large, then the occult metastatic burden might already be consequent and removing the primary tumor might only have a marginal impact.

Virtual simulation of two breast cancer patients

We simulated the quantitative impact of primary tumor surgery in two virtual breast cancer patients having a primary tumor diagnosed at 4.32 cm and two values of μ (median and 90th percentile within a population lognormally distributed according to our fit to the data from [Koscielny et al., 1984]). Results are reported in Figure 3.2[15]. A discrete and stochastic version of the metastatic dissemination process was used here for the simulations. Interestingly, our simulation revealed that at the time of diagnosis, no metastasis was detectable (i.e., below the imaging detection limit, taken here to 10^8 cells) in both cases (Figure 3.2A and B). In clinical terms, this means that both patients would have been diagnosed with a localized disease, which is in line with the aforementioned clinical reports. However, the two size distributions were very different, with a much larger residual burden in the "large μ" case, illustrative of the increased metastatic potential. For the "median μ" case, our model predicted the presence of two small metastases, with respective sizes of 6 and 278 cells. Not surprisingly, when no surgery was simulated, this number continued to increase, reaching 160 secondary lesions after 15 years (Fig. 3.2C). However, most of the metastatic burden (126 tumors, i.e., 78.8% of the total burden) was composed of lesions smaller than 10^9 cells ($\simeq$ 1g). Figures 3.2E and G demonstrate that a substantial relative benefit (larger than 10%) in metastatic burden reduction was eventually obtained, but only after 7.8 years. Nevertheless, at the end of the simulation (15 years after surgery), the predicted two occult metastases at diagnosis had reached substantial sizes (1.41×10^{11} and 1.89×10^{11} cells). Therefore, for this patient with median metastatic potential, the model indicates an important benefit in using surgery and adjuvant therapy. For a patient with higher metastatic potential (at the level of the 90th percentile, see Figure 3.2B, D, F, and H), even with a primary tumor diagnosed at the same size, the predicted metastatic burden at diagnosis was considerably more important, with 76 lesions and the largest comprising 6.23×10^6 cells. This consequent occult burden translated into poor outcome and the metastatic mass would have reached a lethal burden of 10^{12} cells 9.3 years after the initial diagnosis if no therapy would have been administrated.

These results illustrate the potential of the model as a diagnostic and prognostic numerical tool for assessment of the occult metastatic burden and postsurgery growth. In this, it could help to

[15] see also `https://www.youtube.com/watch?v=C2LwnGISfug&index=3&list=PLnuDkx_YTHSxvPMI2QBbKXSoFsD9BU8cI` for a movie of the simulated natural history of the disease

determine the extent of adjuvant therapy necessary to achieve a long-term control of the disease.

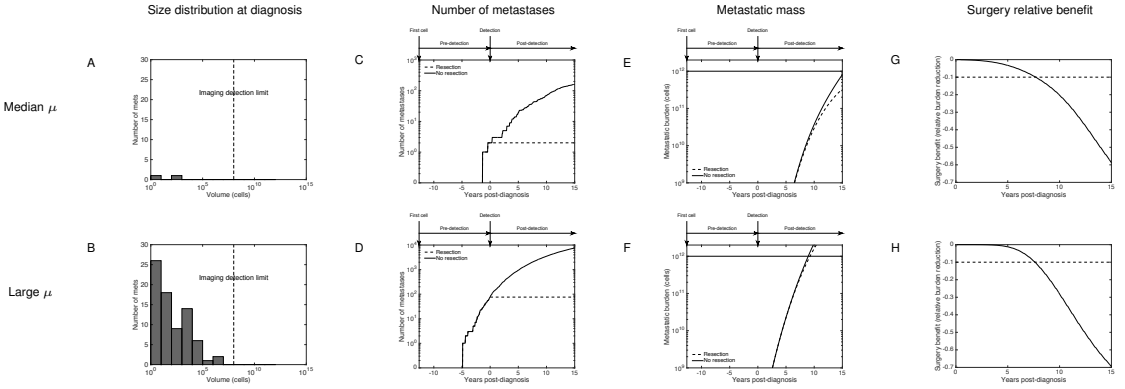

Figure 3.2 – Comparison of surgical/nonsurgical intervention outcomes using the clinical dataset. Simulations were performed using the calibration of the parameter μ from the clinical dataset for the median value and the value of the level of the upper 90th percentile within the population distribution. The primary tumor size at detection was assumed to be 4.32 cm. Simulations were performed using a stochastic version of the model. A and B, size distribution of the metastases at detection. The dashed line corresponds to the detection limit by imaging devices (assumed to be 10^8 cells). C and D, time dynamics of the total number of metastases with and without resection of the primary tumor. The horizontal solid line represents a lethal burden threshold of 10^{12} cells. E and F, time dynamics of the metastatic burden with and without resection of the primary tumor. G and H, surgery metastatic burden benefit as a function of the future, defined by $\frac{B_{res}-B_{nores}}{B_{nores}} \times 100$, where B_{res} and B_{nores} stand for the simulated metastatic burdens with and without resection of the primary tumor, respectively. The dashed line represents a 10% relative benefit.

Impact of tumor size on postsurgical survival

To further examine the relationship between the primary tumor size at surgery and survival, we performed simulations for (i) an individual with fixed value of μ (the population median, see Figure 3.3A) or (ii) an entire population (simulated survival curves in Figure 3.3B) for three primary tumor sizes. Numerical survival was defined by the time to reach a lethal burden of 1 kg [Klein, 2009] from the time of cancer initiation. Interestingly, we observed a highly nonlinear relationship between the primary tumor size and the survival, which suggested three size ranges delimited by two thresholds (Figure 3.3A). The lower threshold—termed "recurrence" threshold (4 cm in Figure 3.3A)—was defined as the maximal limit whereupon no metastasis was present at surgery (number of metastases lower than 1). The upper size threshold—termed "benefit" threshold (5.2 cm in Figure 3.3A)—was defined as the size above which surgery had a negligible (<10%) impact on survival time. Above and below these "recurrence" and "benefit" thresholds, primary tumor size had no important correlative value. Conversely, within the primary tumor size range delimited by these two bounds, the relationship between pre-surgical primary tumor and post-surgical metastatic burden/survival was highly correlative, with a large value of the derivative and a sharp transition between the two extremes. The same qualitative primary tumor size/survival relationship was

obtained for any value of μ sampled within the population distribution, although with substantial quantitative differences [Benzekry et al., 2016].

In Figure 3.3C, we present quantitative estimates of the recurrence and benefit thresholds for various percentiles of μ within the population distribution. Our simulations predicted that for the first half of the population, surgery was almost always leading to negligible metastatic recurrence risk, with large values of the recurrence threshold (larger than the usual detection levels). On the other hand, the patients with large metastatic potential were predicted not to substantially benefit from the surgery, as far as reduction of future metastatic burden was concerned. For instance, a patient with μ at the level of the 90th percentile and a primary tumor diagnosed at 4 cm would have an increase in absolute survival time of only 1.9% following surgery (Figure 3.3C).

3.4 Mathematical modeling of cerebral metastatic apparition and growth for EGFR mutated NSCLC patients

3.4.1 Clinical data of metastatic relapse probability

We performed a review of clinical studies of both the qualitative (growth function) and quantitative (doubling time) features of unperturbed growth of primary lung tumors. A total of 20 publications were found to contain such information, spanning from 1961 to current days. Doubling times (DT) were reviewed from different types of studies, including large screening trials where the tumors were only detected retrospectively, allowing calculation of a doubling time from at least two data points of the tumor size. A few empirical studies with more than 2 time points supported the exponential model during the visible phase of growth of the primary tumor [Friberg and Mattson, 1997, Mizuno et al., 1984]. The Gompertz model was also considered by others [Detterbeck and Gibson, 2008].

In the patient case that we investigated, for a primary tumor (adenocarcinoma) diagnosed at a diameter of about 3.6 cm, the pre-detection time (time elapsed between the first cancer cell and clinical detection) was estimated to 16 years with the exponential model and the assumption of a doubling time of 169 days [Detterbeck and Gibson, 2008]. In contrast, the Gompertz model led to a more reasonable estimate of 4.5 years of undetected history. Thus, we further assumed Gompertzian growth for the pre-treatment phase of the primary tumor.

A published clinical study reported the primary tumor size-stratified frequency of BM, either present at diagnosis or developed during monitoring of the disease, for NSCLC patients (n = 264), including descrition of the ADK patients subgroup (n = 136) [Mujoomdar et al., 2007]. For various values of γ (but constant within the population), we could obtain fits of this data (see Figure 3.4). However, in contrast with our results on breast cancer, the fits that we obtained were rejected by a Pearson χ^2 test.

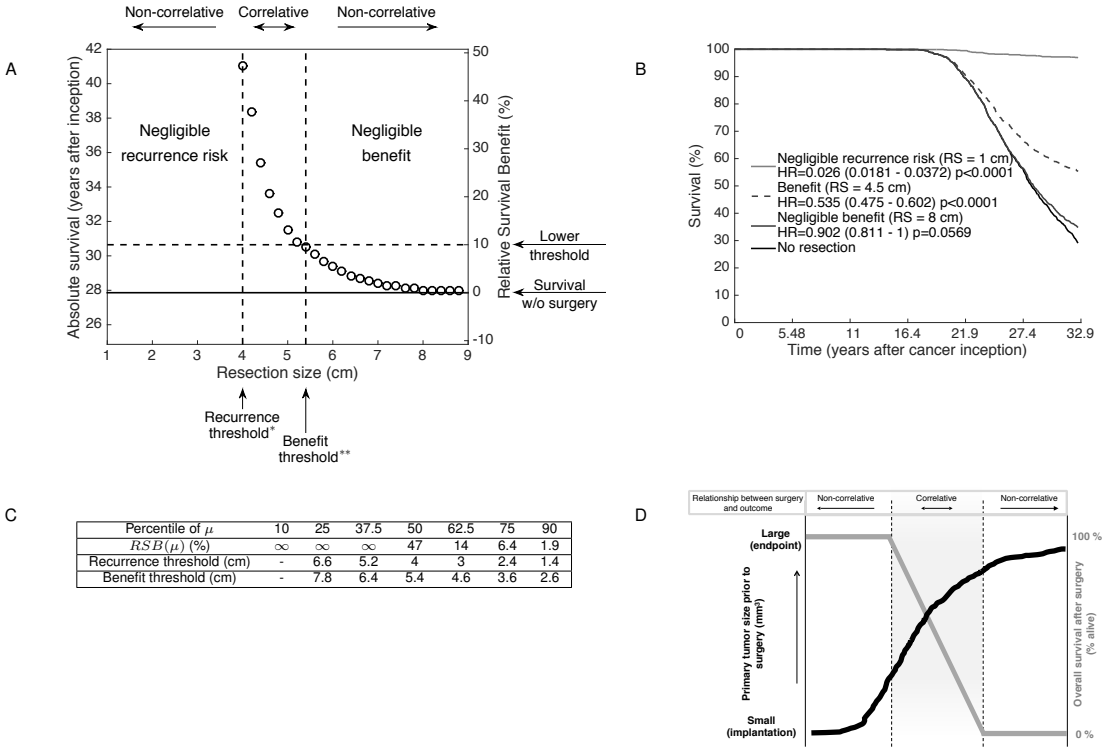

Percentile of μ	10	25	37.5	50	62.5	75	90
$RSB(\mu)$ (%)	∞	∞	∞	47	14	6.4	1.9
Recurrence threshold (cm)	-	6.6	5.2	4	3	2.4	1.4
Benefit threshold (cm)	-	7.8	6.4	5.4	4.6	3.6	2.6

Figure 3.3 – Impact of surgery on survival as a function of primary tumor size. A, simulations of absolute survival time and corresponding relative survival benefit as functions of the primary tumor size at surgery. The relative survival benefit is defined by $RSB = \frac{AS_{res} - AS_{nores}}{AS_{nores}} \times 100$, where AS_{res} and AS_{nores} stand for the simulated absolute survival times with and without surgery of the primary tumor, respectively. * the recurrence threshold was defined as the maximal size below which the patient had no metastasis at diagnosis in the simulation. ** the benefit threshold was defined by a 10% improvement of the absolute survival time due to surgery (horizontal dashed line). The plain line at the bottom corresponds to survival without resection of the primary tumor. Parameter values are those of a virtual patient from with median value of μ. B, survival curves for a simulated population with inter-individual variability on the metastatic potential inferred from the fit to the clinical data (see [Benzekry et al., 2016] for values of the parameters). Three representative primary tumor sizes at resection were considered. RS, resection size; HR, hazard ratio using Cox proportional hazard regression analysis. C, surgical survival benefit, cure, and benefit thresholds as functions of the inter-individual variability in metastatic potential μ. Displayed in the first row are the relative surgical benefits for simulations of a virtual patient with a primary tumor diagnosed at a diameter of 4 cm and values of parameter μ at the indicated percentiles. ∞, the metastatic burden never reached the lethal value of 10^{12} cells during the total simulation time (70 years). RSB, relative survival benefit. Recurrence and benefit thresholds defined as in A. When no value is reported, the value was larger than the larger size considered in the simulations (9 cm). D, schematic of the mutual relationship between primary tumor growth and post-surgery overall survival.

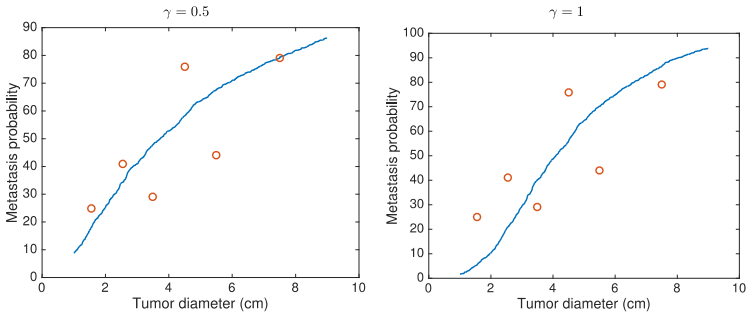

Figure 3.4 – Brain metastasis probability as a function of primary tumor size at diagnosis for ADK (n = 136), with $\gamma = 0.5$ (left) or $\gamma = 1$. Circles = data from [Mujoomdar et al., 2007]. Plain line = fit from the model. Simulation performed over 1000 virtual patients.

3.4.2 Individual description and prediction of cerebral metastases apparition and growth

Data and statement of the problem

We dispose of measurements of the primary tumor and brain metastases (BM) sizes at the times $T_1, \ldots, T_7$. From this data, we are interested in: 1) finding an appropriate, minimal, semi-mechanistic model of the time dynamics of the metastatic population (description of the data) and 2) predict the BM data from data at previous time point(s): either T_1 alone and possibly only the primary tumor (ultimate goal), T_1 and T_2 or T_1, T_2 and additional metastatic time point(s). We will only report results regarding point 1) here.

One patient from the Bergonié EGFR mutated patients has been investigated in details. This patient had a lung adenocarcinoma (ADK) with primary tumor first detected on 08/19/2009, and no overt metastasis at this time. A treatment with erlotinib (tyrosine kinase inhibitor specifically suitable for EGFR-mutated patients) was initiated, which induced an initial decrease of the primary tumor size, followed by a regrowth (Figure 3.5A). At this time, the therapy was changed to cytotoxic chemotherapy. Of note, size variations were small (see the scale in Figure 3.5A). About 20 months after diagnosis, one large (7.5 mm) BM was detected, which kept growing uncontrolled (Figure 3.5B). After a one-year interval without brain imaging examination, five additional BM were detected. These continued to grow and new secondary lesions appeared, reaching a total of 20 BMs on 07/15/2013. We dispose thus of a rich data set for this patient with complete follow-up of the kinetics of BMs at 6 time points (see Figure 3.5B for the growth of the 20 BMs and Figure 3.5C for the longitudinal evolution of the number of visible BMs). Figure 3.5D is an example of a CT image of the brain of the patient with the largest BM apparent, on 07/15/2013. Figure 3.5E depicts the cumulative size distribution of the 20 metastases at this date.

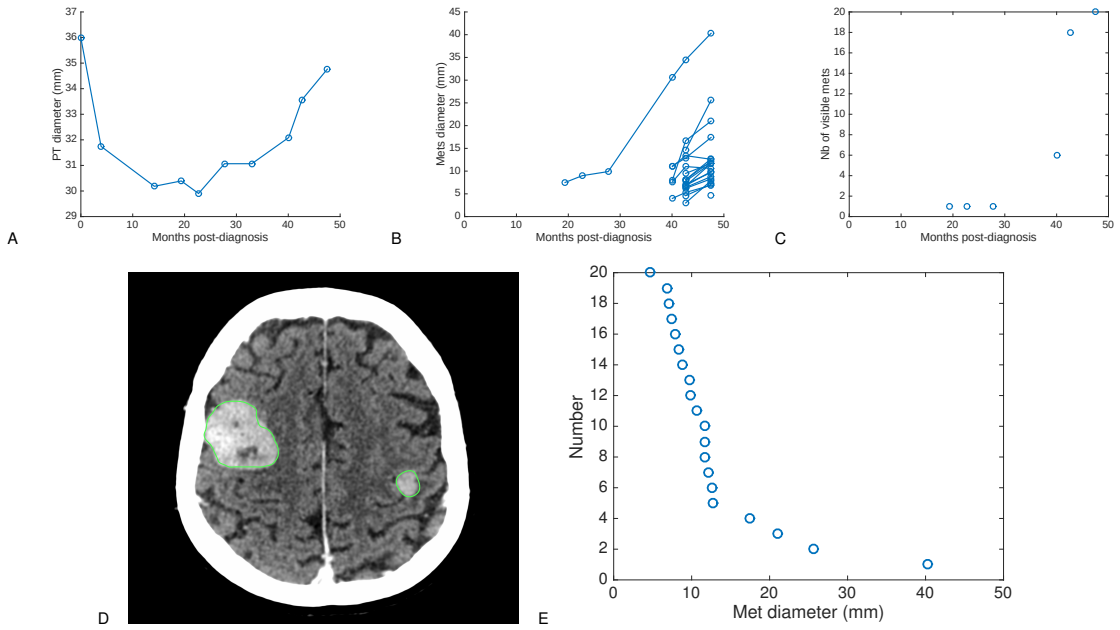

Figure 3.5 – Data on a patient with an EGFR+ lung adenocarcinoma. A. Primary tumor kinetics under erlotinib. B. BMs curves. C. Number of visible BMs. D. CT scan of the brain on 07/15/2013. E. Cumulative size distribution of the BMs on 07/15/2013. primary tumor = Primary Tumor. BM = Brain Metastasis.

Mathematical formalism

The post-diagnosis kinetics of the primary tumor were simply assumed to be bi-exponential and thus determined by: 1) an exponential decrease rate during efficacy of the treatment, 2) a duration of treatment effectiveness before regrowth and 3) an exponential growth rate during relapse. See simulations below (Figure 3.6A). In a first attempt, the effect of therapy on the metastases was ignored, arguing that the observed growth of the metastases did not seem to be impacted by the therapy (this was confirmed by direct fits of the metastases growth showing kinetics not substantially different than the one assumed for the primary tumor from its histological type). Under our formalism (section 2.2), the total number of metastases at time t can be computed by:

$$N(t) = \int_0^t \mu V_p(s)^\gamma ds. \tag{1}$$

In order to use all the data of the size distributions at all time points, since the continuous distribution ρ cannot be directly compared to the data (which would correspond to a sum of Dirac masses), we fitted the cumulative density functions (cdf), defined by:

$$F(t,s) = \int_s^{+\infty} \rho(t,u)du.$$

In a discrete version of the model, if we denote $X_1(t), \ldots, X_{N(t)}(t)$ the sizes of the metastases at time t then

$$F(t,s) = \sum_{n=1}^{N(t)} \mathbb{1}_{X_n(t)\geq s}.$$

These cdfs were to be compared and fitted to their empirical equivalent (Figure 3.5E). In order to do so, it is useful to notice that the number of metastases of size larger than s at time t is the total number of metastases at time $t-\tau(s)$ with $\tau(s)$ the time needed to reach the size s under the mets growth law. For a Gompertz growth with parameters α_0 and β $\left(s(t) = e^{\frac{\alpha_0}{\beta}\left(1-e^{-\beta t}\right)}\right)$, this time is given by

$$\tau(s) = -\frac{1}{\beta}\ln\left(1 - \frac{\beta}{\alpha_0}\ln(s)\right).$$

Therefore, we have, for all t

$$F(t,s) = N(t-\tau(s)),$$

which allows to easily compute the cdfs in view of (1). The fits were then performed by classical likelihood maximization leading to a least squares optimization problem solved with the Matlab function *fminsearch*.

Results

Not all the primary tumor cells have the same metastatic ability When trying to fit the data with $\gamma = 1$, the best-fit of the model predicted a number of metastases (visible + invisible) of 6.2×10^6 at T_1 (diagnosis time) and even 4.8×10^8 metastases at the last time T_7. These values are highly unrealistic and suggest rejection of the $\gamma = 1$ theory.

The model was able to describe the dynamics of the data with (only) three free parameters As expressed above, the primary tumor growth parameters were set from the histologic type and its size at detection. This leaves four free parameters in the model: α_0, β, μ and γ. A reasonable hypothesis would be to assume the same growth parameters for the BMs as for the primary tumor, thus setting $\alpha_0 = \alpha_{0,p}$ and $\beta = \beta_p$. However, this model was not able to accurately fit the data. This suggested a growth difference between the primary tumor and the BMs (which, among themselves, seemed to behave similarly, see Figure 3.5B). Allowing α_0 to differ generated a good fit, for both the dynamics of the number and sizes of the lesions (see Figure 3.6). Therefore,

only three parameters were required to reproduce the BM dynamics over 6 points, with a total of 47 data points.

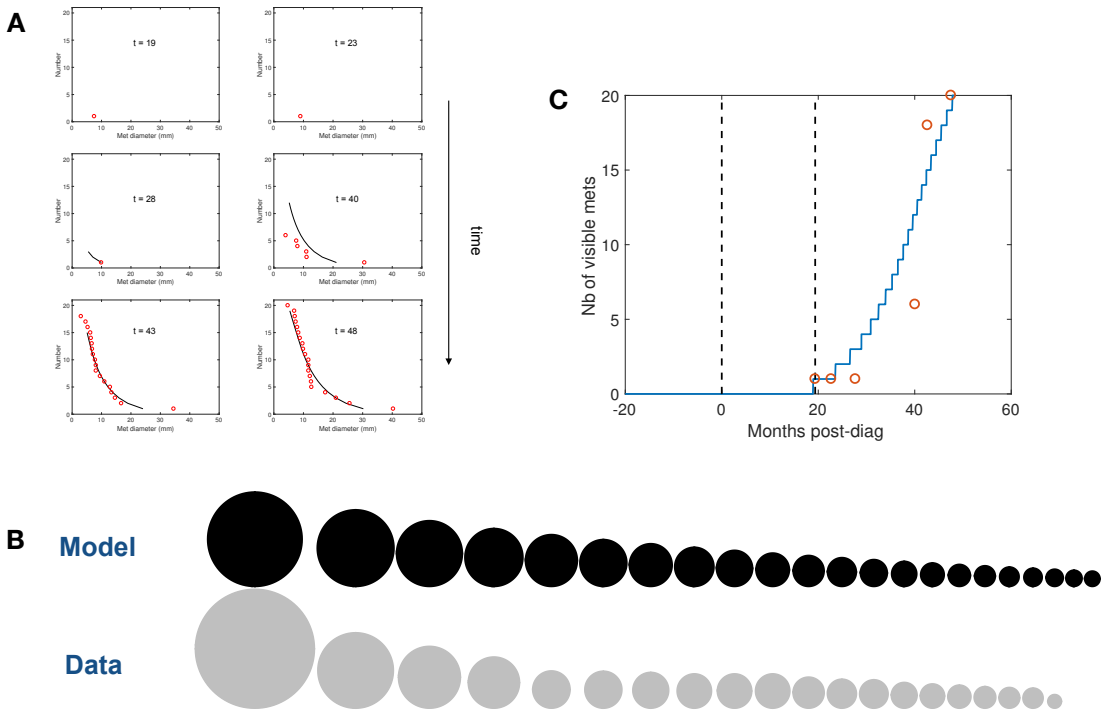

Figure 3.6 – Fit of the model with α_0, μ and γ as free parameters. A. cumulative distribution functions. time expressed in months. Red circles = data. Line = model fit. B. Comparison of the size distributions at T_7. C. number of visible metastases. The two vertical dashed lines correspond to the diagnosis time and the time of first detection of BM. Circles = data. Curve = fit

Clinically meaningful inferences from the model Once the parameters of the model determined (here from an *a posteriori* fit of the longitudinal measurements of visible BMs), several quantities of clinical interest could be derived. First, the sub-clinical phase of the cancer history was estimated to be about 4.5 years (Figure 3.7A). At the time of diagnosis, while no BM was detected, the model predicted that some of the further emerging BMs were already present, with a size distribution plotted in Figure 3.7B. Specifically, 12 out of the 20 BMs that have become visible before death of the patient were predicted to be already present. The largest one was predicted to contain 1.21×10^5 cells ($\simeq 0.61$ mm in diameter) at diagnosis. Its inception was calculated to have occurred 1.8 years before diagnosis (corresponding to 2.7 years after the first primary tumor cancer cell), see Figure 3.7C. The growth curves of all the metastases that were visible on the last patient's exam are plotted in Figure 3.7D.

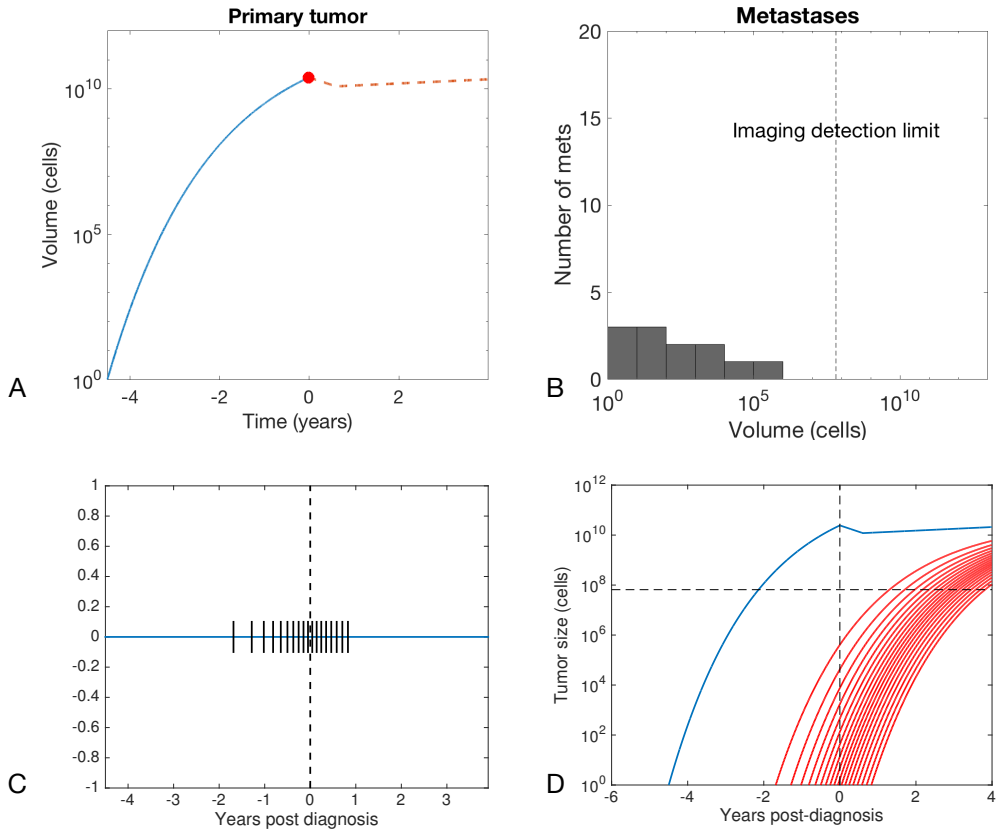

Figure 3.7 – Inference from the model. A. Reconstruction of the primary tumor growth curve. B. Predicted size distribution of metastases at diagnosis. C. Prediction of the birth times of the BMs. D. Prediction of the growth curves of the BMs

3.5 Conclusion

Our modeling philosophy elaborates on Fisher's theory [Fisher, 1977] of cancer as a systemic disease and relates also to the parallel progression model [Klein, 2009]. The dissemination rate d, characterized by the parameters μ and γ, quantifies the metastatic potential and allows for a continuum of possibilities between early and late dissemination. Our results seem to parallel clinical evidence of the impact (and importance) of early surgery—particularly in the case of breast cancer. For example, in a retrospective study of 2 838 breast cancer patients, the postsurgical residual risk of recurrence at 5 years for stage I disease was 7% [Brewster et al., 2008]. Consistently, our quantitative analysis demonstrates that in this case, for most patients, metastases that could have been shed before diagnosis would not develop into overt clinical disease during the remaining life history of the patient. For stage IV breast cancer (that would correspond, in our formalism, to a large value of μ), our analysis predicts only negligible benefit of the surgery (if only considering reduction of metastatic shedding), in accordance with preliminary results of a recent clinical trial

[Badwe et al., 2013].

Clinically, our methodology could be used to refine/optimize therapeutic strategies for patients diagnosed with a localized cancer and inform on the timing of surgery, extent of occult metastatic disease, and probability of recurrence. In turn, this may affect decisions on duration and intensity of presurgical neoadjuvant or postsurgical adjuvant treatments [Early Breast Cancer Trialists' Collaborative Group (EBCTCG), 2005].

Chapter 4

Therapy

Contents

Abstract

After having investigated problems regarding the natural history of tumor growth and metastasis (from both the biological and clinical point of views) in the previous chapters, we report now our contributions regarding quantitative modeling of the effect of systemic therapies.

In the introduction, we perform a short and non-exhaustive review of historical successes of mathematical modeling as underlying theoretical concepts for the administration of systemic therapies (mostly cytotoxic chemotherapies). This review was written mostly in collaboration with Eddy Pasquier, Nicolas André and Joseph Ciccolini and published in [Benzekry et al., 2015b].

So far, we have identified two general classes of therapeutic applications of mathematical modeling. The first concerns the rational design of the scheduling of anti-cancer agents in clinical trials. Given the increasingly diverse arsenal of systemic agents in oncology (from targeted therapies to immune checkpoint inhibitors passing by classical cytotoxic agents and anti-angiogenic drugs), we believe mathematical modeling has the potential to guide rational *combinations* and sequences of administration and improve on the empirical trial-and-error current practice. This is the sense of the combined modeling and experimental studies reported in the second section of this chapter that were the topic of several publications [Imbs et al., 2017, Mollard et al., 2017, Ciccolini et al., 2015]. These were performed in strong interaction with the experimental side of the SMARTc team led by Joseph Ciccolini (Inserm UMR S_911, Marseille, France), who conducted the experiments of the studies of the second section together with Séverine Mollard and Arnaud Boyer. I also co-supervised Diane-Charlotte Imbs and Raouf El Cheikh who performed part of the population fits of the models.

A second class of applications of mathematical modeling that we identified concerns the personalized adaptation of the dosing and timing of the drugs' administrations, given accessible clinical data accessible (e.g. imaging, circulating biomarkers or biopsies). Although this is a trend that has been present in the proceedings of our studies and that we are engaged in in current and future projects, we have not achieved yet any significant contribution in this area.

4.1 Introduction

Innovative technologies have dramatically changed the way we treat cancer. From crude surgery for centuries, to the introduction of radiotherapy in the 1930's and that of chemotherapy in the 1950's [Mukherjee, 2011], we can now envision the development of personalized treatments for cancer patients, thanks to the advances made in biology, chemistry, physics, mathematics and engineering. Immune checkpoint inhibitors, anti-angiogenics and targeted therapies have already entered the clinic with various level of success, and innovative technologies in imaging, PK/PD modeling and the -omics are helping clinicians in their decision making on a daily basis. Yet, chemotherapy is still administered today almost the exact same way it was fifty years ago. In [Benzekry et al., 2015b] we reviewed some of the theoretical concepts that were most influential for the administration of anti-cancer agents.

4.1.1 Historical concepts of chemotherapy

Skipper-Schabel-Wilcox and the log-kill model

Fifty years ago, Skipper, Schabel and Wilcox were the first to introduce theoretical concepts for the optimal design of chemotherapy schedules [Skipper et al., 1964]. Based on experimental studies involving L1210 leukemic cells – which exhibit exponential growth when left untreated –, they introduced and demonstrated the log-kill effect for several cytotoxic agents, including 6-mercaptopurine, 5- fluoruracil and vinblastine [Skipper et al., 1964]. This principle, based on an analogy with the law of mass action for kinetic reactions in chemistry, states that exposure to a given amount of drug kills a constant *fraction* of a cancer cell population, hence reducing it of a constant amount in logarithmic scale (Figure 4.1). Further on, based on their experimental work that demonstrated that the presence of as little as one single leukemic cell was sufficient to lead to the host death, they argued that the goal of the therapy should be to achieve complete cure of the disease, i.e. eradication of *all* malignant cells. In this context, they demonstrated that a large-dose/short-time (single administration) schedule was superior to a chronic (daily) low-dose schedule (with similar or larger total dose), thus leading to the maximum tolerated dose (MTD) paradigm [Skipper, 1965]. However, when this view (that was involved in the calculation of the number of cycles required for cure) was applied to the adjuvant systemic treatment of micrometastases (for breast cancer for instance), it did not lead to the expected results [Early Breast Cancer Trialists' Collaborative Group (EBCTCG), 1992]. Two major criticisms were addressed to the work of Skipper et al.: (1) they considered a homogeneously sensitive population of cancer cells (i.e. no resistance was explicitly taken into account) and (2) the experimental system they employed was limited to a single leukemic cell line and their conclusions might not extend to solid tumors.

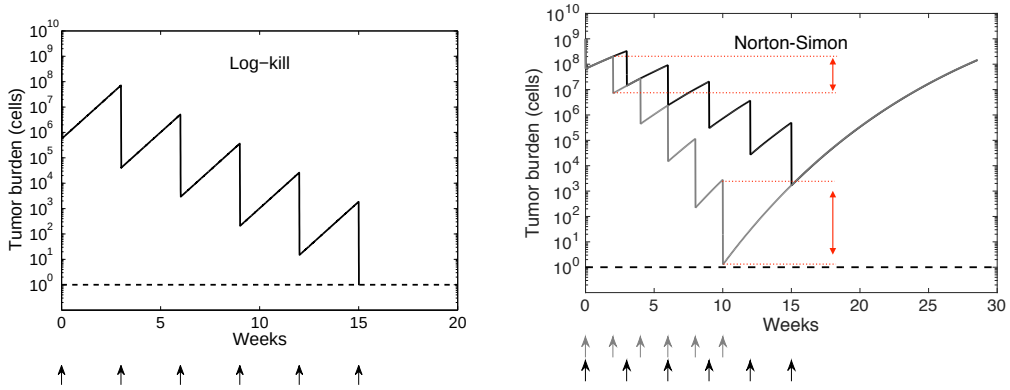

Figure 4.1 – Left: Skipper–Schabel–Wilcox log-kill model. Tumor growth is exponential (linear in log-scale) and each cycle of chemotherapy results in removal of a constant fraction of the tumor volume (as opposed to a constant amount of cells). The dashed line represents the size of one cell, that classical MTD chemotherapy approaches consider as the goal to achieve for eradication of the disease. Right: Norton–Simon model. Untreated tumor growth is Gompertzian and exhibits a decreasing specific growth rate. The Norton–Simon hypothesis implies a larger log-kill for smaller tumors and suggests to densify the chemotherapy administration protocol. This is illustrated by comparison of a three-weeks regimen (black curve) and a densified two-weeks regimen (gray curve). The latter exhibits deeper drop of the tumor burden and thus larger probability of "cure". However, note that when tumor regrows, both schedules have the same time to recurrence.

Clonal resistance and the Goldie-Coldman model

Regarding point (1), substantial efforts in the modeling of resistance to cytotoxic agents have been provided by the work of Goldie and Coldman [Goldie and Coldman, 1979]. The Goldie-Coldman model states that mutation rates toward resistance are relatively high within a population of tumor cells and that mutations develop spontaneously during the natural course of the disease (innate resistance). This implies that the treatment should start as soon as possible in order to avoid the natural tumor progression leading to the presence of more resistant cells. It also implies that if several drugs are to be administered and cannot be given simultaneously for toxicity constraints, they should be delivered alternatively in order to avoid resistance to drug B to develop during therapy with drug A. However, predictions of this model were ruled out by several trials, in breast cancer patients for instance, where strategies that delayed therapy or did not respect strict alternation of combination regimen were proven to perform at least as well as the Goldie–Coldman recommended strategy [Frei et al., 1961]. One of the main hypotheses underlying the Goldie–Coldman model is the concept of absolute resistance, which is discussable. Indeed, there is some evidence that tumors can exhibit various levels of relative drug resistance [Kern et al., 1997].

Kinetic resistance and the Norton-Simon hypothesis

In the 1960s, thorough study of tumor kinetics led to the realization that the specific tumor growth rate for solid tumors, instead of being constant (exponential growth), was rather a decreasing

function of the volume, provided tumor growth is observed long enough [Steel and Lamerton, 1966, Spratt et al., 1993] (see also chapter 1). In mathematical terms, tumor growth can be formalized by means of the following differential equation:

$$\frac{dV}{dt} = f(V)V \tag{1}$$

In the 1970s, Norton and Simon [Norton and Simon, 1977] revisited the Skipper– Schabel–Wilcox log-kill hypothesis, in order to extend it to growing tumors with non-constant specific growth rate. They suggested that since chemotherapy is mostly based on anti-mitotic agents, it should only be active against these cells that are actively proliferating, i.e. precisely the ones that contribute to the volume increase in (1) [Norton and Simon, 1977]. Moreover, the current view of the effect of chemotherapy (log-kill) was in contradiction with clinical observations such as: (a) the effect on small tumors in an adjuvant setting not as pronounced as expected and (b) decreased sensitivity to therapy observed also for very large tumors. Instead of a killing term proportional to the volume of the tumor, they proposed a killing term proportional to the tumor growth rate, i.e.:

$$\frac{dV}{dt} = f(V)V(1 - C(t))$$

They demonstrated that their model was consistent with clinical observations, able to fit preclinical experiments and superior to the log-kill model in predicting the future course of an experimental treated growth curve from a few initial measurements [Norton and Simon, 1977]. This model has profound clinical implications. First, it predicts a superiority of densified dosing regimens. Indeed, if less inter-cycle time is allowed to the tumor to regrow, it reaches a smaller size at the beginning of the next cycle, thus a larger growth rate (Gompertzian growth) and consequently a larger amount of cells killed by the drug. This prediction was confirmed by clinical trials that densified administration drug schedules from every 21 days to every 14 days and showed benefit of applying the second regimen [Held et al., 2006]. Second, extending these concepts to drug combinations, the Norton–Simon model advocates for sequential administration of the drugs (in order to densify the treatment for each drug separately), as opposed to the strict alternation supported by the Goldie–Coldman model. Clinical trials (for the treatment of breast cancer for instance) again confirmed this prediction of the Norton–Simon model [Bonadonna et al., 2004, Citron et al., 2003]. This example demonstrates how rational thinking and mathematical methods, based on phenomenological theories, can help to successfully guide clinical trials [Norton and Simon, 1986, Simon and Norton, 2006]. Under the Norton–Simon hypothesis, larger absolute kill of cancer cells resulting from early chemotherapy, as opposed to late chemotherapy, might be counter-balanced by faster regrowth due to high growth rates of small tumors (see Figure 4.1), thus leading to similar overall survival in both cases, despite significantly different times to relapse [Dang et al., 2003].

4.1.2 Modern cancer biology and metronomics

During the early phases of the development of chemotherapy, the ultimate goal of therapy was always complete cure from the disease. As stated by Skipper et al.: "(...) it appears that high-level, short-term schedules offer considerably greater potential for obtaining "cures" " [Skipper et al., 1964]. Interestingly, even if these investigators were pleading for this option, they already had noticed that this might not be the best strategy to achieve best long-term control of the disease. Indeed, the previous quote continues with "This preference does not necessarily hold with regards to achieving maximum increase in life span of animals which die in spite of therapy". Since several years, there is an increasing trend toward a paradigm shift in clinical oncology: in view of the failure to cure patients using conventional approaches, investigators proposed to change the goal of therapy from complete eradication of the tumor to a long-term management of the disease [Gatenby, 2009]. This suggests that instead of waiting for "magic bullets" that would provide an absolute and complete solution, one might instead look into optimization of already existing therapeutic tools. In order to improve current cancer treatments, historical concepts need to be revised to better take into account the complexity of the disease, including the toxicities of anti-cancer agents, impact of the tumor microenvironment (e.g. vasculature and immune system) and clonal heterogeneity on the efficacy of chemotherapy protocols. While an exhaustive review of the concepts underlying modern anti-cancer biology, even if only from the scope of the contribution of mathematical modeling, is beyond the aim of this review, we mention hereafter specific examples that we believe are illustrative and inspirational for the usefulness of mathematical constructs to counteract cancer dynamics.

Toxicities of cytotoxic agents

Following the implications from the Norton-Simon hypothesis, densification of the cytotoxic treatment protocols in the treatment of breast cancer led to agressive schedules that induced severe toxicities. Of particular importance are hematological toxicities such as neutropenia potentially leading to toxic death of the patients. In an effort of controlling these toxicities, Barbolosi and Iliadis developed a pharmacokinetics/pharmacodynamics model for white blood cell counts and defined an optimal control problem for minimization of the tumor burden under clinically relevant toxicity constraints [Iliadis and Barbolosi, 2000, Barbolosi and Iliadis, 2001, Barbolosi et al., 2003]. This model was further enhanced with an interface model for description of the exposure as a function of the circulating concentration [Meille et al., 2008]. Importantly, these investigators were the first (up to our knowledge) to use such a mathematical model for the design of a phase I/II clinical trial [Meille et al., 2016, Hénin et al., 2016]. The MODEL1 trial was designed for dose-escalation and dose-densification of the combined administration of docetaxel and epirubicin in the treatment of metastatic breast cancer. Not only could the model-based regimen control otherwise life-threatening toxicities, but efficacy was also improved [Hénin et al., 2016]. Extension of this model for the treatment of small cell lung cancer has been considered recently in [Faivre et al., 2017].

Tumor heterogeneity and (epi)-genetic resistances

In a very elegant, simple and conceptually powerful theoretical study, Hahnfeldt, Folkman and Hlatky [Hahnfeldt et al., 2003] re-analyzed the problem of dose repartition in light of tumor heterogeneity. They considered two subpopulations of cancer cells with two distinct sensitivities to a given drug, with transition rates between the two populations. Importantly, the transition rate from the less sensitive population to the most sensitive one was assumed to be positive, thus allowing for a resensitization effect. Under their minimal framework that allows to perform explicit computations, they demonstrated that more regularly spaced dosing of the drug yields better final tumor reduction when compared to irregular spacing, for both single and multiple cycles therapies. Eventually, based on the assumption that the endothelium is more subject to resensitization than the tumor compartment, they also proposed their model as an explanation for the anti-angiogenic basis of metronomic chemotherapy [Kerbel and Kamen, 2004].

Inspired by the example of invasive species in ecology and the use of pesticides, a situation where complete eradication is usually impossible due to high phenotypic diversity that leaves resistant individuals after intervention, Gatenby [Gatenby, 2009] proposes to see a tumor as an ecosystem ruled by evolutionary laws. In this context, high dose chemotherapy might have the deleterious effect of selecting for the most resistant cells, by eliminating the sensitive competitors. On the other hand, a low-dose continuous therapy, by keeping a positive amount of sensitive cells, might provide a better long-term control of the total population [Gatenby, 2009]. In a study using both mathematical and experimental approaches, Gatenby and colleagues further developed this concept and introduced the idea of adaptive therapy. It consists in modulating the dose and frequency of therapeutic administrations in order to maintain a constant tumor volume, as opposed to the conventional approach that administers a fixed dosing regimen repeated over several cycles [Enriquez-Navas et al., 2016, Gatenby et al., 2009].

Applying the same evolutionary concepts to population dynamics of cancer cells, Clairambault et al. developed a modeling framework that revisited the concepts underlying the Delbrück–Luria / Goldie–Coldman model of spontaneous development of resistance [Chisholm et al., 2015]. In their work, they made two major hypotheses: (1) reversible, drug-induced (rather than irreversible and spontaneous) development of resistance, based on a recent experimental study and (2) varying levels of resistance (instead of the classic sensitive/resistant dichotomy). Point (2) was elegantly formalized in mathematical terms within the context of structured evolutionary population dynamics, by means of one (or more) continuous variable representing a phenotyping trait [Lorz et al., 2013, Lorz et al., 2015]. Full implications of these recent studies in terms of optimal scheduling have recently been published and generate non-trivial insights on optimal administration schedules emerging from the complex dynamics due to tumor heterogeneity [Pouchol et al., 2016].

Anti-angiogenesis

In 1999, Hahnfeldt et al. [Hahnfeldt et al., 1999] derived a biologically-based (yet technically simple) mathematical model for tumor growth under endogenous angiogenic signaling that was

able to describe the effect of several anti-angiogenic molecules. Based on this model, Ledzewicz and Schättler performed a full optimal control analysis for theoretical optimization of the scheduling of a drug with anti-angiogenic properties [Ledzewicz and Schättler, 2007]. Interestingly, they found that the optimal control, instead of having a bang-bang expression (constant full-dose sections separated by breaks – i.e. conventional chemotherapy), could exhibit singular arc portions where the drug is administered at a lower dose than the MTD, with varying rates. This is the expression in mathematical terms of the concept of a biologically optimal dose, which might differ from the MTD.

Metronomic chemotherapy

Using the Hahnfeldt model further, d'Onofrio et al. [d'Onofrio et al., 2009] studied the effect of scheduling variations and obtained that a drug targeting the vasculature would have a better effect if administered more frequently at lower doses (assuming constant total dose). When the drug effect was further assumed to depend on the vascular density, a nontrivial optimal metronomic inter-administration time was found [d'Onofrio and Gandolfi, 2010a]. Interestingly, metronomic scheduling additionally exhibited enhanced robustness toward noise-induced transitions (i.e. escape from therapeutic control) in response to stochasticity in the clearance rate [d'Onofrio and Gandolfi, 2010b].

Recently, mathematical models specifically tailored for the analysis of the anti-angiogenic effect of metronomic chemotherapy in various concrete clinical settings were introduced [Benzekry et al., 2012a, Faivre et al., 2013, Barbolosi et al., 2016]. All these rely on the same assumptions: (a) chemotherapy has an anti-angiogenic effect by killing endothelial cells in addition to its cytotoxic effect on cancer cells [Browder et al., 2000, Klement et al., 2000], (b) cancer cells develop resistance whereas endothelial cells do not (due to larger genetic stability) and (c) drug action is stronger on endothelial cells than on tumor cells [Klement et al., 2000]. Using realistic pharmacokinetic models and an interface model for description of the efficacy from the concentration of the drug in the central compartment, MTD and metronomic schedules were compared in silico for the administration of docetaxel [Benzekry et al., 2012a] or temozolomide [Faivre et al., 2013]. A model-designed regimen employing of an adapted version of this model for the use of gemcitabine in the treatment of neuroblastoma was recently shown to be superior to the standard schedule in preclinical experiments [Ciccolini et al., 2017]. In parallel, this model was also used to design the metronomic schedule in a phase Ia/Ib clinical trial of oral vinorelbine in metastatic non-small cell lung cancer [Elharrar et al., 2016].

In the clinic, most cancer-related deaths are not due to the primary tumor, but rather to the metastases [Chaffer and Weinberg, 2011]. To address the issue of treatment on a population of tumors (rather than a single tumor), as well as the effect on the dissemination process, we defined an optimal control problem written for an organism-scale model of metastatic development [Benzekry and Hahnfeldt, 2013]. Although complete mathematical analysis was too complicated to be achieved, we could perform a simulation study and found that the overall efficacy of cytotoxic

agents, either alone or in combination with anti-angiogenic drugs, was generally maximized when employing a metronomic schedule rather than the MTD. Interestingly, in some instances (e.g. values of the parameters, objective function considered), differences in the best strategy occurred between the treatment of the (isolated) primary tumor and the treatment of the (systemic) cancer at the organism scale. These theoretical predictions were independently confirmed in pre-clinical studies using mouse models of spontaneous metastases [Ebos et al., 2014].

4.2 Model-driven optimization of antiangiogenics + cytotoxics

In the previous section, we described how mathematical modeling could be used to improve treatment regimen of *single* anti-cancer drugs or combination of drugs with similar (cytotoxic) action. However, given the current wide scope of possible anti-cancer therapeutic action, even with only chemical weapons, mathematical modeling has also relevance for the matter of the *sequence* of administration of several agents with different modes of action. Of particular relevance is the combination of chemotherapy and anti-angiogenics, in view of the intrinsic link between the vasculature extent and functionality and the drugs' delivery. Relevant to this matter is the phenomenon of *vascular normalization*, a counter-intuitive effect of anti-VEGF agents that transiently *improves* the functional properties of the vasculature and thus the delivery of cytotoxic compounds. Based on previous theoretical modeling work [Benzekry et al., 2012b], in collaboration with the SMARTc team (Inserm S_911, Marseille, France), we conducted a series of experimental and modeling studies to investigate the utility of mathematical modeling in finding an optimal therapeutic window for sequential administration of bevacizumab and cytotoxic agents [Ciccolini et al., 2015]. These were published in two papers, one for breast cancer [Mollard et al., 2017] and the other for non-small cell lung cancer [Imbs et al., 2017]. Experiments were conducted by Joseph Ciccolini, Arnaud Boyer and Séverine Mollard. Part of the modeling analysis of the second study was conducted during the postdoctoral contracts of Diane-Charlotte Imbs and Raouf El Cheikh, who I supervised on this part.

4.2.1 Introduction: vascular normalization and implications for combination of antiangiogenic and cytotoxic agents

Launched in 2004, bevacizumab has been approved since then in a variety of settings in solid tumors such as colorectal, breast, lung or ovarian cancers, with mixed and sometimes still questioned impact on survival [Keating, 2014]. Of note, bevacizumab has always only been approved as a concomitant administration with associated cytotoxics. Several studies from independent academic groups have suggested that anti-angiogenics could induce a transient phase of vasculature normalization with increased tumor blood perfusion, prior to exerting its antiangiogenics properties [Jain, 2001, Jain, 2005, Dickson et al., 2007, Jain, 2014, Arjaans et al., 2016]. Indeed, while

the unaltered tumor vasculature is tortuous, chaotic and poorly functional (Figure 4.2) [Carmeliet and Jain, 2000], bevacizumab prunes and remodels tumor vessels to make them resemble normal tissues in terms of structure and function [Carmeliet and Jain, 2011, Jain, 2013].

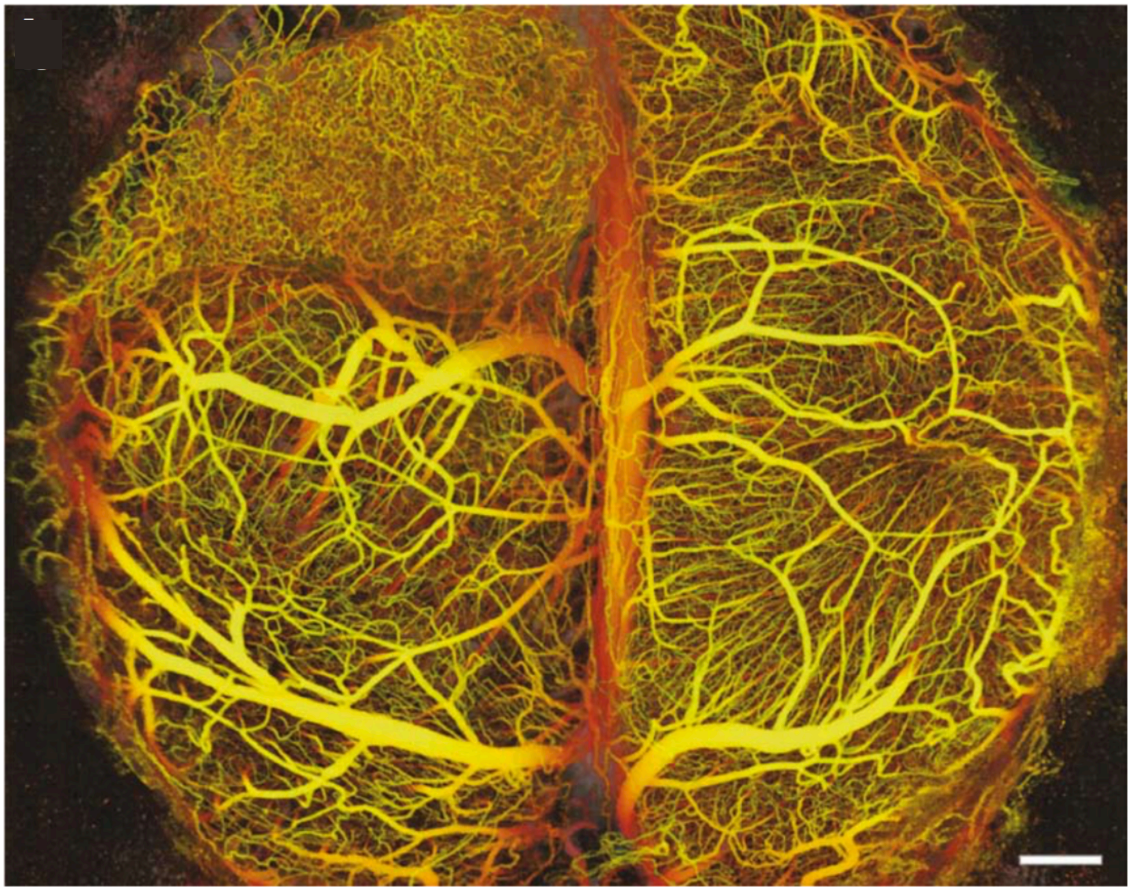

Figure 4.2 – Whole brain vasculature of a mouse bearing a xenografted U87 glioma tumor showing abnormal organization of the tumor vasculature. Reproduced from [Vakoc et al., 2009].

This paradoxical action has been considered as possibly generating a time-window to administrate chemotherapeutic agents, thus suggesting a paradigm shift from concomitant to sequential dosing. Indeed, delaying chemotherapy could allow higher quantities of drugs to reach the tumor, provided that their administration coincides with this normalization phase. This led us to define the following problem, for which we believe mathematical modeling can be of help.

Therapeutic problem 1. *What is the optimal time gap between administration of an anti-angiogenic agent such as bevacizumab and cytotoxic chemotherapy?*

As early as 2004, it has been shown that blocking VEGFR2 could decrease tumor hypoxia at the beginning of the treatment, thus demonstrating that transient normalization of tumor neovessels happens indeed with antiangiogenics [Tong et al., 2004, Winkler et al., 2004]. This was

already associated with improved efficacy of combined radiotherapy or chemotherapy. Indeed, because disrupted tumor vasculature may lead to resistance to chemotherapy and radiotherapy due to subsequent higher interstitial fluid pressure, and reduced blood flow lowering drug delivery [Tejpar et al., 2012], alternate scheduling with antiangiogenics could overcome these resistances. Ever since, several groups have worked on this issue, mostly as part of experimental therapeutics [Arjaans et al., 2016, Cesca et al., 2016, Dickson et al., 2007].

Only few clinical trials have investigated on alternate scheduling with bevacizumab. The BRANCH study evaluated bevacizumab in rectal cancer patients after standard concomitant dosing or alternative sequential administration. Whereas concomitant dosing was little effective, the sequential administration led to 50% of tumor regression rate with 85% of 5-years survival and better tolerance [Avallone et al., 2015]. These promising results supported the ongoing OBELICS study (Optimization of BEvacizumab scheduLIng within Chemotherapy Scheme), a phase-3 trial that will compare different sequences of bevacizumab associated with chemotherapy [Avallone et al., 2016]. Despite these encouraging findings, the need for identifying proper biomarkers to forecast bevacizumab impact on neovessels remains critical [Tredan et al., 2015] and until they are made available, in silico tools could be helpful to optimize alternate schedules.

In contrast to the many pharmacodynamic models describing the action of cytotoxics on tumor growth [Barbolosi et al., 2016], and despite substantial theoretical efforts in the field of cancer modeling to simulate angiogenesis and tumor-vasculature interactions [Anderson and Chaplain, 1998, Chaplain et al., 2006, Billy, 2009, Lignet et al., 2013], relatively few mathematical models of anti-angiogenic therapy have been actually confronted to experimental data [Hahnfeldt et al., 1999, Rocchetti et al., 2013], and even less have investigated combined effects of cytotoxics with antiangiogenics [Rocchetti et al., 2013, Wilson et al., 2015]. To address this issue, we developed a phenomenological model describing the effect of antiangiogenics on vasculature quality throughout time, thus potentially forecasting when the normalization phase occurs (see Figure 4.3) [Benzekry, 2012a]. When coupled with an efficacy component, this model should allow to compare *in silico* differences in efficacy depending on the lag-time between cytotoxics and antiangiogenics, thus helping in decision-making prior to start the actual experiments.

4.2.2 Mathematical modeling of vascular normalization

Semi-mechanistic model

In our studies, we used several models with several purposes. The main idea of all of them was to depart from the Hahnfeldt model which accounts for the effect of anti-angiogenic agents by means of a dynamic carrying capacity $K(t)$ [Hahnfeldt et al., 1999]. While associating the carrying capacity with the vascular supply, this model by itself does not allow for a description of the *quality* of the vasculature. Therefore, we first extended it in a minimal way to account for a description of this feature.

For all drugs, appropriate pharmacokinetic models (often one-compartmental with absorption)

and parameters have been described previously in the literature and were employed to describe the concentrations of the cytotoxic and antiangiogenic drugs , respectively denoted $C(t)$ and $A(t)$ (see [Mollard et al., 2017, Imbs et al., 2017] and references therein) .

The effects of the cytotoxic drugs (paclitaxel for the breast study, cisplatin and pemetrexed for the lung study) were modeled similarly as in [Simeoni et al., 2004] where the authors considered a delay in the effect the drug(s), due to the fact that the cells are not directly removed after cytotoxic administration because they only die when reaching a specific step of the cell cycle. After being affected by the drug(s), the tumor cells thus stop proliferating and go through three compartments Z_1, Z_2 and Z_3 before being removed from the system. Following reported observations, we considered that paclitaxel also had an anti-angiogenic effect [Pasquier et al., 2010].

Following biological rationales [Tong et al., 2004] and previous theoretical work [Lignet et al., 2013], our idea for the definition of a dynamical quality of the vasculature was to divide $K(t)$ into two compartments: a stable one $S(t)$ (mature vessels) and an unstable one $U(t)$ (immature vessels), see Figure 4.3. The anti-angiogenic action of the drugs was then further assumed to occur on U (rather than S), because it represents the component of the vasculature directly affected by VEGF stimulation, which is the target of bevacizumab. Then, the (macroscopic) quality of the vasculature was defined as the ratio of the stable component of the vasculature over the total amount of blood vessels. The drugs delivery was assumed to be modulated by the mature vascular capacity, represented in the model by the variable $S(t)$. The equations write:

$$
\begin{cases}
\frac{dV}{dt} = aV\ln\left(\frac{S}{V}\right) - e_{CT}QSC(t)V & V(t=0) = V_0 \\
\frac{dU}{dt} = bN - dN^{2/3}U - \chi U - (e_{AA} + 5e_{CT})QSA(t)U & U(t=0) = U_0 \\
\frac{dS}{dt} = \chi U - \tau S & S(t=0) = S_0 \\
\frac{dZ_1}{dt} = e_{CT}QSC(t)V - kZ_1 & Z_1(t=0) = 0 \\
\frac{dZ_2}{dt} = kZ_1 - kZ_2 & Z_2(t=0) = 0 \\
\frac{dZ_3}{dt} = kZ_2 - kZ_3 & Z_3(t=0) = V_0 \\
N = V + Z_1 + Z_2 + Z_3 & \\
Q(t) = \frac{S(t)}{U(t)+S(t)} &
\end{cases}
$$

with V_0 denoting the number of cells injected in the experiments and U_0 and S_0 the initial conditions of the vasculature subject to fit to the data. The variable $N(t)$ denoted the total number of tumor cells alive at time t.

In [Mollard et al., 2017] we demonstrated that this model was able to reproduce experimental data that demonstrated the superiority of a sequential scheme where bevacizumab was administrated before paclitaxel (48% reduction in tumor size at study conclusion compared with concomitant dosing). However, due to the high number of variables and parameters in the model in comparison

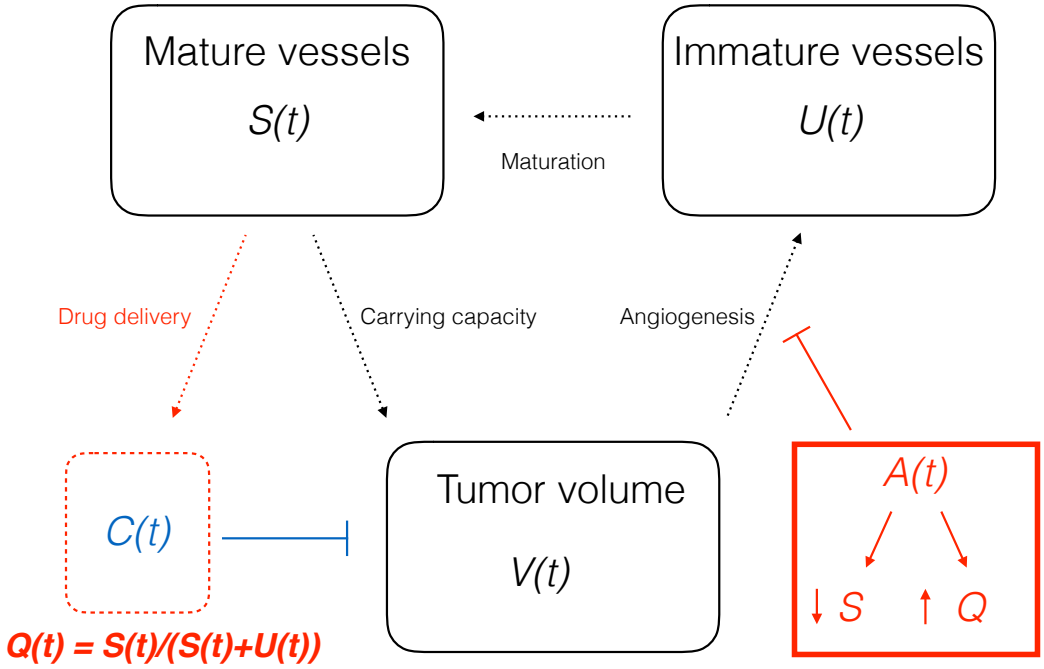

Figure 4.3 – Scheme of the semi-mechanistic mathematical model of vascular normalization

to the relative scarcity of the data obtained in the experiments (only the tumor growth curves), the model was highly unidentifiable with very large standard errors on the parameters estimates [Mollard et al., 2017]. Thus, only moderate confidence can be attributed to the optimal interval predicted by the model (of 2.4 days). To address the identifiability issue, we also built a simpler model with fixed, schedule-dependent quality of the vasculature. While this model was by definition not able to address the therapeutic problem 1, it was nevertheless useful in quantitative inference for the effect of a sequential administration of the two drugs with bevacizumab first, for which it estimated (under our model assumptions) an approximate 5-fold increase in drug delivery.

Simpler model

To address the identifiability issue of the previous model, we :

1. investigated iteratively simpler models that would nevertheless still keep a dynamic quality of the vasculature. This last feature was indeed essential to keep in the model in order to capture the trade-off between vascular normalization and disruption following the administration of anti-angiogenic agents and thus predict the best delay between administration of the two

drugs.

2. employed mixed-effects modeling for fitting population distribution of the parameters to the pooled data of all animals. This reduces the number of parameters to be estimated from $N \times p$ to $p^2 + p$ where N is the number of animals and p the number of parameters.

This new model writes:

$$\begin{cases} \frac{dV}{dt} = aV \ln\left(\frac{K}{V}\right) - e_{CT} Q C(t) V & V(t=0) = V_0 \\ \frac{dK}{dt} = bN - dN^{2/3} K - e_{AA} Q A(t) K & K(t=0) = K_0 \\ \frac{dQ}{dt} = A(t) - g(Q - Q_0) & Q(t=0) = Q_0 \\ \frac{dZ_1}{dt} = e_{CT} Q C(t) V - kZ_1 & Z_1(t=0) = 0 \\ \frac{dZ_2}{dt} = kZ_1 - kZ_2 & Z_2(t=0) = 0 \\ \frac{dZ_3}{dt} = kZ_2 - kZ_3 & Z_3(t=0) = 0 \\ N = V + Z_1 + Z_2 + Z_3 \end{cases}$$

In comparison with the previous one, we abandoned the semi-mechanistic description of the quality of the vasculature as deriving from the division into mature and immature blood vessels. We also removed the dependence of the drugs' delivery on the vasculature (S in the previous model, K in the current one) since simulations showed that this feature had only little impact. The parameter Q_0 corresponds to a baseline value of vascular efficiency, hence thought to be small in view of the poor functionality of untreated tumor blood vessels [Carmeliet and Jain, 2000]. In this simpler model, the dynamics of Q are thus assumed to be stimulated by the presence of the anti-angiogenic agent, whose circulating concentration follows its own pharmacokinetics. The latter has long half-life of the order of ten days for bevacizumab [Lin et al., 1999].

4.2.3 Calibration, predictions and validation of the model in experimental non-small cell lung carcinoma

To investigate the usability of our model and verify its predictions, we employed the following strategy:

1. A first set of experiments (experiment-1) was performed with three arms: a control arm (no treatment), a concomitant arm and a sequential arm, with a delay of 4 days (determined arbitrarily) between bevacizumab and the two cytotoxics (cisplatin and pemetrexed). It demonstrated the superiority of the sequential regimen for both tumor growth and survival (Figure 4.4).

2. Data from experiment-1 were used to calibrate the parameters of the model (Figure 4.5). Simulation of the median behavior from the estimated population parameters confirmed the superiority of the sequential schedule (Figure 4.6A).

3. This calibration allowed to test *in silico* a wide range of possible gaps between the administration of the drugs and predicted an optimal delay of 3 days (Figure 4.6B-C). At the same time, a delay of 8 days was predicted to perform substantially worse. Of note, the model was also able to quantitatively predict inter-animal variability of this optimal delay, which was found to be small but non zero (Figure 4.6D).

4. These predictions were subsequently tested in a second round of experiments (experiment-2) involving two sequential arms (3 days and 8 days). The experiments confirmed the superiority of the 3 days sequential arm over the 8 days one (Figure 4.7).

We refer the interested reader to [Imbs et al., 2017] for materials and methods details.

Together, this proof-of-concept study demonstrated the validity of a simple semi-mechanistic mathematical model for description of tumor growth curves under the action of combined antiangiogenics + cytotoxics therapy with different sequences of administration of the drugs. Moreover, predictions of the model in terms of improved delay between the administration of the two types of drugs were confirmed experimentally, thus emphasizing the utility of mathematical modeling for a rational design of anti-cancer treatment regimen, instead of the empirical, costly, trial-and-error approach.

In addition, our model could be used in a biomarker-based strategy for improving anti-angiogenic therapy. No predictive biomarker has been clearly validated yet with anti-angiogenics [Collinson et al., 2014]. Our model parameters could be quantitatively linked to imaging and predictive circulating biomarkers with bevacizumab [Heist et al., 2015, Lassau et al., 2016]. Consequently, this would provide personalized simulations of tumor growth allowing to predict early the patient's response and to adapt the dose and timing of the treatment in order to maximize the treatment efficacy.

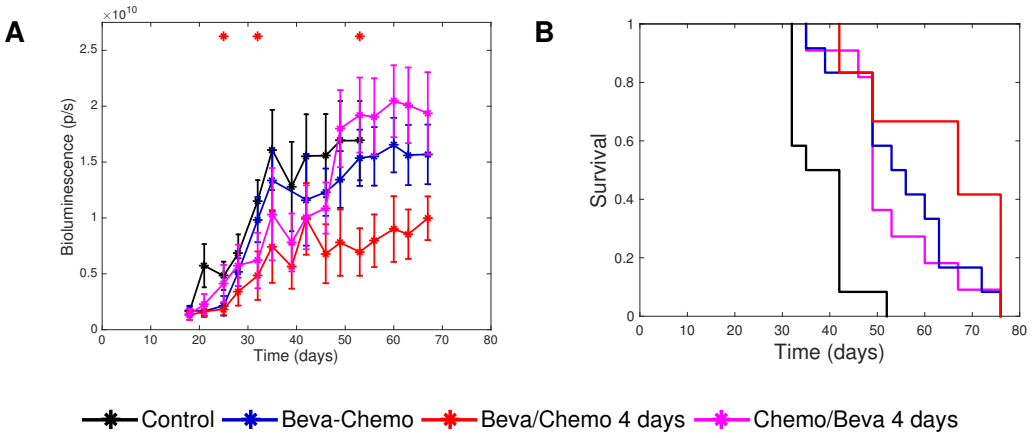

Figure 4.4 – Efficacy and Kaplan-Meier survival curves of experiment-1 A: Mean tumor growth curves for the 4 treatment arms of experiment-1. Signs above curves indicate statistically significant difference with the control arm (Student's t-test, $p < 0.05$). Sequential 4 days versus concomitant: 36% tumor growth reduction at study conclusion. B: Kaplan Meier plot of the overall survival for the 4 treatment arms of experiment-1. Median survival times: 39 days (control), 49 days (concomitant) and 67 days (sequential 4 days). Sequential 4 days was significantly superior to the concomitant group ($p = 0.0485$, log-rank test).

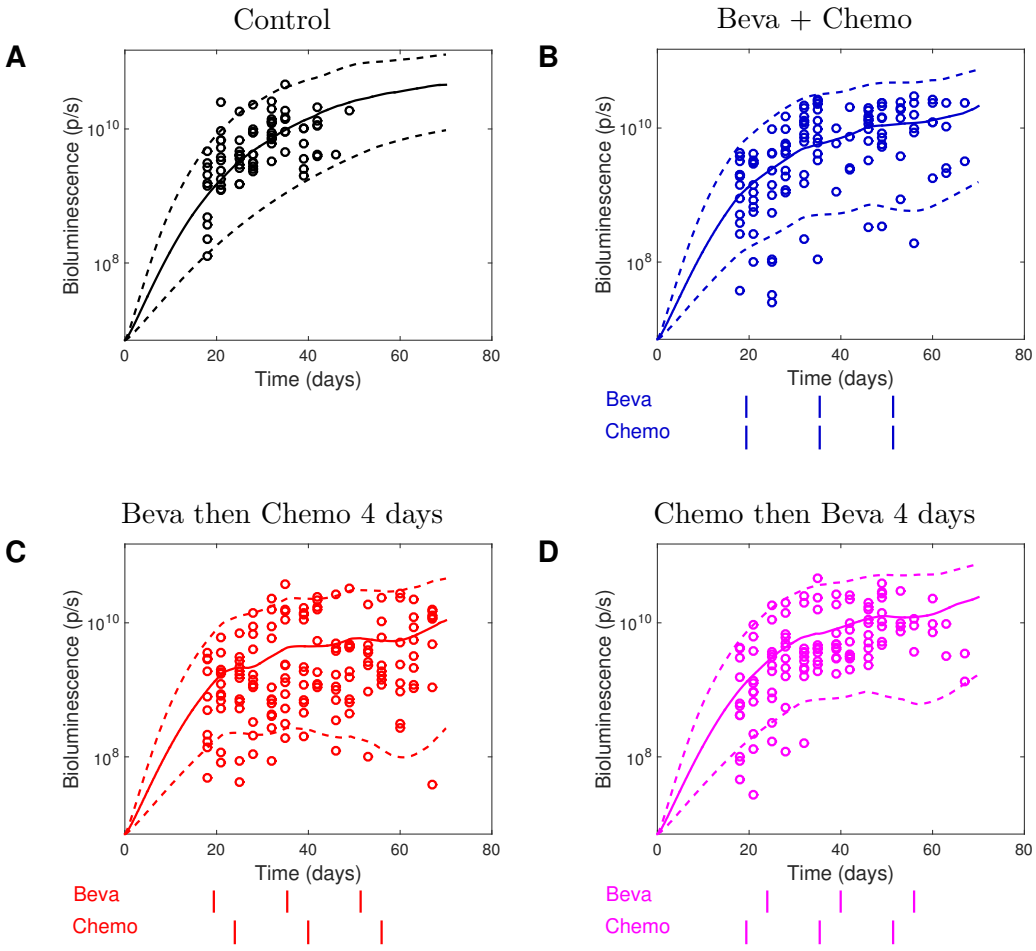

Figure 4.5 – Visual predictive check for experiment-1 population analysis. Circles: experimental data, solid lines: tumor growth simulated curves using median parameter values, dashed lines: 95% intervals for inter-animal variability, generated from the simulation of 1000 virtual animals with parameters distributed according to the distribution estimated by the mixed-effects fit (performed with Monolix).

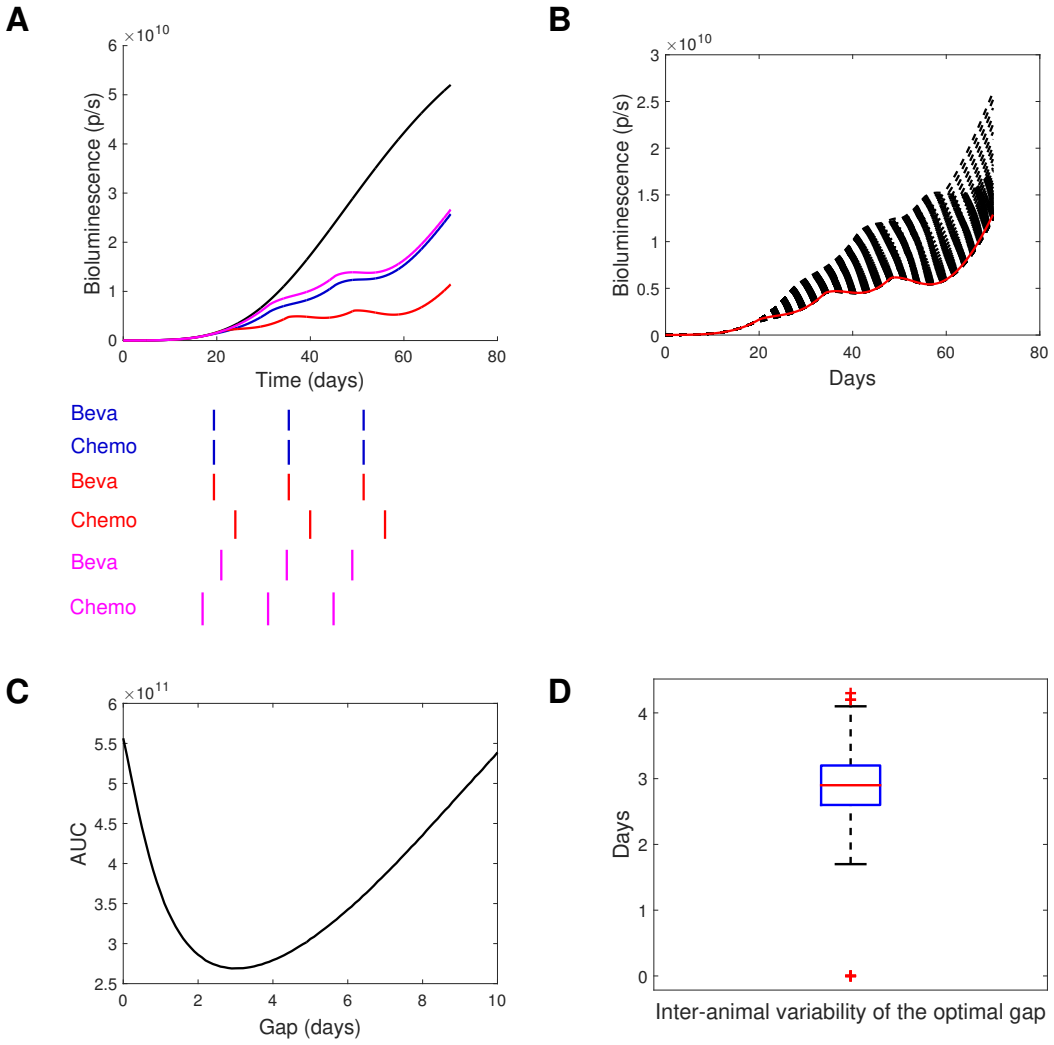

Figure 4.6 – Data-informed modeling simulations of various gaps between bevacizumab and pemetrexed-cisplatin administrations A: Median tumor growth curves. B: Simulations of the tumor growth using different time lags between the administration of bevacizumab and pemetrexed-cisplatin ("Beva then Chemo"). The red curve corresponds to a time lag of 3 days. C: Area under the tumor growth curve as a function of the time lag. D: Inter-animal variability on the optimal lag time between bevacizumab and chemotherapy (median = 2.9 days, standard deviation = 0.45 days).

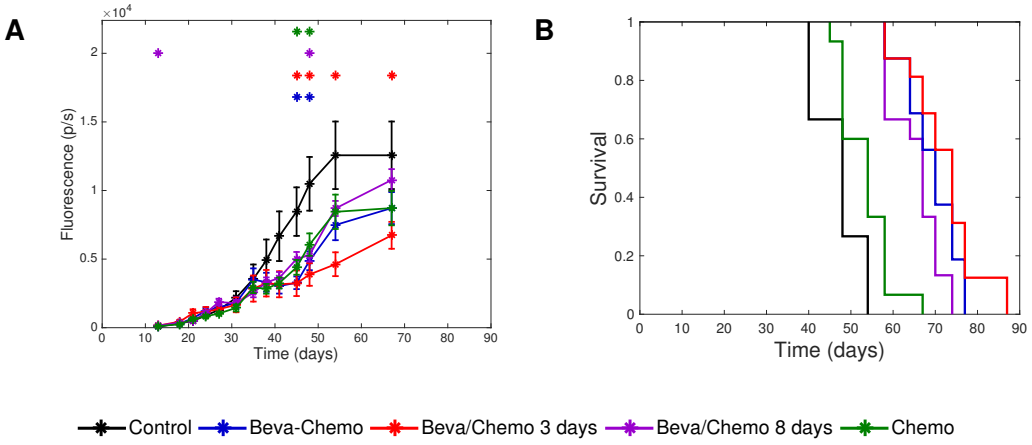

Figure 4.7 – Efficacy and Kaplan-Meier survival curves of experiment-2 A: Mean tumor growth curve for the 5 treatment arms of experiment-2. Signs above curves indicate statistically significant difference with the control arm (Student's t-test, $p < 0.05$). B: Kaplan Meier plot of the overall survival for the 5 treatment arms of experiment-2. Median survival times: 48 days (control), 54 days (chemotherapy), 67 days (sequential 8 days), 70 days (concomitant) and 74 days (sequential 3 days). Sequential 4 days was significantly superior to the sequential 8 days group ($p = 0.0056$, log-rank test)

Chapter 5

Research projects

Contents

Abstract

After having performed several research projects about cancer biology biological that deepened my understanding of the mechanisms of several processes involved in cancer, my current and future projects are now more directed towards a concrete clinical application of the models and methods that I have developed. I still keep a strong interest in the theoretical biology of metastasis and want to continue part of my activity in this area since the results that I obtained have led to opened questions (see below). Nevertheless, the majority of my research projects are within the scope of clinical and therapeutic applications, in line with the aims that I expressed in the introduction.

5.1 Theoretical biology of the metastatic process

In recent years, using sequencing data investigating phylogeny of clones within primary tumors and across metastases, several studies have brought new lights on **systemic-scale metastatic dynamics** [Gundem et al., 2015, Hong et al., 2015, Yachida et al., 2010]. In particular, several of the results from these studies have relevance regarding our own findings about the origin of metastases and the possibility of cells' exchanges between established tumors [Baratchart et al., 2015]. This brings back to the **self-seeding theory** proposed by Larry Norton and Joan Massagué who put forward the hypothesis that metastatic cells from distant lesions might seed back the original tumor [Norton and Massagué, 2006]. While the quantitative contribution of self-seeding to the growth of the primary tumor has been debated (of note, by means of mathematical methods [Scott et al., 2013a]), experimental proof of exchange of cells between artificially implanted tumors was established in [Kim et al., 2009]. Nevertheless, exchange of cells between the primary and the metastases remains to be studied, especially from the quantitative point of view. To this end, our biological collaborators at the LAMC obtained interesting preliminary results supporting the recruitment of circulating cells by established metastatic colonies (Figure 5.1). We want to further pursue these investigations and use modeling for example to quantify the relative amounts of disseminated cells that join established colonies as compared to the ones generating new lesions. Modeling can also be used to compare alternative hypothesis concerning the still open debate of metastases from metastases [Bethge et al., 2012, Tait et al., 2004, Sugarbaker et al., 1971] challenged by the previously cited recent reports [Gundem et al., 2015, Hong et al., 2015].

5.2 Clinical metastasis

In order to transfer the modeling framework for metastasis that I have contributed to develop into a **practical diagnosis and prognosis tool** that could help to refine and individualize adjuvant therapy, the critical next step is to find a way to estimate the parameter μ (for breast cancer) and

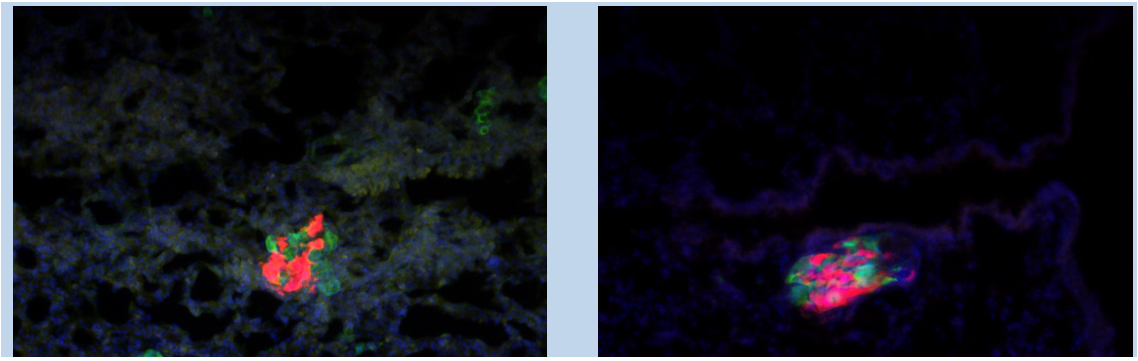

Figure 5.1 – Orthotopic injection of red-tagged (m-cherry) RENCA cells followed 15 days later by intra-caudal intra-veinous injection of green-tagged (GFP) RENCA cells demonstrating that secondary injected cells join already established colonies. Experiments performed by Wilfried Souleyreau and Lin Cooley within the LAMC (Inserm U1029, Bordeaux) led by Andreas Bikfalvi

μ, γ and α_0 (for BMs from lung cancer) in a patient-specific manner. One of the main challenges will be to do so **using data derived from the primary tumor only**, because metastases are often undetectable at the time of diagnosis. Although the value of μ might very likely depend on the combination of several phenomena (including some genetic alterations or the immune status of the patient, which could be linked to different biomarkers [Di Gioia et al., 2015]), recent successes of genetic signatures as prognosis factors for metastasis might allow for patient-specific estimation of μ [Reis-Filho and Pusztai, 2011].

For both breast and lung cancers, our objective now is to up-scale the number of patients and amount of individual information from clinical databases in order to develop the model as a predictive tool that could reach clinical use.

5.2.1 Mechanistic-based prediction of the time to metastatic relapse in breast cancer

I have recently initiated a collaboration with the Bergonié institute in Bordeaux (Véronique Brouste and Carine Bellera) and a team of biostatisticians (Mélanie Prague and Rodolphe Thiebaut, Inria team SISTM) in order to use the breast cancer clinical database of the Bergonié institute to develop the project. This large data set (1070 patients) is particularly interesting because more than half of the patients (642) did not receive adjuvant therapy (the Bergonié Institute was still protecting its patients from toxic chemotherapies several years after the generalization of adjuvant therapy in breast cancer), thus providing data on the natural history of the disease.

The purpose of the project is to further investigate the validity of our model in order to refine the existing classifications and provide **quantitative individualized predictions of the probability of relapse, time to recurrence and survival**. Using machine learning techniques, I want to build a map between the clinical and biological factors present in the database and the

parameters of the model determinant of metastatic relapse and its ocurrence time. In addition to well-established classification variables such as the hormonal and HER2 statuses, quantitative continuous variables reported in the database have the potential to offer a more precise classification through our biologically-based model. Indeed, kinetic parameters such as the Ki-67 level are likely to be related to proliferation rates naturally occurring in the mechanistic model (as part of the growth parameters). Similarly, levels of E-cadherin (a cell-cell transmembrane adhesion protein) or the Trio protein are likely to be related to a cell-scale parameter of the mathematical model of intrinsic metastatatic (disseminative) agressiveness. Cancer stem cells markers (CD44 and CD24), informative on the proportion of tumor-initiating cells, will be integrated in a specific parameter of the model quantifying the proportion of tumor cells susceptible to generate metastases. These factors are all present in the database which thus appears to contain variables ideally suited to be linked to the parameters of our mathematical model.

5.2.2 Brain metastases from lung cancer

In collaboration with several medical teams in Marseille (Fabrice Barlési and Pascale Tomasini from the Multidisciplinary Oncology and Therapeutic Innovations Service, AP-HM and Xavier Muracciole from the radiotherapy unit of the AP-HM), we have started to build a devoted database reporting several clinical entries of interest including **molecular data** (mutation status of EGFR, KRAS, BRAF, PI3KA, HER2, ALK, ROS1 and TTF1) as well as information on the brain metastases. Moreover, in collaboration with Jean-Luc Mari (Laboratoire des Sciences de l'Information et des Systèmes, Marseille) we also plan to apply **computational geometry** tools to clinical images of the lung primary tumors in order to infer and quantify topological and geometrical metrics. While we plan to link the molecular data to the cell-scale parameter μ, the latter geometrical indices will be linked to the tumor-scale parameter γ (see Figure 5.2).

5.3 Tumor-tumor interactions in metastasis from thyroid cancers

In a recent publication, Terroir et al. reported unexpected findings of an absence of correlation between ^{18}fluorodeoxyglucose (FDG) uptake measured by positron emission tomography (PET) and the growth rate of individual tumors [Terroir et al., 2017]. Indeed, this functional imaging metric – supposedly correlated with the metabolic activity of the lesion – is classically thought to be linked to the aggressiveness of the cancer disease, which is in contradiction with the results of [Terroir et al., 2017]. However, these authors considered the tumors **independently from each other**, even if they originated from the same patient. As suggested by and in collaboration with David Taieb (MCU-PH in nuclear medicine, AP-HM, Marseille), we want to reassess the findings of [Terroir et al., 2017] in light of possible **tumor-tumor interactions** that could act as confounding factors and bias the absence of correlations reported. In this context, our tumor-tumor interactions model [Benzekry et al., 2017] could be particularly relevant since: 1) it is minimally parameterized

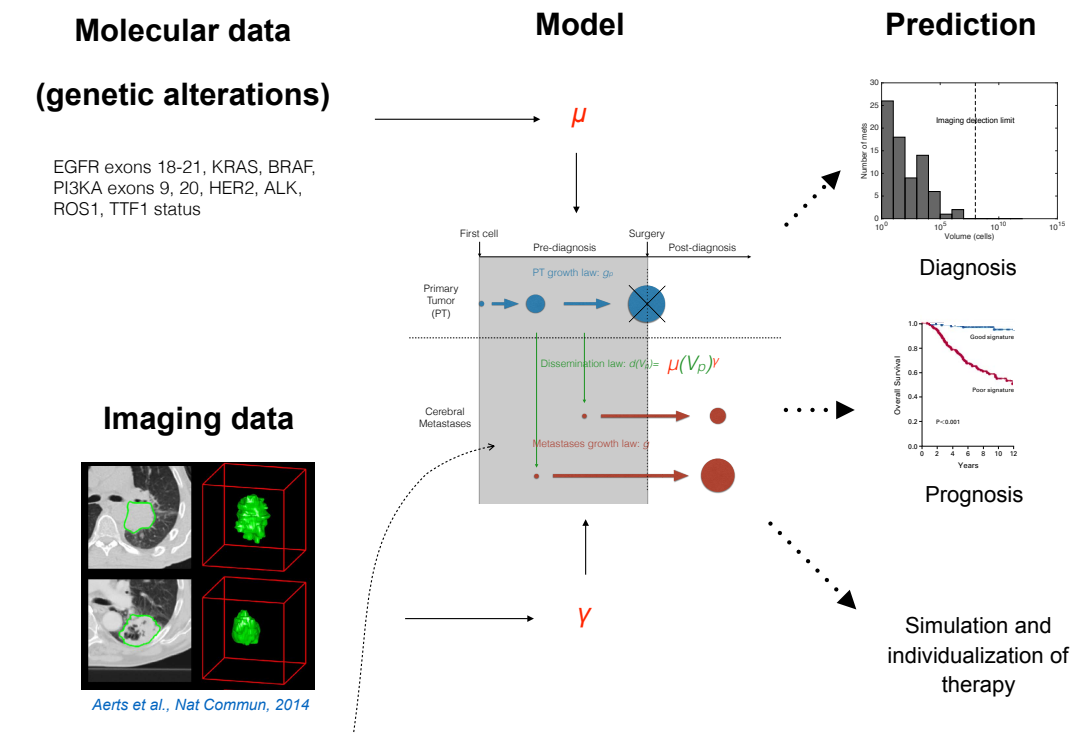

Figure 5.2 – Scheme of the project to identify the model parameters from molecular and imaging data available at diagnosis

(four parameters) and 2) it includes two populations of cells within a tumor which are well suited to be inferred from the two information given by the functional PET imaging and morphometric CT imaging both routinely performed in patients with metastatic thyroid cancer.

In addition, the case of metastatic thyroid cancer is particularly well suited for our model because there is a wait-and-see strategy for some of the patients, thus making the data adapted to be confronted to our model where no validation of the effect of treatments has yet been established. Finally, there is a systemic biomarker measured in the blood (the thyroglobulin) that is produced by each of the cancer cell, thus allowing access to the invisible disseminated burden. A modeling study of the dynamics of thyroglobulin has recently been published and can be used as a starting point [Barbolosi et al., 2017].

In collaboration with David Taieb and Dominique Barbolosi (both authors of the previous study), we want to apply our model to be able to predict, on an per-patient and per-lesion basis, the future evolution of the disease in order to help clinical decision about therapeutic intervention.

5.4 Differential effects of therapies on primary tumor and metastases

Our mathematical methodology for modeling data of metastatic development provides a quantitative *in silico* framework that could be of valuable help for therapeutic preclinical aims. One of my current projects is to address the differential effects of systemic therapies on primary tumor growth and metastases, including possible **acceleration following anti-angiogenic treatment** [Ebos et al., 2009, Ebos et al., 2014]. In collaboration with John Ebos we have access to a large database containing longitudinal data for more than 400 animals treated in the neo-adjuvant setting by two drugs with anti-angiogenic activity (Suntinib and Axitinib), with multiple schemes of administration. These include not only data on primary tumor growth curves but, crucially, also longitudinal measurements of the post-surgical metastatic burden by bioluminescence as well as survival. In addition, quantification of several biomarkers such as the CTCs[16] or myeloid-derived suppressor cells counts and stromal and tumor immuno-histochemistry data (CD31[17] and Ki67[18]) are also available and could be of interest as meaningful covariates in the model.

We will start by establishing a validated model for the **treatment of renal cell carcinoma**. The current standard of care for this cancer in the metastatic setting is sunitinib, an anti-angiogenic drug [Motzer et al., 2007]. However, development of resistance almost inevitably occurs, eventually leading to the patient's death. In 2016, a novel immunotherapy (nivolumab) has been approved as second line treatment [Motzer et al., 2015]. Our model could address several currently open questions, including:

1. What is the best scheduling in the neo-adjuvant (i.e. pre-surgical) setting, considering the

[16] circulating tumor cells
[17] endothelial cells marker
[18] proliferation marker

impact of the "rebound" effect?

2. What are the precise mechanisms of **resistance to sunitinib** and how to delay them?
3. What is the best sequence of administration for **combination of sunitinib and nivolumab**?

In the context of this project, I have supervised several master's internships about the modeling of the effect of Sunitinib on tumor growth (Aristoteles Camillo [Camillo, 2014] and Simon Evain [Evain and Benzekry, 2016]) and I am co-supervising (together with Olivier Saut) a PhD student, Chiara Nicolò (Inria grant, started October 2016).

5.5 Mathematical models for combinations in immunotherapy

Following an ongoing collaboration with Raphaël Serre, Dominique Barbolosi, Xavier Muracciole and Fabrice Barlési about mathematical models of the effect of immune-checkpoint inhibitors [Serre et al., 2016], we plan to use the model to guide the sequence and scheduling of the **combination between radiotherapy, chemotherapy and immunotherapy**. In order to do so, we will first investigate several treatment regimen in experimental systems to validate the applicability of the model. Moreover, **dedicated toxicity models** remain to be established as this topic is the first limiting concern when it comes to clinical anti-cancer therapeutics. This is even more relevant for immune-checkpoint inhibitors which, by their mode of action consisting in releasing immune "brakes" also restores cytotoxicity of lymphocytes against healthy cells, thus increasing the risk of auto-immune diseases.

5.6 Mathematical modeling of anti-cancer nanoparticles

In collaboration with Raphaëlle Fanciullino and Joseph Ciccolini from the SMARTc team (Inserm, Marseille, France) and Clair Poignard from the MONC team (Inria Bordeaux Sud-Ouest, France), we are starting a project about the optimization of the design and scheduling of anticancer nanodrugs using an integrative *in vitro/in vivo/in silico* approach.

One of the major challenge in anti-cancer chemotherapy is the **very high toxicity** associated with cytotoxic agents (such as the folfirinox triplet in the treatment of colorectal cancer). To overcome this issue, nanoparticles conjugated with cancer cell specific antibodies are being developed that ensure delivery of the drug to the therapeutic target only. However, intra-tumor penetration of antibody nanoconjugates (ANC) properties are not fully understood and could be improved. The goal of this project is to establish and to validate a **mathematical model of of the biophysics of these ANC drugs intra-tumor transport** (continuum mechanics partial differential equations) in order to inform on the parameters (size, antibody graft rate, etc...) that will ensure

maximal delivery and cytotoxicity, based on previous research efforts that developed relevant mathematical models for poroelastic description of 3D tissue [Deville et al., 2017].

We also want to perform organism-scale modeling of the pharmacokinetics and pharmacodynamics of the drug. This will allow the *in silico* determination of improved schedules of the drugs that will ensure **optimization of the efficacy/toxicity balance**. See Figure 5.3 for a general scheme of this project.

We have recently obtained an Inria-Inserm PhD grant for a student from the Politecnico di Milano (Cristina Vaghi) who will start her PhD in the fall of 2017.

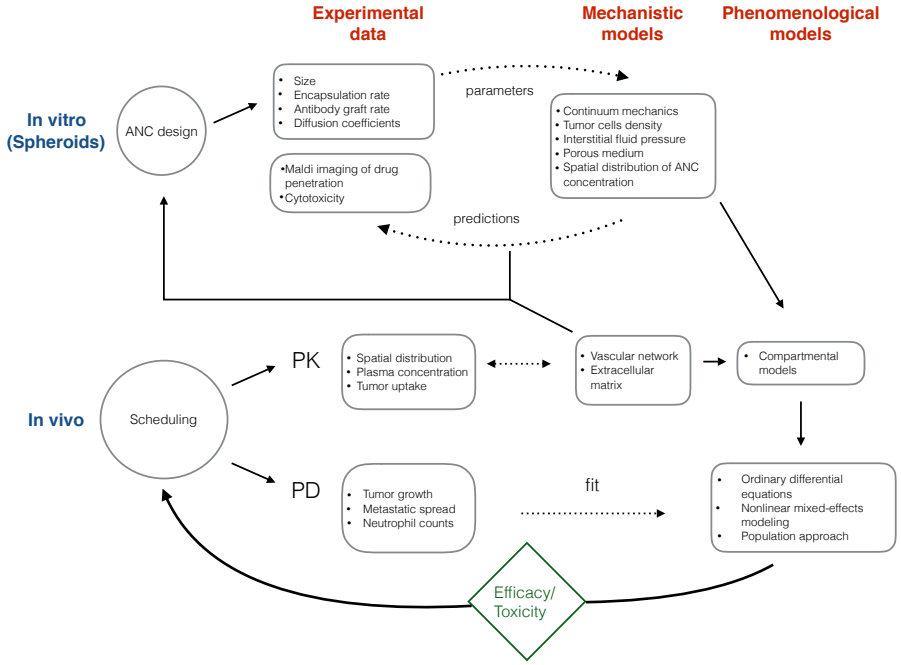

Figure 5.3 – Scheme of the integration between experiments and mathematical models.

Bibliography

[Aceto et al., 2014] Aceto, N., Bardia, A., Miyamoto, D. T., Donaldson, M. C., Wittner, B. S., Spencer, J. A., Yu, M., Pely, A., Engstrom, A., Zhu, H., Brannigan, B. W., Kapur, R., Stott, S. L., Shioda, T., Ramaswamy, S., Ting, D. T., Lin, C. P., Toner, M., Haber, D. A., and Maheswaran, S. (2014). Circulating Tumor Cell Clusters Are Oligoclonal Precursors of Breast Cancer Metastasis. *Cell*, 158(5):1110–1122.

[Aguirre-Ghiso, 2007] Aguirre-Ghiso, J. (2007). Models, mechanisms and clinical evidence for cancer dormancy. *Nat Rev Cancer*, 7(11):834–846.

[Akanuma, 1978] Akanuma, A. (1978). Parameter analysis of Gompertzian function growth model in clinical tumors. *Eur J Cancer*, 14(6):681–8.

[Al-Hajj et al., 2003] Al-Hajj, M., Wicha, M. S., Benito-Hernandez, A., Morrison, S. J., and Clarke, M. F. (2003). Prospective identification of tumorigenic breast cancer cells. *Proc Natl Acad Sci USA*, 100(7):3983–3988.

[Almog, 2010] Almog, N. (2010). Molecular mechanisms underlying tumor dormancy. *Cancer Lett*, 294(2):139–46.

[Almog et al., 2006] Almog, N., Henke, V., Flores, L., Hlatky, L., Kung, A. L., Wright, R. D., Berger, R., Hutchinson, L., Naumov, G. N., Bender, E., Akslen, L. a., Achilles, E.-G., and Folkman, J. (2006). Prolonged dormancy of human liposarcoma is associated with impaired tumor angiogenesis. *FASEB J*, 20(7):947–9.

[Altrock et al., 2015] Altrock, P. M., Liu, L. L., and Michor, F. (2015). The mathematics of cancer: integrating quantitative models. *Nat Rev Cancer*, 15(12):730–745.

[Ambrosi and Preziosi, 2002] Ambrosi, D. and Preziosi, L. (2002). On the closure of mass balance models for tumor growth. *Math Models Methods Appl Sci*, 12(05):737–754.

[Anderson and Quaranta, 2008] Anderson, A. R. and Quaranta, V. (2008). Integrative mathematical oncology. *Nat Rev Cancer*, 8(3):227–234.

[Anderson et al., 2006] Anderson, A. R., Weaver, A. M., Cummings, P. T., and Quaranta, V. (2006). Tumor morphology and phenotypic evolution driven by selective pressure from the microenvironment. *Cell*, 127(5):905–915.

[Anderson and Chaplain, 1998] Anderson, A. R. A. and Chaplain, M. A. J. (1998). Continuous and discrete mathematical models of tumor-induced angiogenesis. *Bull Math Biol*, 60(5):857–899.

[Araujo et al., 2014] Araujo, A., Cook, L. M., Lynch, C. C., and Basanta, D. (2014). An integrated computational model of the bone microenvironment in bone-metastatic prostate cancer. *Cancer Res*, 74(9):2391–2401.

[Araujo and McElwain, 2004] Araujo, R. P. and McElwain, D. L. S. (2004). A history of the study of solid tumour growth: the contribution of mathematical modelling. *Bull Math Biol*, 66(5):1039–1091.

[Arjaans et al., 2016] Arjaans, M., Schröder, C. P., Oosting, S. F., Dafni, U., Kleibeuker, J. E., and de Vries, E. G. E. (2016). VEGF pathway targeting agents, vessel normalization and tumor drug uptake: from bench to bedside. *Oncotarget*, 7(16):21247–21258.

[Avallone et al., 2015] Avallone, A., Pecori, B., Bianco, F., Aloj, L., Tatangelo, F., Romano, C., Granata, V., Marone, P., Leone, A., Botti, G., Petrillo, A., Caracò, C., Iaffaioli, V. R., Muto, P., Romano, G., Comella, P., Budillon, A., and Delrio, P. (2015). Critical role of bevacizumab scheduling in combination with pre-surgical chemo-radiotherapy in MRI-defined high-risk locally advanced rectal cancer: results of the branch trial. *Oncotarget*, 6(30):30394–30407.

[Avallone et al., 2016] Avallone, A., Piccirillo, M. C., Aloj, L., Nasti, G., Delrio, P., Izzo, F., Di Gennaro, E., Tatangelo, F., Granata, V., Cavalcanti, E., Maiolino, P., Bianco, F., Aprea, P., De Bellis, M., Pecori, B., Rosati, G., Carlomagno, C., Bertolini, A., Gallo, C., Romano, C., Leone, A., Caracò, C., de Lutio di Castelguidone, E., Daniele, G., Catalano, O., Botti, G., Petrillo, A., Romano, G. M., Iaffaioli, V. R., Lastoria, S., Perrone, F., and Budillon, A. (2016). A randomized phase 3 study on the optimization of the combination of bevacizumab with FOLFOX/OXXEL in the treatment of patients with metastatic colorectal cancer-OBELICS (Optimization of BEvacizumab scheduLIng within Chemotherapy Scheme). *BMC Cancer*, 16.

[Badwe et al., 2013] Badwe, R., Parmar, V., Hawaldar, R., Nair, N., Kaushik, R., Siddique, S., Navale, A., Budrukkar, A., Mittra, I., and Gupta, S. (2013). Surgical removal of primary tumor and axillary lymph nodes in women with metastatic breast cancer at first presentation: A randomized controlled trial. In *San Antonio Breast Cancer Symposium*, pages S2–02.

[Bajzer and Vuk-Pavlović, 2000] Bajzer, Ž. and Vuk-Pavlović, S. (2000). New Dimensions in Gompertzian Growth. *Journal of Theoretical Medicine*, 2(4):307–315.

[Baldock et al., 2013] Baldock, a. L., Rockne, R. C., Boone, a. D., Neal, M. L., Hawkins-Daarud, A., Corwin, D. M., Bridge, C. A., Guyman, L. a., Trister, A. D., Mrugala, M. M., Rockhill, J. K., and Swanson, K. R. (2013). From patient-specific mathematical neuro-oncology to precision medicine. *Front Oncol*, 3:62.

[Baratchart, 2016] Baratchart, E. (2016). *Etude quantitative des aspects dynamiques et spatiaux du développement métastatique à l'aide de modèles mathématiques*. PhD thesis, Bordeaux.

[Baratchart et al., 2015] Baratchart, E., **Benzekry *, S.**, Bikfalvi *, A., Colin *, T., Cooley, L. S., Pineau, R., Ribot, E. J., Saut, O., and Souleyreau, W. (2015). Computational Modelling of Metastasis Development in Renal Cell Carcinoma. *PLoS Comput Biol*, 11(11):e1004626.

[Barbolosi et al., 2013] Barbolosi, D., Benabdallah, A., **Benzekry, S.**, Ciccolini, J., Faivre, C., Hubert, F., Verga, F., and You, B. (2013). A Mathematical Model for Growing Metastases on Oncologists's Service. In *Computational Surgery and Dual Training*, pages 331–338. Springer New York, New York, NY.

[Barbolosi et al., 2009] Barbolosi, D., Benabdallah, A., Hubert, F., and Verga, F. (2009). Mathematical and numerical analysis for a model of growing metastatic tumors. *Math Biosci*, 218(1):1–14.

[Barbolosi et al., 2016] Barbolosi, D., Ciccolini, J., Lacarelle, B., Barlesi, F., and André, N. (2016). Computational oncology–mathematical modelling of drug regimens for precision medicine. *Nat Rev Clin Oncol*, 13(4):242–254.

[Barbolosi et al., 2003] Barbolosi, D., Freyer, G., Ciccolini, J., and Iliadis, A. (2003). Optimisation de la posologie et des modalités d'administration des agents cytotoxiques à l'aide d'un modèle mathématique. *Bull Cancer*, 90(2):167–175.

[Barbolosi and Iliadis, 2001] Barbolosi, D. and Iliadis, A. (2001). Optimizing drug regimens in cancer chemotherapy: a simulation study using a PK-PD model. *Comput Biol Med*, 31(3):157–172.

[Barbolosi et al., 2017] Barbolosi, D., Summer, I., Meille, C., Serre, R., Kelly, A., Zerdoud, S., Bournaud, C., Schvartz, C., Toubeau, M., Toubert, M.-E., Keller, I., and Taïeb, D. (2017). Modeling Therapeutic Response to Radioiodine in Metastatic Thyroid Cancer: A proof-of-concept study for individualized medicine. *Oncotarget*.

[Barbolosi et al., 2011] Barbolosi, D., Verga, F., You, B., Benabdallah, A., Hubert, F., Mercier, C., Ciccolini, J., and Faivre, C. (2011). Modélisation du risque d'évolution métastatique chez les patients supposés avoir une maladie localisée. *Oncologie*, 13(8):528–533.

[Barlesi et al., 2013] Barlesi, F., Khobta, N., Tallet, A., Goncalves, A., Azria, D., Spano, J.-P., Carpentier, A. F., Régis, J., and Métellus, P. (2013). Management of brain metastases for lung cancer patients. *Bull Cancer*, 100(3):303–308.

[Barnholtz-Sloan et al., 2004] Barnholtz-Sloan, J. S., Sloan, A. E., Davis, F. G., Vigneau, F. D., Lai, P., and Sawaya, R. E. (2004). Incidence proportions of brain metastases in patients diagnosed (1973 to 2001) in the Metropolitan Detroit Cancer Surveillance System. *J Clin Oncol*, 22(14):2865–2872.

[Bazhenova et al., 2014] Bazhenova, L., Newton, P., Mason, J., Bethel, K., Nieva, J., and Kuhn, P. (2014). Adrenal metastases in lung cancer: clinical implications of a mathematical model. *J Thorac Oncol*, 9(4):442–446.

[Beheshti et al., 2015] Beheshti, A., **Benzekry, S.**, McDonald, J. T., Ma, L., Peluso, M., Hahnfeldt, P., and Hlatky, L. (2015). Host age is a systemic regulator of gene expression impacting cancer progression. *Cancer Res*, 75(6):1134–1143.

[Bellomo et al., 2008] Bellomo, N., de Angelis, E., and Chaplain, M. A. J. (2008). Selected topics in cancer modeling: genesis, evolution, immune competition, and therapy. Springer.

[Benguigui et al., 2017] Benguigui, M., Alishekevitz, D., Timaner, M., Shechter, D., Raviv, Z., **Benzekry *, S.**, and Shaked *, Y. (2017). Dose- and time-dependence of the host-mediated response to paclitaxel therapy: a mathematical modeling approach. *submitted*.

[Benzekry, 2011a] **Benzekry, S.** (2011a). Mathematical analysis of a two-dimensional population model of metastatic growth including angiogenesis. *J Evol Equ*, 11(1):187–213.

[Benzekry, 2011b] **Benzekry, S.** (2011b). *Modeling, mathematical and numerical analysis of anti-cancerous therapies for metastatic cancers*. PhD thesis, Aix-Marseille University.

[Benzekry, 2012a] **Benzekry, S.** (2012a). Mathematical and numerical analysis of a model for anti-angiogenic therapy in metastatic cancers. *ESAIM Math Model Numer Anal*, 46(2):207–237.

[Benzekry, 2012b] **Benzekry, S.** (2012b). Passing to the limit 2D–1D in a model for metastatic growth. *J Biol Dynam*, 6(sup1):19–30.

[Benzekry, 2017] **Benzekry, S.** (2017). Les lois de la croissance tumorale. *Bibliothèque Tangente*, Hors Série.

[Benzekry et al., 2012a] **Benzekry, S.**, André, N., Benabdallah, A., Ciccolini, J., Faivre, C., Hubert, F., and Barbolosi, D. (2012a). Modelling the impact of anticancer agents on metastatic spreading. *Math Model Nat Phenom*, 7(1):306–336.

[Benzekry et al., 2015a] **Benzekry, S.**, Beheshti, A., Hahnfeldt, P., and Hlatky, L. (2015a). Capturing the Driving Role of Tumor-Host Crosstalk in a Dynamical Model of Tumor Growth. *bio-protocol*, 5(21).

[Benzekry et al., 2012b] **Benzekry, S.**, Chapuisat, G., Ciccolini, J., Erlinger, A., and Hubert, F. (2012b). A new mathematical model for optimizing the combination between antiangiogenic and cytotoxic drugs in oncology. *C R Acad Sci Paris, Ser I*, 350(1-2):23–28.

[Benzekry and Ebos, 2015] **Benzekry, S.** and Ebos, J. M. (2015). On the growth and dissemination laws in a mathematical model of metastatic growth. *ITM Web of Conferences*, 5:00007.

[Benzekry et al., 2014a] **Benzekry, S.**, Gandolfi, A., and Hahnfeldt, P. (2014a). A mathematical model of systemic inhibition of angiogenesis in metastatic development. *ESAIM Proc Surv*, 45:75–87.

[Benzekry et al., 2014b] **Benzekry, S.**, Gandolfi, A., and Hahnfeldt, P. (2014b). Global Dormancy of Metastases Due to Systemic Inhibition of Angiogenesis. *PLoS ONE*, 9(1):e84249–11.

[Benzekry and Hahnfeldt, 2013] **Benzekry, S.** and Hahnfeldt, P. (2013). Maximum tolerated dose versus metronomic scheduling in the treatment of metastatic cancers. *J Theor Biol*, 335:235–244.

[Benzekry et al., 2017] **Benzekry, S.**, Lamont, C., Barbolosi, D., Hlatky, L., and Hahnfeldt, P. (2017). Mathematical Modeling of Tumor-Tumor Distant Interactions Supports a Systemic Control of Tumor Growth. *Cancer Res*, 77(18):5183–5193.

[Benzekry et al., 2014c] **Benzekry, S.**, Lamont, C., Beheshti, A., Tracz, A., Ebos, J. M. L., Hlatky, L., and Hahnfeldt, P. (2014c). Classical mathematical models for description and prediction of experimental tumor growth. *PLoS Comput Biol*, 10(8):e1003800.

[Benzekry et al., 2015b] **Benzekry, S.**, Pasquier, E., Barbolosi, D., Lacarelle, B., Barlesi, F., André, N., and Ciccolini, J. (2015b). Metronomic reloaded: Theoretical models bringing chemotherapy into the era of precision medicine. *Semin Cancer Biol*, 35:53–61.

[Benzekry et al., 2016] **Benzekry, S.**, Tracz, A., Mastri, M., Corbelli, R., Barbolosi, D., and Ebos, J. M. L. (2016). Modeling Spontaneous Metastasis following Surgery: An In Vivo-In Silico Approach. *Cancer Res*, 76(3):535–547.

[Benzekry et al., 2015c] **Benzekry, S.**, Tuszynski, J. A., Rietman, E. A., and Lakka Klement, G. (2015c). Design principles for cancer therapy guided by changes in complexity of protein-protein interaction networks. *Biol Direct*, 10:32.

[Bernard et al., 2012] Bernard, A., Kimko, H., Mital, D., and Poggesi, I. (2012). Mathematical modeling of tumor growth and tumor growth inhibition in oncology drug development. *Expert Opin Drug Metab Toxicol*, 8(9):1057–1069.

[Bertalanffy, 1957] Bertalanffy, L. V. (1957). Quantitative laws in metabolism and growth. *Q Rev Biol*, 32(3):217–231.

[Bethge et al., 2012] Bethge, A., Schumacher, U., Wree, A., and Wedemann, G. (2012). Are metastases from metastases clinical relevant? Computer modelling of cancer spread in a case of hepatocellular carcinoma. *PLoS ONE*, 7(4):e35689–e35689.

[Billy, 2009] Billy, F. (2009). *Modélisation mathématique multi-échelle de l'angiogenèse tumorale: analyse de la réponse tumorale aux traitements anti-angiogéniques.* PhD thesis, University Claude Bernard - Lyon 1, University Claude Bernard - Lyon 1.

[Black and Welch, 1993] Black, W. C. and Welch, H. G. (1993). Advances in diagnostic imaging and overestimation of disease prevalence and the benefits of therapy. *N Engl J Med*, 328(17):1237–1243.

[Bonadonna et al., 2004] Bonadonna, G., Zambetti, M., Moliterni, A., Gianni, L., and Valagussa, P. (2004). Clinical relevance of different sequencing of doxorubicin and cyclophosphamide, methotrexate, and Fluorouracil in operable breast cancer. *J Clin Oncol*, 22(9):1614–1620.

[Boyer et al., 2017a] Boyer, A., Ciccolini, J., Mascaux, C., Imbs, D. C., El Cheikh, R., Barlesi, F., and **Benzekry, S.** (2017a). Étude de l'effet séquence bévacizumab/pémétrexed/cisplatine chez la souris porteuse de cancer du poumon non à petites cellules. *Rev Mal Respir*, 34:A52.

[Boyer et al., 2017b] Boyer, A., Imbs, D.-C., Cheikh, R. E., Mascaux, C., Barlesi, F., Barbolosi, D., **Benzekry, S.**, and Ciccolini, J. (2017b). Abstract 4529: Optimization of the sequence for the administration of bevacizumab in combination with pemetrexed and cisplatin in NSCLC : a pharmacology based in vivo study . *Cancer Res*, 77(13 Supplement):4529 –4529.

[Brackstone et al., 2007] Brackstone, M., Townson, J. L., and Chambers, A. F. (2007). Tumour dormancy in breast cancer: an update. *Breast Cancer Res*, 9(3):208–208.

[Brewster et al., 2008] Brewster, A. M., Hortobagyi, G. N., Broglio, K. R., Kau, S.-W., Santa-Maria, C. A., Arun, B., Buzdar, A. U., Booser, D. J., Valero, V., Bondy, M., and Esteva, F. J. (2008). Residual risk of breast cancer recurrence 5 years after adjuvant therapy. *J Natl Cancer Inst*, 100(16):1179–1183.

[Brodbeck et al., 2014] Brodbeck, T., Nehmann, N., Bethge, A., Wedemann, G., and Schumacher, U. (2014). Perforin-dependent direct cytotoxicity in natural killer cells induces considerable knockdown of spontaneous lung metastases and computer modelling-proven tumor cell dormancy in a HT29 human colon cancer xenograft mouse model. *Mol Cancer*, 13(1):244.

[Browder et al., 2000] Browder, T., Butterfield, C. E., Kraling, B. M., Shi, B., Marshall, B., O'Reilly, M. S., and Folkman, J. (2000). Antiangiogenic scheduling of chemotherapy improves efficacy against experimental drug-resistant cancer. *Cancer Res*, 60(7):1878–1886.

[Burnham and Anderson, 2003] Burnham, K. P. and Anderson, D. R. (2003). Model selection and multimodel inference: a practical information-theoretic approach. Springer Science & Business Media.

[Byrne, 2010] Byrne, H. M. (2010). Dissecting cancer through mathematics: from the cell to the animal model. *Nat Rev Cancer*, 10(3):221–230.

[Camillo, 2014] Camillo, A. (2014). An experimentally-based modeling study of the effect of anti-angiogenic therapies on primary tumor kinetics for data analysis of clinically relevant animal models of metastasis. Master's thesis, Inria Bordeaux Sud-Ouest.

[Carmeliet and Jain, 2000] Carmeliet, P. and Jain, R. K. (2000). Angiogenesis in cancer and other diseases. *Nature*, pages 249–257.

[Carmeliet and Jain, 2011] Carmeliet, P. and Jain, R. K. (2011). Principles and mechanisms of vessel normalization for cancer and other angiogenic diseases. *Nat Rev Drug Discov*, 10(6):417–427.

[Ceelen et al., 2014] Ceelen, W., Pattyn, P., and Mareel, M. (2014). Surgery, wound healing, and metastasis: recent insights and clinical implications. *Crit Rev Oncol Hematol*, 89(1):16–26.

[Cesca et al., 2016] Cesca, M., Morosi, L., Berndt, A., Nerini, I. F., and Decio, A. (2016). Bevacizumab-improved distribution of paclitaxel in ovarian cancer xenografts potentiates anti-tumor efficacy. *Cancer Res*, 76(14 Supplement):3377–3377.

[Chaffer and Weinberg, 2011] Chaffer, C. L. and Weinberg, R. A. (2011). A perspective on cancer cell metastasis. *Science*, 331(6024):1559–1564.

[Chambers et al., 2002] Chambers, A. F., Groom, A. C., and MacDonald, I. C. (2002). Dissemination and growth of cancer cells in metastatic sites. *Nat Rev Cancer*, 2(8):563–572.

[Chaplain et al., 2006] Chaplain, M. A. J., McDougall, S. R., and Anderson, A. R. A. (2006). Mathematical modeling of tumor-induced angiogenesis. *Annu Rev Biomed Eng*, 8:233–257.

[Chiarella et al., 2012] Chiarella, P., Bruzzo, J., Meiss, R. P., and Ruggiero, R. A. (2012). Concomitant tumor resistance. *Cancer Lett*, 324(2):133–141.

[Chibon, 2013] Chibon, F. (2013). Cancer gene expression signatures – The rise and fall? *Eur J Cancer*, 49(8):2000–2009.

[Chisholm et al., 2015] Chisholm, R. H., Lorenzi, T., Lorz, A., Larsen, A. K., Almeida, L. N. d., Escargueil, A., and Clairambault, J. (2015). Emergence of Drug Tolerance in Cancer Cell Populations: An Evolutionary Outcome of Selection, Nongenetic Instability, and Stress-Induced Adaptation. *Cancer Res*, 75(6):930–939.

[Chmielecki et al., 2011] Chmielecki, J., Foo, J., Oxnard, G. R., Hutchinson, K., Ohashi, K., Somwar, R., Wang, L., Amato, K. R., Arcila, M., Sos, M. L., Socci, N. D., Viale, A., de Stanchina, E., Ginsberg, M. S., Thomas, R. K., Kris, M. G., Inoue, A., Ladanyi, M., Miller, V. a., Michor, F., and Pao, W. (2011). Optimization of dosing for EGFR-mutant non-small cell lung cancer with evolutionary cancer modeling. *Sci Transl Med*, 3(90):90ra59–90ra59.

[Ciccolini et al., 2017] Ciccolini, J., Barbolosi, D., Meille, C., Lombard, A., Serdjebi, C., Giacometti, S., Padovani, L., Pasquier, E., and André, N. (2017). Pharmacokinetics and pharmacodynamics-based mathematical modeling identifies an optimal protocol for metronomic chemotherapy. *Cancer Res*, pages canres.3130.2016–37.

[Ciccolini et al., 2015] Ciccolini, J., **Benzekry, S.**, Lacarelle, B., Barbolosi, D., and Barlesi, F. (2015). Improving efficacy of the combination between antiangiogenic and chemotherapy: Time for mathematical modeling support. *Proc Natl Acad Sci USA*, 112(27):E3453.

[Citron et al., 2003] Citron, M. L., Berry, D. A., Cirrincione, C., Hudis, C., Winer, E. P., Gradishar, W. J., Davidson, N. E., Martino, S., Livingston, R., Ingle, J. N., Perez, E. A., Carpenter, J., Hurd, D., Holland, J. F., Smith, B. L., Sartor, C. I., Leung, E. H., Abrams, J., Schilsky, R. L., Muss, H. B., and Norton, L. (2003). Randomized trial of dose-dense versus conventionally scheduled and sequential versus concurrent combination chemotherapy as postoperative adjuvant treatment of node-positive primary breast cancer: first report of Intergroup Trial C9741/Cancer and Leukemia Group B Trial 9741. *J Clin Oncol*, 21(8):1431–1439.

[Clare et al., 2000] Clare, S. E., Nakhlis, F., and Panetta, J. C. (2000). Molecular biology of breast metastasis The use of mathematical models to determine relapse and to predict response to chemotherapy in breast cancer. *Breast Cancer Res*, 2(6):1569.

[Coffey et al., 2003] Coffey, J. C., Wang, J. H., Smith, M. J. F., Bouchier-Hayes, D., Cotter, T. G., and Redmond, H. P. (2003). Excisional surgery for cancer cure: therapy at a cost. *Lancet Oncology*, 4(12):760–768.

[Colin et al., 2015] Colin, T., Cornelis, F., Jouganous, J., Palussière, J., and Saut, O. (2015). Patient-specific simulation of tumor growth, response to the treatment, and relapse of a lung metastasis: a clinical case. *J Comput Surg*, 2(1):841–17.

[Colin et al., 2010] Colin, T., Iollo, A., Lombardi, D., and Saut, O. (2010). Prediction of the Evolution of Thyroidal Lung Nodules Using a Mathematical Model. *ERCIM News*.

[Colin et al., 2012] Colin, T., Iollo, A., Lombardi, D., and Saut, O. (2012). System identification in tumor growth modeling using semi-empirical eigenfunctions. *Math Models Methods Appl Sci*, 22(6):1250003–1250030.

[Collins et al., 1956] Collins, V. P., Loeffler, R. K., and Tivey, H. (1956). Observations on growth rates of human tumors. *Am J Roentgenol Radium Ther Nucl Med*, 76(5).

[Collinson et al., 2014] Collinson, F., Hutchinson, M., Craven, R. A., Cairns, D. A., Alexandre, Z., Wind, T. C., Gahir, N., Messenger, M. P., Jackson, S., Thompson, D., Adusei, C., Ledermann, J., Hall, G., Jayson, G. C., Selby, P. J., and Banks, R. E. (2014). Biomarkers and response to bevacizumab–response. *Clin Cancer Res*, 20(4):1058–1058.

[Comen et al., 2011] Comen, E., Norton, L., and Massagué, J. (2011). Clinical implications of cancer self-seeding. *Nat Rev Cancer*, 8(6):369–377.

[Cornelis et al., 2013] Cornelis, F., Saut, O., Cumsille, P., Lombardi, D., Iollo, A., Palussiere, J., and Colin, T. (2013). In vivo mathematical modeling of tumor growth from imaging data: Soon to come in the future? *Diagn Interv Imaging*, 94(6):593–600.

[Coumans et al., 2013] Coumans, F. A. W., Siesling, S., and Terstappen, L. W. M. M. (2013). Detection of cancer before distant metastasis. *BMC Cancer*, 13(1):283.

[Dang et al., 2003] Dang, C., Gilewski, T. A., Surbone, A., and Norton, L. (2003). Growth curve analysis. In Kufe, D. W., Pollock, R. E., Weichselbaum, R. R., Bast, R. C. J., Gansler, T. S., Holland, J. F., and Frei, E., editors, *Holland-Frei Cancer Medicine. 6th edition*. BC Decker, Hamilton (ON).

[de Mascarel et al., 2015] de Mascarel, I., Debled, M., Brouste, V., Mauriac, L., Sierankowski, G., Velasco, V., Croce, S., Chibon, F., Boudeau, J., Debant, A., and MacGrogan, G. (2015). Comprehensive prognostic analysis in breast cancer integrating clinical, tumoral, micro-environmental and immunohistochemical criteria. *SpringerPlus 2015 4:1*, 4(1):528.

[Demicheli, 1980] Demicheli, R. (1980). Growth of testicular neoplasm lung metastases: Tumor-specific relation between two Gompertzian parameters. *Eur J Cancer*, 16(12):1603–1608.

[Demicheli et al., 1996] Demicheli, R., Abbattista, A., Miceli, R., Valagussa, P., and Bonadonna, G. (1996). Time distribution of the recurrence risk for breast cancer patients undergoing mastectomy: Further support about the concept of tumor dormancy. *Breast Cancer Res Treat*, 41(2):177–185.

[Demicheli et al., 1989] Demicheli, R., Foroni, R., and Ingrosso, A. (1989). An exponential-Gompertzian description of LoVo cell tumor growth from in vivo and in vitro data. *Cancer Res*, 49:6543–6546.

[Demicheli et al., 2007] Demicheli, R., Retsky, M. W., Hrushesky, W. J. M., and Baum, M. (2007). Tumor dormancy and surgery-driven interruption of dormancy in breast cancer: learning from failures. *Nat Clin Rev Oncol*, 4(12):699–710.

[Demicheli et al., 2008] Demicheli, R., Retsky, M. W., Hrushesky, W. J. M., Baum, M., and Gukas, I. D. (2008). The effects of surgery on tumor growth: a century of investigations. *Ann Oncol*, 19(11):1821–8.

[Dethlefsen et al., 1968] Dethlefsen, L. a., Prewitt, J. M., and Mendelsohn, M. L. (1968). Analysis of tumor growth curves. *J Natl Cancer Inst*, 40(2):389–405.

[Detterbeck and Gibson, 2008] Detterbeck, F. C. and Gibson, C. J. (2008). Turning gray: the natural history of lung cancer over time. *J Thorac Oncol*, 3(7):781–792.

[Deville et al., 2017] Deville, M., Natalini, R., and Poignard, C. (2017). A continuum mechanics model of enzyme-based tissue degradation in cancer therapies. *submitted*.

[Dewys, 1972] Dewys, W. D. (1972). Studies correlating the growth rate of a tumor and its metastases and providing evidence for tumor-related systemic growth-retarding factors. *Cancer Res*, 32(2):374–379.

[Di Gioia et al., 2015] Di Gioia, D., Stieber, P., Schmidt, G. P., Nagel, D., Heinemann, V., and Baur-Melnyk, A. (2015). Early detection of metastatic disease in asymptomatic breast cancer patients with whole-body imaging and defined tumour marker increase. *Br J Cancer*, 112(5):809–818.

[Dickson et al., 2007] Dickson, P. V., Hamner, J. B., Sims, T. L., Fraga, C. H., Ng, C. Y. C., Rajasekeran, S., Hagedorn, N. L., McCarville, M. B., Stewart, C. F., and Davidoff, A. M. (2007). Bevacizumab-induced transient remodeling of the vasculature in neuroblastoma xenografts results in improved delivery and efficacy of systemically administered chemotherapy. *Clin Cancer Res*, 13(13):3942–3950.

[d'Onofrio and Gandolfi, 2004] d'Onofrio, A. and Gandolfi, A. (2004). Tumour eradication by antiangiogenic therapy: analysis and extensions of the model by Hahnfeldt et al. (1999). *Math Biosci*, 191(2):159–184.

[d'Onofrio and Gandolfi, 2010a] d'Onofrio, A. and Gandolfi, A. (2010a). Chemotherapy of vascularised tumours: role of vessel density and the effect of vascular "pruning". *J Theor Biol*, 264(2):253–265.

[d'Onofrio and Gandolfi, 2010b] d'Onofrio, A. and Gandolfi, A. (2010b). Resistance to antitumor chemotherapy due to bounded-noise-induced transitions. *Phys Rev E Stat Nonlin Soft Matter Phys*, 82(6 Pt 1):061901.

[d'Onofrio et al., 2009] d'Onofrio, A., Gandolfi, A., and Rocca, A. (2009). The dynamics of tumour-vasculature interaction suggests low-dose, time-dense anti-angiogenic schedulings. *Cell Prolif*, 42(3):317–329.

[Drasdo and Höhme, 2005] Drasdo, D. and Höhme, S. (2005). A single-cell-based model of tumor growth in vitro: monolayers and spheroids. *Phys. Biol.*, 2(3):133–147.

[Early Breast Cancer Trialists' Collaborative Group (EBCTCG), 1992] Early Breast Cancer Trialists' Collaborative Group (EBCTCG) (1992). Systemic treatment of early breast cancer by hormonal, cytotoxic, or immune therapy. 133 randomised trials involving 31,000 recurrences and 24,000 deaths among 75,000 women. *Lancet*, 339(8784):1–15.

[Early Breast Cancer Trialists' Collaborative Group (EBCTCG), 2005] Early Breast Cancer Trialists' Collaborative Group (EBCTCG) (2005). Effects of chemotherapy and hormonal therapy for early breast cancer on recurrence and 15-year survival: an overview of the randomised trials. *Lancet*, 365(9472):1687–1717.

[Ebos et al., 2008] Ebos, J. M. L., Lee, C. R., Bogdanovic, E., Alami, J., Van Slyke, P., Francia, G., Xu, P., Mutsaers, A. J., Dumont, D. J., and Kerbel, R. S. (2008). Vascular endothelial growth factor-mediated decrease in plasma soluble vascular endothelial growth factor receptor-2 levels as a surrogate biomarker for tumor growth. *Cancer Res*, 68(2):521–529.

[Ebos et al., 2009] Ebos, J. M. L., Lee, C. R., Cruz-Munoz, W., Bjarnason, G. A., Christensen, J. G., and Kerbel, R. S. (2009). Accelerated metastasis after short-term treatment with a potent inhibitor of tumor angiogenesis. *Cancer Cell*, 15(3):232–239.

[Ebos et al., 2014] Ebos, J. M. L., Mastri, M., Lee, C. R., Tracz, A., Hudson, J. M., Attwood, K., Cruz-Munoz, W. R., Jedeszko, C., Burns, P., and Kerbel, R. S. (2014). Neoadjuvant antiangiogenic therapy reveals contrasts in primary and metastatic tumor efficacy. *EMBO Mol Med*, 6(12):1561–1576.

[Ehrlich, 1906] Ehrlich, P. (1906). Experimentelle Karzinomstudien an Mäusen. *Arb Inst exp Ther Frankfurt*, 1:65.

[Elharrar et al., 2016] Elharrar, X., Barbolosi, D., Ciccolini, J., Meille, C., Faivre, C., Lacarelle, B., André, N., and Barlesi, F. (2016). A phase Ia/Ib clinical trial of metronomic chemotherapy based on a mathematical model of oral vinorelbine in metastatic non- small cell lung cancer and malignant pleural mesothelioma: rationale and study protocol. *BMC Cancer*, pages 1–8.

[Enderling et al., 2009] Enderling, H., Hlatky, L., and Hahnfeldt, P. (2009). Migration rules: tumours are conglomerates of self-metastases. *Br J Cancer*, 100(12):1917–25.

[Enriquez-Navas et al., 2016] Enriquez-Navas, P. M., Kam, Y., Das, T., Hassan, S., Silva, A., Foroutan, P., Ruiz, E., Martinez, G., Minton, S., Gillies, R. J., and Gatenby, R. a. (2016). Exploiting evolutionary principles to prolong tumor control in preclinical models of breast cancer. *Sci Transl Med*, 8(327):327ra24–327ra24.

[Evain and Benzekry, 2016] Evain, S. and **Benzekry, S.** (2016). Mathematical modeling of tumor and metastatic growth when treated with sunitinib. Technical report, Inria Bordeaux Sud-Ouest.

[Faivre et al., 2013] Faivre, C., Barbolosi, D., Pasquier, E., and André, N. (2013). A mathematical model for the administration of temozolomide: comparative analysis of conventional and metronomic chemotherapy regimens. *Cancer Chemother Pharmacol*, 71(4):1013–1019.

[Faivre et al., 2017] Faivre, C., El Cheikh, R., Barbolosi, D., and Barlesi, F. (2017). Mathematical optimisation of the cisplatin plus etoposide combination for managing extensive-stage small-cell lung cancer patients. *Br J Cancer*, 116(3):344–348.

[Fanciullino et al., 2017] Fanciullino, R., **Benzekry, S.**, Lacarelle, B., Ciccolini, J., and Rodallec, A. (2017). Pharmacokinetics of nanoparticles in oncology: clues for anticipating interpatient variability. *submitted*.

[Ferlay et al., 2013] Ferlay, J., Soerjomataram, I., Ervik, M., Dikshit, R., Eser, S., Mathers, C., Rebelo, M., Parkin, D. M., Forman, D., and Bray, F. (2013). GLOBOCAN 2012 v1.0, Cancer Incidence and Mortality Worldwide: IARC CancerBase No. 11. World Health Organization.

[Fidler and Paget, 2003] Fidler, I. J. and Paget, S. (2003). The pathogenesis of cancer metastasis: the 'seed and soil' hypothesis revisited. *Nat Rev Cancer*, 3(6):453–458.

[Fidler and Talmadge, 1986] Fidler, I. J. and Talmadge, J. E. (1986). Evidence that intravenously derived murine pulmonary melanoma metastases can originate from the expansion of a single tumor cell. *Cancer Res*, 46(10):5167–5171.

[Fisher, 1977] Fisher, B. (1977). Biological and clinical considerations regarding the use of surgery and chemotherapy in the treatment of primary breast cancer. *Cancer*, 40(1 Suppl):574–587.

[Fisher, 1980] Fisher, B. (1980). Laboratory and clinical research in breast cancer–a personal adventure: the David A. Karnofsky memorial lecture. *Cancer Res*, 40(11):3863–3874.

[Fisher et al., 1989] Fisher, B., Gunduz, N., Coyle, J., Rudock, C., and Saffer, E. (1989). Presence of a growth-stimulating factor in serum following primary tumor removal in mice. *Cancer Res*, 49(8):1996–2001.

[Fisher et al., 1983] Fisher, B., Gunduz, N., and Saffer, E. A. (1983). Influence of the interval between primary tumor removal and chemotherapy on kinetics and growth of metastases. *Cancer Res*, 43(4):1488–1492.

[Folkman, 1971] Folkman, J. (1971). Tumor angiogenesis: therapeutic implications. *N Engl J Med*, 285(21):1182–1186.

[Folkman, 1995a] Folkman, J. (1995a). Angiogenesis in cancer, vascular, rheumatoid and other disease. *Nat Med*, 1(1):27–31.

[Folkman, 1995b] Folkman, J. (1995b). Angiogenesis inhibitors generated by tumors. *Mol Med*, 1(2):120–2.

[Folkman, 2007] Folkman, J. (2007). Angiogenesis: an organizing principle for drug discovery? *Nature Rev Drug Discov*, 6(4):273–86.

[Folkman and Kalluri, 2004] Folkman, J. and Kalluri, R. (2004). Cancer without disease. *Nature*, 427(6977):787–787.

[Frei et al., 1961] Frei, E., Freireich, E. J., Gehan, E., Pinkel, D., Holland, J. F., Selawry, O., Haurani, F., Spurr, C. L., Hayes, D. M., James, G. W., Rothberg, H., Sodee, D. B., Rundles, R. W., Schroeder, L. R., Hoogstraten, B., Wolman, I. J., Traggis, D. G., Cooper, T., Gendel, B. R., Ebaugh, F., and Taylor, R. (1961). Studies of Sequential and Combination Antimetabolite Therapy in Acute Leukemia: 6-Mercaptopurine and Methotrexate. *Blood*, 18(4):431–454.

[Frenzen and Murray, 1986] Frenzen, C. L. and Murray, J. D. (1986). A Cell Kinetics Justification for Gompertz' Equation. *SIAM J Appl Math*, 46(4):614–629.

[Friberg and Mattson, 1997] Friberg, S. and Mattson, S. (1997). On the growth rates of human malignant tumors: implications for medical decision making. *J Surg Oncol*, 65(4):284–297.

[Gatenby, 2009] Gatenby, R. a. (2009). A change of strategy in the war on cancer. *Nature*, 459(7246):508–509.

[Gatenby and Maini, 2003] Gatenby, R. a. and Maini, P. K. (2003). Mathematical oncology: cancer summed up. *Nature*, 421(6921):321–321.

[Gatenby et al., 2009] Gatenby, R. a., Silva, A. S., Gillies, R. J., and Frieden, B. R. (2009). Adaptive therapy. *Cancer Res*, 69(11):4894–4903.

[Gerlee, 2013] Gerlee, P. (2013). The model muddle: in search of tumor growth laws. *Cancer Res*, 73(8):2407–11.

[Gershon et al., 1967] Gershon, R. K., Carter, R. L., and Kondo, K. (1967). On concomitant immunity in tumour-bearing hamsters. *Nature*, 213(5077):674–676.

[Goldie and Coldman, 1979] Goldie, J. H. and Coldman, a. J. (1979). A mathematic model for relating the drug sensitivity of tumors to their spontaneous mutation rate. *Cancer Treat Rep*, 63(11-12):1727–1733.

[Gompertz, 1825] Gompertz, B. (1825). On the Nature of the Function Expressive of the Law of Human Mortality, and on a New Mode of Determining the Value of Life Contingencies. *Phil Trans R Soc B*, 115:513–584.

[Gorelik, 1983] Gorelik, E. (1983). Resistance of tumor-bearing mice to a second tumor challenge. *Cancer Res*, 43(1):138–145.

[Gorelik et al., 1978] Gorelik, E., Segal, S., and Feldman, M. (1978). Growth of a local tumor exerts a specific inhibitory effect on progression of lung metastases. *Int J Cancer*, 21(5):617–625.

[Gorelik et al., 1981] Gorelik, E., Segal, S., and Feldman, M. (1981). On the mechanism of tumor "concomitant immunity". *Int J Cancer*, 27(6):847–856.

[Greenspan, 1972] Greenspan, H. P. (1972). Models for the Growth of a Solid Tumor by Diffusion. *Studies in Applied Mathematics*, 51(4):317–340.

[Guiguet et al., 1982] Guiguet, M., Tubiana, M., and Valleron, A. J. (1982). Distribution des tailles des métastases a la détection et traitement adjuvant. Approche biomathématique. *C R Seances Acad Sci III*, 294:15–18.

[Guiot et al., 2003] Guiot, C., Degiorgis, P. G., Delsanto, P. P., Gabriele, P., and Deisboeck, T. S. (2003). Does tumor growth follow a “universal law”? *J Theor Biol*, 225(2):147–151.

[Gundem et al., 2015] Gundem, G., Van Loo, P., Kremeyer, B., Alexandrov, L. B., Tubio, J. M. C., Papaemmanuil, E., Brewer, D. S., Kallio, H. M. L., Högnäs, G., Annala, M., Kivinummi, K., Goody, V., Latimer, C., O’Meara, S., Dawson, K. J., Isaacs, W., Emmert-Buck, M. R., Nykter, M., Foster, C., Kote-Jarai, Z., Easton, D., Whitaker, H. C., Neal, D. E., Cooper, C. S., Eeles, R. A., Visakorpi, T., Campbell, P. J., McDermott, U., Wedge, D. C., and Bova, G. S. (2015). The evolutionary history of lethal metastatic prostate cancer. *Nature*, 520(7547):353–357.

[Gunduz et al., 1979] Gunduz, N., Fisher, B., and Saffer, E. A. (1979). Effect of surgical removal on the growth and kinetics of residual tumor. *Cancer Res*, 39(10):3861–5.

[Gupta and Massagué, 2006] Gupta, G. P. and Massagué, J. (2006). Cancer metastasis: building a framework. *Cell*, 127(4):679–695.

[Haeno et al., 2012] Haeno, H., Gonen, M., Davis, M. B., Herman, J. M., Iacobuzio-Donahue, C. A., and Michor, F. (2012). Computational modeling of pancreatic cancer reveals kinetics of metastasis suggesting optimum treatment strategies. *Cell*, 148(1-2):362–375.

[Hahnfeldt et al., 2003] Hahnfeldt, P., Folkman, J., and Hlatky, L. (2003). Minimizing long-term tumor burden : the logic for metronomic chemotherapeutic dosing and its antiangiogenic basis. *J Theor Biol*, 220(4):545–554.

[Hahnfeldt et al., 1999] Hahnfeldt, P., Panigrahy, D., Folkman, J., and Hlatky, L. (1999). Tumor development under angiogenic signaling: a dynamical theory of tumor growth, treatment response, and postvascular dormancy. *Cancer Res*, 59(19):4770–4775.

[Hanahan and Folkman, 1996] Hanahan, D. and Folkman, J. (1996). Patterns and emerging mechanisms of the angiogenic switch during tumorigenesis. *Cell*, 86(3):353–364.

[Hanahan and Weinberg, 2000] Hanahan, D. and Weinberg, R. A. (2000). The hallmarks of cancer. *Cell*, 100(1):57–70.

[Hanahan and Weinberg, 2011] Hanahan, D. and Weinberg, R. A. (2011). Hallmarks of cancer: the next generation. *Cell*, 144(5):646–674.

[Hanin and Bunimovich-Mendrazitsky, 2014] Hanin, L. and Bunimovich-Mendrazitsky, S. (2014). Reconstruction of the natural history of metastatic cancer and assessment of the effects of surgery: Gompertzian growth of the primary tumor. *Math Biosc*, 247:47–58.

[Hanin and Rose, 2016] Hanin, L. and Rose, J. (2016). Uncovering the natural history of cancer from post-mortem cross-sectional diameters of hepatic metastases. *Math Med Biol*, 33(4):397–416.

[Hanin et al., 2006] Hanin, L., Rose, J., and Zaider, M. (2006). A stochastic model for the sizes of detectable metastases. *J Theor Biol*, 243(3):407–417.

[Hanin et al., 2015] Hanin, L., Seidel, K., and Stoevesandt, D. (2015). A "universal" model of metastatic cancer, its parametric forms and their identification: what can be learned from site-specific volumes of metastases. *J. Math. Biol.*, 72(6):1633–1662.

[Hart et al., 1998] Hart, D., Shochat, E., and Agur, Z. (1998). The growth law of primary breast cancer as inferred from mammography screening trials data. *Br J Cancer*, 78(3):382–7.

[Hartung, 2015] Hartung, N. (2015). Efficient resolution of metastatic tumor growth models by reformulation into integral equations. *Discrete Contin Dyn Syst Ser B*, 20(2):445–467.

[Hartung and Christophe, 2014] Hartung, N. and Christophe, G. (2014). A stochastic framework for secondary metastatic emission.

[Hartung et al., 2014] Hartung, N., Mollard, S., Barbolosi, D., Benabdallah, A., Chapuisat, G., Henry, G., Giacometti, S., Iliadis, A., Ciccolini, J., Faivre, C., and Hubert, F. (2014). Mathematical modeling of tumor growth and metastatic spreading: validation in tumor-bearing mice. *Cancer Res*, 74(22):6397–6407.

[Heist et al., 2015] Heist, R. S., Duda, D. G., Sahani, D. V., Ancukiewicz, M., Fidias, P., Sequist, L. V., Temel, J. S., Shaw, A. T., Pennell, N. A., Neal, J. W., Gandhi, L., Lynch, T. J., Engelman, J. A., and Jain, R. K. (2015). Improved tumor vascularization after anti-VEGF therapy with carboplatin and nab-paclitaxel associates with survival in lung cancer. *Proc Natl Acad Sci USA*, 112(5):1547–1552.

[Held et al., 2006] Held, G., Schubert, J., Reiser, M., and Pfreundschuh, M. (2006). Dose-Intensified Treatment of Advanced-Stage Diffuse Large B-Cell Lymphomas. *Seminars in Hematology*, 43(4):221–229.

[Henares-Molina et al., 2017a] Henares-Molina, A., **Benzekry, S.**, Lara, P., García-Rojo, M., Pérez-García, V., and Martínez-González, A. (2017a). OS06.6 Optimized radiotherapy protocols delay the malignant transformation of low-grade gliomas in-silico. *Neuro-Oncology*, 19(suppl 3):iii12–iii12.

[Henares-Molina et al., 2017b] Henares-Molina, A., **Benzekry, S.**, Lara, P. C., García-Rojo, M., Pérez-García, V. M., and Martínez-González, A. (2017b). Non-standard radiotherapy fractionations delay the time to malignant transformation of low-grade gliomas. *PLoS ONE*, 12(6):e0178552.

[Hénin et al., 2016] Hénin, E., Meille, C., Barbolosi, D., You, B., Guitton, J., Iliadis, A., and Freyer, G. (2016). Revisiting dosing regimen using PK/PD modeling: the MODEL1 phase I/II trial of docetaxel plus epirubicin in metastatic breast cancer patients. *Breast Cancer Res Treat*, 156(2):331–341.

[Herman et al., 2011] Herman, A. B., Savage, V. M., and West, G. B. (2011). A Quantitative Theory of Solid Tumor Growth, Metabolic Rate and Vascularization. *PLoS ONE*, 6(9):e22973.

[Heuser et al., 1979] Heuser, L., Spratt, J. S., and Polk, H. C. (1979). Growth rates of primary breast cancers. *Cancer*, 43(5):1888–94.

[Hiratsuka et al., 2006] Hiratsuka, S., Watanabe, A., Aburatani, H., and Maru, Y. (2006). Tumour-mediated upregulation of chemoattractants and recruitment of myeloid cells predetermines lung metastasis. *Nat Cell Biol*, 8(12):1369–1375.

[Holmgren et al., 1995] Holmgren, L., O'Reilly, M. S., and Folkman, J. (1995). Dormancy of micrometastases: balanced proliferation and apoptosis in the presence of angiogenesis suppression. *Nat Med*, 1(2):149–153.

[Hong et al., 2015] Hong, W. S., Shpak, M., and Townsend, J. P. (2015). Inferring the Origin of Metastases from Cancer Phylogenies. *Cancer Res*, 75(19):4021–4025.

[Howlader et al., 2014] Howlader, N., Noone, A., Krapcho, M., Garshell, J., Miller, D., Altekruse, S., Kosary, C., Kosary, M., Ruhl, J., Tatalovich, Z., Mariotto, A., Mariotto, D., Chen, H., Feuer, E., and Cronin, K. (2014). SEER Cancer Statistics Review, 1975-2011, National Cancer Institute.

[Huang et al., 2002] Huang, X., Wong, M. K., Yi, H., Watkins, S., Laird, A. D., Wolf, S. F., and Gorelik, E. (2002). Combined therapy of local and metastatic 4T1 breast tumor in mice using SU6668, an inhibitor of angiogenic receptor tyrosine kinases, and the immunostimulator B7.2-IgG fusion protein. *Cancer Res*, 62(20):5727–5735.

[Iliadis and Barbolosi, 2000] Iliadis, A. and Barbolosi, D. (2000). Optimizing drug regimens in cancer chemotherapy by an efficacy-toxicity mathematical model. *Comput Biomed Res*, 33:211–226.

[Imbs et al., 2017] Imbs, D.-C., El Cheikh, R., Boyer, A., Ciccolini, J., Mascaux, C., Lacarelle, B., Barlesi, F., Barbolosi, D., and **Benzekry, S.** (2017). Revisiting bevacizumab + cytotoxics scheduling using mathematical modeling: proof of concept study in experimental non-small cell lung carcinoma. *CPT Pharmacometrics Syst Pharmacol*, accepted.

[InVS and INCa, 2011] InVS and INCa (2011). Projection de l'incidence et de la mortalité par cancer en France en 2011. Technical report, Institut de veille sanitaire et Institut National du Cancer, Saint Maurice.

[Iwata et al., 2000] Iwata, K., Kawasaki, K., and Shigesada, N. (2000). A Dynamical Model for the Growth and Size Distribution of Multiple Metastatic Tumors. *J Theor Biol*, 203(2):177–186.

[Jain, 2001] Jain, R. K. (2001). Normalizing tumor vasculature with anti-angiogenic therapy: A new paradigm for combination therapy. *Nat Med*, 7(9):987–989.

[Jain, 2005] Jain, R. K. (2005). Normalization of tumor vasculature: an emerging concept in antiangiogenic therapy. *Science*, 307(5706):58–62.

[Jain, 2013] Jain, R. K. (2013). Normalizing tumor microenvironment to treat cancer: bench to bedside to biomarkers. *J Clin Oncol*, 31(17):2205–2218.

[Jain, 2014] Jain, R. K. (2014). Antiangiogenesis strategies revisited: from starving tumors to alleviating hypoxia. *Cancer Cell*, 26(5):605–622.

[Joyce and Pollard, 2009] Joyce, J. A. and Pollard, J. W. (2009). Microenvironmental regulation of metastasis. *Nat Rev Cancer*, 9(4):239–252.

[Kaplan et al., 2005] Kaplan, R. N., Riba, R. D., Zacharoulis, S., Bramley, A. H., Vincent, L., Costa, C., MacDonald, D. D., Jin, D. K., Shido, K., Kerns, S. A., Zhu, Z., Hicklin, D., Wu, Y., Port, J. L., Altorki, N., Port, E. R., Ruggero, D., Shmelkov, S. V., Jensen, K. K., Rafii, S., and Lyden, D. (2005). VEGFR1-positive haematopoietic bone marrow progenitors initiate the pre-metastatic niche. *Nature*, 438(7069):820–7.

[Keating, 2014] Keating, G. M. (2014). Bevacizumab: a review of its use in advanced cancer. *Drugs*, 74(16):1891–1925.

[Kerbel and Kamen, 2004] Kerbel, R. S. and Kamen, B. A. (2004). The anti-angiogenic basis of metronomic chemotherapy. *Nat Rev Cancer*, 4(6):423–436.

[Kern et al., 1997] Kern, M. A., Helmbach, H., Artuc, M., Karmann, D., Jurgovsky, K., and Schadendorf, D. (1997). Human melanoma cell lines selected in vitro displaying various levels of drug resistance against cisplatin, fotemustine, vindesine or etoposide: modulation of proto-oncogene expression. *Anticancer research*, 17(6D):4359–4370.

[Ketcham et al., 1961] Ketcham, a. S., Kinsey, D. L., Wexler, H., and Mantel, N. (1961). The development of spontaneous metastases after the removal of a "primary" tumor. II. Standardization protocol of 5 animal tumors. *Cancer*, 14:875–882.

[Kim et al., 2009] Kim, M.-Y., Oskarsson, T., Acharyya, S., Nguyen, D. X., Zhang, X. H. F., Norton, L., and Massagué, J. (2009). Tumor self-seeding by circulating cancer cells. *Cell*, 139(7):1315–26.

[Kimmel and Flehinger, 1991] Kimmel, M. and Flehinger, B. J. (1991). Nonparametric estimation of the size-metastasis relationship in solid cancers. *Biometrics*, 47(3):987–1004.

[Klein, 2009] Klein, C. A. (2009). Parallel progression of primary tumours and metastases. *Nat Rev Cancer*, 9(4):302–312.

[Klein and Bartoszyński, 1991] Klein, J. P. and Bartoszyński, R. (1991). Estimation of growth and metastatic rates of primary breast cancer. In Arino, O., Axelrod, D. E., and Kimmel, M., editors, *Mathematical Population Dynamics*, pages 397–412.

[Klement et al., 2000] Klement, G., Baruchel, S., Rak, J., Man, S., Clark, K., Hicklin, D. J., Bohlen, P., and Kerbel, R. S. (2000). Continuous low-dose therapy with vinblastine and VEGF receptor-2 antibody induces sustained tumor regression without overt toxicity. *J Clin Invest*, 105(8):15–24.

[Koscielny and Tubiana, 1999] Koscielny, S. and Tubiana, M. (1999). The link between local recurrence and distant metastases in human breast cancer. *Int J Radiat Oncol Biol Phys*, 43(1):11–24.

[Koscielny et al., 1984] Koscielny, S., Tubiana, M., Le, M. G., Valleron, A., Mouriesse, H., Contesso, G., and Sarrazin, D. (1984). Breast cancer: relationship between the size of the primary tumour and the probability of metastatic dissemination. *Br J Cancer*, 49(6):709–15.

[Koscielny et al., 1985] Koscielny, S., Tubiana, M., and Valleron, A. J. (1985). A simulation model of the natural history of human breast cancer. *Br J Cancer*, 52(4):515–524.

[Kuhn and Lavielle, 2005] Kuhn, E. and Lavielle, M. (2005). Maximum likelihood estimation in nonlinear mixed effects models. *Comput. Statist. Data Anal.*, 49(4):1020–1038.

[Laird, 1964] Laird, A. K. (1964). Dynamics of tumor growth. *Br J Cancer*, 13:490–502.

[Laird, 1965] Laird, A. K. (1965). Dynamics of Tumour Growth: Comparison of Growth Rates and Extrapolation of Growth Curve To One Cell. *Br J Cancer*, 19:278–91.

[Lakhani et al., 2012] Lakhani, S. R., Ellis, I. O., Schnitt, S. J., Tan, P. H., and van de Vijver, M. J., editors (2012). *WHO Classification of Tumours, Volume 4*. IARC, Lyon, 4 edition.

[Lassau et al., 2016] Lassau, N., Coiffier, B., Kind, M., Vilgrain, V., Lacroix, J., Cuinet, M., Taieb, S., Aziza, R., Sarran, A., Labbe-Devilliers, C., Gallix, B., Lucidarme, O., Ptak, Y., Rocher, L., Caquot, L. M., Chagnon, S., Marion, D., Luciani, A., Feutray, S., Uzan-Augui, J., Benatsou, B., Bonastre, J., and Koscielny, S. (2016). Selection of an early biomarker for vascular normalization using dynamic contrast-enhanced ultrasonography to predict outcomes of metastatic patients treated with bevacizumab. *Ann Oncol*, 27(10):1922–1928.

[Lavielle, 2014] Lavielle, M. (2014). *Mixed Effects Models for the Population Approach*. Models, Tasks, Methods and Tools. CRC Press.

[Ledzewicz and Schättler, 2007] Ledzewicz, U. and Schättler, H. (2007). Antiangiogenic therapy in cancer treatment as an optimal control problem. *SIAM J Control Optim*, 46(3):1052–1079.

[Lefebvre et al., 2016] Lefebvre, G., Cornelis, F., Cumsille, P., Colin, T., Poignard, C., and Saut, O. (2016). Spatial modelling of tumour drug resistance: the case of GIST liver metastases. *Math Med Biol*.

[Li et al., 2001] Li, T. S., Kaneda, Y., Ueda, K., Hamano, K., Zempo, N., and Esato, K. (2001). The influence of tumour resection on angiostatin levels and tumour growth–an experimental study in tumour-bearing mice. *Eur J Cancer*, 37(17):2283–8.

[Lignet et al., 2013] Lignet, F., **Benzekry, S.**, Wilson, S., Billy, F., Saut, O., Tod, M., You, B., Adda Berkane, A., Kassour, S., Wei, M. X., Grenier, E., and Ribba, B. (2013). Theoretical investigation of the efficacy of antiangiogenic drugs combined to chemotherapy in xenografted mice. *J Theor Biol*, 320:86–99.

[Lin et al., 1999] Lin, Y. S., Nguyen, C., Mendoza, J. L., Escandon, E., Fei, D., Meng, Y. G., and Modi, N. B. (1999). Preclinical pharmacokinetics, interspecies scaling, and tissue distribution of a humanized monoclonal antibody against vascular endothelial growth factor. *J Pharmacol Exp Ther*, 288(1):371–378.

[Liotta et al., 1976a] Liotta, L. A., Saidel, G. M., and Kleinerman, J. (1976a). Stochastic model of metastases formation. *Biometrics*, 32(3):535–550.

[Liotta et al., 1976b] Liotta, L. A., Saidel, M. G., and Kleinerman, J. (1976b). The significance of hematogenous tumor cell clumps in the metastatic process. *Cancer Res*, 36(3):889–894.

[Litière et al., 2012] Litière, S., Werutsky, G., Fentiman, I. S., Rutgers, E., Christiaens, M.-R., Van Limbergen, E., Baaijens, M. H. A., Bogaerts, J., and Bartelink, H. (2012). Breast conserving therapy versus mastectomy for stage I-II breast cancer: 20 year follow-up of the EORTC 10801 phase 3 randomised trial. *Lancet Oncol*, 13(4):412–419.

[Lixoft, 2013] Lixoft (2013). Monolix software.

[Lorz et al., 2015] Lorz, A., Lorenzi, T., Clairambault, J., Escargueil, A., and Perthame, B. (2015). Modeling the effects of space structure and combination therapies on phenotypic heterogeneity and drug resistance in solid tumors. *Bull Math Biol*, 77(1):1–22.

[Lorz et al., 2013] Lorz, A., Lorenzi, T., Hochberg, M. E., Clairambault, J., and Perthame, B. (2013). Populational adaptive evolution, chemotherapeutic resistance and multiple anti-cancer therapies. *ESAIM Math Model Numer Anal*.

[Lowengrub et al., 2010] Lowengrub, J. S., Frieboes, H. B., Jin, F., Chuang, Y.-L., Li, X., Macklin, P., Wise, S. M., and Cristini, V. (2010). Nonlinear modelling of cancer: bridging the gap between cells and tumours. *Nonlinearity*, 23(1):R1–R9.

[Marie and Clunet, 1910] Marie, P. and Clunet, J. (1910). Frequency of visceral metastases in tumor bearing mice following surgical removal of their tumor [French]. *Bull Assoc Fr Etud Cancer*, 3:19–23.

[Mayneord, 1932] Mayneord, W. V. (1932). On a Law of Growth of Jensen's Rat Sarcoma. *Cancer Res*, 16(4):841–846.

[McMillin et al., 2013] McMillin, D. W., Negri, J. M., and Mitsiades, C. S. (2013). The role of tumour-stromal interactions in modifying drug response: challenges and opportunities. *Nat Rev Drug Discov*, 12(3):217–228.

[Mehrara et al., 2013] Mehrara, E., Forssell-Aronsson, E., Johanson, V., Kölby, L., Hultborn, R., and Bernhardt, P. (2013). A new method to estimate parameters of the growth model for metastatic tumours. *Theor Biol Med Model*, 10:31–31.

[Meille et al., 2016] Meille, C., Barbolosi, D., Ciccolini, J., Freyer, G., and Iliadis, A. (2016). Revisiting Dosing Regimen Using Pharmacokinetic/Pharmacodynamic Mathematical Modeling: Densification and Intensification of Combination Cancer Therapy. *Clin Pharmacokinet*, 55(8):1015–1025.

[Meille et al., 2008] Meille, C., Iliadis, A., Barbolosi, D., Frances, N., and Freyer, G. (2008). An interface model for dosage adjustment connects hematotoxicity to pharmacokinetics. *J Pharmacokinet Pharmacodyn*, 35(6):619–633.

[Métellus et al., 2013] Métellus, P., Faillot, T., Guyotat, J., Farah, W., Bauchet, L., Mornex, F., and Menei, P. (2013). Place of surgery in brain metastases. *Bull Cancer*, 100(1):51–56.

[Michelson et al., 1987] Michelson, S., Glicksman, a. S., and Leith, J. T. (1987). Growth in solid heterogeneous human colon adenocarcinomas: comparison of simple logistical models. *Cell Prolif*, 20(3):343–355.

[Michor, 2008] Michor, F. (2008). Mathematical models of cancer stem cells. *J Clin Oncol*, 26(17):2854–2861.

[Michor et al., 2006] Michor, F., Nowak, M. A., and Iwasa, Y. (2006). Stochastic dynamics of metastasis formation. *J Theor Biol*, 240(4):521–530.

[Milsom et al., 2013] Milsom, C. C., Lee, C. R., Hackl, C., Man, S., and Kerbel, R. S. (2013). Differential post-surgical metastasis and survival in SCID, NOD-SCID and NOD-SCID-IL-2Rγ(null) mice with parental and subline variants of human breast cancer: implications for host defense mechanisms regulating metastasis. *PLoS ONE*, 8(8):e71270.

[Miyake et al., 1999] Miyake, H., Hara, I., Gohji, K., and Yamanaka, K. (1999). Relative Expression of Matrix Metalloproteinase-2 and Tissue Inhibitor of Metalloproteinase-2 in Mouse Renal Cell Carcinoma Cells Regulates Their Metastatic Potential. *Clin Cancer Res*, pages 2824–2829.

[Mizuno et al., 1984] Mizuno, T., Masaoka, A., Ichimura, H., Shibata, K., Tanaka, H., and Niwa, H. (1984). Comparison of actual survivorship after treatment with survivorship predicted by actual tumor-volume doubling time from tumor diameter at first observation. *Cancer*, 53(12):2716–2720.

[Mollard et al., 2014] Mollard, S., **Benzekry, S.**, Giacometti, S., Faivre, C., Hubert, F., Ciccolini, J., and Barbolosi, D. (2014). Abstract 3677: Model-based optimization of combined antiangiogenic + cytotoxics modalities: application to the bevacizumab-paclitaxel association in breast cancer models. *Cancer Res*, 74(19 Supplement):3677–3677.

[Mollard et al., 2017] Mollard, S., Ciccolini, J., Imbs, D.-C., El Cheikh, R., Barbolosi, D., and **Benzekry, S.** (2017). Model driven optimization of antiangiogenics + cytotoxics combination: application to breast cancer mice treated with bevacizumab + paclitaxel doublet leads to reduced tumor growth and fewer metastasis. *Oncotarget*, 8(14):23087–23098.

[Mollard et al., 2016] Mollard, S., Fanciullino, R., Giacometti, S., Serdjebi, C., **Benzekry, S.**, and Ciccolini, J. (2016). In Vivo Bioluminescence Tomography for Monitoring Breast Tumor Growth and Metastatic Spreading: Comparative Study and Mathematical Modeling. *Nature Sci Rep*, 6:36173.

[Montel et al., 2012] Montel, F., Delarue, M., Elgeti, J., Vignjevic, D., Cappello, G., and Prost, J. (2012). Isotropic stress reduces cell proliferation in tumor spheroids. *New J Phys*, 14(5):055008.

[Motzer et al., 2015] Motzer, R. J., Escudier, B., McDermott, D. F., George, S., Hammers, H. J., Srinivas, S., Tykodi, S. S., Sosman, J. A., Procopio, G., Plimack, E. R., Castellano, D., Choueiri, T. K., Gurney, H., Donskov, F., Bono, P., Wagstaff, J., Gauler, T. C., Ueda, T., Tomita, Y., Schutz, F. A., Kollmannsberger, C., Larkin, J., Ravaud, A., Simon, J. S., Xu, L.-A., Waxman, I. M., Sharma, P., and CheckMate 025 Investigators (2015). Nivolumab versus Everolimus in Advanced Renal-Cell Carcinoma. *N Engl J Med*, 373(19):1803–1813.

[Motzer et al., 2007] Motzer, R. J., Hutson, T. E., Tomczak, P., Michaelson, M. D., Bukowski, R. M., Rixe, O., Oudard, S., Negrier, S., Szczylik, C., Kim, S. T., Chen, I., Bycott, P. W., Baum, C. M., and Figlin, R. A. (2007). Sunitinib versus Interferon Alfa in Metastatic Renal-Cell Carcinoma. *N Engl J Med*, 356(2):115–124.

[Mujoomdar et al., 2007] Mujoomdar, A., Austin, J. H. M., Malhotra, R., Powell, C. A., Pearson, G. D. N., Shiau, M. C., and Raftopoulos, H. (2007). Clinical Predictors of Metastatic Disease to the Brain from Non–Small Cell Lung Carcinoma: Primary Tumor Size, Cell Type, and Lymph Node Metastases1. *Radiology*, 242(3):882–888.

[Mukherjee, 2011] Mukherjee, S. (2011). *The Emperor of All Maladies: A Biography of Cancer*. Scribner, New York.

[Mulvenna et al., 2016] Mulvenna, P., Nankivell, M., Barton, R., Faivre-Finn, C., Wilson, P., McColl, E., Moore, B., Brisbane, I., Ardron, D., Holt, T., Morgan, S., Lee, C.,

Waite, K., Bayman, N., Pugh, C., Sydes, B., Stephens, R., Parmar, M. K., and Langley, R. E. (2016). Dexamethasone and supportive care with or without whole brain radiotherapy in treating patients with non-small cell lung cancer with brain metastases unsuitable for resection or stereotactic radiotherapy (QUARTZ): results from a phase 3, non-inferiority, randomised trial. *Lancet*, 388(10055):2004–2014.

[Neal et al., 2013] Neal, M. L., Trister, A. D., Ahn, S., Baldock, A., Bridge, C. a., Guyman, L., Lange, J., Sodt, R., Cloke, T., Lai, A., Cloughesy, T. F., Mrugala, M. M., Rockhill, J. K., Rockne, R. C., and Swanson, K. R. (2013). Response classification based on a minimal model of glioblastoma growth is prognostic for clinical outcomes and distinguishes progression from pseudoprogression. *Cancer Res*, 73(10):2976–2986.

[Newton et al., 2013] Newton, P. K., Mason, J., Bethel, K., Bazhenova, L., Nieva, J., Norton, L., and Kuhn, P. (2013). Spreaders and sponges define metastasis in lung cancer: a Markov chain Monte Carlo mathematical model. *Cancer Res*, 73(9):2760–2769.

[Newton et al., 2012] Newton, P. K., Mason, J., Bethel, K., Bazhenova, L. A., Nieva, J., and Kuhn, P. (2012). A Stochastic Markov Chain Model to Describe Lung Cancer Growth and Metastasis. *PLoS ONE*, 7(4):e34637.

[Nguyen et al., 2009] Nguyen, D. X., Bos, P. D., and Massagué, J. (2009). Metastasis: from dissemination to organ-specific colonization. *Nat Rev Cancer*, 9(4):274–284.

[Nielsen et al., 1987] Nielsen, M., Thomsen, J. L., Primdahl, S., Dyreborg, U., and Andersen, J. A. (1987). Breast cancer and atypia among young and middle-aged women: a study of 110 medicolegal autopsies. *Br J Cancer*, 56(6):814–819.

[Norton, 1988] Norton, L. (1988). A Gompertzian model of human breast cancer growth. *Cancer Res*, 48(24):7067–7071.

[Norton and Massagué, 2006] Norton, L. and Massagué, J. (2006). Is cancer a disease of self-seeding? *Nat Med*, 12(8):875–878.

[Norton and Simon, 1977] Norton, L. and Simon, R. (1977). Tumor size, sensitivity to therapy, and design of treatment schedules. *Cancer Treat Rep*, 61:1307–1317.

[Norton and Simon, 1986] Norton, L. and Simon, R. (1986). The Norton-Simon hypothesis revisited. *Cancer Treat Rep*, 70(1):163–169.

[Norton et al., 1976] Norton, L., Simon, R., Brereton, H. D., and Bogden, A. E. (1976). Predicting the course of Gompertzian growth. *Nature*, 264:542–544.

[Oh et al., 2009] Oh, Y., Taylor, S., Bekele, B. N., Debnam, J. M., Allen, P. K., Suki, D., Sawaya, R., Komaki, R., Stewart, D. J., and Karp, D. D. (2009). Number of metastatic sites is a strong predictor of survival in patients with nonsmall cell lung cancer with or without brain metastases. *Cancer*, 115(13):2930–2938.

[O'Reilly et al., 1997] O'Reilly, M. S., Boehm, T., Shing, Y., Fukai, N., Vasios, G., Lane, W. S., Flynn, E., Birkhead, J. R., Olsen, B. R., and Folkman, J. (1997). Endostatin: an endogenous inhibitor of angiogenesis and tumor growth. *Cell*, 88(2):277–285.

[O'Reilly et al., 1994] O'Reilly, M. S., Holmgren, L., Shing, Y., Chen, C., Rosenthal, R. A., Moses, M., Lane, W. S., Cao, Y., Sage, E. H., and Folkman, J. (1994). Angiostatin: a novel angiogenesis inhibitor that mediates the suppression of metastases by a Lewis lung carcinoma. *Cell*, 79(2):315–328.

[Ossowski et al., 2010] Ossowski, L., Aguirre-Ghiso, J. A., and Manuscript, A. (2010). Dormancy of metastatic melanoma. *Pigment Cell Melanoma Res*, 23(1):41–56.

[Owonikoko et al., 2014] Owonikoko, T. K., Arbiser, J., Zelnak, A., Shu, H.-K. G., Shim, H., Robin, A. M., Kalkanis, S. N., Whitsett, T. G., Salhia, B., Tran, N. L., Ryken, T., Moore, M. K., Egan, K. M., and Olson, J. J. (2014). Current approaches to the treatment of metastatic brain tumours. *Nat Rev Clin Oncol*, 11(4):203–222.

[Paik et al., 2004] Paik, S., Shak, S., Tang, G., Kim, C., Baker, J., Cronin, M., Baehner, F. L., Walker, M. G., Watson, D., Park, T., Hiller, W., Fisher, E. R., Wickerham, D. L., Bryant, J., and Wolmark, N. (2004). A multigene assay to predict recurrence of tamoxifen-treated, node-negative breast cancer. *N Engl J Med*, 351(27):2817–2826.

[Pantziarka et al., 2016] Pantziarka, P., Hutchinson, L., André, N., **Benzekry, S.**, Bertolini, F., Bhattacharjee, A., Chiplunkar, S., Duda, D. G., Gota, V., Gupta, S., Joshi, A., Kannan, S., Kerbel, R., Kieran, M., Palazzo, A., Parikh, A., Pasquier, E., Patil, V., Prabhash, K., Shaked *, Y., Saulnier Sholler, G., Sterba, J., Waxman, D. J., and Banavali, S. (2016). Next generation metronomic chemotherapy—report from the Fifth Biennial International Metronomic and Anti-angiogenic Therapy Meeting, 6–8 May 2016, Mumbai. *Ecancermedicalscience*, 10.

[Parfitt and Fyhrie, 1997] Parfitt, A. M. and Fyhrie, D. P. (1997). Gompertzian growth curves in parathyroid tumours: further evidence for the set-point hypothesis. *Cell Prolif*, 30(8-9):341–349.

[Pasquier et al., 2010] Pasquier, E., Kavallaris, M., and André, N. (2010). Metronomic chemotherapy: new rationale for new directions. *Nat Rev Clin Oncol*, 7:455–465.

[Pechoux et al., 2016] Pechoux, C. L., Dhermain, F., and Besse, B. (2016). Whole brain radiotherapy in patients with NSCLC and brain metastases. *Lancet*, 388(10055):1960–1962.

[Peeters et al., 2008] Peeters, C. F., de Waal, R. M., Wobbes, T., and Ruers, T. J. (2008). Metastatic dormancy imposed by the primary tumor: does it exist in humans? *Ann Surg Oncol*, 15(11):3308–15.

[Peeters et al., 2006] Peeters, C. F. J. M., de Waal, R. M. W., Wobbes, T., Westphal, J. R., and Ruers, T. J. M. (2006). Outgrowth of human liver metastases after resection of the primary colorectal tumor: a shift in the balance between apoptosis and proliferation. *Int J Cancer*, 119(6):1249–53.

[Perou et al., 2000] Perou, C. M., S rlie, T., Eisen, M. B., van de Rijn, M., Jeffrey, S. S., Rees, C. A., Pollack, J. R., Ross, D. T., Johnsen, H., Akslen, L. a., Fluge, y., Pergamenschikov, A., Williams, C., Zhu, S. X., L nning, P. E., B rresen Dale, A.-L., Brown, P. O., and Botstein, D. (2000). Molecular portraits of human breast tumours : Abstract : Nature. *Nature*, 406(6797):747–752.

[Poleszczuk et al., 2016] Poleszczuk, J., Luddy, K. A., Prokopiou, S., Robertson-Tessi, M., Moros, E. G., Fishman, M., Djeu, J. Y., Finkelstein, S. E., and Enderling, H. (2016). Abscopal benefits of localized radiotherapy depend on activated T cell trafficking and distribution between metastatic lesions. *Cancer Res*.

[Pollard, 2016] Pollard, J. W. (2016). Defining Metastatic Cell Latency. *N Engl J Med*, 375(3):280–282.

[Portz et al., 2012] Portz, T., Kuang, Y., and Nagy, J. D. (2012). A clinical data validated mathematical model of prostate cancer growth under intermittent androgen suppression therapy. *AIP Advances*, 2(1):011002–011002.

[Pouchol et al., 2016] Pouchol, C., Clairambault, J., Lorz, A., and Trélat, E. (2016). Asymptotic analysis and optimal control of an integro-differential system modelling healthy and cancer cells exposed to chemotherapy. *arXiv*.

[Prehn, 1991] Prehn, R. T. (1991). The inhibition of tumor growth by tumor mass. *Cancer Res*, 51(1):2–4.

[Prehn, 1993] Prehn, R. T. (1993). Two competing influences that may explain concomitant tumor resistance. *Cancer Res*, 53(14):3266–3269.

[Psaila and Lyden, 2009] Psaila, B. and Lyden, D. (2009). The metastatic niche: adapting the foreign soil. *Nat Rev Cancer*, 9(4):285–293.

[Raman et al., 2016] Raman, F., Scribner, E., Saut, O., Wenger, C., Colin, T., and Fathallah-Shaykh, H. M. (2016). Computational Trials: Unraveling Motility Phenotypes, Progression Patterns, and Treatment Options for Glioblastoma Multiforme. *PLoS ONE*, 11(1):e0146617.

[Ravdin et al., 2001] Ravdin, P. M., Siminoff, L. A., Davis, G. J., Mercer, M. B., Hewlett, J., Gerson, N., and Parker, H. L. (2001). Computer program to assist in making decisions about adjuvant therapy for women with early breast cancer. *J Clin Oncol*, 19(4):980–991.

[Reis-Filho and Pusztai, 2011] Reis-Filho, J. S. and Pusztai, L. (2011). Gene expression profiling in breast cancer: classification, prognostication, and prediction. *Lancet*, 378(9805):1812–1823.

[Retsky and Demicheli, 2014] Retsky, M. and Demicheli, R. (2014). Multimodal Hazard Rate for Relapse in Breast Cancer: Quality of Data and Calibration of Computer Simulation. *Cancers*, 6(4):2343–2355.

[Retsky et al., 2010] Retsky, M., Demicheli, R., Hrushesky, W., Baum, M., and Gukas, I. (2010). Surgery triggers outgrowth of latent distant disease in breast cancer: an inconvenient truth? *Cancers*, 2(2):305–337.

[Retsky et al., 2008] Retsky, M. W., Demicheli, R., Hrushesky, W. J. M., Baum, M., and Gukas, I. D. (2008). Dormancy and surgery-driven escape from dormancy help explain some clinical features of breast cancer. *APMIS*, 116(7-8):730–741.

[Retsky et al., 1997] Retsky, M. W., Demicheli, R., Swartzendruber, D. E., Bame, P. D., Wardwell, R. H., Bonadonna, G., Speer, J. F., and Valagussa, P. (1997). Computer simulation of a breast cancer metastasis model. *Breast Cancer Res Treat*, 45(2):193–202.

[Ribba et al., 2006a] Ribba, B., Colin, T., and Schnell, S. (2006a). A multiscale mathematical model of cancer, and its use in analyzing irradiation therapies. *Theor Biol Med Model*, 3(1):7.

[Ribba et al., 2012] Ribba, B., Kaloshi, G., Peyre, M., Ricard, D., Calvez, V., Tod, M., Cajavec-Bernard, B., Idbaih, A., Psimaras, D., Dainese, L., Pallud, J., Cartalat-Carel, S., Delattre, J.-Y., Honnorat, J., Grenier, E., and Ducray, F. (2012). A tumor growth inhibition model for low-grade glioma treated with chemotherapy or radiotherapy. *Clin Cancer Res*, 18(18):5071–5080.

[Ribba et al., 2006b] Ribba, B., Saut, O., Colin, T., Bresch, D., Grenier, E., and Boissel, J. P. (2006b). A multiscale mathematical model of avascular tumor growth to investigate the therapeutic benefit of anti-invasive agents. *J Theor Biol*, 243(4):532–541.

[Rocchetti et al., 2013] Rocchetti, M., Germani, M., Bene, F., Poggesi, I., Magni, P., Pesenti, E., and Nicolao, G. (2013). Predictive pharmacokinetic–pharmacodynamic modeling of tumor growth after administration of an anti-angiogenic agent, bevacizumab, as single-agent and combination therapy in tumor xenografts. *Cancer Chemother Pharmacol*, 71(5):1147–1157.

[Rofstad and Graff, 2001] Rofstad, E. and Graff, B. (2001). Thrombospondin-1-mediated metastasis suppression by the primary tumor in human melanoma xenografts. *J Invest Dermatol*, 117(5):1042–9.

[Ruggiero et al., 2012] Ruggiero, R. A., Bruzzo, J., Chiarella, P., Bustuoabad, O. D., Meiss, R. P., and Pasqualini, C. D. (2012). Concomitant tumor resistance: the role of tyrosine isomers in the mechanisms of metastases control. *Cancer Res*, 72(5):1043–1050.

[Ruggiero et al., 2011] Ruggiero, R. A., Bruzzo, J., Chiarella, P., di Gianni, P., Isturiz, M. A., Linskens, S., Speziale, N., Meiss, R. P., Bustuoabad, O. D., and Pasqualini, C. D. (2011). Tyrosine isomers mediate the classical phenomenon of concomitant tumor resistance. *Cancer Res*, 71(22):7113–7124.

[Ruggiero et al., 1985] Ruggiero, R. A., Bustuoabad, O. D., Bonfil, R. D., Meiss, R. P., and Pasqualini, C. D. (1985). "Concomitant immunity" in murine tumours of non-detectable immunogenicity. *Br J Cancer*, 51(1):37–48.

[Saidel et al., 1976] Saidel, G. M., Liotta, L. A., and Kleinerman, J. (1976). System dynamics of metastatic process from an implanted tumor. *J Theor Biol*, 56(2):417–434.

[Sánchez-Chapado et al., 2003] Sánchez-Chapado, M., Olmedilla, G., Cabeza, M., Donat, E., and Ruiz, A. (2003). Prevalence of prostate cancer and prostatic intraepithelial neoplasia in Caucasian Mediterranean males: an autopsy study. *Prostate*, 54(3):238–47.

[Sckell et al., 1998] Sckell, A., Safabakhsh, N., Dellian, M., and Jain, R. K. (1998). Primary tumor size-dependent inhibition of angiogenesis at a secondary site: an intravital microscopic study in mice. *Cancer Res*, 58(24):5866–5869.

[Scott et al., 2013a] Scott, J. G., Basanta, D., Anderson, A. R., and Gerlee, P. (2013a). A mathematical model of tumour self-seeding reveals secondary metastatic deposits as drivers of primary tumour growth. *J R Soc Interface*, 10(82):20130011–20130011.

[Scott et al., 2014] Scott, J. G., Fletcher, A. G., Maini, P. K., Anderson, A. R., and Gerlee, P. (2014). A filter-flow perspective of haematogenous metastasis offers a non-genetic paradigm for personalised cancer therapy. *Eur J Cancer*, 50(17):3068–3075.

[Scott et al., 2013b] Scott, J. G., Gerlee, P., Basanta, D., Fletcher, A. G., Maini, P. K., and Anderson, A. R. (2013b). Mathematical Modeling of the Metastatic Process. In Malek, A., editor, *Experimental Metastasis: Modeling and Analysis*, pages 189–208. Springer Netherlands, Dordrecht.

[Scribner et al., 2014] Scribner, E., Saut, O., Province, P., Bag, A., Colin, T., and Fathallah-Shaykh, H. M. (2014). Effects of anti-angiogenesis on glioblastoma growth and migration: model to clinical predictions. *PLoS ONE*, 9(12):e115018.

[Seber and Wild, 2003] Seber, G. A. and Wild, C. J. (2003). *Nonlinear regression.* Wiley-Interscience, Hoboken (NJ).

[Serre et al., 2016] Serre, R., **Benzekry, S.**, Padovani, L., Meille, C., André, N., Ciccolini, J., Barlesi, F., Muracciole, X., and Barbolosi, D. (2016). Mathematical Modeling of Cancer Immunotherapy and Its Synergy with Radiotherapy. *Cancer Res*, 76(17):4931–4940.

[Simeoni et al., 2004] Simeoni, M., Magni, P., Cammia, C., De Nicolao, G., Croci, V., Pesenti, E., Germani, M., Poggesi, I., and Rocchetti, M. (2004). Predictive pharmacokinetic-pharmacodynamic modeling of tumor growth kinetics in xenograft models after administration of anticancer agents. *Cancer Res*, 64(3):1094–1101.

[Simon and Norton, 2006] Simon, R. and Norton, L. (2006). The Norton-Simon hypothesis: designing more effective and less toxic chemotherapeutic regimens. *Nat Clin Rev Oncol*, 3(8):406–7.

[Simpson-Herren et al., 1976] Simpson-Herren, L., AH, S., and Holmquist, J. P. (1976). Effects of surgery on the cell kinetics of residual tumor. *Cancer Treat Rep*, 60(12):1749–1760.

[Skipper, 1965] Skipper, H. E. (1965). The effects of chemotherapy on the kinetics of leukemic cell behavior. *Cancer Res*, 25(9):1544–50.

[Skipper et al., 1964] Skipper, H. E., SCHABEL, F. M., and WILCOX, W. S. (1964). Experimental evaluation of potential anticancer agents XIII. On the criteria and kinetics associated with "curability" of experimental leukemia. *Cancer Chemother Rep*, 35:1–111.

[Slack et al., 1969] Slack, N. H., Blumenson, L. E., and Bross, I. D. (1969). Therapeutic implications from a mathematical model characterizing the course of breast cancer. *Cancer*, 24(5):960–971.

[Spratt et al., 1993] Spratt, J. A., von Fournier, D., Spratt, J. S., and Weber, E. E. (1993). Decelerating growth and human breast cancer. *Cancer*, 71(6):2013–2019.

[Spratt et al., 1995] Spratt, J. S., Meyer, J. S., and Spratt, J. A. (1995). Rates of growth of human solid neoplasms: Part I. *J Surg Oncol*, 60(2):137–146.

[Spratt et al., 1996] Spratt, J. S., Meyer, J. S., and Spratt, J. A. (1996). Rates of growth of human neoplasms: Part II. *J Surg Oncol*, 61(1):68–83.

[Steeg, 2016] Steeg, P. S. (2016). Targeting metastasis. *Nat Rev Cancer*, 16(4):201–218.

[Steel, 1977] Steel, G. G. (1977). *Growth kinetics of tumours*. Clarendon Press. Oxford.

[Steel and Lamerton, 1966] Steel, G. G. and Lamerton, L. F. (1966). The growth rate of human tumours. *Br J Cancer*, 20(1):74–86.

[Stylianopoulos et al., 2012] Stylianopoulos, T., Martin, J. D., Chauhan, V. P., Jain, S. R., Diop-Frimpong, B., Bardeesy, N., Smith, B. L., Ferrone, C. R., Hornicek, F. J., Boucher, Y., Munn, L. L., and Jain, R. K. (2012). Causes, consequences, and remedies for growth-induced solid stress in murine and human tumors. *Proc Natl Acad Sci USA*, 109(38):15101–15108.

[Stylianopoulos et al., 2013] Stylianopoulos, T., Martin, J. D., Snuderl, M., Mpekris, F., Jain, S. R., and Jain, R. K. (2013). Coevolution of solid stress and interstitial fluid pressure in tumors during progression: implications for vascular collapse. *Cancer Res*, 73(13):3833–3841.

[Sugarbaker et al., 1971] Sugarbaker, E. V., Cohen, a. M., and Ketcham, a. S. (1971). Do metastases metastasize? *Annals of surgery*, 174(2):161–6.

[Sullivan and Salmon, 1972] Sullivan, P. W. and Salmon, S. E. (1972). Kinetics of tumor growth and regression in IgG multiple myeloma. *J Clin Invest*, 51(7):1697–1708.

[Sutherland et al., 1971] Sutherland, R. M., McCredie, J. A., and Inch, W. R. (1971). Growth of multicell spheroids in tissue culture as a model of nodular carcinomas. *J Natl Cancer Inst*, 46(1):113–120.

[Swanson et al., 2002] Swanson, K. R., Alvord, E. C., and Murray, J. D. (2002). Virtual brain tumours (gliomas) enhance the reality of medical imaging and highlight inadequacies of current therapy. *Br J Cancer*, 86(1):14–18.

[Tabouret et al., 2013] Tabouret, E., Métellus, P., Tallet-Richard, A., Figarella-Branger, D., Charaffe-Jauffret, E., Viens, P., and Goncalves, A. (2013). Surgical resection of brain metastases from breast cancer in the modern era: clinical outcome and prognostic factors. *Anticancer research*, 33(5):2159–2167.

[Tait et al., 2004] Tait, C. R., Dodwell, D., and Horgan, K. (2004). Do metastases metastasize? *J Pathol*, 203(1):515–8.

[Tallet et al., 2012] Tallet, A. V., Azria, D., Barlesi, F., Spano, J.-P., Carpentier, A. F., Gonçalves, A., and Métellus, P. (2012). Neurocognitive function impairment after whole brain radiotherapy for brain metastases: actual assessment. *Radiat Oncol*, 7(1):77.

[Talmadge and Fidler, 2010] Talmadge, J. E. and Fidler, I. J. (2010). AACR centennial series: the biology of cancer metastasis: historical perspective. *Cancer Res*, 70(14):5649–69.

[Talmadge et al., 1982] Talmadge, J. E., Wolman, S. R., and Fidler, I. J. (1982). Evidence for the clonal origin of spontaneous metastases. *Science*, 217(4557):361–363.

[Tejpar et al., 2012] Tejpar, S., Prenen, H., and Mazzone, M. (2012). Overcoming resistance to antiangiogenic therapies. *The Oncologist*, 17(8):1039–1050.

[Terroir et al., 2017] Terroir, M., Borget, I., Bidault, F., Ricard, M., Deschamps, F., Hartl, D., Tselikas, L., Dercle, L., Lumbroso, J., Baudin, E., Berdelou, A., Deandreis, D., Schlumberger, M., and Leboulleux, S. (2017). The intensity of 18FDG uptake does not predict tumor growth in patients with metastatic differentiated thyroid cancer. *Eur J Nucl Med Mol Imaging*, 44(4):638–646.

[Tong et al., 2004] Tong, R. T., Boucher, Y., Kozin, S. V., Winkler, F., Hicklin, D. J., and Jain, R. K. (2004). Vascular normalization by vascular endothelial growth factor receptor 2 blockade induces a pressure gradient across the vasculature and improves drug penetration in tumors. *Cancer Res*, 64(11):3731–3736.

[Torre et al., 2015] Torre, L. A., Bray, F., Siegel, R. L., Ferlay, J., Lortet Tieulent, J., and Jemal, A. (2015). Global cancer statistics, 2012. *CA Cancer J Clin*, 65(2):87–108.

[Tredan et al., 2015] Tredan, O., Lacroix-Triki, M., Guiu, S., Mouret-Reynier, M.-A., Barrière, J., Bidard, F.-C., Braccini, A.-L., Mir, O., Villanueva, C., and Barthélémy, P. (2015). Angiogenesis and tumor microenvironment: bevacizumab in the breast cancer model. *Target Oncol*, 10(2):189–198.

[Vakoc et al., 2009] Vakoc, B. J., Lanning, R. M., Tyrrell, J. A., Padera, T. P., Bartlett, L. A., Stylianopoulos, T., Munn, L. L., Tearney, G. J., Fukumura, D., Jain, R. K., and Bouma, B. E. (2009). Three-dimensional microscopy of the tumor microenvironment in vivo using optical frequency domain imaging. *Nat Med*, 15(10):1219–1223.

[Valastyan and Weinberg, 2011] Valastyan, S. and Weinberg, R. A. (2011). Tumor metastasis: molecular insights and evolving paradigms. *Cell*, 147(2):275–92.

[van de Ven et al., 2012] van de Ven, A. L., Wu, M., Lowengrub, J., McDougall, S. R., Chaplain, M. A. J., Cristini, V., Ferrari, M., and Frieboes, H. B. (2012). Integrated intravital microscopy and mathematical modeling to optimize nanotherapeutics delivery to tumors. *AIP Advances*, 2(1):011208.

[van de Vijver et al., 2002] van de Vijver, M. J., He, Y. D., van 't Veer, L. J., Dai, H., Hart, A. A. M., Voskuil, D. W., Schreiber, G. J., Peterse, J. L., Roberts, C., Marton, M. J., Parrish, M., Atsma, D., Witteveen, A., Glas, A., Delahaye, L., van der Velde, T., Bartelink, H., Rodenhuis, S., Rutgers, E. T., Friend, S. H., and Bernards, R. (2002). A Gene-Expression Signature as a Predictor of Survival in Breast Cancer. *N Engl J Med*, 347(25):1999–2009.

[van 't Veer et al., 2002] van 't Veer, L. J., Dai, H., van de Vijver, M. J., He, Y. D., Hart, A. A. M., Mao, M., Peterse, H. L., van der Kooy, K., Marton, M. J., Witteveen, A. T., Schreiber, G. J., Kerkhoven, R. M., Roberts, C., Linsley, P. S., Bernards, R., and Friend, S. H. (2002). Gene expression profiling predicts clinical outcome of breast cancer. *Nature*, 415(6871):530–536.

[Volpert et al., 1998] Volpert, O. V., Lawler, J., and Bouck, N. P. (1998). A human fibrosarcoma inhibits systemic angiogenesis and the growth of experimental metastases via thrombospondin-1. *Proc Natl Acad Sci U S A*, 95(11):6343–8.

[Waclaw et al., 2015] Waclaw, B., Bozic, I., Pittman, M. E., Hruban, R. H., Vogelstein, B., and Nowak, M. A. (2015). A spatial model predicts that dispersal and cell turnover limit intratumour heterogeneity. *Nature*, 525(7568):261–264.

[Wang et al., 2009] Wang, C. H., Rockhill, J. K., Mrugala, M., Peacock, D. L., Lai, A., Jusenius, K., Wardlaw, J. M., Cloughesy, T., Spence, A. M., Rockne, R., Alvord, E. C., and Swanson, K. R. (2009). Prognostic significance of growth kinetics in newly diagnosed glioblastomas revealed by combining serial imaging with a novel biomathematical model. *Cancer Res*, 69(23):9133–9140.

[Weis et al., 2015] Weis, J. A., Miga, M. I., Arlinghaus, L. R., Li, X., Abramson, V., Chakravarthy, A. B., Pendyala, P., and Yankeelov, T. E. (2015). Predicting the Response of Breast Cancer to Neoadjuvant Therapy Using a Mechanically Coupled Reaction-Diffusion Model. *Cancer Res*, 75(22):4697–4707.

[Weis et al., 2013] Weis, J. A., Miga, M. I., Arlinghaus, L. R., Li, X., Chakravarthy, A. B., Abramson, V., Farley, J., and Yankeelov, T. E. (2013). A mechanically coupled reaction-diffusion model for predicting the response of breast tumors to neoadjuvant chemotherapy. *Phys Med Biol*, 58(17):5851–5866.

[Welch and Black, 2010] Welch, H. G. and Black, W. C. (2010). Overdiagnosis in cancer. *J Natl Cancer Inst*, 102(9):605–13.

[Welter and Rieger, 2013] Welter, M. and Rieger, H. (2013). Interstitial Fluid Flow and Drug Delivery in Vascularized Tumors: A Computational Model. *PLoS ONE*, 8(8):e70395–23.

[West et al., 2001] West, G. B., Brown, J. H., and Enquist, B. J. (2001). A general model for ontogenetic growth. *Nature*, 413(6856):628–31.

[Wheldon, 1988] Wheldon, T. E. (1988). *Mathematical models in cancer research*. Hilger, Bristol.

[Wigner, 1960] Wigner, E. P. (1960). The unreasonable effectiveness of mathematics in the natural sciences. Richard courant lecture in mathematical sciences delivered at New York University, May 11, 1959. *Comm Pure Appl Math*, 13(1):1–14.

[Wilson et al., 2015] Wilson, S., Tod, M., Ouerdani, A., Emde, A., Yarden, Y., Adda Berkane, A., Kassour, S., Wei, M. X., Freyer, G., You, B., Grenier, E., and Ribba, B. (2015). Modeling and predicting optimal treatment scheduling between the antiangiogenic drug sunitinib and irinotecan in preclinical settings. *CPT Pharmacometrics Syst Pharmacol*, 4(12):720–727.

[Winkler et al., 2004] Winkler, F., Kozin, S. V., Tong, R. T., Chae, S.-S., Booth, M. F., Garkavtsev, I., Xu, L., Hicklin, D. J., Fukumura, D., di Tomaso, E., Munn, L. L., and Jain, R. K. (2004). Kinetics of vascular normalization by VEGFR2 blockade governs brain tumor response to radiation: Role of oxygenation, angiopoietin-1, and matrix metalloproteinases . *Cancer Cell*, 6(6):553–563.

[Wishart et al., 2010] Wishart, G. C., Azzato, E. M., Greenberg, D. C., Rashbass, J., Kearins, O., Lawrence, G., Caldas, C., and Pharoah, P. D. P. (2010). PREDICT: a new UK prognostic model that predicts survival following surgery for invasive breast cancer. *Breast Cancer Res*, 12(1):R1.

[Yachida et al., 2010] Yachida, S., Jones, S., Bozic, I., Antal, T., Leary, R., Fu, B., Kamiyama, M., Hruban, R. H., Eshleman, J. R., Nowak, M. A., Velculescu, V. E., Kinzler, K. W., Vogelstein, B., and Iacobuzio-Donahue, C. A. (2010). Distant metastasis occurs late during the genetic evolution of pancreatic cancer. *Nature*, 467(7319):1114–1117.

[Yankeelov et al., 2013] Yankeelov, T. E., Atuegwu, N., Hormuth, D., Weis, J. A., Barnes, S. L., Miga, M. I., Rericha, E. C., and Quaranta, V. (2013). Clinically relevant modeling of tumor growth and treatment response. *Sci Transl Med*, 5(187):187ps9–187ps9.

[Yorke et al., 1993] Yorke, E. D., Fuks, Z., Norton, L., Whitmore, W., and Ling, C. C. (1993). Modeling the development of metastases from primary and locally recurrent tumors: comparison with a clinical data base for prostatic cancer. *Cancer Res*, 53(13):2987–2993.

Abstract

Accumulation of new biological and clinical data thanks to the development and generalization of novel measurement techniques (especially in imaging or molecular biology) is currently driving oncology towards a quantitative science. Meanwhile, mathematical models developed by theoreticians have often remained confined to qualitative conclusions and rarely been confronted to the observations. The work presented here aims to bridge this gap.

Motivated by concrete biological or clinical questions, I have conducted combined experimental and theoretical studies with two main objectives: 1) better understand and 2) better predict. The contributions belong to three axis of research: tumor growth, metastasis and scheduling of anti-cancer treatments. The mathematical tools are mostly ordinary differential equations or physiologically structured partial differential equations. Statistical tools were also largely employed to fit the models to the data and test the hypotheses, with a major focus on nonlinear mixed-effects models.

Together, these contributions represent a step forward towards the development of quantitative methods in cancer biology. They also set the basis for computational tools of clinical value to help defining the design of clinical trials (at the population level) but also to better assess the diagnosis and prognosis of a cancer disease in a personalized way, in order to individually tailor the therapeutic intervention.

Keywords: Mathematical modeling, Cancer, Metastasis, Pharmacometrics, Nonlinear mixed-effect models, Personalized oncology